UNIVERSITÉ DE
SHERBROOKE
Faculté de génie
Département de génie civil

PUNCHING SHEAR BEHAVIOUR OF CONCRETE TWO-WAY SLABS REINFORCED WITH GLASS FIBER-REINFORCED POLYMER (GFRP) BARS

COMPORTEMENT AU POINÇONNEMENT DE DALLES BIDIRECTIONNELLES EN BÉTON ARMÉ DE BARRES D'ARMATURE EN POLYMÈRE RENFORCÉS DE FIBRES

Thèse de doctorat ès sciences appliquées
Spécialité: génie civil

Jury:
Brahim Benmokrane (directeur de recherche)
Edward Sherwood (Examinateur)
Marie-Josée Nollet (Examinateur)
Charles-Philippe Lamarche (Rapporteur)

Mohamed Ashour Wardany HASSAN

Sherbrooke (Québec) Canada **August 2013**

Your file Votre référence
ISBN: 978-0-494-96322-7

Our file Notre référence
ISBN: 978-0-494-96322-7

PUBLICATION DISSERTATION OPTION

This dissertation consists of the following four articles that have been accepted or submitted for publication in referred journals:

The first paper, presented in Chapter 4, has been accepted for publication in the ACI Structural Journal.

The second paper, presented in Chapter 5, has been accepted for publication in the Canadian Journal for Civil Engineering (CJCE).

The third paper, presented in Chapter 6, has been accepted to the ASCE Journal of Composites for Construction.

Finally, the fourth paper, presented in Chapter 7, has been submitted to the ASCE Journal of Composites for Construction.

ABSTRACT

Deterioration of reinforced-concrete (RC) structures due to corrosion of steel limits the service-life and increases the rehabilitation costs. Concrete slabs in parking structures deteriorate faster than any other structural elements because of direct exposure to high concentrations of chlorides used for snow and ice removal during winter seasons. The use of fiber-reinforced polymer (FRP) bars as an alternative to conventional steel has emerged as a realistic and cost-effective solution to overcome the corrosion problems, particularly for concrete structure exposed to harsh environmental conditions.

Design of RC flat slabs is often compromised by their ability to resist shear stresses at the punching-shear surface area. The connections between slabs and supporting columns could be susceptible to high shear stresses and might cause brittle and sudden punching-shear failure. These connections may become the starting points leading to catastrophic punching-shear failure of a flat slab system when the steel reinforcement corrodes. Extensive research work has been conducted on the punching-shear behaviour of steel-reinforced flat slabs. The punching-shear strength of RC flat slabs reinforced with glass fiber-reinforced polymer (GFRP) bars, however, is yet to be fully investigated and understood. This is due to the limited research work on the subject and to the numerous parameters affecting punching-shear behaviour. In addition, the current FRP design codes and guidelines do not provide rational design models addressing the contribution of the FRP as shear reinforcement (stirrups) for FRP-RC flat slabs.

Thus, this study aims at investigating the punching-shear behaviour of concrete two-way slabs reinforced in flexure with GFRP bars. The investigation included two-way test specimens without shear reinforcement and others with carbon or glass FRP stirrups to evaluate the performance of specimens without shear reinforcement and the effect of shear reinforcement on the punching-capacity and performance. To achieve this, experimental and analytical studies were conducted. The experimental program included twenty-six interior slab-column connections reinforced with GFRP bars and two specimens reinforced with steel

bars for comparisons. The specimens were tested through two phases. Phase I, focused on the two-way slabs without shear reinforcement and the investigated parameters were: (i) flexural reinforcement ratio (ranged from 0.34% to 1.66%) and type (steel and GFRP); (ii) GFRP compression reinforcement; (iii) slab thickness (200 mm and 350 mm); (v) column dimensions (300 × 300 mm and 450 × 450 mm); (iv) concrete strength (normal and high-strength concretes). Phase II, focused on the use of FRP shear reinforcement (stirrups) and its effectiveness and contribution to the punching-shear capacity. The test variables considered in Phase II were: (i) the material of stirrups (carbon and glass FRP); (ii) shear reinforcement ratio; (iii) stirrup spacing; (iv) the effect of flexural reinforcement ratio on the effectiveness of the shear reinforcement. The effect of the different parameters considered in the two phases of the experimental work were presented and discussed in four journal papers. Moreover, the test results and the findings contributed to the first field implementation of GFRP bars in two flat slabs parking garages in Québec's city, which were Québec's city hall (Québec, Canada, 2010) and La Chancelière parking garage (the world's first flat-slab parking garage totally reinforced with GFRP bars) (Québec, Canada, 2011).

On the other hand, the analytical study included assessing the accuracy of the current punching-shear design provisions through comparing the test results of the specimens tested herein and 35 specimens from literature. The provisions included CSA S806-12 (2012), ACI 440 (2006), BS 8110 (1997), and JSCE (1997).

Keywords: Punching-shear, two-way, slab, flat slab, parking garage, fiber-reinforced polymer, FRP, strength, prediction, design, shear reinforcement, stirrups, concrete.

RÉSUMÉ

La détérioration des structures en béton armé due à la corrosion de l'acier limite leur durée de vie et augmente les coûts de réparation. Les dalles en béton dans les structures de stationnements étagés se détériorent plus vite que n'importe quel autre élément structural à cause de l'exposition directe à de hautes concentrations de chlorures utilisés comme sels de déglaçage. L'utilisation de barres en polymère renforcé de fibres (PRF) est une bonne alternative à l'armature conventionnelle en acier particulièrement pour les structures en béton exposées à des conditions environnementales sévères.

Comportement au poinçonnement de dalles bidirectionnelles peut mener à une rupture fragile sans aucun avertissement. De nombreux travaux de recherche ont été consacrés à l'étude du comportement au poinçonnement de dalles en béton armé. Cependant la résistance au poinçonnement de dalles renforcées de barres en polymères renforcés de fibres de verre (PRFV) n'a pas encore été pleinement investiguée. Aussi, les codes et guides de design actuels des PRF ne fournissent pas d'équations pour le calcul de la contribution des PRF comme armature de cisaillement (étriers).

Cette étude vise l'investigation du comportement au poinçonnement de dalles bidirectionnelles renforcées en flexion avec des barres PRFV. L'étude inclut des spécimens d'essais bidirectionnels sans et avec armature de cisaillement. Des étriers en carbone ou en verre ont fait l'objet de ces essais. Le programme expérimental comprend vingt-six spécimens de dalles renforcées de barres en PRFV et deux spécimens renforcés avec des barres en acier pour des fins de comparaison. Les échantillons ont été testés en deux étapes. L'étape I a porté sur les dalles bidirectionnelles sans armature de cisaillement et les paramètres investigués sont: (i) le pourcentage d'armature en flexion (variant de 0,34% à 1,66%) et le type d'armature (acier et PRFV); (ii) l'armature en compression en PRFV; armature d'intégrité; (iii) l'épaisseur de dalle (200 mm et 350 mm); (v) les dimensions des colonnes (300 × 300 mm et 450 × 450 mm); (iv) la résistance en compression du béton (bétons normal et à haute résistance). L'étape II a porté, quant à elle, sur l'utilisation de renforcement de cisaillement en PRF (étriers) et sa contribution à la résistance au poinçonnement. Les variables d'essais

considérées dans l'étape II sont: (i) le matériau des étriers (carbone ou verre); (ii) le pourcentage d'armature de cisaillement; (iii) l'espacement des étriers; (iv) le pourcentage d'armature en flexion. L'effet des différents paramètres considérés dans les deux étapes de l'étude expérimentale est présentée et analysée à travers quatre articles scientifiques. Les résultats d'essais ont contribué à l'utilisation de barres en PRFV dans deux dalles de stationnements étagés à Québec : le stationnement de l'Hôtel de Ville de Québec en 2010 et le stationnement La Chancelière (le premier stationnement au monde entièrement renforcé de barres en PRFV) en 2011.

Enfin, une étude analytique comprenant l'utilisation d'équations de calcul de la résistance au poinçonnement a été réalisée dans le cadre de cette thèse. Cette étude a également compris l'analyse de 35 essais de dalles bidirectionnelles retrouvés dans la littérature.

Keywords: Cisaillement, poinçonnement, dalle bidirectionnelle, polymère renforcé de fibres, PRF, prédiction, design, étrier, béton.

The candidate has participated in the following publications during his doctorate study at the University of Sherbrooke:

Accepted/Submitted Journal Publications:

Dulude, C., **Hassan, M.**, Ahmed, E. and Benmokrane, B., (2013), "Punching-Shear Behavior of Flat Slabs Reinforced with Glass Fiber-Reinforced Polymer Bars", *ACI Structural Journal*, 110(5): 723-734.

Hassan, M., Ahmed, E. and Benmokrane, B., (2013), "Punching-Shear Behavior of Flat Slabs Reinforced with Glass Fiber-Reinforced Polymer Bars", *Canadian Journal of Civil Engineering (CJCE)*, in press.

Hassan, M., Ahmed, E. and Benmokrane, B., (2013), "Punching-Shear Strength of Normal- and High-Strength Two-Way Concrete Slabs Reinforced with GFRP Bars", *ASCE Journal of Composites for Construction*, in press.

Hassan, M., Ahmed, E. and Benmokrane, B., (2013), "Punching-Shear Behavior of Two-Way Slabs Reinforced with FRP Shear Reinforcement.", *ASCE Journal of Composites for Construction*, submitted.

Conference Publications:

Hassan, M., Ahmed, E. and Benmokrane, B., (2013), "Preliminary Investigation on Punching-Shear Strength of Flat Slabs with FRP Flexural and Shear Reinforcement.", *CSCE 2013, 3rd Specialty Conference on Material Engineering & Applied Mechanics*, Montreal, Quebec, May 29 to 1 June, 10 p.

Hassan, M., Ahmed, E. and Benmokrane, B., (2012) "Punching shear strength prediction of FRP-reinforced concrete flat slabs.", *6th International Conference on Advanced Composite Materials in Bridges and Structures*, Kingston, Ontario, Canada, 22 – 25 May, 10p.

Hassan, M., Dulude, C., Ahmed, E. and Benmokrane, B., (2011), "Punching Shear Strength of Flat Slabs Reinforced with Glass Fiber-Reinforced Polymer (GFRP) Bars", *CSCE 2011, General Conference*, Ottawa, Ontario, June 14-17, 10 p. (CD-ROM).

Selected Technical Reports:

Hassan, M., Afifi, M., Ahmed, E. and Benmokrane, B., (2013), "Caractérisation d'un nouvel étrier de cisaillement en matériaux composites pour les dalles de stationnements étagés et les colonnes en béton : Essais structuraux en laboratoire sur des spécimens grandeur nature.". (Rapport d'avancement II), for the Ministère du Développement économique, Innovation et Exportation, 33 p.

Hassan, M., Afifi, M., Ahmed, E. and Benmokrane, B., (2012), "Caractérisation d'un nouvel étrier de cisaillement en matériaux composites pour les dalles de stationnements étagés et les colonnes en béton : Essais structuraux en laboratoire sur des spécimens grandeur nature.".

(Rapport d'avancement I), for the Ministère du Développement économique, Innovation et Exportation, 22 p.

Hassan, M., Ahmed, E. and Benmokrane, B., (2011), "Punching-Shear Behavior of Two-way Flat Slabs Concrete Reinforced with FRP Bars.". (Rapport d'avancement), for the Ministère du Développement économique, Innovation et Exportation, 17 p.

Dulude.C, **Hassan M.**, Ahmed E., Benmokrane B., (2010), "Conception et essais expérimentaux sur des dalles de stationnements étagés en béton armé d'armature en matériaux composites de PRFV", (*projet de recherche MDEIE, N/Réf.: 08-09-PSVT2-13462*), (Technical report), Département de génie civil, Université de Sherbrooke, 74p.

Hassan M., Ahmed E., Benmokrane B., (2010), "Punching shear behavior of reinforced concrete slabs reinforced with FRP bars.", *Definition of doctorate research project* (Technical report), Université de Sherbrooke, Québec.

Benmokrane B., Dulude C. et **Hassan M.**, (2010), "Évaluation de la performance structurale des étriers en polymères renforcés de fibres dans les dalles bidirectionnelles de stationnements étagés", (Technical report), Pultrall inc., mai, 14p.

Poster Presentations:

Hassan, M., Ahmed, E. and Benmokrane, B., (2011), "Punching shear behaviour of two-way concrete flat slabs reinforced with FRP bars", *Poster in CRIB conference*, 21 June, Université Laval, Quebec.

Hassan, M., Ahmed, E. and Benmokrane, B., (2010), "Punching shear behaviour of two-way concrete flat slabs reinforced with and without FRP shear reinforcement", *NSERC annual meeting*, 22 February, Université de Sherbrooke, Quebec.

ACKNOWLEDGEMENTS

I would like to express my sincere and deep gratitude to my supervisor, Prof. Brahim Benmokrane for his guidance, valuable advice, encouragement, and support throughout all stages of the research project. Also, I would like to thank very much Dr. Ehab Ahmed, postdoctoral researcher, for his technical support and help.

Deep appreciation is due to the technical staff of the Civil Engineering Department at the Université de Sherbrooke, in particular Mr. Francois Ntacorigira, Martin Bernier, and Simon Kelley for their help in constructing and testing the specimens.

The financial support received from Quebec's Ministry of Economic Development, Innovation, and Export Trade, the Natural Sciences and Engineering Research Council of Canada (NSERC) (Canada Research Chair Programme), Pultrall Inc. (Thetford Mines, Québec), and the Fonds québécois de la recherche sur la nature et les technologies (FQRNT) (volet équipe de recherche) is deeply appreciated.

Many thanks also go to all my colleagues and friends in the Department of Civil Engineering at the Université de Sherbrooke who in one way or another contributed and supported me throughout my study and my life style.

I would like to express my deep appreciation and thanks to my parents, my sisters, and my wife's family, for their endless love, support, encouragement, duas, and prayers. The spiritual support of all of them cannot be praised enough. Finally, my words stand helpless, and cannot express my deep love and appreciation to my wife (Asmaa) for her continuous encouragement, and steadfast support throughout these years - without you I would never have gotten this far. I cannot present this work without expressing my love to my son (Omar) who enlightened my life with his smile; to them this thesis is dedicated.

Dedication

To my mother and father

To the memory of my father in law "Abdel-daim"

To my lovely wife "Asmaa" and my son "Omar"

with all my love and respect

TABLE OF CONTENTS

LIST OF TABLES

LIST OF FIGURES

LIST OF SYMBOLS

SI units are used throughout this study presented herein. Unless otherwise stated, the symbols most frequently used have the following meanings:

Symbol	Definition
A_f	total area of the reinforcing bars in one direction;
$A_{f,Ave.}$	average area of the reinforcing bars in the two directions;
A_{rx}	area of steel or FRP flexural reinforcement in X direction (mm^2);
A_{fv}	cross-sectional area of the FRP shear reinforcement on a concentric line parallel to the perimeter of the column;
$b_{o;0.5d}$	critical perimeter at a distance of $0.5d$ from the column face (mm);
$b_{o;1.5d}$	critical perimeter at a distance of $1.5d$ from the column face (mm);
d	average effective slab depth (mm) = slab thickness − 50/or 45 mm − d_b;
d_x	effective slab depth in X directions (mm); d_x=t-d_b/2-50/or 45 mm;
d_y	effective slab depth in Y directions (mm); d_y=t-1.5d_b-50/or 45 mm;
d_b	reinforcing bar diameter (mm);
E_r	modulus of elasticity of the tensile reinforcing bars (MPa);
E_s	modulus of elasticity of steel reinforcing bars (MPa);
E_f	modulus of elasticity of FRP reinforcing bars (MPa);
E_{fv}	modulus of elasticity of FRP stirrups straight portion (MPa);
E_c	modulus of elasticity of the concrete (MPa) (=$4750\sqrt{f_c'}$);
E_fA_f	FRP flexural reinforcement axial stiffness (N);
f_c'	cylinders concrete compressive strength (MPa);
f_t	split cylinder tensile strength of concrete (MPa);
f_u	ultimate tensile strength of steel bars;
f_y	yield strength of steel bars;
f_{fu}	ultimate tensile strength of FRP bars;

f_{fu}^*	guaranteed tensile strength FRP bars (MPa);
f_{fv}	ultimate tensile strength of the straight portion of FRP stirrups (MPa);
f_{fvb}	ultimate tensile strength of FRP stirrups at bend location (MPa);
n_f	modular ratio (E_f/E_c);
n_s	numbers of stirrups on a concentric line parallel to the perimeter of the column;
r_b	radius of the bend (mm);
S_{fv}	stirrup spacing, shall not exceed d/2, with the first stirrup placed at d/4 from the column face according to (CSA 23.4-2004);
t	slab thickness (mm);
u	perimeter of the loaded area (mm);
$v_{u.}$	ultimate shear stress at the column face (MPa);
$v_{u,\ 0.5d}$	ultimate shear stress at *d/2* from the column face (MPa);
v_c	ultimate punching-shear stress provided by the concrete (MPa);
v_{sf}	ultimate punching-stress provided by the FRP shear reinforcement (MPa);
V_u	ultimate/peak punching shear load (measured in test) (kN);
V_c	ultimate punching shear capacity provide by the concrete (kN);
V_{cr}	first radial cracking load (kN);
$V_{tang.}$	tangent cracking load (measured in test) (kN);
$V_{\Delta u}$	post-peak load (kN);
X_{cone}	distance from the column face to the observed failure surface;
$X_{\varepsilon fmax}$	distance from the column face to the maximum strains in the FRP bars;
α_{xcone}	estimated angel cone calculated from the X_{cone} distance in the horizontal direction = $(\tan^{-1}(t/X_{cone})$;
α_{cone}	actual average punching shear-angle cone in the horizontal direction;
α	a new parameter function for FRP tensile stiffness;
λ	factor to account for concrete density (λ=1 for normal-density concrete);
α_s	factor that adjusts V_c for support dimensions;
β_c	the ratio of long side to short side of the concentrated load or reaction area;
γ_b	safety factor (1.3);

Δ_{fu}	deflection at the peak load (mm);
Δ_u	defection at failure (post-peak) (mm);
ρ	reinforcement ratio;
ρ_b	balanced reinforcement ratio;
ρ_f	FRP reinforcement ratio = $A_{f,Ave.}$ / (2500×d);
ρ_s	steel reinforcement ratio = $A_{f,Ave.}$ / (2500×d);
ρ_{fb}	FRP bars balanced reinforcement ratio calculated according to ACI 440.1R (2006);
ρ_{fv}	shear reinforcement ratio at a perimeter at 0.5d; = (n_s*A_{fv}/S_{fv}.$b_{o;0.5d}$);
$\rho_{fv}E_{fv}$	shear reinforcement index;
ϕ_c	material resistance factor for concrete;
ε_y	yield strain of steel bar (με);
ε_{fu}	ultimate tensile strain for FRP bar (με);
ε_{fVu}	ultimate tensile strength of FRP bars at peak load (με);
ε_{fmax}	maximum tensile strength of FRP bars at the post-peak load (με);
ε_{cmax}	ultimate concrete strength (με);

CHAPTER 1
INTRODUCTION

1.1 Background and Problem Definition

The expansive corrosion of steel reinforcing bars is a significant factor shortening the service life of reinforced concrete (RC) structures. The deleterious effects due to significant temperature fluctuations, de-icing salts, and chlorides have created harsh environment conditions accelerating the corrosion of steel reinforcement in concrete structures such as parking garages. Furthermore, the expansive corrosion of steel causes cracking and spalling of the concrete cover, which typically lead to significant deterioration and rehabilitation needs. Several methods have been proposed to control the corrosion process by means of stopping chlorides and carbonation attack reaching to the surface of the steel and/or making the steel corrosion-resistant, for instance, increasing the concrete cover, decreasing the permeability of concrete, waterproofing membranes, epoxy coating, and galvanizing and stainless steel bars (Broomfield 2007). None of these techniques, however, has been proven to be cost-effective or a long-term solution.

A significant research effort over the past twenty years has shown that fibre-reinforced polymer (FRP) reinforcing bars can be used effectively as an alternative to the steel bars in RC structures, particularly where steel corrosion is a major concern. FRPs are corrosion-free and nonmagnetic materials with high strength-to-weight ratios, in addition to their possibility to provide embedded microwire sensors into the matrix (used as a kind of "smart" reinforcement) (Komová et al. 2008), makes them an attractive alternative reinforcement for concrete structures. Using FRP reinforcing bars in RC two-way slabs such as in parking garages, the most component structural element vulnerable to corrosion deteriorations because of the direct exposure to high concentration of chlorides used for snow and ice removal, can extend the lifetime serviceability, reduce maintenance costs, and improve life-cycle cost efficiency.

Moreover, FRP bars may also reduce construction costs by eliminating the need for waterproofing membranes and pavement items (Benmokrane et al. 2006).

Since glass FRP (GFRP) bar is more economical than the available types (carbon and aramid) of FRP bars, it is more attractive for the construction industry. Furthermore, recent advances in polymer technology have led to the development of a new generation of GFRP bars designated with high modulus of elasticity, which is expected to advance the use of GFRP reinforcing bars in many applications. Several successful field applications have been built with GFRP bars as internal reinforcement, especially concrete bridge deck slabs (El-Salakawy et al. 2005, and Benmokrane et al. 2006 & 2007). However, to date, the number of practical applications in two-way flat slabs parking garages reinforced internally with GFRP bars is very limited because of insufficient knowledge of the punching-shear behaviour of FRP-RC two-way flat slabs.

The shear design of RC flat slabs structures has received a great challenge for decades. The shear failure of the slab-column connection, commonly known as punching-shear failure, can lead to catastrophic collapse of the entire floor system (Cheng and Parra-Montesinos 2010). Punching-shear failure of slabs without shear reinforcement is brittle in nature with limited deflections and followed by a sudden loss of the load-carrying capacity. Several ways can be used to increase the punching-shear capacity of RC two-way slabs such as increasing slab thickness and/or column dimensions, using drop panels and/or column heads or both, concrete compressive strength (f'_c), and placing shear reinforcement in the punching-shear zone of the slab. The well-designed punching-shear reinforcement significantly improves the slab behaviour, as it not only increases the punching-shear strength but also the deformation capacity of the slab (Lips et al., 2012). The principle effect of the shear reinforcement is to restrain the discontinuity of the slabs at the shear crack and transfers most of the forces across the shear crack, which delays the further widening of the shear crack, thus increasing the punching-shear and deformation capacity (Rizk et al. 2011). Moreover, using the shear reinforcement in two-way flat slabs is a preferred way when the increase in slab thickness is restricted which, in turn, reduces the slabs self-weight, the total height, and the overall cost of the structure.

The FRP mechanical properties have a brittle linear elastic response, a lower modulus of elasticity, and different bond characteristics than that of steel reinforcement, which results

in differences in the punching-shear behaviour. Few studies were conducted to evaluate the punching-shear behaviour of FRP bars and/or grids in RC two-way slabs reinforced with and without FRP shear reinforcement (Ahmad et al. 1993; Banthia et al. 1995; Matthys and Taerwe, 2000 a & b; El-Ghandour et al. 2003; Ospina et al. 2003; Hussein et al. 2004; Zhang et al. 2005; Zaghloul 2007; Lee et al. 2009, and Nguyen-Minh and Rovank 2013). Through these investigations, it was demonstrated that the difference in mechanical properties and bond characteristics between FRP and steel reinforcement significantly affect the slab behaviour and strength. This results in the development of wider and deeper cracks. Deeper cracks decrease the contribution to shear strength from the uncracked concrete due to the lower depth of concrete in compression. Wider cracks, in turn, decrease the contributions from aggregate interlock and residual tensile stresses. Additionally, due to the relatively small transverse strength of FRP bars and relatively wider cracks, the contribution of dowel action may be negligible (El-Gamel et al. 2005 b). Besides, given the difference in mechanical properties, the punching-shear equations for steel-RC flat slabs cannot be directly employed for FRP-RC sections.

Most of the current equations predicting the punching-shear strength of FRP-RC elements are modified forms of those for steel-reinforced elements, in which an equivalent FRP ratio was included to account for the lower elastic stiffness of FRP bars. Recently, the Canadian Standard Association provided its first equations for predicting the punching-shear strength of FRP-RC members without shear reinforcement in the CAN/CSA S806-12 (2012), which provides a step forward for the design of such elements. These equations are based on the CSA A23.3 (2004) equations for a steel-reinforced section with some modifications to account for the FRP axial stiffness as well as the cubic root of the concrete compressive strength was proposed. Nevertheless, no codes and design guidelines or rational design models addressed the contribution of the FRP as shear reinforcement (stirrups) for FRP-RC two-way slabs. In addition, the use of FRP as shear reinforcement in two-way flat slabs was not fully investigated. Thus, this extensive experimental study is designed to investigate the punching shear behaviour of GFRP-RC two-way flat slabs reinforced with and without FRP shear reinforcement (stirrups) under concentric loading.

1.2 Research Significance

This research project examines the punching shear behaviour of interior two-way slab-column connections reinforced with GFRP bars under concentric loading. In addition, it pays attention to use of glass and carbon fiber-reinforced polymer (GFRP and CFRP) closed and spiral stirrups as shear reinforcement to enhance the punching-shear capacity of GFRP two-way slabs. The effects of most relevant parameters influencing the punching-shear capacity such as flexural reinforcement ratio and type, GFRP compression reinforcement, slab thickness, column dimensions, concrete strength (normal- and high-strength concretes), and FRP shear reinforcement contribution were also investigated.

The results of this research has contributed to implementing the GFRP bars in parking structures, which is an innovative solution of the corrosion problem of parking garages' slabs (Benmokrane et al. 2012). On the other hand, it introduces experimental results on the effects of FRP flexure and shear reinforcement on punching-shear capacity of flat slabs. The accuracy of current equations in the FRP design codes and guidelines (CSA S806 (2012); ACI 440 (2006); BS 8110 (1997) and JSCE (1997), and other design approaches from the literature were assessed. This research work also enriches the state-of-the-art and the databank of concentric punching shear tests of GFRP two-way slabs as well as provides useful information to all researchers and practicing engineers.

1.3 Objectives and Originality

The GFRP reinforcing bars are standing out as a realistic and cost-effective alternative reinforcement to conventional steel bars for concrete structures under severe environmental conditions. However, to date, the number of practical applications in RC two-way slabs parking garages reinforced internally with GFRP bars is very limited because of the lack of research and data on the punching-shear behaviour of FRP-RC two-way slabs. Besides, most of the experiments on slab-column connections conducted to date are based on slabs with a thickness of around 175 mm and a concrete strength ranging from 26 MPa to 50 MPa while few specimens constructed with high strength concrete (HSC) as well as FRP shear reinforcement. Therefore, more experimental results on slab-column connections are needed to clearly understand the structural performance of such elements.

Through the Natural Sciences and Engineering Research Council of Canada (NSERC) Industrial Research Chair in FRP for Concrete Infrastructure at the University of Sherbrooke, a joint effort with *the* Ministère du Développement Économique, de l'Innovation et de l'Exportation (MDEIE) of Québec was established to develop and implement GFRP reinforcement bars for RC two-way slabs parking garages. This effort was initiated by evaluating the punching-shear behaviour of GFRP-reinforced interior slab-column connections without FRP shear reinforcement (Phase I) and with FRP shear reinforcement (stirrups) (Phase II) focusing on evaluating their contribution on the punching-shear capacity.

Recently, the CAN/CSA S806-12 (2012) has published its new equations for predicting the punching-shear strength of FRP-RC members without shear reinforcement, which provides a step forward for the design an application of such elements. The accuracy and the validity of these equations as well as other available equations in the design guidelines and the literature will be evaluated. The main objectives of the current investigation can be summarized as follow:

1. To investigate the punching-shear behaviour of GFRP-RC two-way flat slabs with and without FRP shear reinforcement under concentric loading.
2. To investigate the FRP-stirrups' contribution to the punching-shear capacity of the GFRP-RC two-way flat slabs.
3. To evaluate the accuracy of the new proposed equations in the CAN/CSA S806-12 (2012) design code and current equations in the design guidelines for punching shear strength of FRP two-way flat slabs.
4. To establish design recommendations for the use of FRP materials as flexural and shear reinforcement in two-way flat slabs parking garages.

1.4 Methodology

Experimental and analytical studies were designed to achieve the aforementioned objectives of this research. The experimental study comprised two phases (Phase I and II). The two phases included construction and testing of twenty-six full-scale interior slab-column connections reinforced with GFRP bars and two specimens reinforced with steel bars for comparisons. Whereas, the first Phase I included twenty-one specimens without shear reinforcement, and Phase II included seven specimens with FRP shear reinforcement. The test

specimens were designed to simulate real thicknesses of flat slabs being used in the first implementation for GFRP bars in two-way flat slab parking garages (Benmokrane et al. 2012). Each specimen had a side dimension of 2500 mm in both directions and a central column stub extending 300 mm beyond the top and bottom surfaces of the slabs. The test specimens were simply supported along all four edges. A concentric load was applied to the slabs through the column stub from down. Through the experimental program, the effects of the following parameters were investigated: (i) flexural reinforcement ratio (ranged from 0.34% to 1.66%) and type (steel and GFRP); (ii) GFRP compression reinforcement; (iii) slab thickness (200 mm and 350 mm); (v) column dimensions (300 x 300 mm and 450 x 450 mm); (iv) concrete strength (normal and high-strength concretes); (vi) FRP shear reinforcement contribution.

On the other hand, the analytical study included assessing the accuracy of the current punching-shear design provisions through comparing the test results of the specimens tested herein and 35 specimens from literature. The provisions included CSA S806-12 (2012), ACI 440 (2006), BS 8110 (1997), and JSCE (1997).

1.5 Organization of the Dissertation

This dissertation consists of eight chapters. The following is a brief description of each:

Chapter 1: This chapter defines the problem and summarizes the main objectives and originality of the research program. The methodology followed to achieve these objectives is also emphasized.

Chapter 2: This chapter provides brief description of the FRP composites materials and their characteristics. The available literature review focusing on the punching-shear behaviour of the FRP two-way slabs reinforced with and without FRP shear reinforcement is also presented. The available punching-shear design provisions for concrete members reinforced with FRP recently introduced in Japan, Europe, USA, and Canada are also presented.

Chapter 3: This chapter describes the experimental program conducted at the University of Sherbrooke to test 28 GFRP concrete two-way slabs reinforced with and without shear

reinforcement. In this chapter, the details of test specimens, configurations, test setups, and instrumentations are given. The chapter provides detailed characteristics of the materials used in this research program.

Chapter 4: This chapter presents the first paper in this dissertation entitled "Punching-Shear Behavior of Flat Slabs Reinforced with Glass Fiber-Reinforced Polymer Bars." The presented materials in this chapter are collaborative joint research work between the author of this dissention during his doctorate studying and a master candidate (Dulude 2011). The experimental work is based on testing 10 interior slab-column connections without shear reinforcement with five specimens of each author. Factors influencing the punching-shear strength and deformation capacity such as the effect of reinforcement type (GFRP and steel) and ratio, slab thickness and column dimensions are addressed. Additionally, the test results are employed to evaluate the accuracy of current equations predicting the punching-shear strength of FRP-RC two-way slabs provided by codes, design guidelines, and others models from the literature are presented.

Chapter 5: This chapter presents the second paper in this dissertation entitled "Punching-Shear Strength of GFRP-Reinforced Concrete Flat-Slabs." The experimental study was extended to complete the test matrix presented in the first paper. The punching-shear behaviour of 17 test specimens without shear reinforcement divided into 4 Series was discussed and analysed. Extended parameters such as concrete strength (30 to 47 MPa) and GFRP compression reinforcement crossing the column cross section were highlighted. Comparisons between the experimental test results and the theoretical predictions values by the Canadian Standards code CSA S806-12 (2012), design guidelines and other models from the literatures are performed.

Chapter 6: This chapter presents the third paper in this dissertation entitled "Punching-Shear Strength of Normal and High-Strength Concrete Slabs Reinforced with GFRP Bars" In this study, a total of 10 full-scale interior slab-column connections without shear reinforcement were fabricated with normal- and high-strength concretes. The main objective of this paper is to investigate the punching-shear behaviour of two-way flat slabs reinforced with different grades of GFRP bars and constructed with different concrete grades (NSC and HSC).

Comparisons between 54 specimens without shear reinforcement tested to date including the specimens in this investigation, using punching-shear design models presented in CSA S806 (2012), ACI 440 (2006), BS 8110 (1997), and JSCE (1997) were assessed.

Chapter 7: This chapter presents the fourth paper in this dissertation entitled "Punching Shear Behavior of GFRP Reinforced Concrete Slabs Using FRP Shear Reinforcement." It presents the results of an experimental investigation on the behaviour of GFRP-RC two-way flat slabs reinforced with and without FRP shear reinforcement. A total of 10 full-scale interior slab-column connections were tested under concentrated load up to failure. The tests were performed to evaluate the effectiveness and contribution of using the FRP as shear reinforcement in the GFRP-RC slabs.

Chapter 8: A summary of this investigation is given in this chapter. The chapter also presents the general conclusions drawn from the work presented in this dissertation. Recommendations for future research are also given.

Although the complete description of the research work conducted herein was presented and discussed in the four papers listed above, more information was introduced in Appendix A concerning the failure envelop for all the test specimens.

CHAPTER 2

LITERATURE REVIEW

2.1 General

In many parts of the world, corrosion of steel reinforcement in concrete structures is a major durability problem, leading to structural degradation and consequent costly repairs and loss of serviceability. In the recent decade, the use of advanced composites, normally called fiber reinforced polymers (FRP), as reinforcement for concrete structures has emerged as one of the most promising new technologies in construction to overcome the problem of corrosion. Several design guides and codes on reinforcing structural concrete members with FRP reinforcement were developed and published in several countries (JSCE (1997); ISIS design manual No. 3 (2007); CSA S6-06 (2006); ACI 440.1R-06 (2006); CNR-DT 204-06 (2006); FIB *Task Group 9.3* (2007); and CSA S806-12 (2012). Countries such as, Canada, United States (USA), Japan and some other European countries have already implemented the use of FRP in bridges deck slabs, parking structures, barrier walls, continuous pavement, and other concrete structures.

This chapter provides brief information on the FRP materials and their characteristics. The previous research studies carried out to investigate the punching-shear behaviour of FRP-reinforced concrete two-way slabs with and without FRP shear reinforcement are reviewed. The punching-shear design provisions for concrete two-way slabs reinforced with FRP recently published in Japan, Europe, USA, and Canada are also presented.

2.2 FRP Composite Materials

"FRP" is an acronym for fiber reinforced polymers, which some also call fiber reinforced plastics. The term composite material is a generic term used to describe a judicious combination of two or more materials to yield a product that is more efficient from its constituents. One constituent is called the reinforcing or fiber phase (one that provides

strength); the other in which the fibers are embedded is called the matrix phase. The matrix, such as a cured resin-like epoxy, polyester, vinyl ester, or other matrix acts as a binder and holds the fibers in the intended position, giving the composite material its structural integrity by providing shear transfer capability. Figure 2.1 shows typical stress-strain curves for fibers, matrices, and the FRP materials that result from the combination of fibers and matrix.

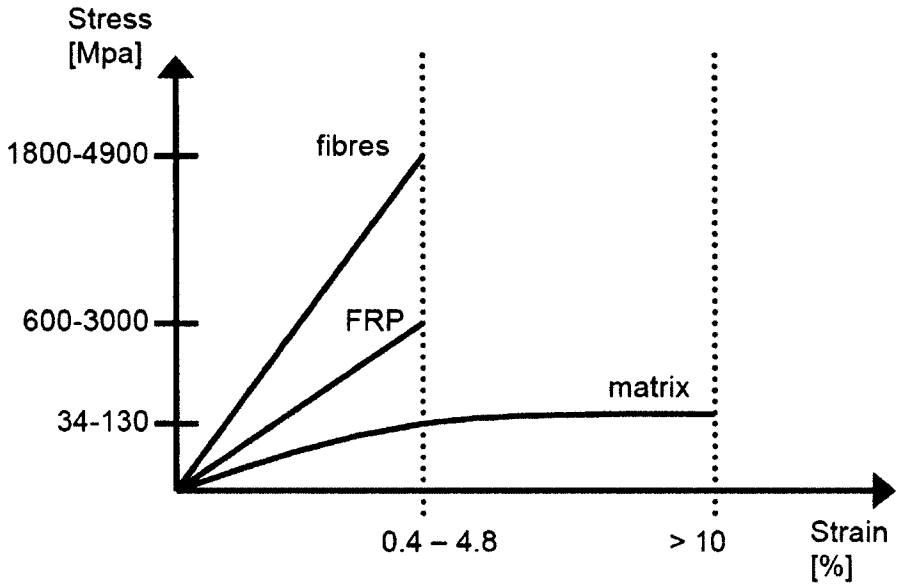

Figure 2.1: Stress-strain relationships for fibres, matrix, and FRP
ISIS design manual No. 3 (2007)

Three FRPs are commonly used (among others): composites containing glass fibers are called glass fiber reinforced polymers (GFRP); those containing carbon fibers are called carbon fiber reinforced polymers (CFRP); and those reinforced with aramid fibers are referred to as aramid fiber reinforced polymers (AFRP). GFRPs are the most inexpensive compared to the other commercially available FRPs, consequently the most commonly used fibers in structural engineering applications.

Use of composite materials was pioneered by the aerospace industry beginning in the 1940s, primarily because of the material's high-performance and lightweight qualities. Today their potential is being harnessed for many uses. Advanced composite materials, so called because of their many desirable properties, such as high performance, high strength-to-weight and high stiffness-to-weight ratios, high-energy absorption, and outstanding corrosion and fatigue damage resistance are now increasingly used for civil engineering infrastructure such as buildings and bridges. FRP products are manufactured in different forms such as bars,

fabrics, 2D grid, 3D grid, or standard structural shapes. Figure 2.2 shows various types and shapes of currently available FRP products.

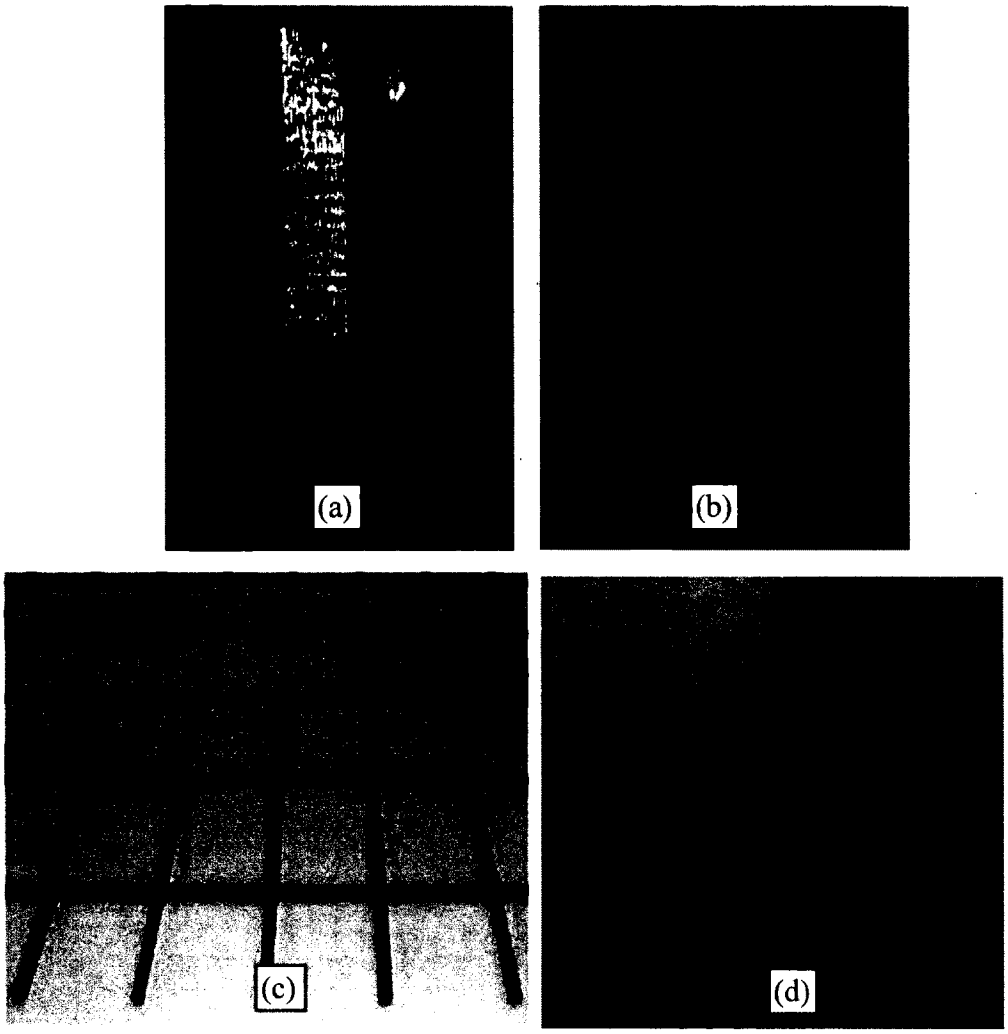

Figure 2.2: Different FRP products: (a) fabrics and strips; (b) straight bars; (c) grids; (d) spiral stirrups and curved bars.

2.3 General Characteristics of FRP Reinforcing Bars

FRP reinforcing bars are manufactured from continuous fibers (such as carbon, glass, and aramid) embedded in matrices (thermosetting or thermoplastic). A key element in evaluation of FRP properties is the characterization of the relative volume and/or mass content of the various constituent materials. The FRP reinforcing bars in concrete structures is strongly

influenced by their physical and mechanical properties. Available design variables include the choice of constituents (fiber and polymeric matrix), the volume fractions of fiber and matrix, fiber orientation and the manufacturing process. Other factors such as dimensional effects and quality control during fabrication play an important role in determining the characteristics of FRP bars. The properties of FRP materials are also influenced by loading history, duration of loading, temperature and humidity.

Similar to steel reinforcement, FRP bars are produced in different diameters, depending on the manufacturing process. FRP bars normally have tensile strength higher than the tensile strength of conventional steel bars. This relatively high tensile strength makes FRP bars suitable as reinforcement for concrete structures. The tensile behaviour of FRP bars having one type of fiber material is characterized by a linearly elastic stress-strain relationship up to failure. They do not exhibit any plastic behaviour before rupture. Typical tensile stress-strain relationships of FRP reinforcement compared to conventional steel bars are shown in Figure 2.3. The figure also shows that the modulus of elasticity of FRP bars is lower than that of steel bars. The CFRP has the highest modulus of elasticity, which ranged from 60% to 75% of that for steel. While the GFRP bars has the lowest modulus of elasticity, which ranged from 20% to 25% of that for steel. Table 2.1 shows the mechanical properties of some commercially available FRP reinforcing bars.

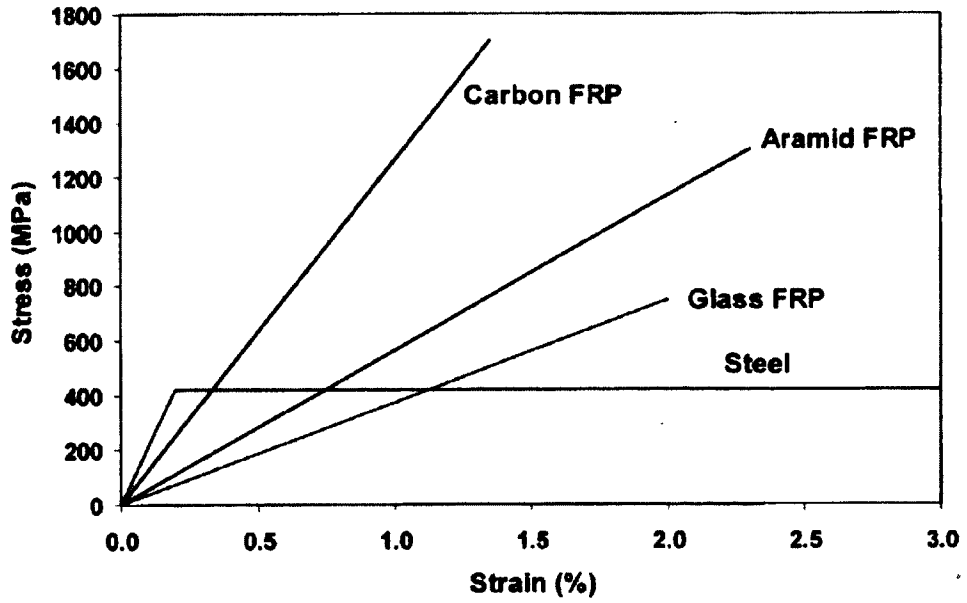

Figure 2.3: Typical stress-strain relationships of FRPs compared to steel bars (Ahmed 2009)

Bond behaviour of an FRP bar depends on the surface preparation and mechanical properties of the bar itself as well as the environmental conditions. The FRP bars surface preparations can be divided into two general categories according to the technique in which bond stresses between the FRP bar and the concrete are transferred, friction forming preparations and bearing forming preparations. The bars in the first category are coated with a granular material before the bars completely cured. These granular particles increase bond transfer through friction between the bars and concrete. Another way of increasing the bond strength of the bars is through the formation of indentations or deformations on the bar before full curing. The V-ROD FRP bars; which have sand-coated surface and are produced by Pultrall Inc., Quebec, Canada, stand as example of the bars of first category, whereas Leadline^{TM} CFRP bars; which have indented surface and are produced by Mitsubishi Chemical Cooperation, Japan, stand as example of the bars of second category. On the other hand, the surface of the Aslan FRP bars produced by the Hughes Brothers Inc., USA, contains indentations as well as a granular coating. Figure 2.4 shows different surfaces types of sand-coated and deformed FRP bars.

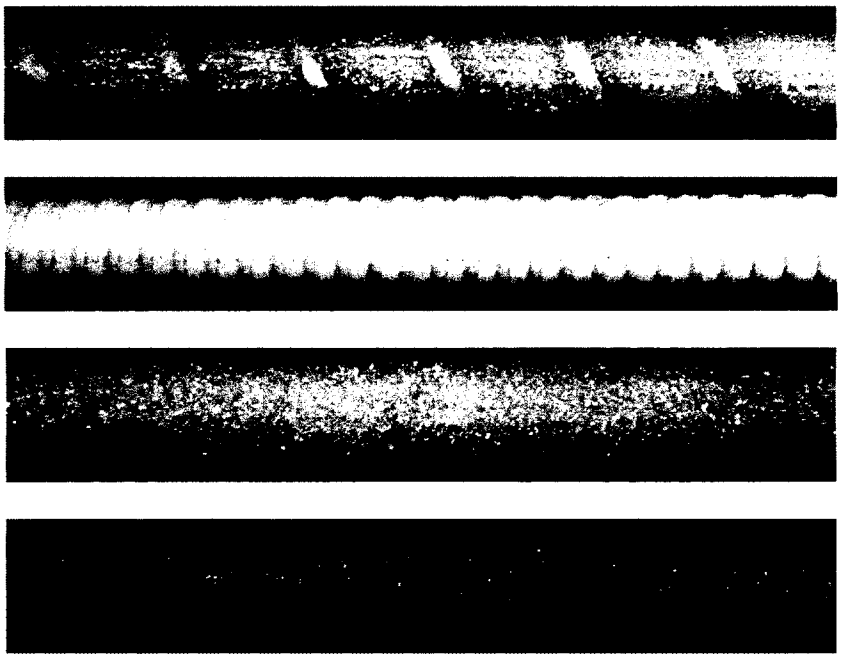

Figure 2.4: Different surfaces types of FRP bars

Further information concerning the physical and mechanical properties, time dependent behaviour, and durability of FRP reinforcement, can be found in the following:

JSCE (1997); ACI 440.1R-06 (2006); ISIS design manual No. 3 (2007); CAN/CSA-S806 (2012), S807 (2010), and S6-06 (2006).

Table 2.1: Typical mechanical properties of FRP reinforcement bars

Trade name	Fiber type	Guaranteed tensile strength (MPa)	Modulus of elasticity (GPa)	Ultimate tensile strain (%)
V- ROD[1]	Carbon	1356-1765	120-144	1.18-1.13
V- ROD LM[1]	Glass	666-804	43-45	1.34-1.89
V- ROD SM[1]	Glass	703-941	53-57	1.33-1.79
V- ROD HM[1]	Glass	1000-1372	63-66	1.15-2.11
Aslan 200[2]	Carbon	2068-2241	124	1.17-1.81
Aslan 100[2]	Glass	551-896	46	1.19-1.94
ComBAR[3]	Glass	> 1000	> 64	1.17
Leadline[4]	Carbon	2250	147	1.50
RockBAR[5]	Basalt	1107-1350	43-48	2.72-3.10
Dost Re-Bar[6]	Carbon	2300*	130	1.80
Dost Re-Bar[6]	Aramid	1400*	60	2.40
Dost Re-Bar[6]	Glass	1000*	40	2.8

[1] Pultrall Inc. (http://www.pultrall.com).

[2] Hughes Brothers Inc. (http://www.aslanfrp.com).

[3] Schöck Inc. (http://www.schoeck.ca).

[4] Mitsubishi Chemical Coporation Inc.(ISIS manual 3, 2007).

[5] Kammeny Vek Inc. (Serbescu, A. 2009).

[6] DostKimya Inc. (http://www.dostkimya.com); (*) tensile strength.

2.4 Shear Strength of Concrete Two-Way Slabs

Shear failure of concrete two-way slabs in the vicinity of concentrated loads may be due to beam action or two-way action. In case of the beam action, the slab behaves as a wide beam and the failure surface extends along the entire width of the slab. This type of failure occurs rarely in flat slab system.

In case of two-way action, the slab fails in a local area around the concentrated load. The critical section extends around the concentrated load or column. A punching shear failure occurs along a truncated cone or pyramid caused by the critical diagonal tension crack around the concentrated load or column. Figure 2.5 shows the slab shear-failure mechanisms.

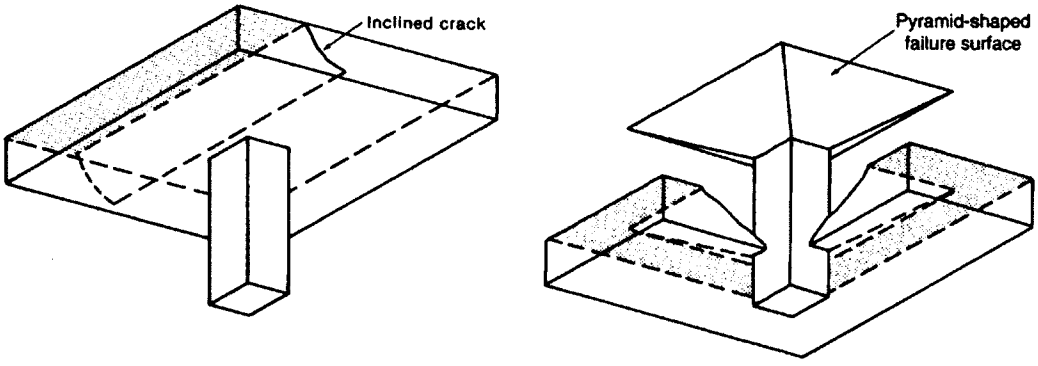

(a) One-way shear (b) Two-way shear

Figure 2.5: Shear-failure in a slab (MacGregor 1997)

Shear failure at a slab-column connection can result in progressive failures of adjacent connections of the same floor, as the load is transferred elsewhere, causing the adjacent connections to be more heavily loaded. In addition, the lower floor may fail progressively as they become unable to support the impact of material dropping from above. Hence, caution is clearly needed in shear strength calculation, and attention should be given to the low ductility associated with shear strength in order to avoid brittle failure conditions if possible.

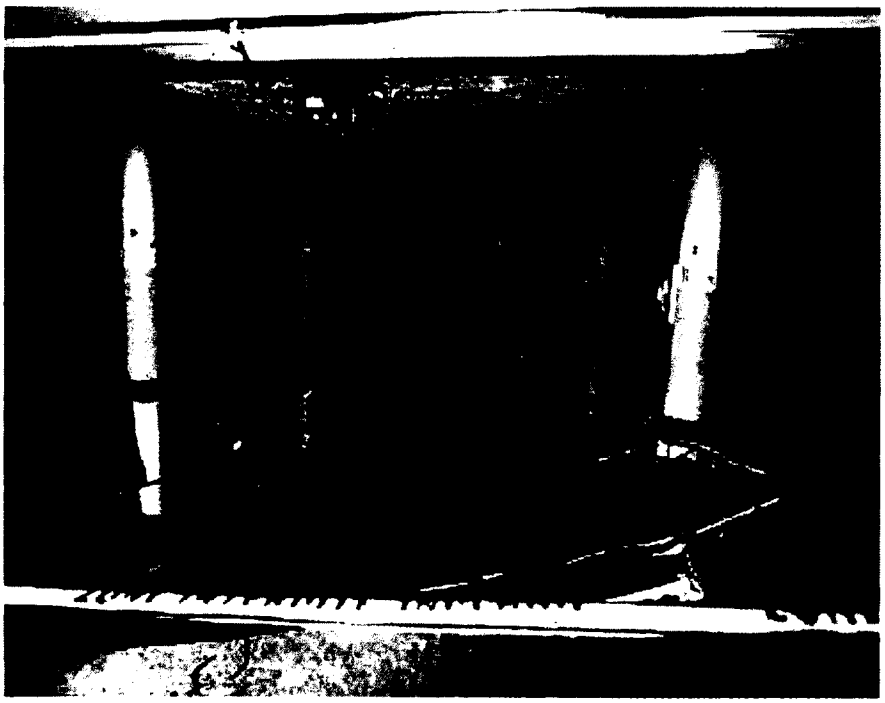

Figure 2.6: Punching failure in slabs (Montreal parking garage roof collapse 2008)

2.4.1 Punching shear failure mechanism of steel two-way slabs without shear reinforcement

After the diagonal tension cracking has occurred in the vicinity of the critical section of the slab around the perimeter of the load area, the slab carries the shear forces by shear across the compression zone, aggregate interlock, and dowel action. However, where two-way bending occurs, the nominal ultimate shear stress that can be developed in a slab at the assumed critical section is much higher than in a beam. This increase in punching shear strength of slabs is due to the three-dimensional nature of the slab shear-failure mechanism.

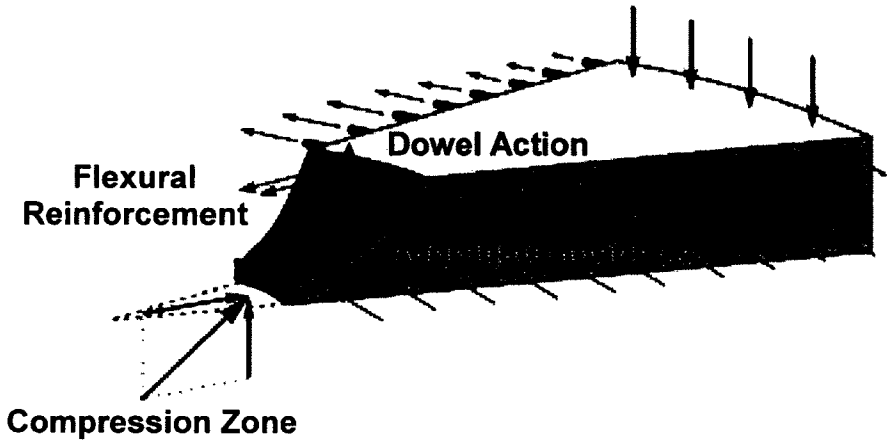

Figure 2.7: Shear failure mechanism in a cracked RC slab section without shear reinforcement (Adapted from Muttoni 2008).

When the load is applied to the slab, the first crack to form is a roughly circular tangential crack around the perimeter of the loaded area due to the negative bending moments in the radial direction. Radial cracks, due to negative bending moments in the tangential direction, then extend from that perimeter. Figure 2.8 shows a typical symmetric punching-shear failure. Because the radial moment decreases rapidly away from the loaded area, a significant increase in load is necessary before tangential cracks form around the load area some distance out in the slab. The diagonal tension cracks that developed in the slab tend to originate near mid-depth and therefore more similar to web-shear cracks than to flexural-shear cracks (Park and Gamble 2000). Test results by Kinnunen and Nylander (1960) reported that the first shear crack opened up at a load which ranged from 45 to 75 percent of the ultimate load. In most cases, only radial cracks were observed in the slab portion situated outside the

shear crack. At higher loads some tangential cracks forming circles around the column develop. The final punching failure occurs suddenly as a result of the propagation of the outermost tangential crack.

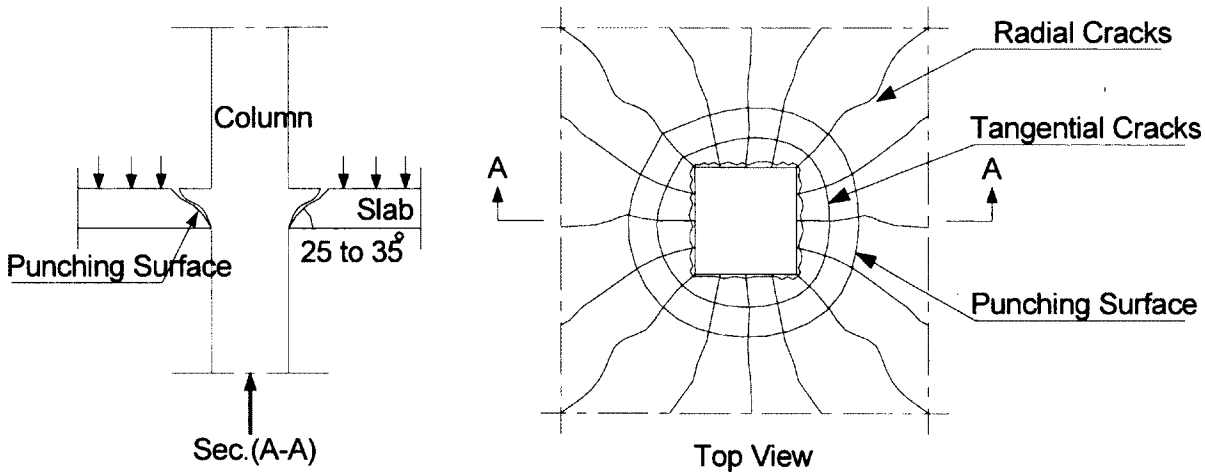

Figure 2.8: Typical symmetrical punching failure around an interior column (Sherif 1996)

2.4.2 Failure mode and shear strength of steel two-way slabs with shear reinforcement

Flat flab systems hold an inherent risk of brittle punching failure, which is a sudden and undesirable type of failure. One way to increase the shear capacity of slabs is providing shear reinforcement, which not only enhances the punching capacity but also helps to increase slab ductility (Hawkins et al. 1974). In order to reach yield, and therefore be fully effective, shear reinforcement has to be well-anchored (Hawkins 1974). Deformations at failure in slabs with well-anchored shear reinforcement are two to three times greater than for slabs without shear reinforcement (Regan and Bræstrup 1985). Due to anchorage problems, cost of shear reinforcement, and problems in placing the shear elements, some researchers find shear reinforcement unnecessary and recommend overcoming shear problems by providing additional flexural reinforcement (Whitney 1957), using higher strength concrete, or increasing the column size or slab thickness (Dragosavic and Van den Beukel, 1974). All of these methods have been shown to improve the punching capacity but cannot increase the

connection ductility and may impact the story height as well as the usable floor space (Birkle 2004).

The principle effect of shear reinforcement is to restraint the discontinuity of the slab at the shear crack, so that rotation is concentrated to the vertical crack at the face of the column (Sherif 1996). While after the development of inclined shear cracks, the shear reinforcement transfers most of the forces across the shear cracks and delays further widening. This, in turn, increases the punching-shear and deformation capacity of the slab (Rizk et al. 2011).

Design of slabs with punching shear reinforcement typically considers several potential failure modes (see Figure 2.9):

a) Crushing of compression struts (Figure 2.9 a). This failure mode becomes governing for high amounts of bending and transverse reinforcement, where large compressive stresses develop in the concrete near the column region. Crushing of concrete struts limits thus the maximum strength that can be provided by a shear reinforcing system. This is instrumental for design as it determines the applicability of such systems with respect to the effective depth of the slab and size of support region.

b) Punching within the shear-reinforced zone (Figure 2.9 b). Such failure develops for moderate or low amounts of shear reinforcement, when a shear crack localizes the strains within the shear-reinforced zone. Shear strength is thus governed by the contribution of concrete and of the transverse reinforcement. For design, this failure mode is used to determine the amount of shear reinforcement to be arranged.

c) Punching outside the shear-reinforced zone (Figure 2.9 c), this failure mode may be governing when the shear-reinforced zone extends over a small region. Check of this failure mode is typically performed in design to determine the extent of the slab to be shear reinforced.

d) Delamination of concrete core (Figure 2.9 d), when the shear reinforcement is not enclosing the flexural reinforcement, delamination of the concrete core may occur. This leads to a rather ductile failure mode but with limited strength and with loss of

development on the flexural reinforcement. Typical detailing provided in codes of practice avoids the use of shear reinforcement systems leading to such failure mode.

e) Flexural yielding (Figure 2.9 e), slabs with low flexural reinforcement ratios and with sufficient transverse reinforcement can fail by development of a flexural plastic mechanism. Bending strength and not punching shear strength is thus governing for the strength of the slab.

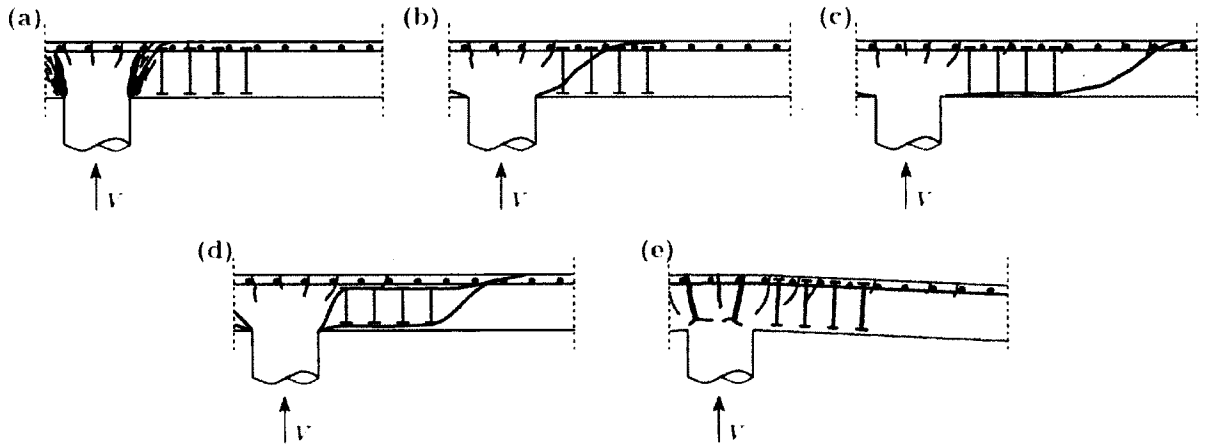

Figure 2.9 : Failure modes in flat slabs: (a) crushing of concrete struts; (b) punching within the shear-reinforced zone; (c) punching outside the shear-reinforced zone; (d) delamination; and (e) flexural yielding (Ruiz and Muttoni 2010).

2.4.3 Punching shear of FRP concrete two-way slabs reinforced with and without FRP shear reinforcement

Shear behaviour of reinforced concrete (RC) members is a complex phenomenon that relies on the development of internal carrying mechanisms, the magnitude and combination of which is still a subject of debate. The punching-shear failure of two-way slabs without shear reinforcement is brittle in nature with limited deflections and followed by a sudden loss of the load-carrying capacity. When the steel reinforcement corrodes in concrete slab, the slab-column connection may become the starting points leading to catastrophic collapse of the entire floor system. Because of direct exposure to high concentrations of chlorides used for snow and ice removal during winter seasons, concrete slabs deteriorate faster than any other structural elements. To overcome the corrosion-related problems, the steel should be protected

from elements causing corrosion or replaced with alternative non-corrodible materials, such as fiber-reinforced-polymer (FRP) composites reinforcement. Using FRP reinforcing bars in RC two-way slabs, can extend the service life, reduce maintenance cost and improve-life cycle cost efficiency. Moreover, FRP bars may also reduce construction costs by eliminating the need for membrane and pavement items (Benmokrane et al. 2006). The direct implementation of FRP instead of steel bars, however, is not possible due to the differences in the mechanical and bond characterises compared to steel bars. This results development of wider and deeper cracks affected the shear strength from the uncracked concrete compression zone below the neutral axis (N.A) depth and the contribution of aggregate interlock to decrease which, in turn, the ultimate punching-shear capacity to decrease. A summary of the previous studies on the punching shear behaviour of FRP-RC two-way slabs are briefly reviewed as follow:

Ahmad et al. (1993) tested six simply supported square concrete slabs under central concentrated loads. All test specimens had a side dimension of 690 mm with a thickness of 80 mm. The average effective depth in both directions was 61 mm and the concrete strength was 30 MPa. Four specimens were reinforced with 3-D carbon fiber grids and two slabs were reinforced with conventional mild steel. The flexural reinforcement ratios in the three directions (x, y, and z) for the CFRP-reinforced specimens were 0.95% whilst the reinforcement ratios of the control specimens were 1.18% and 1.35%. The average modulus of elasticity of the CFRP reinforcement was 113 GPa and an ultimate strain ranged between 0.8% and 1.18%. The test results indicated that all the CFRP-reinforced specimens failed in a punching shear failure with a smaller failure surface surrounding the loaded area compared to steel-reinforced slabs. Furthermore, the CFRP-reinforced specimens showed a significant reduction in the post-cracking stiffness stage compared to the steel slabs with a non-linear behaviour before the peak load, and also exhibited a post-peak load deformation softening response.

Banthia et al. (1995) tested four specimens 600x600x75 mm in dimensions with an effective depth of 55 mm. The slabs were simply supported on all four sides and a concentrated load was applied at the centre of the slabs. Three specimens were reinforced with FRP NEFMAC grids (reinforcement ratio = 0.37%) and one control specimen was reinforced with a steel grid (reinforcement ratio = 0.35%). The tensile strength and modulus of elasticity

of the FRP grids were 1200 MPa, and 100 GPa while the steel mesh was made of high-carbon steel with yield and ultimate strengths of 448 MPa and 917 MPa, respectively. The three FRP-reinforced slabs constructed with normal strength concrete, high strength concrete, and fiber-reinforced concrete with normal concrete strength, respectively, while the slab reinforced with steel had a normal strength concrete. The test results showed that all specimens failed in punching and the punched area was more pronounced in the steel-reinforced slab. It was observed that the specimens reinforced with FRP grids absorb less energy than comparable specimen reinforced with a steel grid. This is presumably due to the brittle nature of the FRP composites. Further, the use of fiber-reinforced concrete is found to improve the ultimate load-carrying capacity and the energy-absorption capability of slabs reinforced with FRP grids. Failure pattern of the various slabs and the acquired strain data indicate that the general cohesiveness, capability to transfer stresses across a crack, and the improved strain capacity of fiber-reinforced concrete delay the formation of large cracks, and thus, assist the low-modulus FRP reinforcement in achieving its full potential.

Matthys and Taerwe (2000 a) performed bending tests under concentrated load on one-way slabs: 4500 mm long x 1000 mm width x 120 or 150 mm depth. The tested specimens were reinforced with different types of FRP grids. While, Matthys and Taerwe (2000 b) tested 17 square slabs were obtained, except two, by saw-cutting 1000 mm (long) from those one-way slabs previously tested. The remaining two specimens were steel reinforced slabs, which were cast later and used as reference (R2 and R3). The average concrete strength ranged from 26.3 MPa to 35.1 MPa except for one specimen, which was constructed with high-strength concrete of 96.7 MPa. All slabs were simply supported by eight supports arranged in a circular pattern with a diameter of 0.9 m and the load was applied concentrically with a circular steel loading plate (diameters 80 mm, 150 mm, or 230 mm). These slabs were designed based on two different criteria, the first being the flexural strength and the second the flexural stiffness to satisfy serviceability requirements. The investigated parameters were flexural reinforcement ratio, slab thickness, and loaded area. It is worth mentioning that these slabs did not have reinforcement near the compression face. The specimens were divided into three series: the first series had four specimens reinforced with S500 steel mesh (the reinforcement ratio (ρ) ranged between 0.58% to 1.79%); the second series had eight specimens reinforced with different types of CFRP grids (ρ = 0.19 to 1.05%);

and the third series had five specimens reinforced with a hybrid type of FRP comprising glass and carbon FRP (ρ = 0.62% to 3.76%). The test results showed that there is a strong interaction between shear and flexural effects. However, most slabs showed a punching cone failure. The average angle of inclination for the punching cone were 30.7° for steel reinforced slabs, 29.2° for different CFRP grids and 26.8° for H type slabs. For all slabs, slip of the flexural reinforcement was noticed near failure or shortly after cracking and the bond behaviour of the grids was of considerable influence on the crack development and brittleness of the punching failure. Furthermore, they found that the FRP-reinforced specimens with a similar flexural strength as the steel-reinforced reference specimens, the obtained punching load and stiffness in the cracked state were considerably less. However, for the FRP-reinforced specimens with an increased reinforcement ratio or an increased slab depth, the behaviour of the slabs were comparable to steel-reinforced reference slabs. In addition, higher failure loads were found with increasing loading plate diameter; however, this parameter was less important than the reinforcement ratio and slab thickness.

Matthys and Taerwe also calculated the punching failure load of their tested specimens using some well-known empirical or code equations and compared the results with their experimental data. They found that these equations give fairly good predictions, but with an underestimation for FRP-reinforced slabs. The latter aspect was solved by introducing the equivalent reinforcement ratio $\rho_f E_f/E_s$. They suggested a modification to the empirical formula of the BS 8110-97 (1997) to adapt it for determining the punching-shear capacity of FRP-reinforced slabs. They multiplied the reinforcement ratio by the modular ratio E_f/E_s to obtain the modified punching capacity, as shown in the following equation:

$$V_c = 1.36 \frac{\left(100\rho_f \frac{E_f}{E_s} f_c'\right)^{1/3}}{d^{1/4}} b_{o,1.5d} d \qquad (2.1)$$

El-Ghandour et al. (1999, 2000, and 2003) investigated the punching shear behaviour of FRP-RC two-way slabs with and without CFRP shear reinforcement (corrugated shearbands). They conducted a two-phase experimental program to test eight square simply supported specimens with 2.0 m side length, a 175 mm thickness, and a 200x200 mm square column. All specimens were tested using a concentrated load at the center of the slabs. The first phase consisted of four specimens. Two slabs were reinforced with GFRP bars (ρ =

0.18%) and two were reinforced with CFRP bars (ρ = 0.15%). In the second phase, they increased the flexural reinforcement ratio to 0.38%. In the first phase, the specimens had rather low reinforcement ratio and wide spacing between the reinforcement bars and consequently failed due to bond slip of the flexural bars at loads less than their expected flexural and punching shear capacities. The shear reinforcement increased the slab load capacity, and it hampered slip initiation, but did not eliminate it. In the second phase, the smaller flexural bar spacing eliminated the problems of concrete splitting and prevented the bond slip failure in these slabs, which failed in punching shear. The shear reinforcement increased the apparent bond of the flexural reinforcement and reduced its slippage. It also prevented splitting of concrete around flexural bars; consequently, it increased the strength of the connection by 17%. These investigators recommended the use of 0.5d spacing between the shearband legs instead of the 0.75d used in their tests and also a maximum strain of 0.0045 for calculating the shear capacity of the CFRP shearband reinforcement.

Moreover, the analysis involved modifications to the punching-shear design equations used for steel-reinforced slabs in ACI-318-95 (1995) and BS-8110 (1997) to predict the punching-shear capacity of tested specimens accurately. They suggested modifying the ACI 318-95 (1995) equation by multiplying it in a stiffness correction factor $(E_f/E_s)^{1/3}$ while a strain limit of 0.0045 was proposed for FRP reinforcement in BS 8110 (1997) equation, yielding these equations for FRP slabs, as shown in Eqns. (2.2 and 2.3), respectively.

$$V_c = 0.33\sqrt{f_c}\left(E_f/E_s\right)^{1/3} b_{o;0.5d}\, d \tag{2.2}$$

$$V_c = 0.79\left[100\rho_f\left(E_f/E_s\right)\cdot\left(0.0045/\varepsilon_y\right)\right]^{1/3}\left(f_{cu}/25\right)^{1/3}\left(400/d\right)^{1/4} b_{o;1.5d}\, d \tag{2.3}$$

Zaghloul (2002 & 2007) investigated the punching-shear behaviour of CFRP grids interior slab-column connections reinforced with and without special fabricated CFRP shear rail used as shear reinforcement. The slabs were tested under shear and unbalanced moments. A total of 13 specimens were tested, 10 specimens were reinforced with CFRP grids in flexural only and one specimen with traditional steel reinforcement without shear reinforcement while the remaining two specimens were reinforced with CFRP grids in flexural and CFRP shear reinforcement in shear. The investigated parameters were: (i) the ratio of the applied moment to shear (M/V) = 0.22 or 0.30 m; (ii) reinforcement ratios (0.87%, 1.33%, and 1.48%); (iii) reinforcement type (steel or CFRP grids); (iv) slab thickness (100 mm or 125

mm); (v) column aspect ratio (1.0 or 1.4); and (vi) CFRP shear reinforcement. The test specimens comprised a 1760 x 1760 mm slab and a 250 x 250 mm or 250 x 350 mm column stub extending above and below the slab, and were made of 35 MPa concrete strength. The specimens was loaded via the cantilever that was a part of the upper column stub, and by adjusting the eccentricity of the axial load P, the desired moment to shear (M/V) was achieved. During the tests, the slabs were supported on four sides and were prevented from lifting. Due to the constant eccentricity of the axial load from the column center, the ratio of the moment to the shear was held constant throughout the test. Based on their study they reported the following:

1. The basic punching shear behaviour of CFRP reinforced slab-column connections is the same as that of steel reinforced connections.
2. The punching shear strength of slabs without shear reinforcement is proportional to the cubic root of their flexural reinforcement rigidity.
3. The column aspect ratio has an effect on the punching shear capacity of the slabs. Doubling the column aspect ratio caused a 15 % reduction in the punching strength.
4. The proposed shear reinforcement increased the punching shear strength of the specimens by 24.6% and 30.4%, when the first leg of the shear reinforcement was located 0.5d and 0.85d from the column face, respectively. This increase in punching capacity is comparable to the increase that can be achieved when using steel-headed studs.
5. A 25% increase in the slab thickness would cancel the negative effects of the lower elastic modulus of CFRP reinforcement on the stiffness and strength of the interior slab-column connections.

Ospina et al. (2003) investigated the punching shear behaviour of four full-scale interior slab-column connections measuring 2150 x 2150 x 155 mm in dimensions reinforced with FRP reinforcing bars and grids. All slabs were tested under a concentric load applied to the column stub. This load reacted against eight loading points on the slab, at a distance of 0.9 m from the center of the column stub. The main variables were the reinforcement material (steel or GFRP), the type of reinforcement mat (individual bars or two-dimensional grid) and the slab reinforcement ratio (0.73% to 1.46%). Two specimens were reinforced with GFRP deformed bars (C-bars), the third with a GFRP NEFMAC grid, and the last one with ordinary steel. The

experimental results of this study showed that the punching failure in FRP-reinforced specimens is affected by the elastic stiffness of the FRP mat as well as its bond characteristics. Whereas, the FRP grids in two-way flat slabs might not provide the same punching-shear capacity as FRP bars due to the difference in bond behaviour and concentration of stresses in the grids where the orthogonal reinforcement intersected. Furthermore, it would be improbable for a punching shear failure in an FRP reinforced slab to be triggered by FRP rupture. Even in the most lightly reinforced test specimens, the FRP did not rupture. The results also suggested that concrete crushing did not necessarily trigger punching shear failure in steel- or FRP-reinforced concrete slabs. For the purposes of calculating the ultimate shear strength of their test specimens, they adopted the expression recommended by Matthys and Taerwe (2000 b) (Eq. 2.1), as shown in the following Eq. (2.4).

$$V_c = 2.77\left(\rho_f f_c'\right)^{1/3}\sqrt{\frac{E_f}{E_s}}\, b_{o;1.5d} d \qquad (2.4)$$

Hussein et al. (2004) investigate the punching-shear behaviour of two-way slabs reinforced with GFRP bars. Four isolated interior slab-column connections were tested. The reinforcement ratio of the slabs varied between 0.95% and 1.67%. The slabs had a side dimension of 1900 mm square and thickness of 150 mm. A concentric load was applied on the slabs through a 250 x 250 column stub. The test results revealed that the crack pattern at failure and the strain distribution of the FRP reinforcement were different from those reported in the literature from similar investigations. The cracking along the reinforcement reported by other investigators was not observed and there was no apparent bond failure. The test results revealed that increasing the reinforcement ratio would not increase the connection capacity significantly.

El-Gamal et al. (2005 a & b) tested a total of six full size deck slabs: 3000 mm long x 2500 mm wide x 200 mm deep were constructed and tested to failure. The deck slabs were tested under monotonic concentrated load over a contact area of 600 x 250 mm to simulate the footprint of sustained truck wheel load (87.5 kN CL-625 truck) acting on the center of the slab. The deck slabs were supported on two steel girders (restrained edges) spaced at 2000 mm center-to-center. Five deck slabs were reinforced with GFRP and CFRP bars and one slab was reinforced with steel bars for comparisons. The test parameters were the type and amount of FRP reinforcement in the bottom transverse direction (1.0 to 2.0% for GFRP and 0.34 to 0.68% for CFRP). It was observed that the mode of failure for all deck slabs was punching

shear with carrying capacities of more than three times the design factored load specified by the Canadian Highway Bridge Design Code (CAN/CSA-S6). It was also concluded that the maximum measured crack widths and deflections at service load level were below the allowable code limits.

Based on the experimental and others researchers results from the literature, they proposed a new model to predict the punching shear capacity of two-way concrete slabs reinforced with FRP or steel reinforcement. This model takes into consideration a new parameter to give better agreement with the experimental results and is given by Eqn. (2.5).

$$V_c = V_{c,ACI\,318} \times \alpha = 0.33\sqrt{f_c'}\, b_{o;0.5d}\, d \times \alpha \qquad (2.5)$$

$$\alpha = 0.5\left(\rho_f\, E_f\right)^{1/3}\left(1 + 8d/b_o\right) \qquad (2.5\ a)$$

α is a new parameter which is a function of the flexural stiffness of the tensile reinforcement ($\rho_f E_f$), the perimeter of the applied load (b_o), and the effective depth of the slab (d) was introduced.

Zhang et al. (2005) investigate the punching-shear behaviour of two-way slabs reinforced with GFRP bars and constructed with normal and high-strength concrete. Three isolated interior slab-column connections were tested. The reinforcement ratio of the specimens was around 1.10%. The slabs had a side dimension of 1900 mm square and thickness of 150 mm. A central load was applied on a slab through a 250 x 250 mm column stub. The test results revealed that the reinforcement type significantly influences the punching strength of slabs. Using GFRP bars offsets the brittleness characteristics of punching failure. The concrete strength significantly affects the load carrying capacity and the post-punching capacity of slabs, but it has a little influence on the stiffness of the cracked slabs.

Lee et al. (2009) tested six specimens under punching shear test. The slabs had a side dimension of 2300 mm square and thickness of 150 mm. The slab was loaded with either equal concentrated loads around the perimeter to simulate a uniformly distributed load on the test specimen. The main variables were the reinforcement material, the concentration of reinforcement around the column, and the presence of steel fibers in the concrete. Four specimens were reinforced with uniform and banded distribution (within a distance 1.5h from the column faces, where h is the slab thickness) GFRP bars while two control steel specimens for comparisons. The flexural reinforcement ratios of the specimens were varied between

1.18% and 3%. The test results indicated that concentrating the top mat of flexural reinforcement within a distance 1.5 times the slab thickness from the column faces resulted in slightly higher punching shear strength, more uniform distribution of strains in the top flexural bars and better crack control compared to the companion slab with a uniform distribution of the same amount of reinforcement. The increase in punching shear strength due to the banded distribution of top reinforcement was 5% and 11% for the steel and GFRP specimens, respectively. In addition, the punching shear failure plane for the slabs with banded reinforcement surfaced at a greater distance from the column faces. However, excessive concentrations of the reinforcement (ρ = 3%) seems to be ineffective in increasing the punching resistance of GFRP-reinforced concrete slabs. They also compared the results in study including other experimental results performed by various researchers with the nominal punching-shear strength predicted using the design equations in ACI 440.1R-06 (2006) and JSCE (1997). It was concluded that the predictions using the equations of ACI 440.1R-06 (2006) were very conservative, while JSCE (1997) equations gave better predictions. The predictions using JSCE (1997) equations were unconservative for specimens with reinforcement ratios ranged between 2% to 3%.

Nguyen-Minh and Rovnak (2013) investigated the punching shear behaviour of concrete two-way slabs reinforced with GFRP bars. A total of six large-scale interior GFRP and steel reinforced slab-column connections (2200 x 2200 x 150 mm) with a column dimension 200 x 200 mm, consisting of three GFRP reinforced slabs and three control steel reinforced slabs, were tested. The flexural reinforcement ratios varied between 0.4% and 0.8% with no compression reinforcement was used in the slabs. All slabs simply supported on all four sides were tested under a concentrated load, acting on the column stub in the middle of each slab. Based on the results obtained from the study, it can be concluded that the increase of the GFRP reinforcement ratio in tested slabs increased the punching shear strengths up to 36% and deflections was reduced up to 35%. Both the size factor and the effect of the span to effective depth ratio L/d should be taken into account in calculations of the punching shear resistance of the FRP reinforced slab-column connections. Furthermore, the punching shear angles cone of steel and GFRP reinforced slabs was varied between 23° to 18° and 27° to 23°, respectively. The latter values differ from the angles of the punching cone of GFRP reinforced slabs varying from 26.8° to 30.7° by Matthys and Taerwe (2000 b).

2.5 Summary

The available literature of the FRP-RC two-way has been demonstrated that the punching shear strength was depended on many variables were discussed in this chapter. The main variables affecting the punching capacity are the concrete strength, the slab thickness, the column shape and size, the reinforcing material (steel or FRP), the reinforcement type (individual bars or grids), the FRP flexural reinforcement ratio, and the FRP shear reinforcement. However, to date the punching-shear strength of FRP-RC two-way slabs has yet to be fully investigated and clearly understood. This is due to the limited research work on the subject, especially in FRP two-way slabs reinforced with FRPs as shear reinforcement, and the numerous parameters affecting punching-shear behaviour. On the other hand, most of the previous research work on FRP-RC two-way slabs employed on slab thicknesses ranged from 75 mm to 175 mm. Thus, there was a need to investigate the punching-shear performance of full-scale slab-column connections simulating real thicknesses of flat slabs used in the field applications. In this regard, this study aims at investigating the punching-shear behaviour of GFRP-RC two-way slabs reinforced with and without FRP shear reinforcement, which contributes to understanding the general behaviour of such reinforced concrete elements. The test parameters in the current experimental program described in the following chapter.

CHAPTER 3

EXPERIMENTAL PROGRAM

3.1 General

The experimental program is aimed at investigating the punching-shear behaviour of GFRP-interior slab-column connections reinforced with and without FRP shear reinforcement. The experimental program presented herein consists of two phases. The two phases included construction and testing of twenty-six full-scale interior slab-column connections reinforced with GFRP bars and two specimens reinforced with steel bars for comparisons. Whereas, the first Phase I comprised twenty-one specimens without shear reinforcement including the steel-reinforced specimens, and Phase II included seven specimens with FRP shear reinforcement. The test specimens are designed to simulate real thicknesses of two-way flat slabs used in the first implementation for GFRP bars in two-way flat slab parking garages (Benmokrane et al. 2012). Each specimen had a side dimension of 2500 mm in both directions and a central column stub extending 300 mm beyond the top and bottom surfaces of the slabs. The test specimens were simply supported along all four edges to simulate the lines of contra-flexure. A concentric load was applied to the slabs through the column stub from down. Through the experimental program, the effects of the following parameters are investigated:

- Reinforcement type (steel and GFRP);
- Flexural reinforcement ratio (ranged from 0.34% to 1.66%);
- GFRP axial stiffness;
- GFRP compression reinforcement concentration around the column;
- Slab thickness (200 mm and 350 mm);
- Square column size (300 x 300 mm and 450 x 450 mm);
- Concrete compressive strength (normal and high-strength concretes);
- FRP shear reinforcement spacing;
- FRP shear reinforcement ratio and index;

- Flexural reinforcement ratio.

This chapter presents the details of test specimens, fabrication, instrumentation, test setup, and test procedure. In addition, this chapter gives the detailed properties of the different materials used in the experimental program, and obtained by testing representative samples of each material.

3.2 Material Properties

3.2.1 FRP and steel bars

Sand-coated GFRP bars (V-ROD) of sizes No. 15, No. 20, and No. 25, designated according to the CSA S807 (2010), were used as flexural reinforcement of the test specimens. The GFRP bars were classified according to their modulus of elasticity (E_f): Grade I (E_f <50 GPa), Grade II (50 GPa $\leq E_f$ < 60 GPa), and Grade III ($E_f \geq$ 60 GPa). The bars were manufactured by combining the pultrusion process with an in-line sand coating to enhance the bond between the bars and the surrounding concrete. Figure 3.1 shows a photo of the GFRP bars from different batches used in this research project. The tensile properties of the GFRP bars were determined by testing five representative bars for each diameter in accordance with ASTM D7205M (2011). All the test samples were prepared by attaching steel tubes at both ends as anchorages using commercially available cement grout known as Bristar 10. Then, the samples were tested in tension using BALDWIN machine up to failure. Figure 3.2 shows a typical tensile test and bars rupture. Table 3.1 summaries the mechanical properties of the GFRP bars as determined from testing. The reference specimens, however, were reinforced with 20M steel bars (Type 44W) with a yield stress of 470 MPa and a modulus of elasticity of 200 GPa (as provided by the manufacturer). Figure 3.3 shows typical stress-strain relationships for the reinforcing bars.

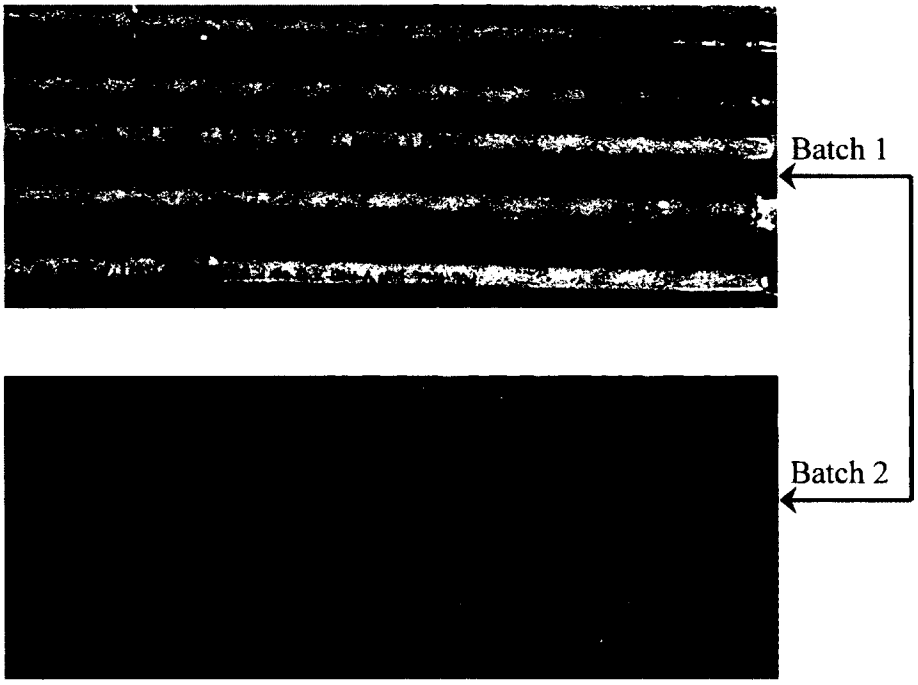

Figure 3.1: Sand-coated GFRP bars

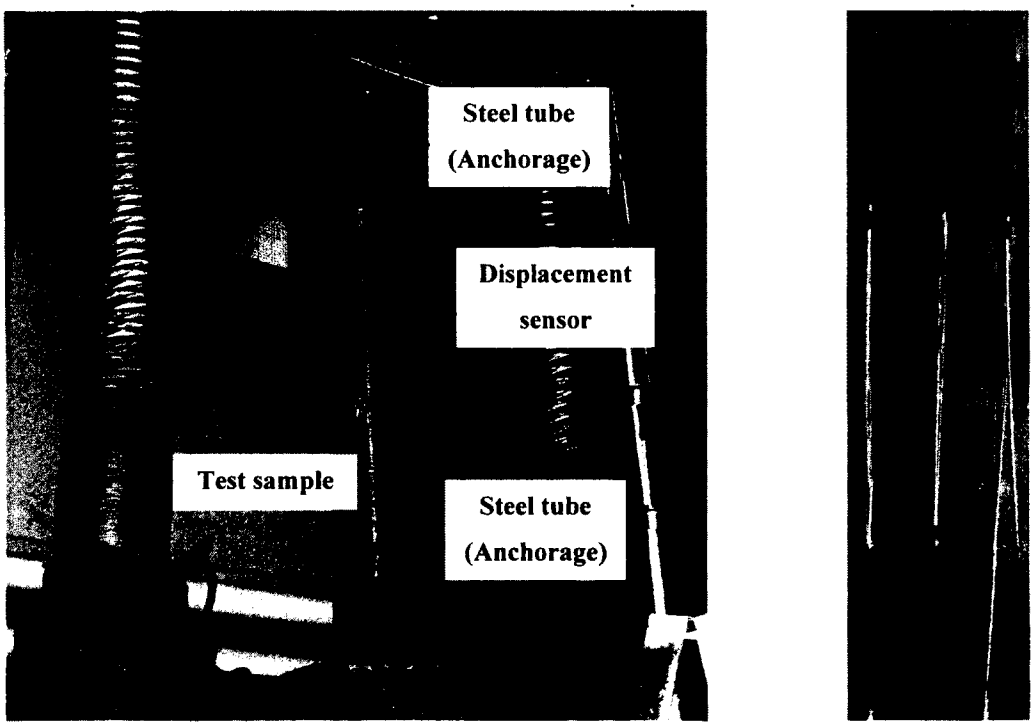

(a) (b)

Figure 3.2: Typical tension testing of GFRP bar: (a) Test setup; (b) GFRP bar rupture

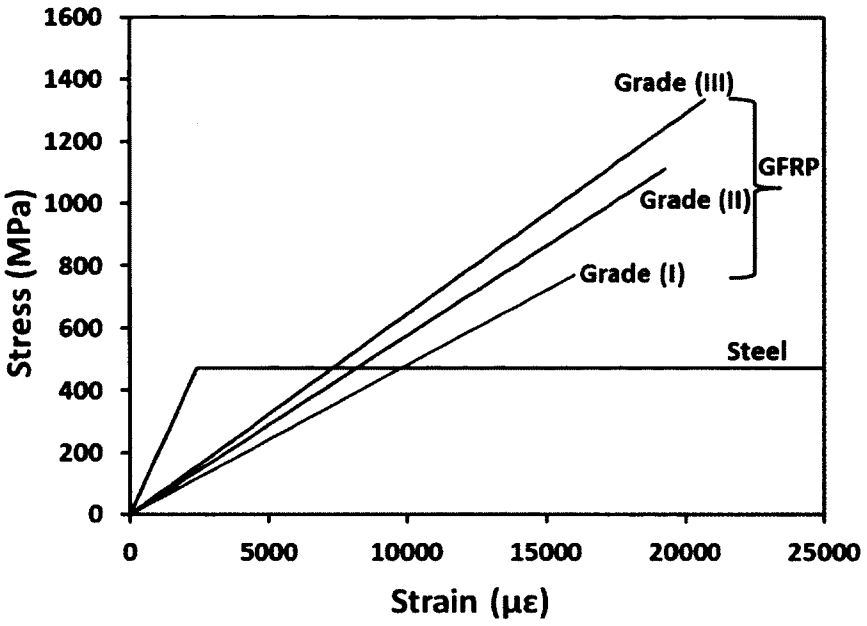

Figure 3.3: Typical stress-strain relationships for the reinforcing bars

Table 3.1: Properties of the reinforcing bars

RFT type	Grade [a]	Bar size [a]	Area [a], mm^2	Elastic tensile modulus, E_f, GPa	Ultimate tensile strength, MPa	Characteristic tensile strength [b], MPa	Ultimate tensile elongation, %
GFRP	I	No. 15	199	48.2±0.4	769±23	700	1.60±0.05
		No. 20	284	48.1±0.7	765±31	672	1.59±0.08
		No. 25	510	46.1±0.7	660±11	626	1.43±0.02
	II	No. 20	284	57.4±0.3	1109±21	1046	1.93±0.04
		No. 25	510	56.7±0.3	1065±22	999	1.88±0.04
	III	No. 20	284	64.9±0.6	1334±85	1079	2.07±0.13
Steel*	44W	No. 20	300	200	f_u=620	f_y=470	ε_y = 0.24

* f_u, f_y, and ε_y Ultimate, yield tensile strengths and yield strain for steel type 44W (as provided by the manufacturer), respectively.

[a] According to CSA S807 (2010).

[b] Characteristic tensile strength = Average value of five specimens – 3× standard deviation (CSA S806, 2012).

3.2.2 FRP stirrups

3.2.2.1. Tension characteristic of the straight portion

Two types of sand-coated FRP stirrups were used, namely CFRP and GFRP. Closed discreet and spiral continuous stirrups diameters No. 10 and No. 13 were used in the test specimens with a thickness of 200 mm and 350 mm, respectively. All the FRP stirrups were

delivered prefabricated and produced by Pultrall Inc. Figure 3.4 shows the configurations of the investigated stirrups. Five straight samples of each FRP type and diameter were directly cut from the FRP stirrups and tested in accordance with ASTM D7205M (2011). The mechanical properties of the GFRP and CFRP stirrups are reported in Table 3.2.

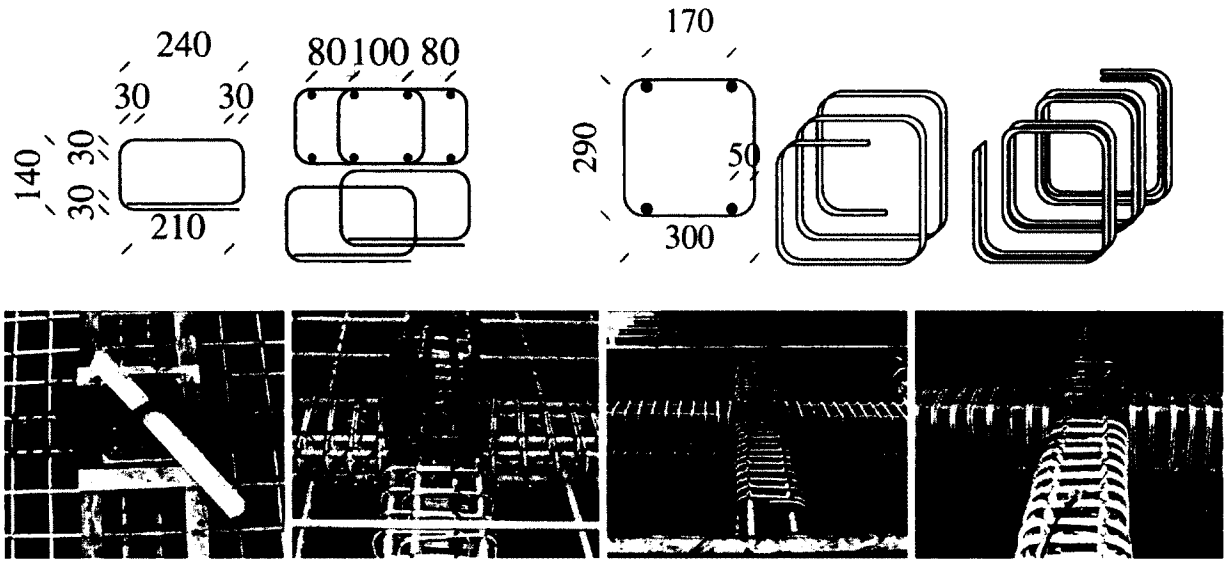

(a) CCS (b) GCS (c) GSS (d) GBSS

Figure 3.4: Details and configurations of investigated stirrups

3.2.2.2. Bend strength of the FRP stirrups

The bend strengths of the GFRP and CFRP stirrups were determined by testing five specimens of each diameter using the B.5 test method in accordance with ACI 440.3R-04 (2004). The B.5 test method evaluates the bend strength of C-shaped FRP stirrups through embedment in two concrete blocks, which are pushed apart until the rupture of the FRP stirrups. Figure 3.5 shows the dimensions of the C-shaped specimens for B.5 test method. The C-shaped FRP specimens were prepared keeping the two sides of the stirrups as continuous end in the concrete block. One side of the stirrups was provided with de-bonding tubes. These de-bonding tubes were secured into the desired position with silicone and duct tape. The dimensions of the concrete blocks were 500 mm × 300 mm × 200 mm. The free length of the stirrup between the two blocks was kept constant at 400 mm. Each block was reinforced transversally with 10 mm-diameter steel stirrups spaced 65 mm to prevent any premature splitting prior to rupture of the FRP stirrups. The test specimens were cast using ready-mixed

normal weight concrete (Type V, MTQ with a target compressive strength of 35 MPa after 28 days). The actual concrete strength obtained from standard cylinders at the day of test was 41 MPa (average of three cylinders). Figure 3.6 shows the preparation of the specimens while Figure 3.7 shows casting of the concrete blocks. After casting, all concrete blocks were cured and stored indoor for 28 days before testing.

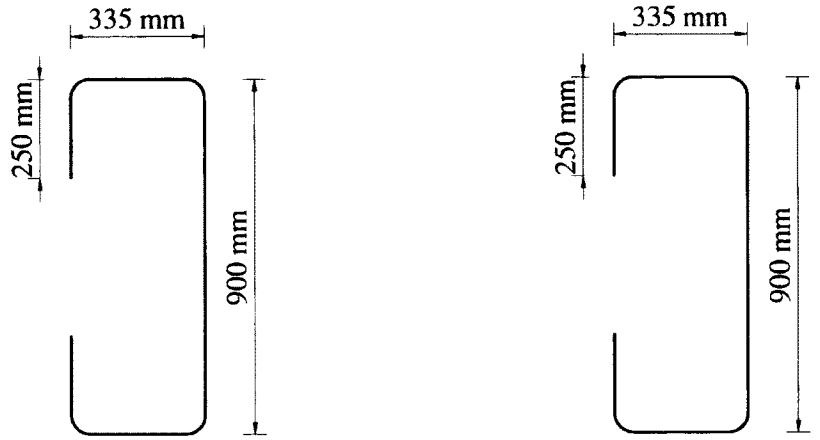

C/GFRP (No.13)
r_b/d_b=4, r_b=50 mm

C/GFRP (No.10)
r_b/d_b=4, r_b=40 mm

Figure 3.5: Dimensions of the C-shaped specimens for B.5 test method

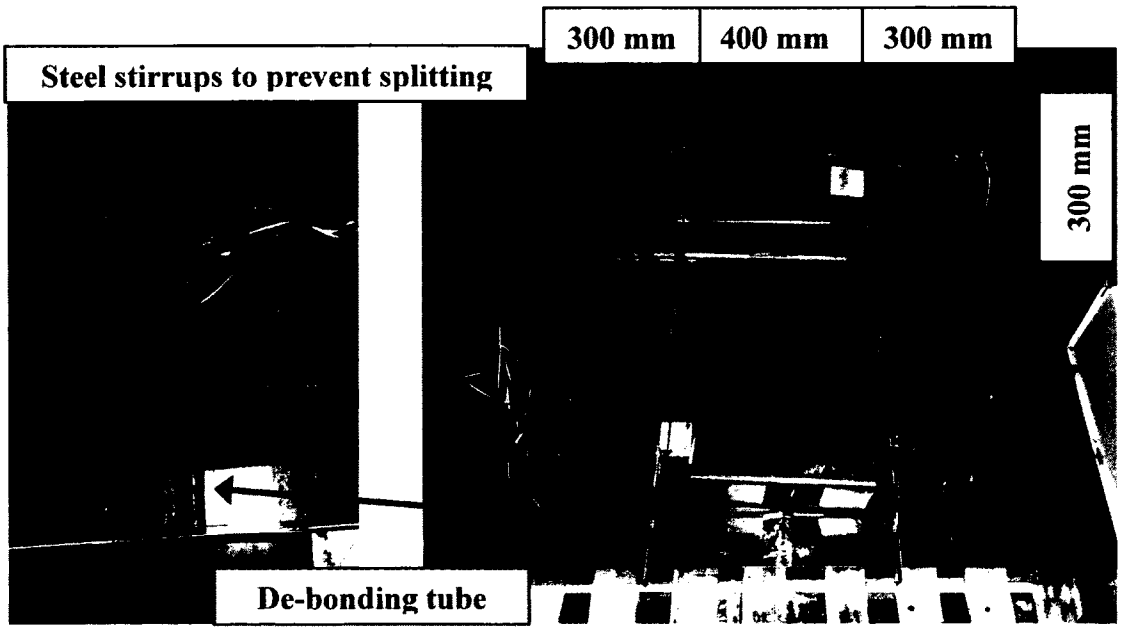

Figure 3.6: Preparation of the test specimens

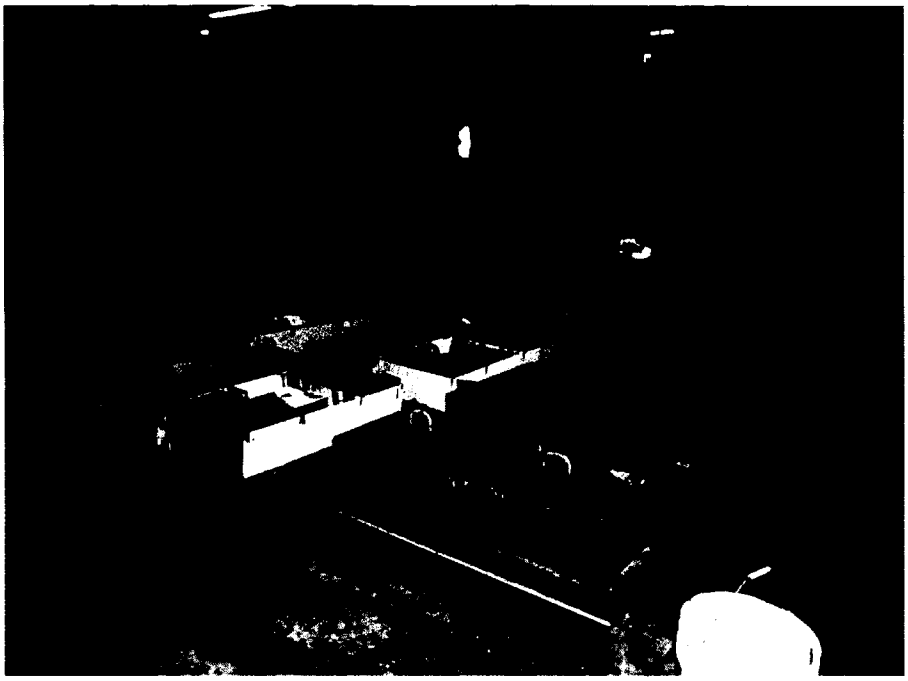

Figure 3.7: Casting of the concrete blocks

The two blocks (for each test) were adjusted on the horizontal testing bed and the inner concrete surface of each block was cleaned. One of two blocks was placed over a moving roller (the moving side) to allow for the horizontal movement and minimize the friction between the block and the testing bed. Following the preparation and placing the moving side block on the roller, two steel plates were placed in front of the inner faces of the concrete blocks to distribute the hydraulic jack loading. The load was applied by pushing the two concrete blocks apart until the failure of the bent specimen. Figure 3.8 shows the setup during testing of FRP stirrup in concrete blocks (B.5). The test specimens failed due to the rupture of FRP bars at the bend, which was followed by slippage of FRP bars out of the concrete blocks as shown in Figure 3.9. The failure load was recorded and the bend strength was calculated from Eq. (3.1). The measured strengths of the GFRP and CFRP stirrups at the bend location were reported in Table 3.3.

$$f_{bend} = \frac{P_u}{2A} \tag{3.1}$$

Where f_{bend} is the bend strength (MPa), P_u is the failure load (N), and A is the FRP bar cross sectional area (mm^2). Some specimens were instrumented using electrical resistance strain

gauges to measure the tensile strain in the start, middle, and end of the bend portion of the FRP stirrup. The test results indicated the strains in the outer side of the middle part of bend portion was the highest strains developed. Further tests, however, are needed to confirm these findings. Figure 3.10 shows the load-strain relationships at different locations of the bend radius.

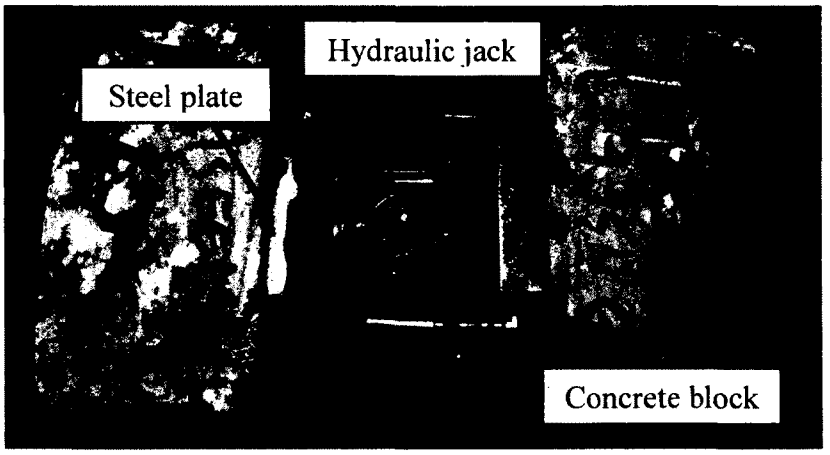

(a)

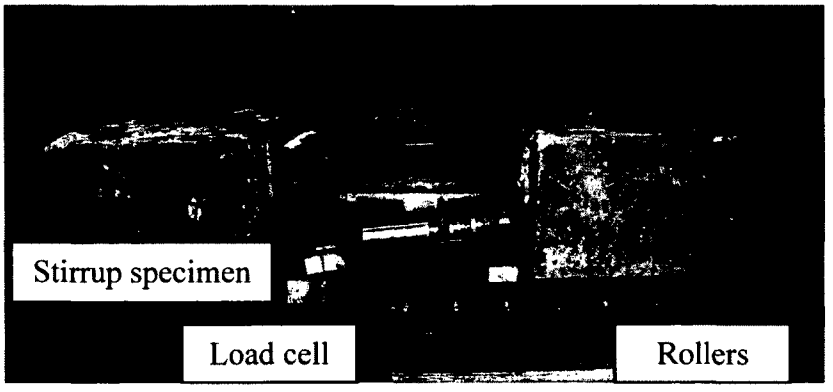

(b)

Figure 3.8: B.5 method test setup

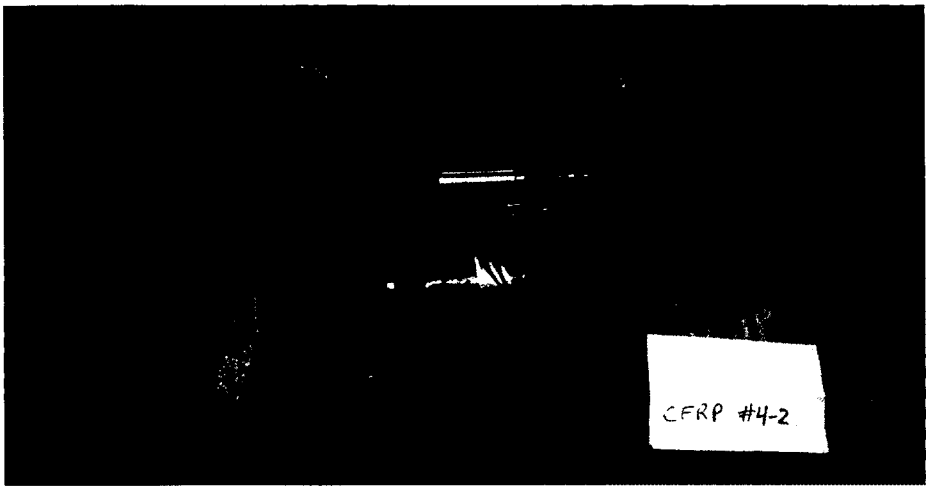

(a)

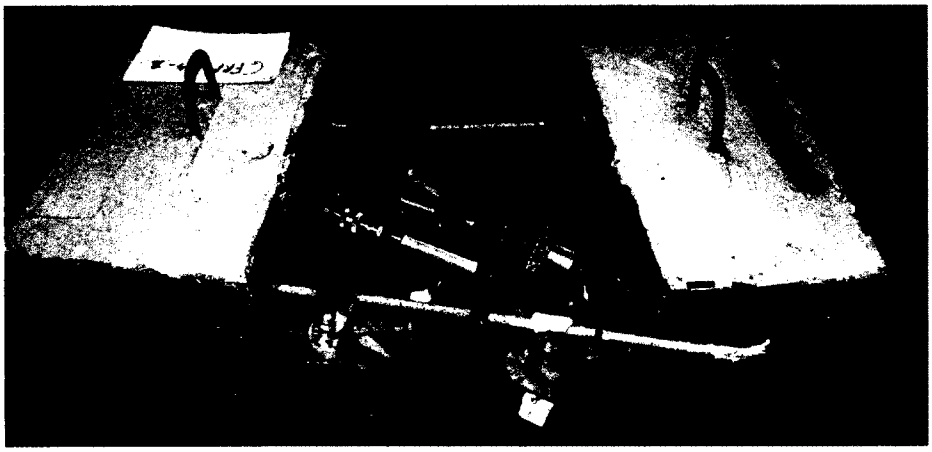

(b)

Figure 3.9: Rupture of the FRP stirrups at the corner in concrete blocks followed by stirrups slippage

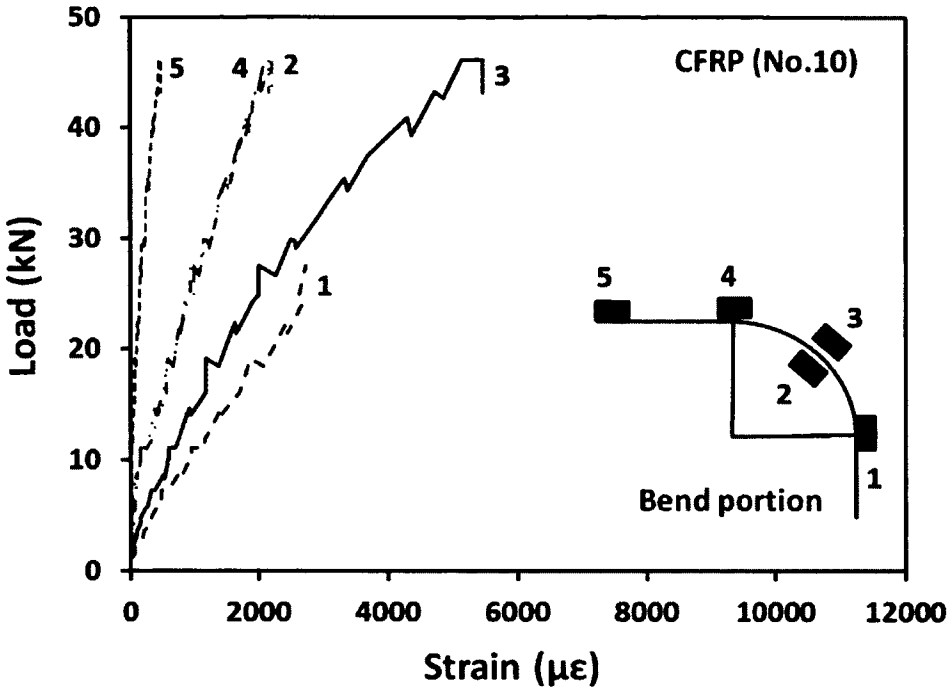

(a)

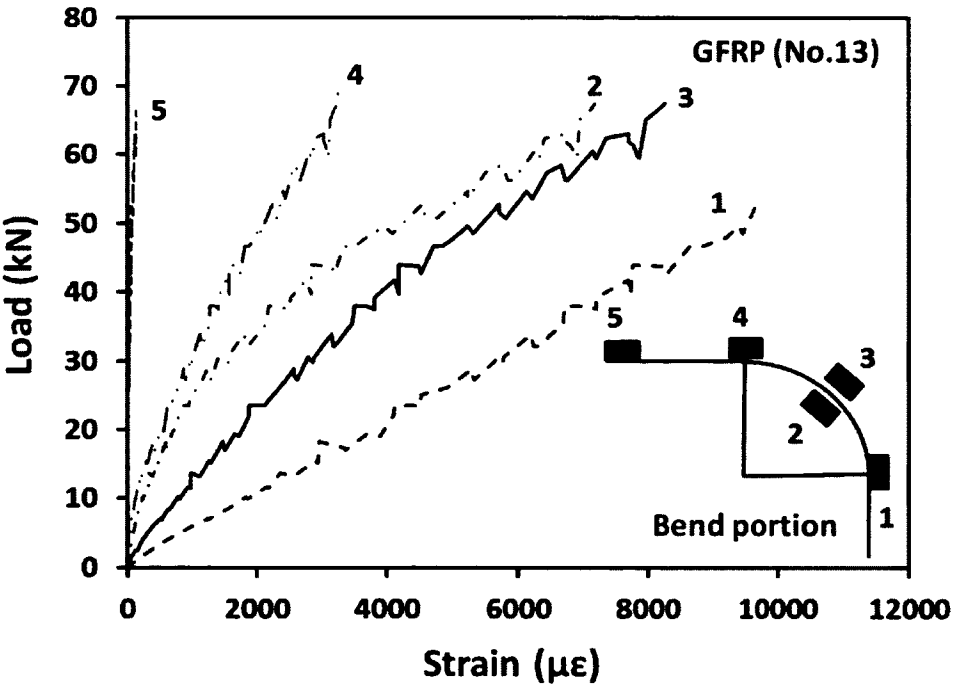

(b)

Figure 3.10: Load-strain relationships at different locations of the bend radius

Table 3.2: Test results of the tension characteristics of GFRP and CFRP No.10 and No.13 (9.5 mm and 12.7 mm)

Specimen	GFRP No.10 (9.5 mm)			CFRP No.10 (9.5 mm)			GFRP No.13 (12.7 mm)			CFRP No.13 (12.7 mm)		
	f_{fv} (MPa)	E_{fv} (GPa)	ε_{fu} (%)	f_{fv} (MPa)	E_{fv} (GPa)	ε_{fu} (%)	f_{fv} (MPa)	E_{fv} (GPa)	ε_{fu} (%)	f_{fv} (MPa)	E_{fv} (GPa)	ε_{fu} (%)
1	971	45	2.13	1582	130	1.22	1004	45	2.25	-	-	-
2	968	44	2.18	-	-	-	978	45	2.18	1544	124	1.24
3	973	45	2.16	-	-	-	1005	45	2.24	1578	123	1.28
4	881	44	1.98	1568	130	1.21	1032	44	2.34	1595	125	1.28
5	946	45	2.11	1536	131	1.18	1002	45	2.25	1531	125	1.22
Average	948	45	2.11	1562	130	1.23	1004	45	2.25	1562	124	1.26
SD	39	0.45	0.08	24	0.61	0.04	19	0.36	0.06	30	0.71	0.03
COV%	4.08	1.00	3.66	1.51	0.47	2.98	1.88	0.80	2.63	1.92	0.57	2.28

Table 3.3: Test results of the bend strength of FRP C-shaped stirrups

Specimen	GFRP No.10 (9.5 mm)		CFRP No.10 (9.5 mm)		GFRP No.13 (12.7 mm)		CFRP No.13 (12.7 mm)	
	P_u (kN)	f_{fvb} (MPa)	P_u (kN)	f_{fvb} (MPa)	P_u (kN)	f_{fvb} (MPa)	P_u (kN)	f_{fvb} (MPa)
1	58	407	100	704	-	-	42	163
2	72	508	105	739	71	275	142	549
3	49	344	120	845	-	-	182	705
4	89	629	115	810	-	-	92	358
5	55	386	110	658	86	332	92	356
Average	65	455	110	751	78	551	110	774
SD	16	115	8	76	10	73	53	377
COV%	25	25	7	10	13	13	49	49
f_{fvb}/f_{fv}	-	0.48	-	0.48	-	0.50	-	0.50

3.2.3 Concrete

The slab-column connections were cast using a ready-mixed, normal-strength concrete (NSC) and high-strength concrete (HSC) with an entrained-air ratio of 5% to 8%. The target compressive strengths of NSC and HSC were 35 and 65 MPa, respectively. The slump of the fresh concrete was measured before casting and was between 80 mm to 100 mm. Six concrete cylinders 150 × 300 mm were cast from each concrete batch and cured under the same conditions as the test slabs. Three cylinders were tested in compression at the day of slab testing and the stress–strain relationships were measured. The last three cylinders were tested in tension by performing the split cylinder test at the day of slab testing. The compression and splitting testing of concrete cylinders are shown in Figure 3.11 and 3.12, respectively. The average concrete compressive strength for the NSC ranged from 29.6 to 48.6 MPa, while that of the HSC was 75.8 MPa. The average tensile strength ranged from 2.3 to 3.5 MPa for the NSC and was 4.4 MPa for the HSC. The measured stress-strain relationships for different batches are shown in Figure 3.13.

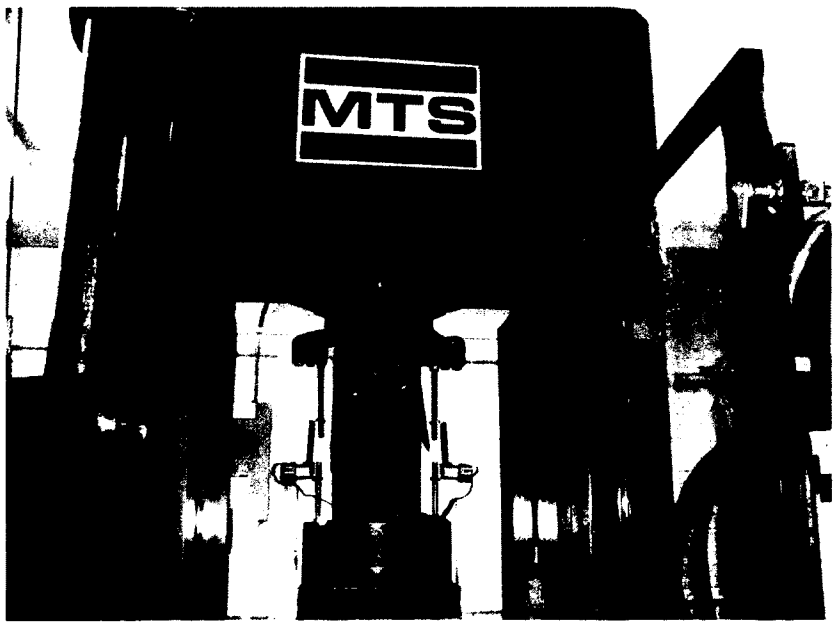

Figure 3.11: Compression test of the standard concrete cylinders

Figure 3.12: Splitting test of the standard concrete cylinders

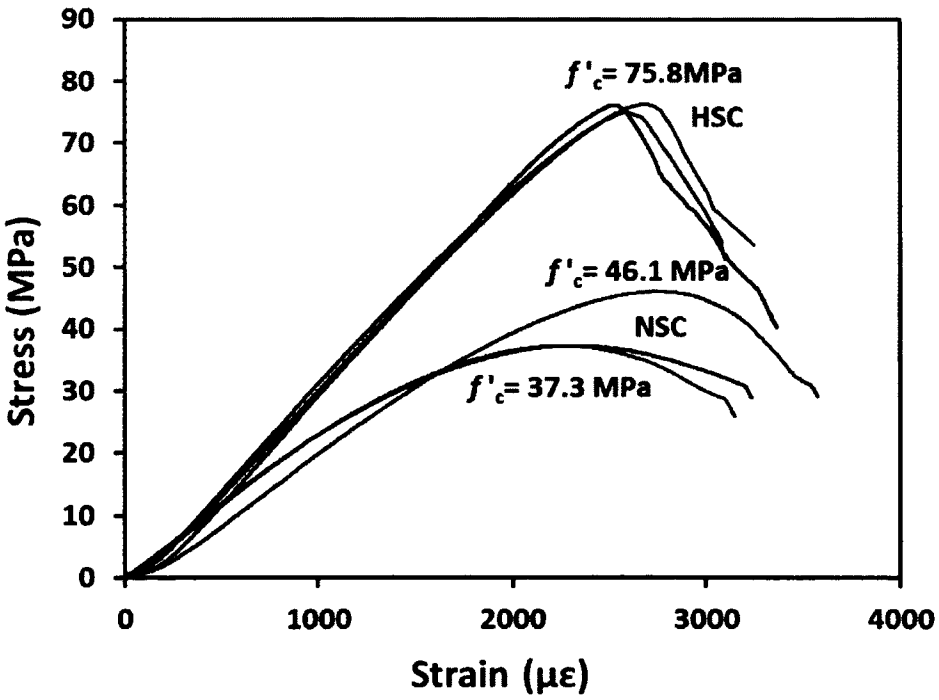

Figure 3.13: Stress-strain relationship for different concrete batches

3.3 Test Specimens' Details

A total of twenty-six full-scale interior slab-column connections were reinforced with GFRP bars and two specimens were reinforced with steel bars for comparisons. All specimens were simply supported on all four edges and tested under a concentrated load acting on the column stub in the middle of each slab from down. The test specimens measured 2500 mm × 2500 mm with thicknesses of either 200 mm or 350 mm, while the square column stub measured 300 mm × 300 mm or 450 mm × 450 mm. The column stub extended 300 mm beyond the top and bottom surfaces of the slabs. The clear concrete cover was between 45 to 50 mm. Figure 3.14 to Figure 3.28 show the geometry and typical reinforcement configuration of the test specimens.

The experimental Phase I consisted of twenty-one specimens without shear reinforcement including the steel-reinforced specimens. The effects of the following parameters were investigated as follows: (i) reinforcement type (GFRP and steel) and ratio (0.34% to 1.66%); (ii) GFRP axial stiffness; (iii) GFRP compression reinforcement concentration around the column; (iv) slab thickness (200 mm and 350 mm); and (v) column dimensions (300 mm × 300 mm and 450 mm × 450 mm); (vi) concrete strength (ranged between 29.6 MPa to 75.8 MPa). The specimens of Phase I were categorized into two groups according to thickness: Group I (1) with a thickness of 200 mm and Group I (2) with a thickness of 350-mm. Table 3.4 presents the test matrix and characteristics of each test specimen. Group I (1) comprised 9 GFRP-RC specimens with a reinforcement ratio ranging from 0.71% to 1.56% and one reference steel-reinforced slab. Group I (2) comprised 10 GFRP-RC specimens with a reinforcement ratio (ρ) ranging from 0.34% to 1.61% and one reference steel-reinforced slab. The reinforcement ratio was selected to cover a wide range of ρ/ρ_b, which ranged from 0.58 to 5.04. All specimens were fabricated using NSC, except two specimens were fabricated with HSC to investigate the effects of concrete type and strength. Three specimens in each series were fabricated with a square column dimension of 450 mm to study the influence of the column dimensions on the strength. While one specimen ($G_{(1.2)}30/20$) in Group I (1) was reinforced with high modulus (Grade-III) GFRP bars; this slab had the same axial reinforcement stiffness (E_fA_f) as $G_{(1.6)}30/20$ reinforced with normal bars (Grade II).

The test specimens of Phase I were labeled with a letter denoting the reinforcement type (G for GFRP and S for steel bars) with a subscript indicating the reinforcement ratio, followed by the column dimension in centimeters (30 cm or 45 cm) and ending with the slab thickness in centimeters (20 cm or 35 cm) while other letters (B & H) denoting the GFRP compression reinforcement and high-strength concrete, respectively, if any. For example, the prototype $G_{(0.7)}30/20$ was reinforced with GFRP bars with a reinforcement ratio of 0.7% in each orthogonal direction, a 30 cm square column, and a slab thickness of 20 cm.

The experimental Phase II comprised seven specimens reinforced in flexure with GFRP bars and in shear with CFRP and GFRP stirrups. Specimens included in Phase I (without shear reinforcement), served as reference specimens to evaluate the stirrups' contribution on punching-shear and deformation capacities. The effects of the following parameters were investigated: (i) FRP stirrups shear reinforcement ratio and index; (ii) FRP stirrups shear reinforcement spacing; (iii) flexural reinforcement ratio. The clear concrete cover was between 45 to 50 mm. Figure 3.4 shows details and configurations of investigated stirrups. The test specimens were provided with GFRP flexural reinforcement ratios (ρ_f) ranged from 0.34% to 1.61%. This range was chosen to evaluate the efficiency of the FRP stirrups in relatively low and high flexural reinforcement ratios.

The test matrix was categorized according to slab thickness into two groups. Group II (1) (200 mm thick) comprised two specimens reinforced in flexure with GFRP bars with a reinforcement ratio (ρ_f) of 1.21%. The two specimens were reinforced with GFRP or CFRP closed discreet stirrups. The GFRP and CFRP stirrups were of size No. 10 and were distributed along the orthogonal directions with a spacing of $d/2$=70 mm. Figure 3.16 and Figure 3.17 show the test specimens' details.

Group II (2) (350 mm thick) comprised five specimens reinforced in flexure with GFRP bars with a reinforcement ratio of either 0.34% or 1.61%. The five specimens were fabricated with GFRP and CFRP spiral stirrups including one specimen ($G_{(1.6)}$350-GBSS(d/4) with GFRP spiral stirrups in bundled configuration (see Figure 3.27). In this test group, the spiral stirrups were chosen because of their fast and easy installation in the construction than the closed discreet ones. Both of the used GRRP and CFRP spiral were of size No. 13 and were distributed along the orthogonal directions of the slabs with spacing ranged from $d/3$ to $d/4$ (100 mm to 70 mm). The shear reinforcement ratio (ρ_{fv}) was calculated by the cross-

sectional area of the FRP stirrups on a concentric line parallel to the perimeter of the column at 0.5*d* from the column face as specified by ACI 318-08 (2008) and CSA 23.4 (2004). Figure 3.15 to Figure 3.28 depict the reinforcement layout prior to casting.

The test specimens of Phase II were labeled with a letter denoting the flexural reinforcement type (G for GFRP bars) with a subscript indicating the reinforcement ratio, followed by the slab thickness in millimeters (350 mm) and ended by the stirrups configurations (shear reinforcement type, shape, and spacing), if any. For example, the specimen $G_{(1.6)}350$-GSS(d/4) was reinforced with GFRP bars with a reinforcement ratio of 1.6% in each direction, a slab thickness of 350 mm, and GFRP shear reinforcement spiral stirrups with spaced at distance *d*/4, where *d* is the effective slab depth (= 280 mm).

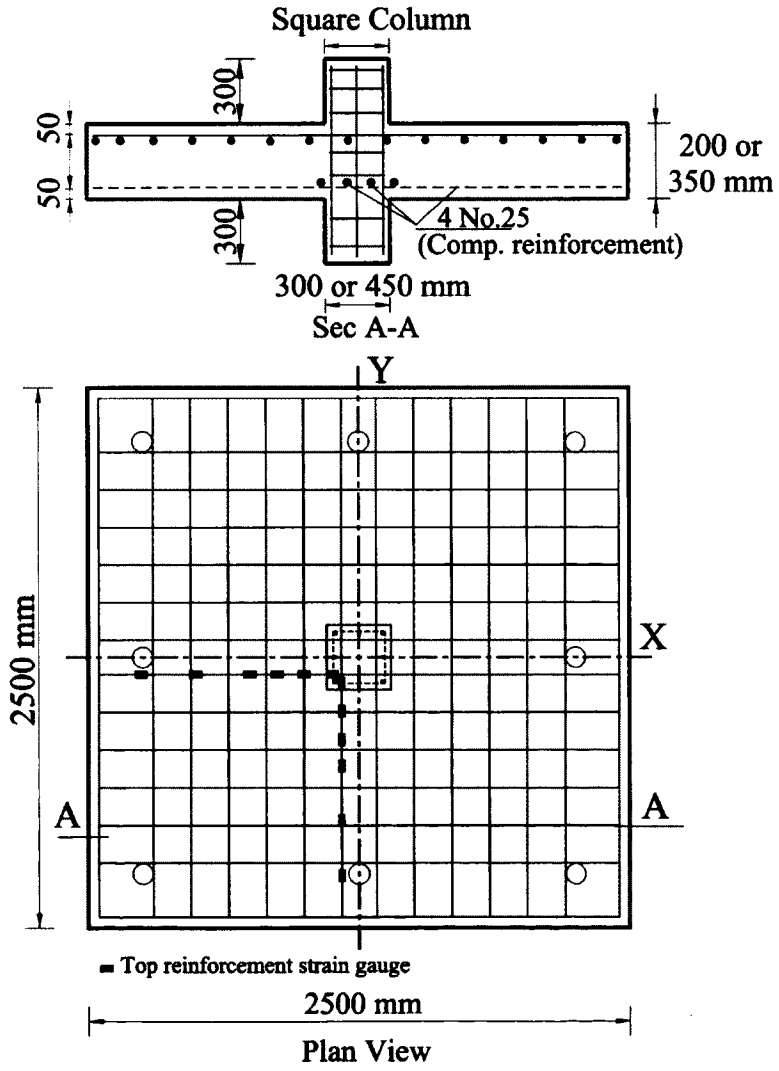

Figure 3.14: Typical details for specimens without shear reinforcement

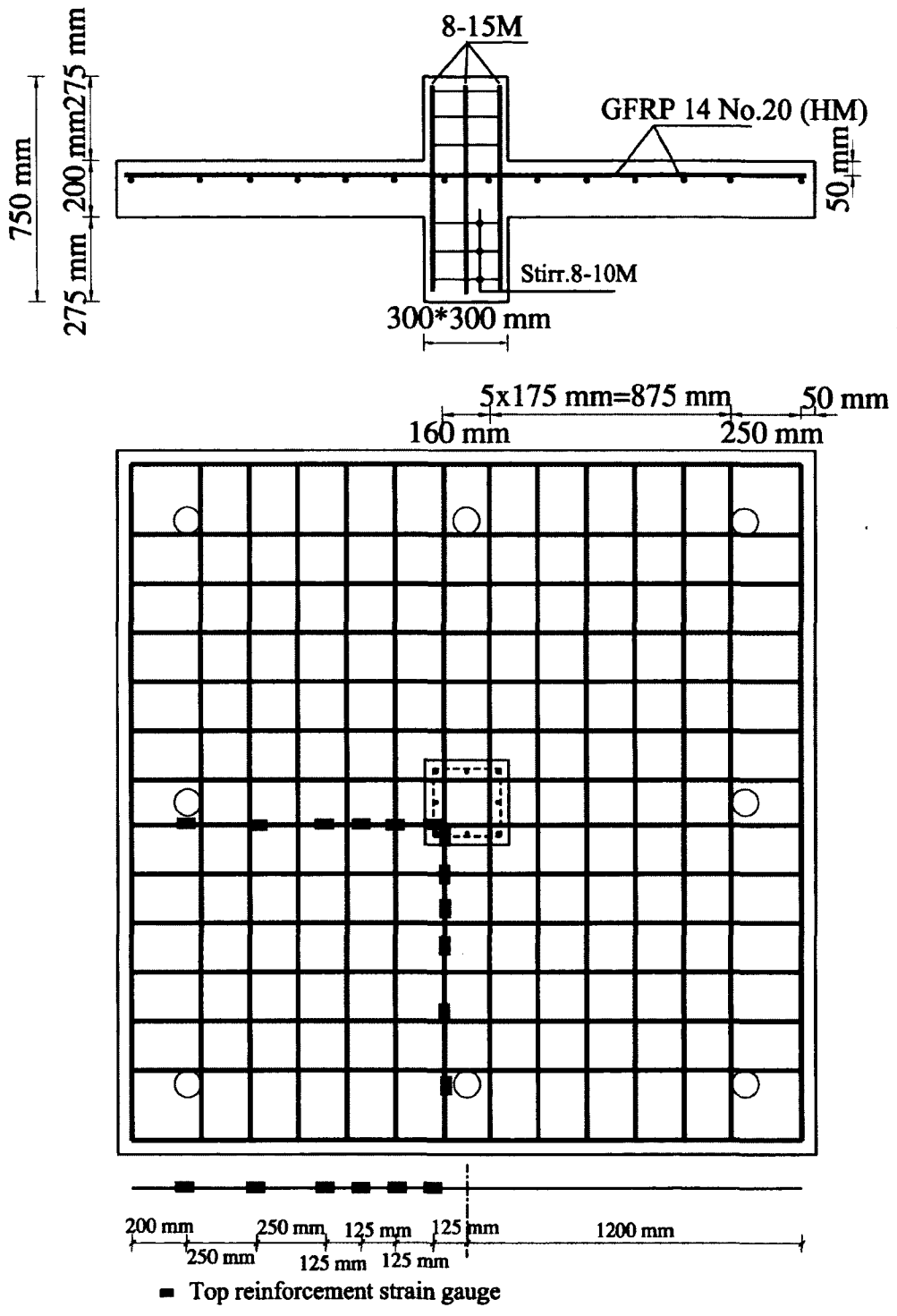

Figure 3.15: Specimen $G_{(1.2)}200$ [reference slab of Group II (1)]

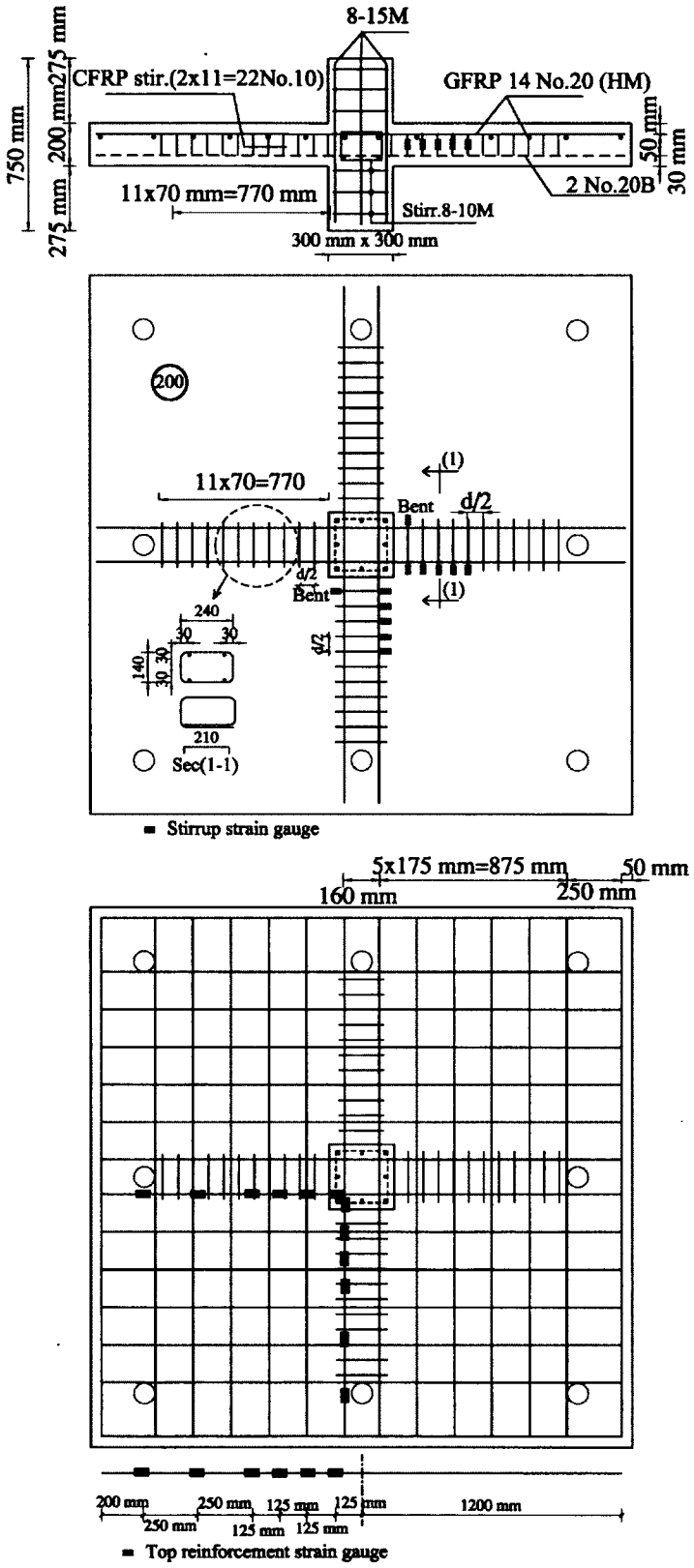

Figure 3.16: Specimen $G_{(1.2)}$200-GGS(d/2) (closed stirrups)

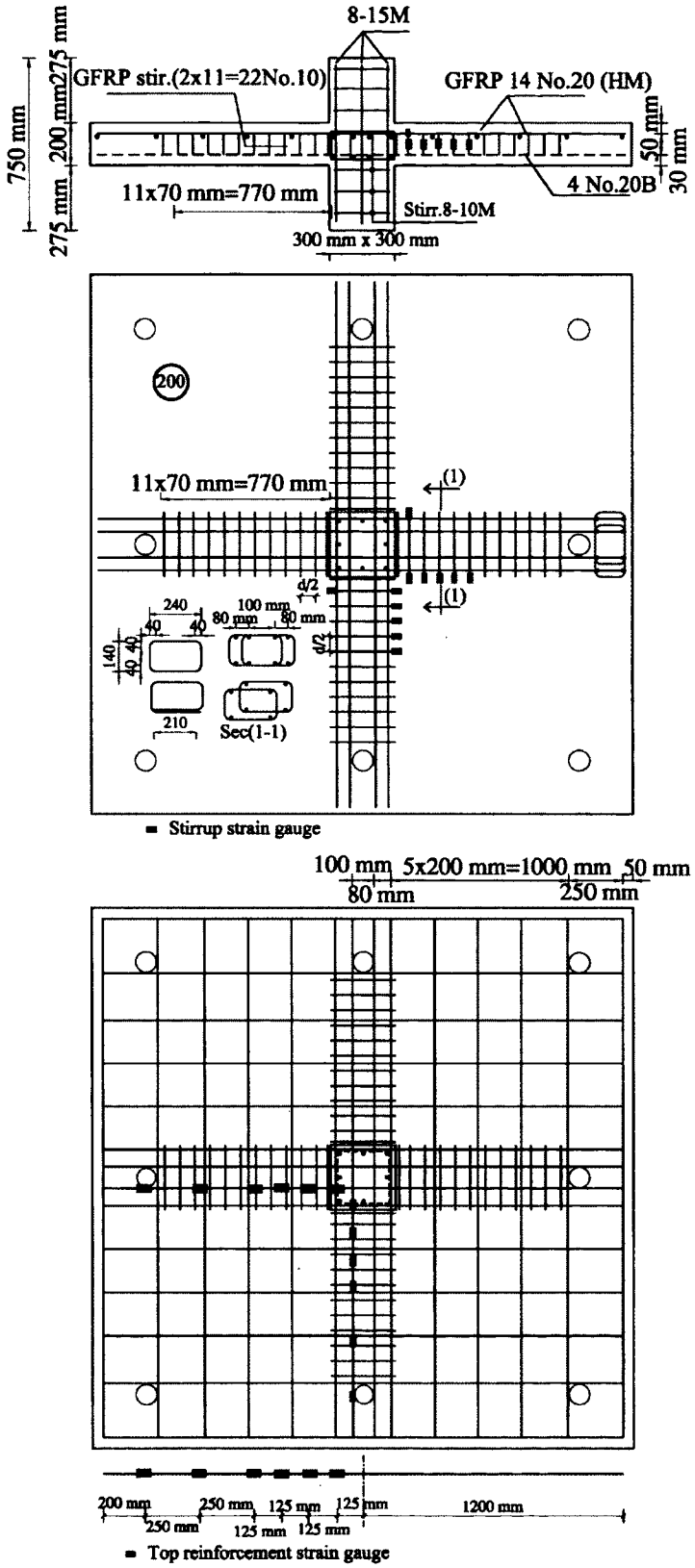

Figure 3.17: Specimen $G_{(1.2)}$200-CCS(d/2) (closed stirrups)

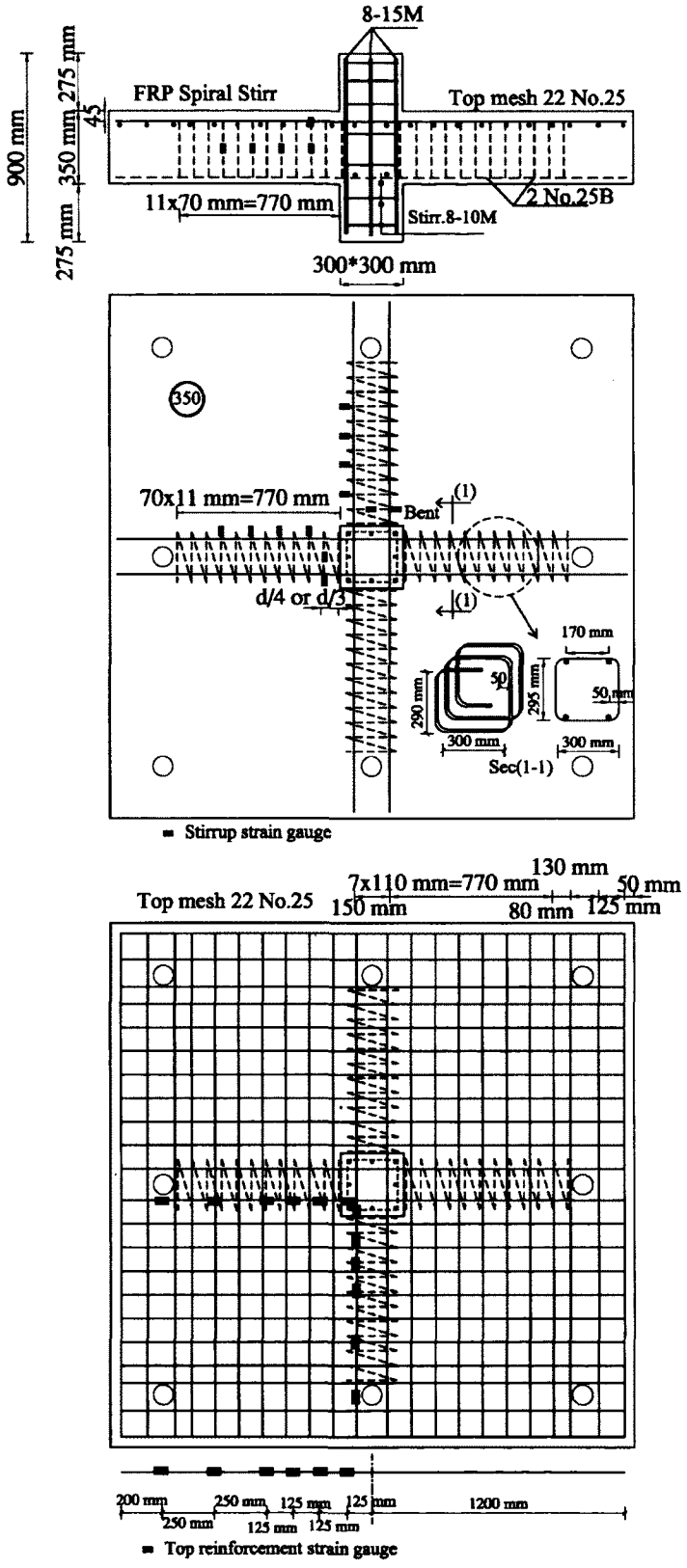

Figure 3.18: Typical details for specimens with spiral stirrups

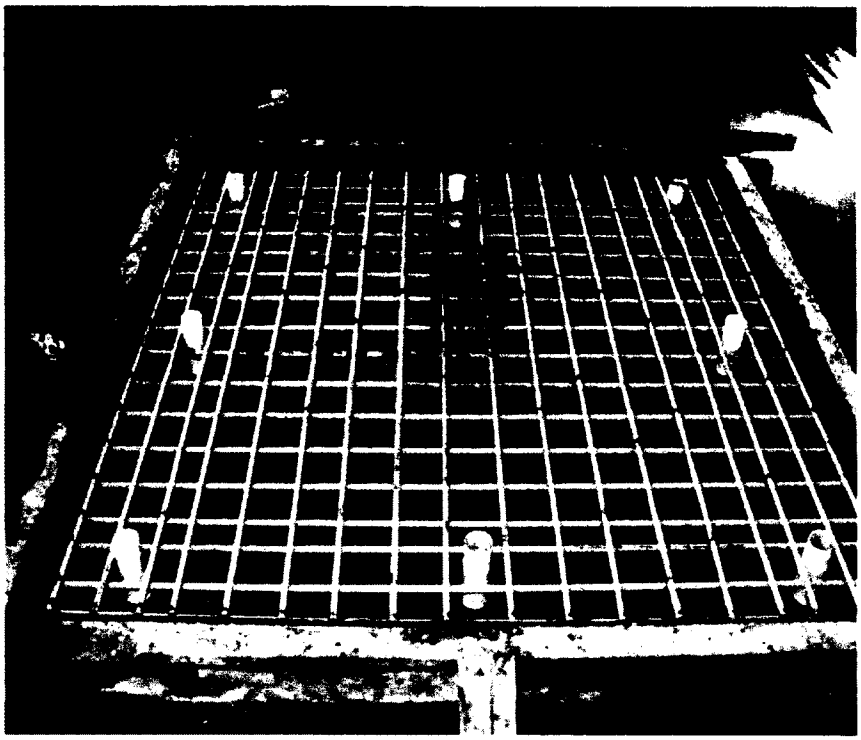

Figure 3.19: Specimen $G_{(1.2)}30/20$ (without bottom reinforcement)

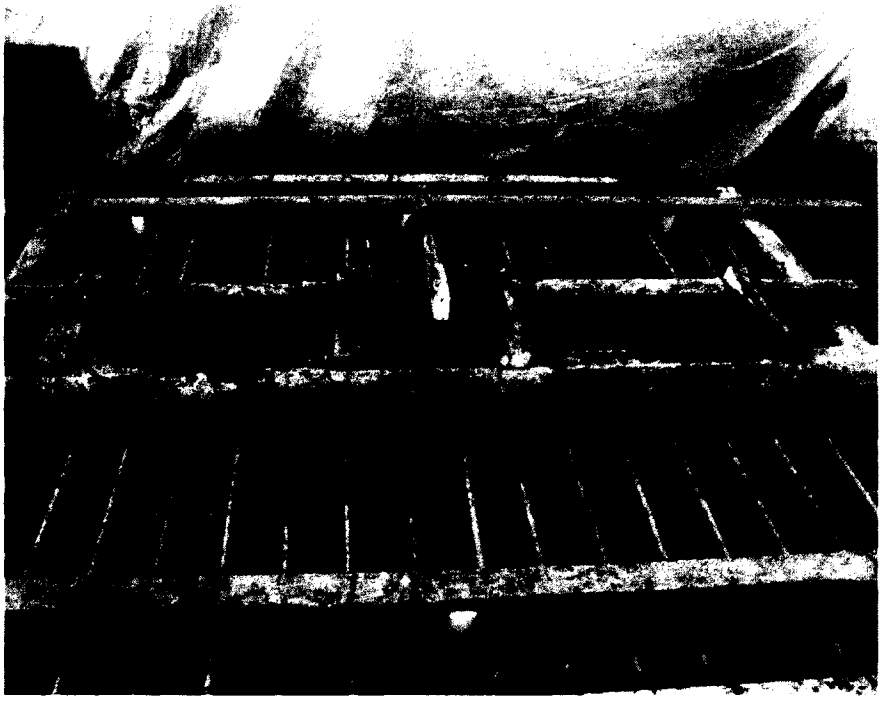

Figure 3.20: Specimen $G_{(1.6)}30/20$-B (with GFRP bottom reinforcement crossing the column cross-section)

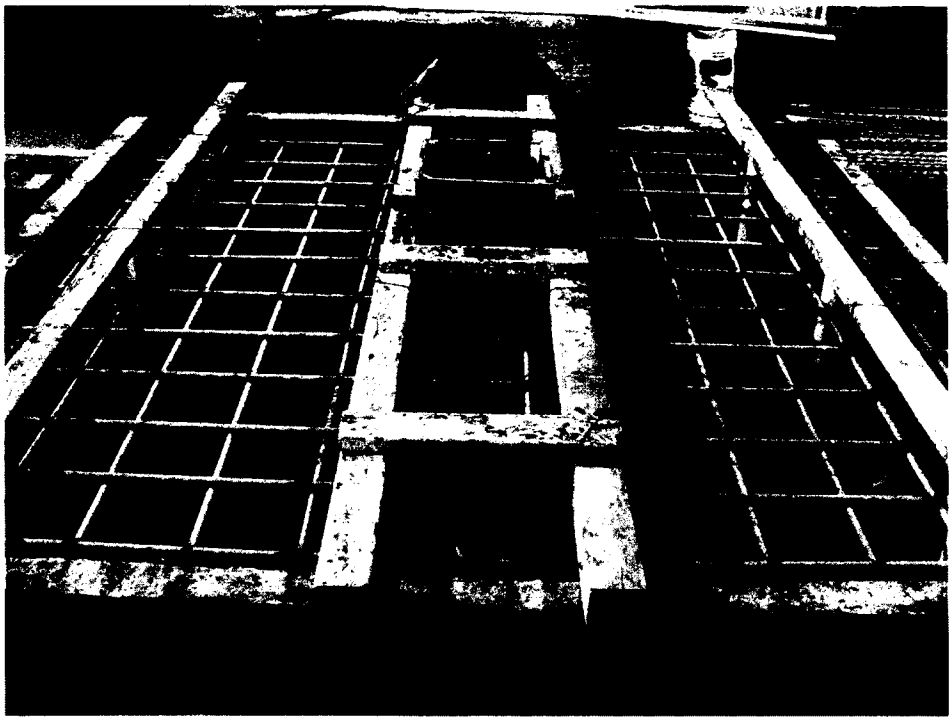

Figure 3.21: Specimen $G_{(0.3)}30/35$ (with low flexural reinforcement ratio)

Figure 3.22: Specimen $G_{(1.6)}30/35$ (with high flexural reinforcement ratio)

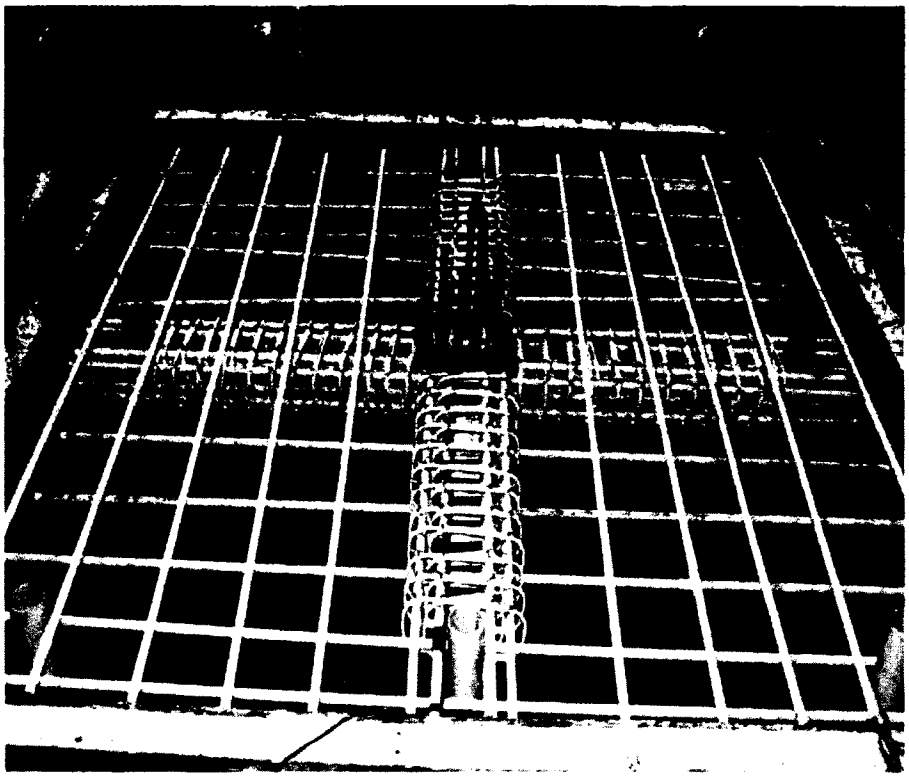

Figure 3.23: Specimen $G_{(1.2)}$200-GCS(d/2)

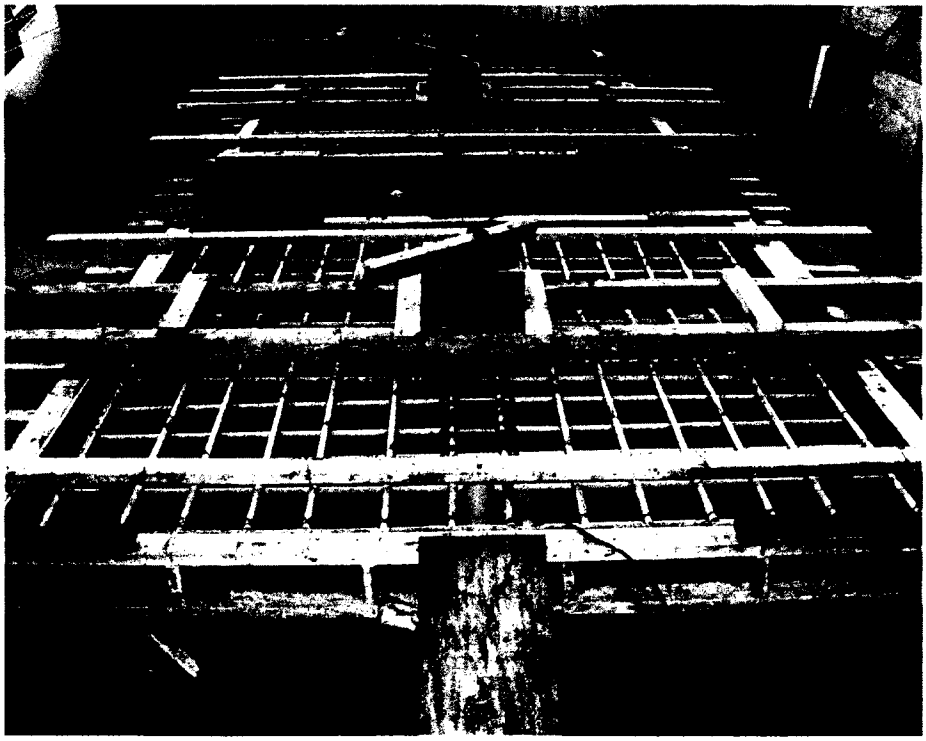

Figure 3.24: Specimen $G_{(1.2)}$200-CCS(d/2)

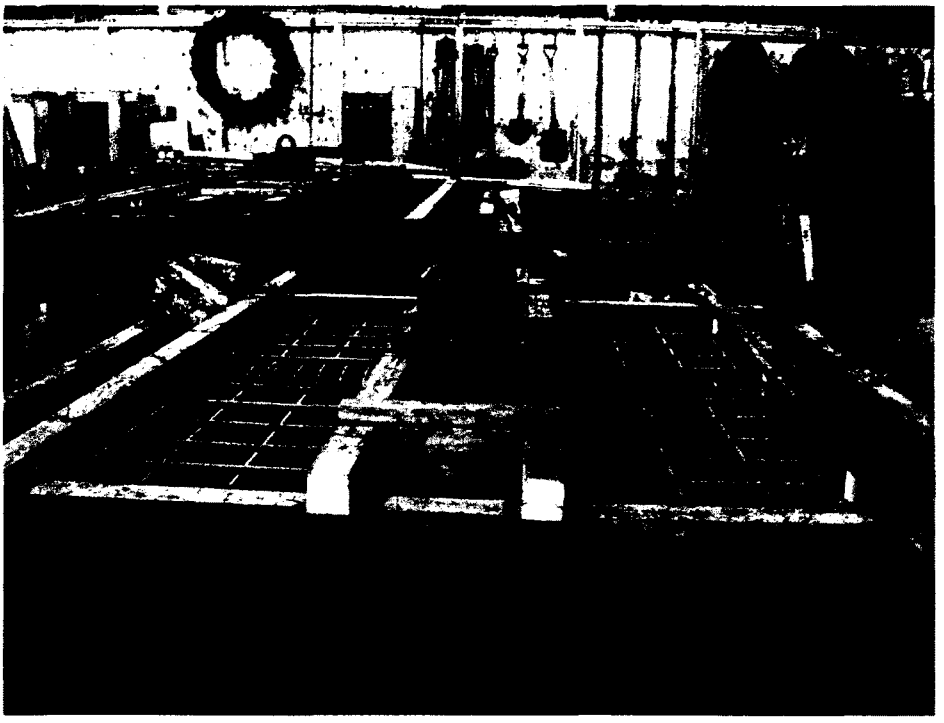

Figure 3.25: Specimen $G_{(0.3)}$350-GSS(d/4)

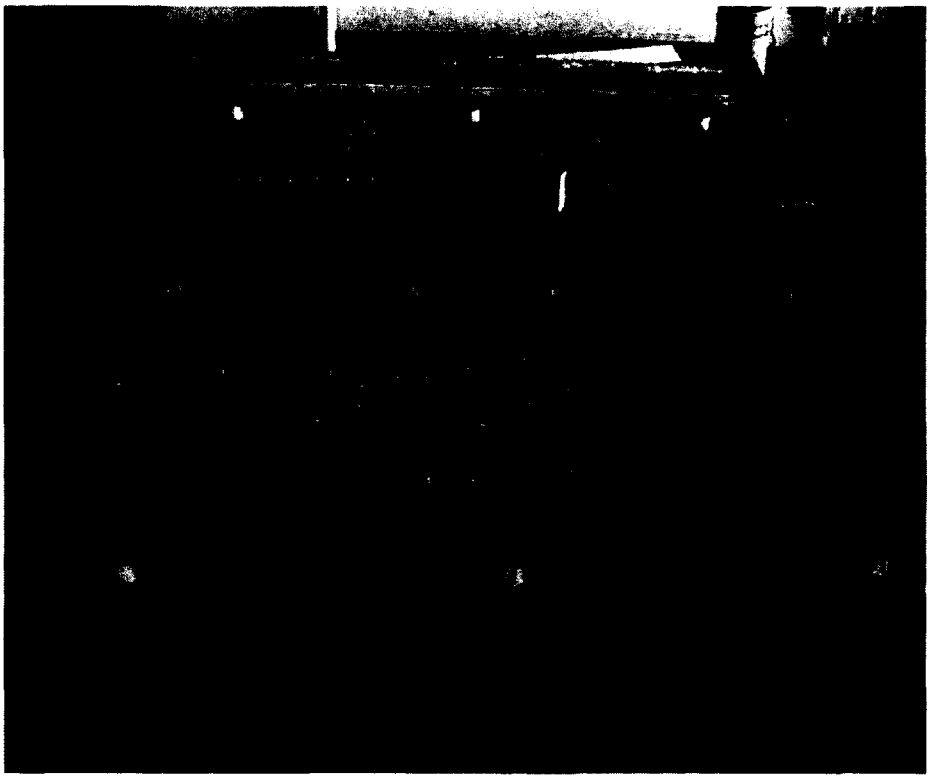

Figure 3.26: Specimen $G_{(1.6)}$350-GSS(d/4)

Figure 3.27: Specimen $G_{(1.6)}350$-GBSS(d/4)

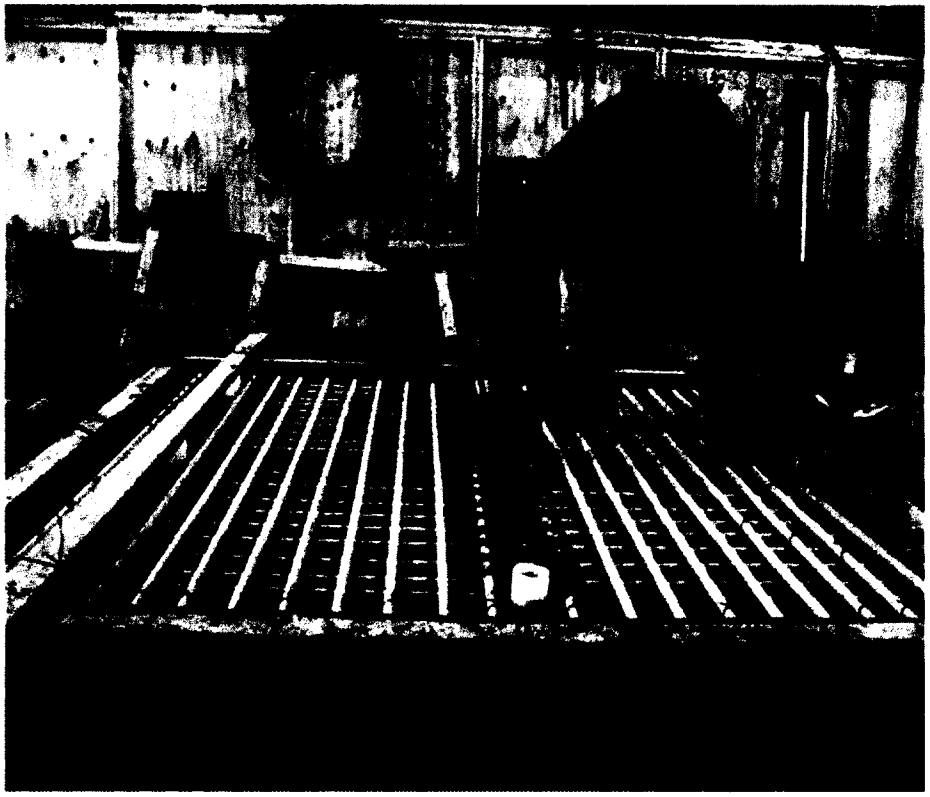

Figure 3.28: Specimen $G_{(1.6)}350$-CSS(d/4)

Table 3.4: Details of test specimens

Phases	Specimen	Slab thick. mm	d_x, mm	d_y, mm	Col. dim. mm	a/d	Tens. & comp. RFT grade	Tension RFT.	Comp. RFT.	ρ, %	ρ_b %	ρ/ρ_b	$\rho(E_r/E_s)$, %	f'_c MPa	f_t MPa	Shear reinforcement ρ_{fv}, %	RFT type	Diam.	Spacing mm
I (1)	$G_{(0.7)}30/20$	200	142	126	300	6.34	I	12 No. 15	-	0.71	0.49	1.45	0.17	34.3	2.5	Without shear reinforcement			
	$G_{(0.7)}30/20$-B		142	126		6.34		12 No. 15	4 No. 25	0.71	0.49	1.45	0.17	38.6	2.8				
	$G_{(1.6)}30/20$*		141	122		6.46		18 No. 20	-	1.56	0.52	3.00	0.38	38.6	2.8				
	$G_{(1.6)}30/20$-B		141	122		6.46		18 No. 20	4 No. 25	1.56	0.52	3.00	0.38	32.4	2.3				
	$G_{(1.6)}30/20$-H		141	122		6.46	II	18 No. 20	-	1.56	0.51	3.06	0.45	75.8	4.4				
	$G_{(1.2)}30/20$		141	122		6.46	III	14 No. 20	-	1.21	0.24	5.04	0.39	37.5	3.5				
	$G_{(0.7)}45/20$*		142	126	450	5.78	I	12 No. 15	-	0.71	0.57	1.25	0.17	45.4	2.9				
	$G_{(1.6)}45/20$		141	122		5.92		18 No. 20	-	1.56	0.47	3.32	0.38	32.4	2.3				
	$G_{(1.6)}45/20$-B		141	122		5.92		18 No. 20	4 No. 25	1.56	0.53	2.94	0.38	38.6	2.3				
	$S_{(1.7)}30/20$*		141	122	300	6.46	Steel	18-20M	-	1.66	4.92	0.34	1.66	45.4	2.8				
I (2)	$G_{(0.3)}30/35$	350	292	276	300	2.99	I	12 No. 15	-	0.34	0.49	0.69	0.08	34.3	2.5				
	$G_{(0.3)}30/35$-B		292	276		2.99		12 No. 15	4 No. 25	0.34	0.53	0.64	0.08	38.6	2.3				
	$G_{(0.7)}30/35$*		291	272		3.02		18 No. 20	-	0.73	0.53	1.38	0.18	39.4	2.3				
	$G_{(0.7)}30/35$-B-1		291	272		3.02		18 No. 20	4 No. 25	0.73	0.59	1.24	0.18	29.6	2.7				
	$G_{(0.7)}30/35$-B-2		291	272		3.02		18 No. 20	4 No. 25	0.73	0.44	1.66	0.18	46.7	2.7				
	$G_{(1.6)}30/35$		287	262		3.09	II	22 No. 25		1.61	0.33	4.88	0.46	38.2	3.3				
	$G_{(1.6)}30/35$-H		287	262		3.09		22 No. 25		1.61	0.54	2.98	0.46	75.8	4.4				
	$G_{(0.3)}45/35$*		292	276	450	2.73	I	12 No. 15		0.34	0.59	0.58	0.08	48.6	2.6				
	$G_{(0.3)}45/35$-B		292	276		2.72		12 No. 15	4 No. 25	0.34	0.46	0.74	0.08	32.4	2.3				
	$G_{(0.7)}45/35$		291	272		2.75		18 No. 20		0.73	0.44	1.66	0.18	29.6	2.7				
	$S_{(0.8)}30/35$		291	272	300	3.02	Steel	18-20M	-	0.77	4.18	0.18	0.77	38.6	2.8				
II (1)	$G_{(1.2)}$ 200-GCS(d/2)	200	141	122		6.46	III	14 No. 20	4 No. 20	1.21	0.24	5.04	0.39	37.5	3.5	0.94	GFRP	No.10	70
	$G_{(1.2)}$ 200-CCS(d/2)		141	122		6.46		14 No. 20	2 No. 20	1.21	0.24	5.04	0.39	37.5	3.5	0.47	CFRP	No.10	70
II (2)	$G_{(0.3)}$350-GSS(d/4)	350	292	276	300	2.99	I	12 No. 15	2 No. 25	0.34	0.43	0.79	0.08	29.5	2.3	0.63	GFRP	No.13	70
	$G_{(1.6)}$ 350-GSS(d/4)		287	262		3.09	II	22 No. 25	2 No. 25	1.61	0.34	4.74	0.46	40.2	3.3	0.64	GFRP	No.13	70
	$G_{(1.6)}$ 350-GBSS(d/4)		287	262		3.09		22 No. 25	2 No. 25	1.61	0.32	5.03	0.46	37.5	3.5	1.27	GFRP	No.13	70
	$G_{(1.6)}$ 350-CSS(d/4)		287	262		3.09		22 No. 25	2 No. 25	1.61	0.33	4.88	0.46	38.2	3.3	0.64	CFRP	No.13	70
	$G_{(1.6)}$ 350-CSS(d/3)		287	262		3.09		22 No. 25	2 No. 25	1.61	0.34	4.74	0.46	40.2	3.3	0.45	CFRP	No.13	100

* Tests by Dulude (2011).

3.4 Fabrication of Test Specimens

All specimens were cast in a wood formwork designed to cast four specimens each time. The bottom column stub was fabricated in the wood formwork 300 mm beyond the slab. The orientation of the specimens during production was the same as during testing. Before assembling the reinforcing cage, the formwork was lubricated to provide ease in formwork removal. Eight 10 mm-diameter holes were cast close to the slab edges to enable anchorage during testing by fixing PVC pipe at those locations. The steel cage of the column was installed first thereafter the tension reinforcement was placed on chairs and tied together (the compression reinforcement was placed and tied before the tension reinforcement, if any) and finally a vertical steel hook was placed centrally inside the column to carry the slabs after removing from the formwork. While the test specimens with shear reinforcement, four GFRP reinforcement bars passing through the column cross-section (top and bottom) and FRP shear reinforcement were assembled together first in each direction separately. Then the reinforcement cage was assembled together inside the slab. After that, the steel cage of the column was installed followed by the placing of tension reinforcement bars in both directions and tied together. Figure 3.29 show the shutting and fabrication of the test specimens.

The concrete was cast in the slabs and was internally vibrated and when casting was completed, the surface of the concrete slab was adjusted. The bottom and top column stub were cast with the slab on the same day. Figure 3.30 shows the concrete casting of the test specimens. Test cylinders were cast simultaneously with the slabs. Twenty-four hours after casting, the cylinders and the external sides of the formworks were stripped and then the slabs and the concrete cylinders were covered with wet burlap. After one week, the specimens were moved out from the formwork, and placed outdoor until the day of testing. Before testing, each slab was coated with whitewash to facilitate the observation of cracking during testing. The slabs were tested after at least 28 days from the date of casting. The average compressive concrete strength at the day of slab testing was determined based on testing three standard cylinders as given in Table 3.4 for each specimen.

(a) Wood formwork preparations

(b) Completed reinforcing cage and formwork

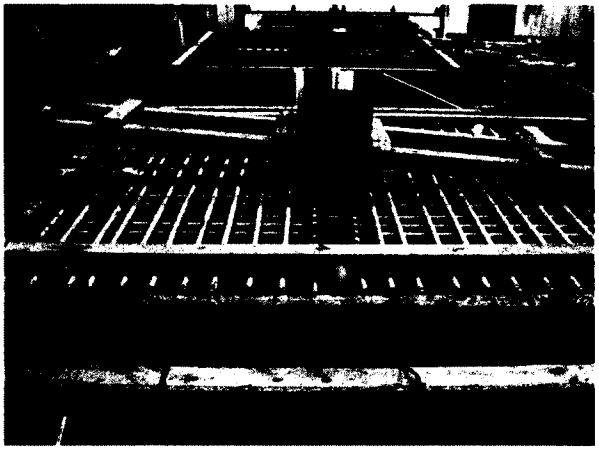

(c) Assembling the top column wood formwork

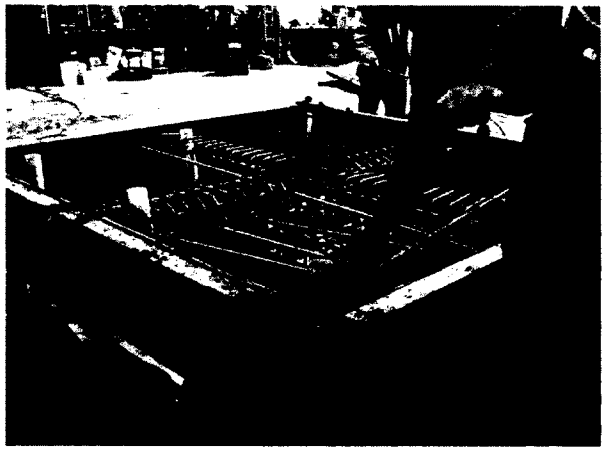

(d) Installation of stirrups and top bars

Figure 3.29: Shuttering and fabrication of the test specimens

(a) Slump test of the fresh concrete before casting

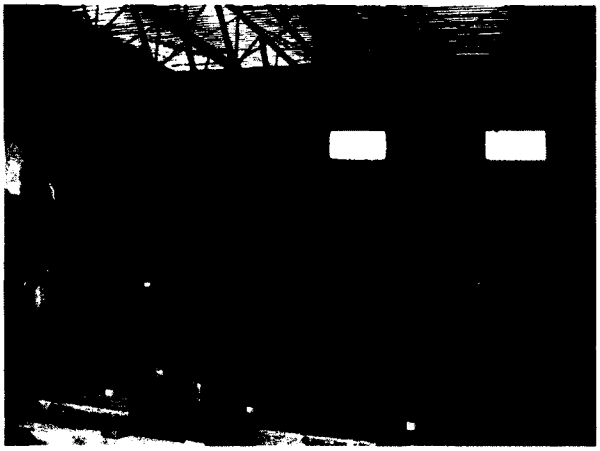

(b) Concrete casting

(c) Concrete cylinders

(d) Adjusting the concrete surface

(e) Concrete slabs just after casting

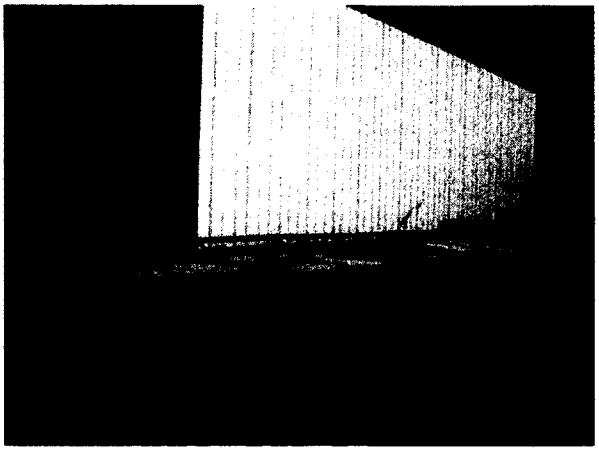

(f) Outdoor storage of the test specimens

Figure 3.30: Concrete casting of the test specimens

3.5 Instrumentations

Systematic measurements (such as the load, the vertical deflections, strains in flexural reinforcement and concrete, strains in the shear reinforcement, and crack widths) allow for an understanding of the behaviour of the tested specimens. Instrumentation of the slabs included Linear Variable Displacement Transducers (LVDT) for deflection and crack widths measurements, and electrical resistance strain gauges for strain measurements. Detailed descriptions of the electrical resistance gauges and LVDTs instrumentations are shown in Figure 3.14 to Figure 3.18 and Figure 3.31 to Figure 3.35, respectively.

To measure the reinforcement and concrete strains, electrical resistance gauges produced by Kyowa Electronic Instruments Co., Ltd., Tokyo, Japan of resistance of 120 ohms were attached to the reinforcing (bars and stirrups), and concrete surface. Each specimen was provided with 2-instrumented bars in the orthogonal directions in the top reinforcing mat (tension side) with 6 electrical-resistance strain gauges (10-mm long with gauge factor 2.08) attached to each bar as shown in Figure 3.36. While, 6 electrical strain gauges (6-mm long with gauge factor 2.07) in each orthogonal direction were glued in the straight, bend locations top and bottom of the stirrups as shown in Figure 3.37 and Figure 3.38. In addition, the slab was placed in a vertical position to enable gluing 8 concrete electrical strain gauges (60-mm long with gauge factor 2.08) labeled C1 to C8 in the slab's bottom surface (compression side) before testing (see Figure 3.39). Moreover, the 8 steel tie rods supporting the test specimen were instrumented with electrical strain gauges to verify the loading symmetry during the test.

The deflection of the test specimens was captured at the different locations with 11 linear variable differential transformers (LVDTs) whereas the crack width was measured using three high-accuracy LVDTs (± 0.001 mm). The crack appearance was monitored during the test by visual inspection until the first three cracks (two flexural orthogonal and one tangential cracks) appeared. Thereafter, their initial widths were measured using a hand-held microscope with a magnifying power of 50X. Then, the three LVDTs were installed at the locations of the first three cracks. The strain gauges and LVDTs were connected to a data-acquisition system to record the readings during the test. Figure 3.32 shows the different locations of LVDTs measuring the crack width. During the test, the propagation of cracks was marked and the corresponding loads were recorded.

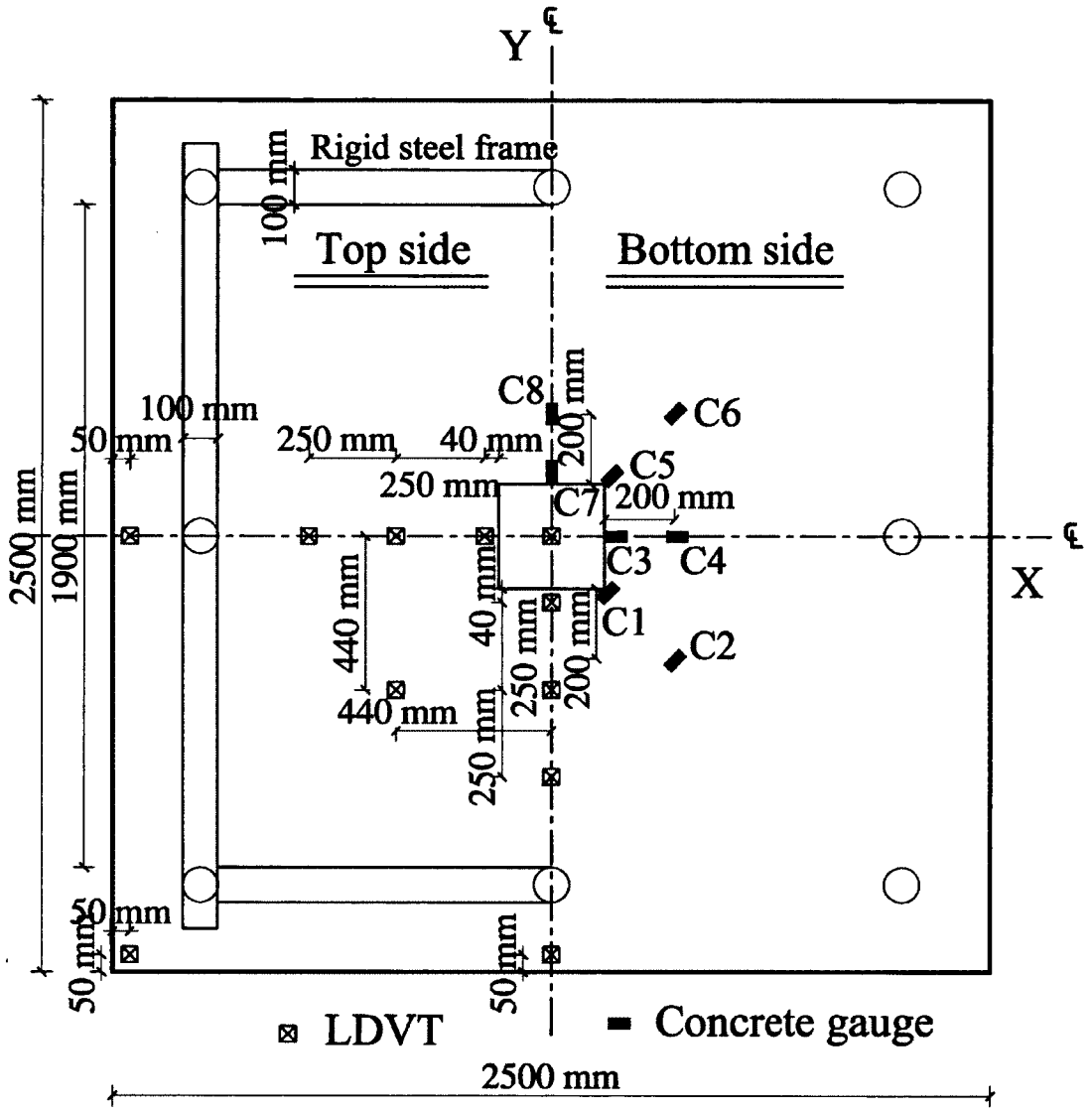

Figure 3.31: LVDTs and concrete gauges placing in the top and bottom sides

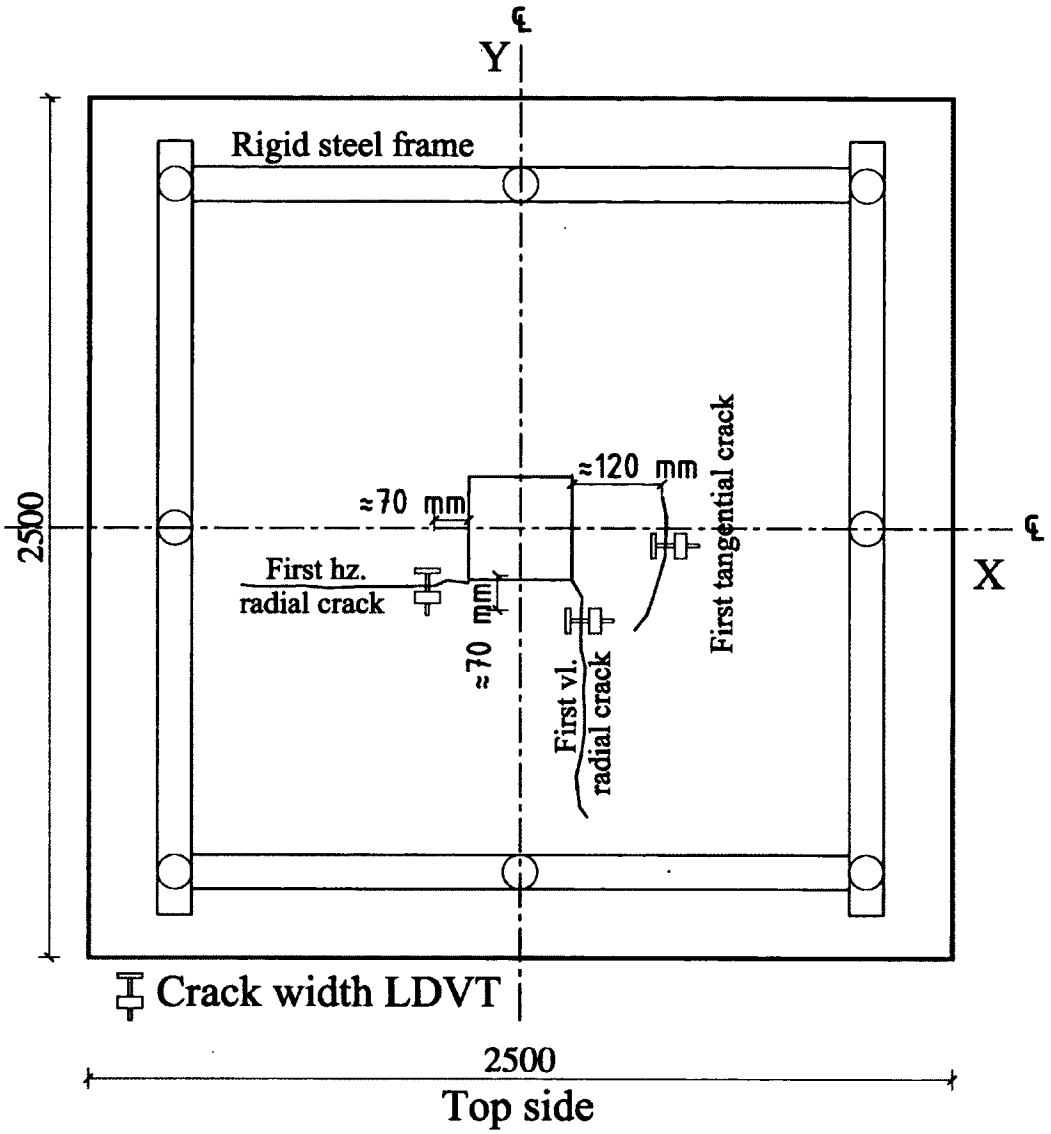

Figure 3.32: Crack width LVDTs placing

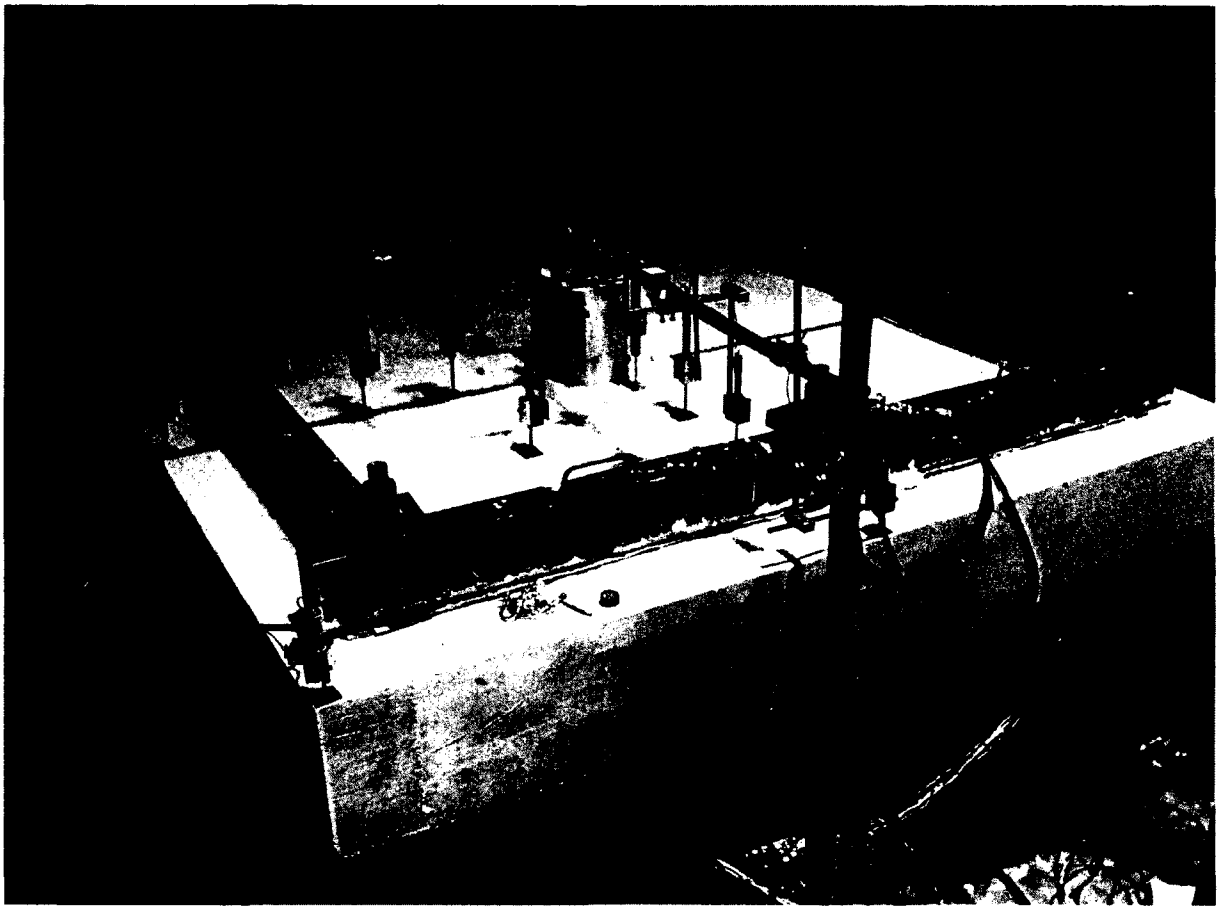

Figure 3.33: A photograph for the deflection measurement using LVDTs

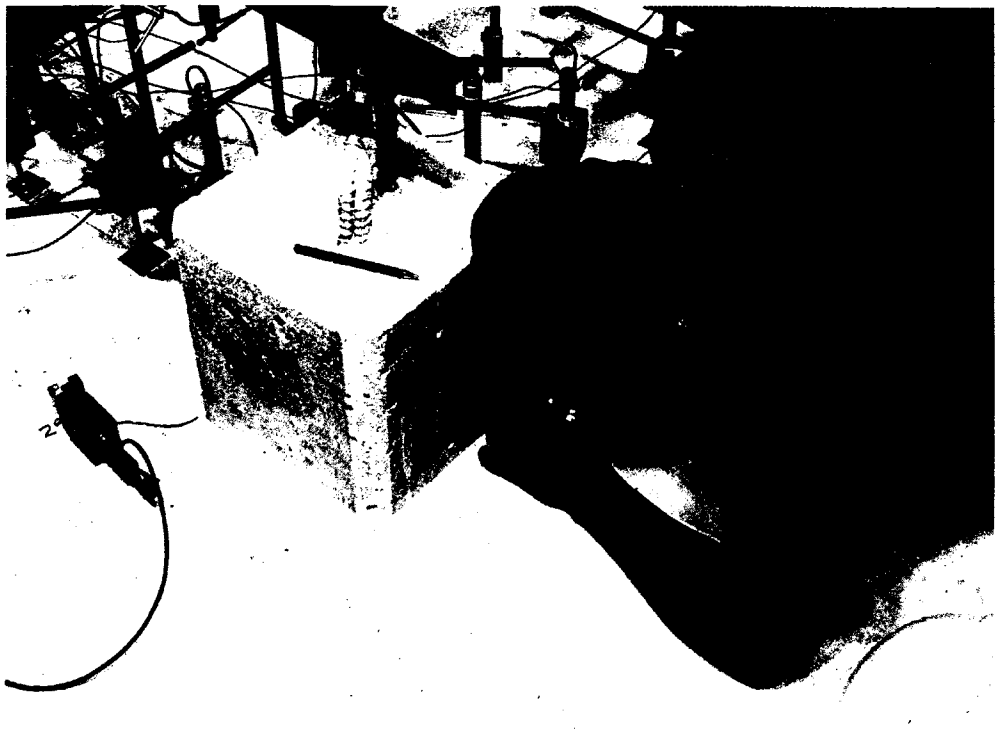

Figure 3.34: Measuring the initial flexural crack width using the hand-held microscope

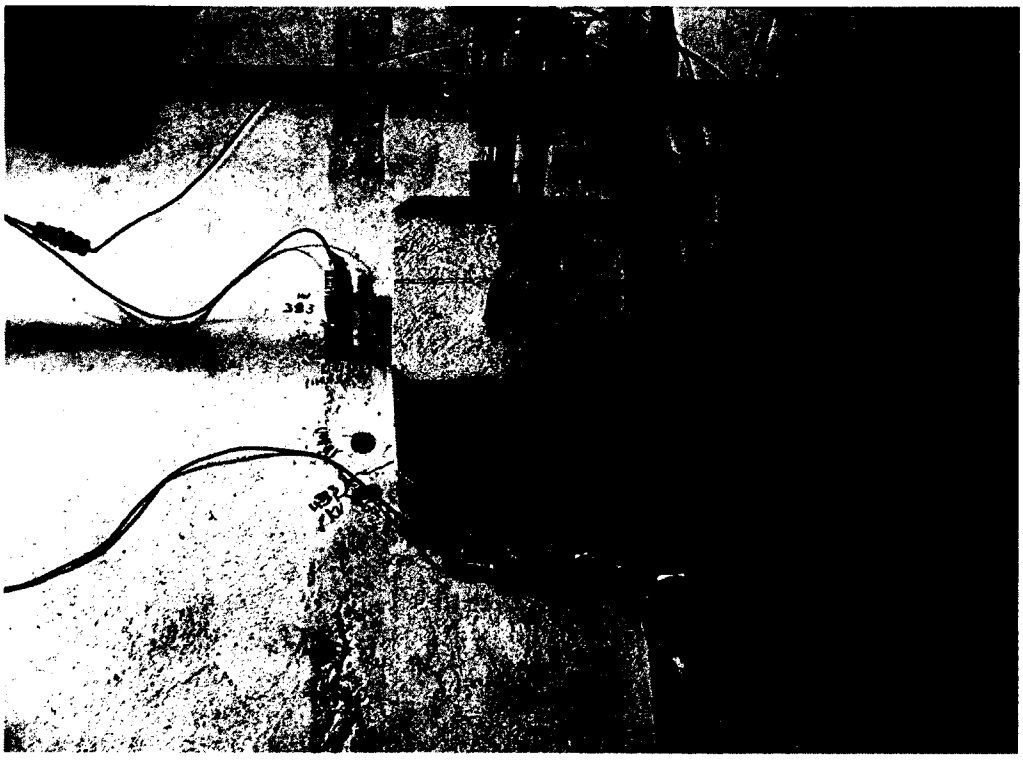

Figure 3.35: A photograph for the placing of the crack widths measurement using LVDTs

Figure 3.36: GFRP bars electrical strain gauges

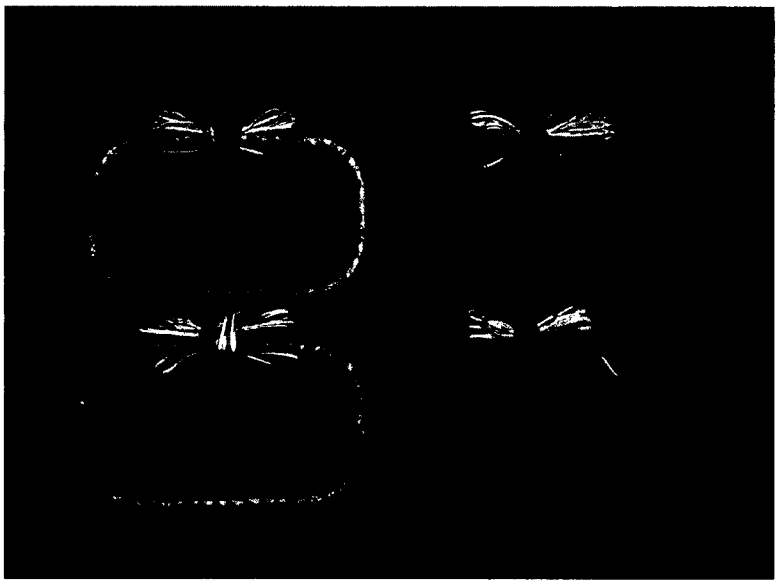

Figure 3.37: FRP closed stirrups electrical strain gauges

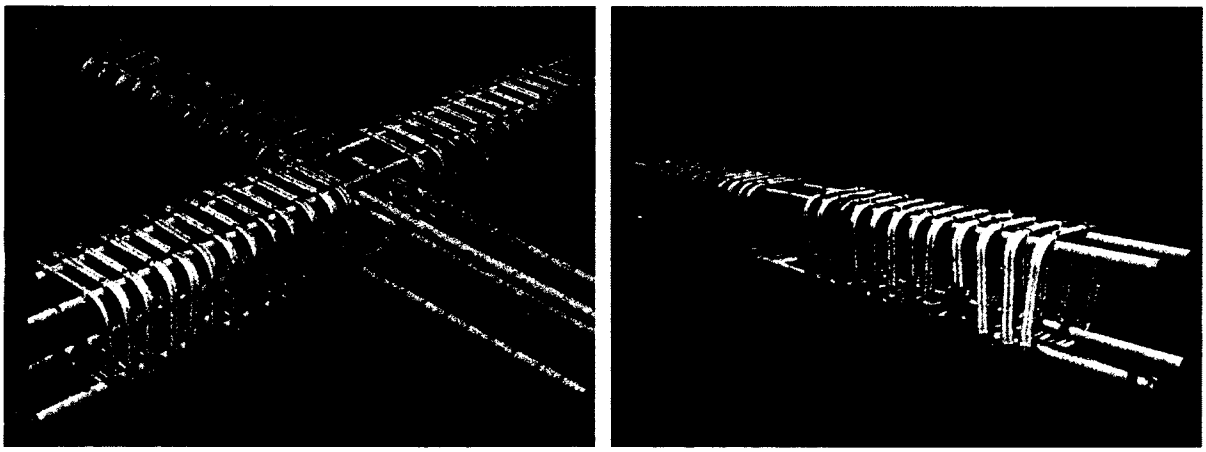

Figure 3.38: FRP spiral stirrups electrical strain gauges

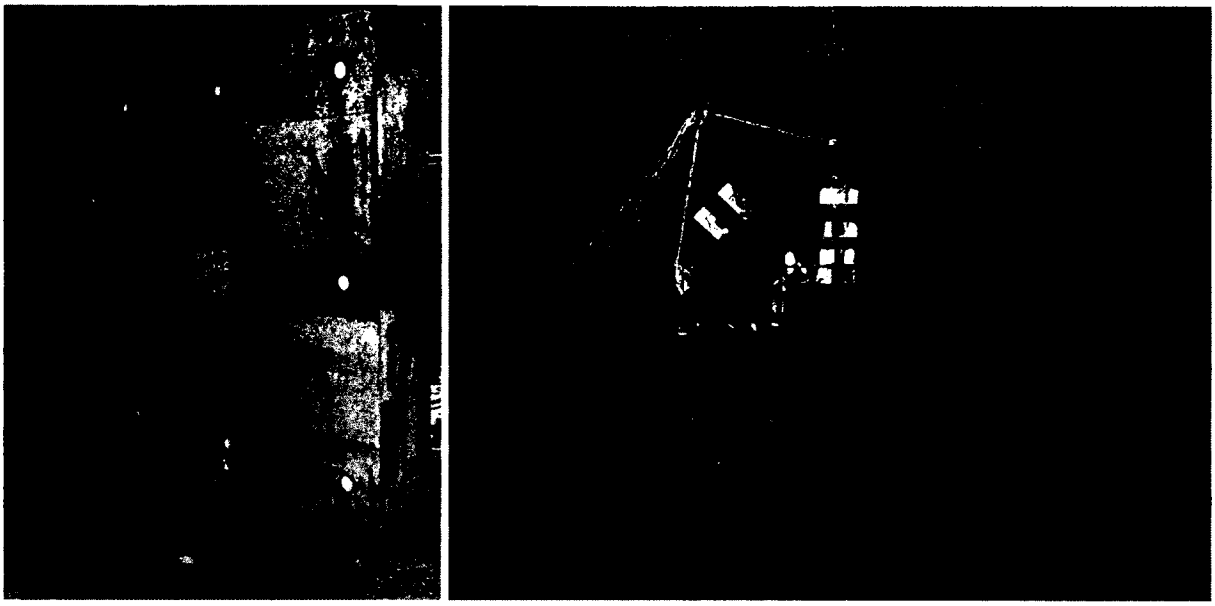

Figure 3.39: Concrete electrical strain gauges in the slab bottom side

3.6 Test Setup and Procedure

All specimens were tested in the structural laboratory at the University of Sherbrooke under monotonic concentrated load, acting on the column stub from the bottom side of the slabs until failure. The specimens were simply supported on all four sides and were held against the laboratory's rigid floor using a rigid steel frame 100 mm in width supported by 8 steel tie rods, each measuring 38 mm in diameter. The specimens were placed supported on temporary frame (see Figure 3.40) and its leveling was adjusted. A 15 mm-thick layer of cement mortar was placed on the concrete surface at the location of the rigid steel frame (see Figure 3.41). In addition, 10 mm-thick neoprene sheets were used over the loading plate and between the supporting frame and the slab. Thereafter, the load was applied using one or two 1500 kN hydraulic jacks according to the expected capacity of each specimen, at a loading rate of 5 kN/min. When two hydraulic jacks were used, they were connected to the same pump and calibrated to work simultaneously. Figure 3.42 and Figure 3.43 provide the details of the test setup and a photograph of the test setup.

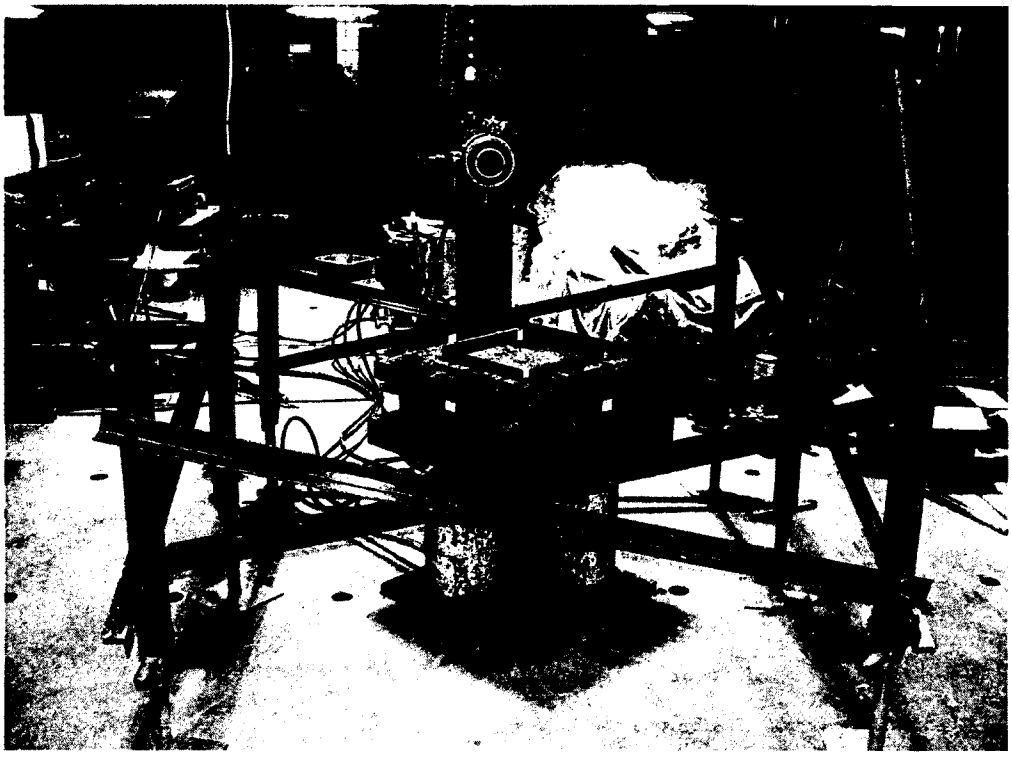

Figure 3.40: Temporary steel supports and the loading units placing

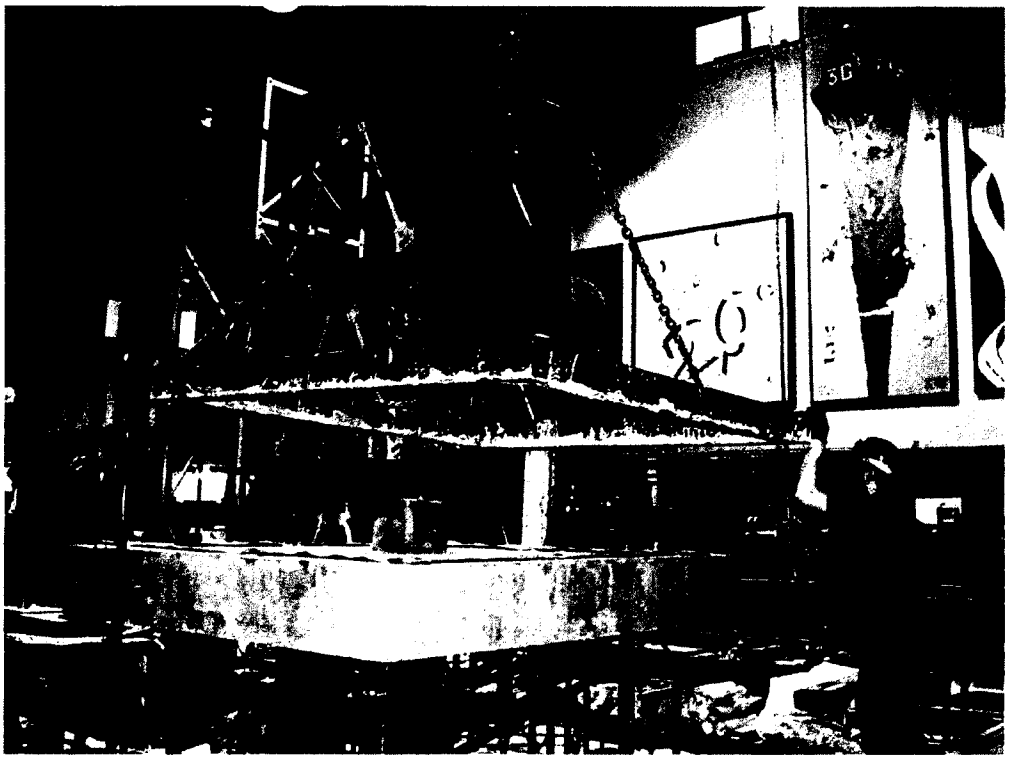

Figure 3.41: Placing the rigid steel frame on slab

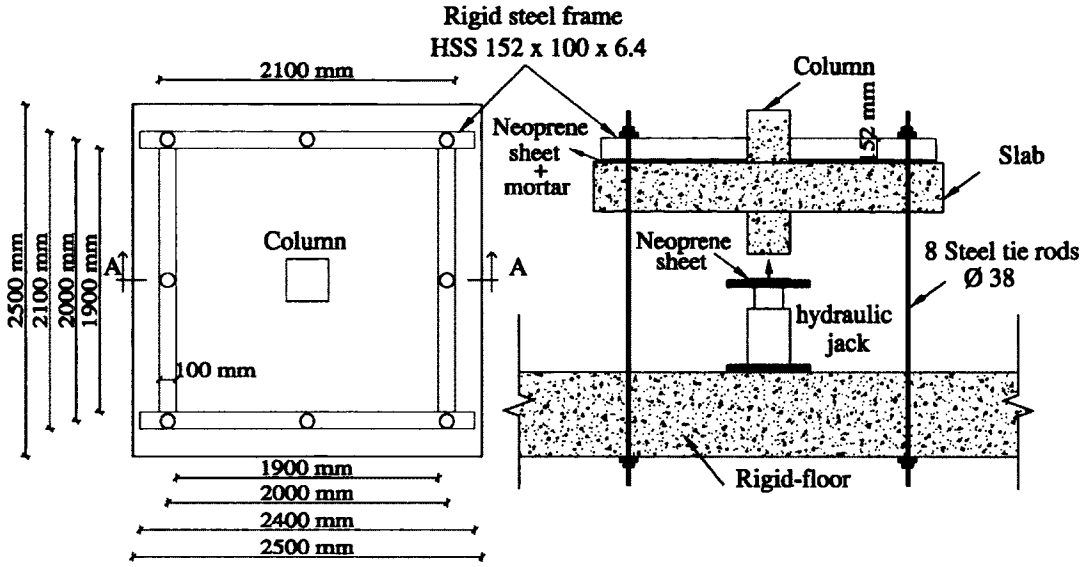

Figure 3.42: Schematic for the test setup

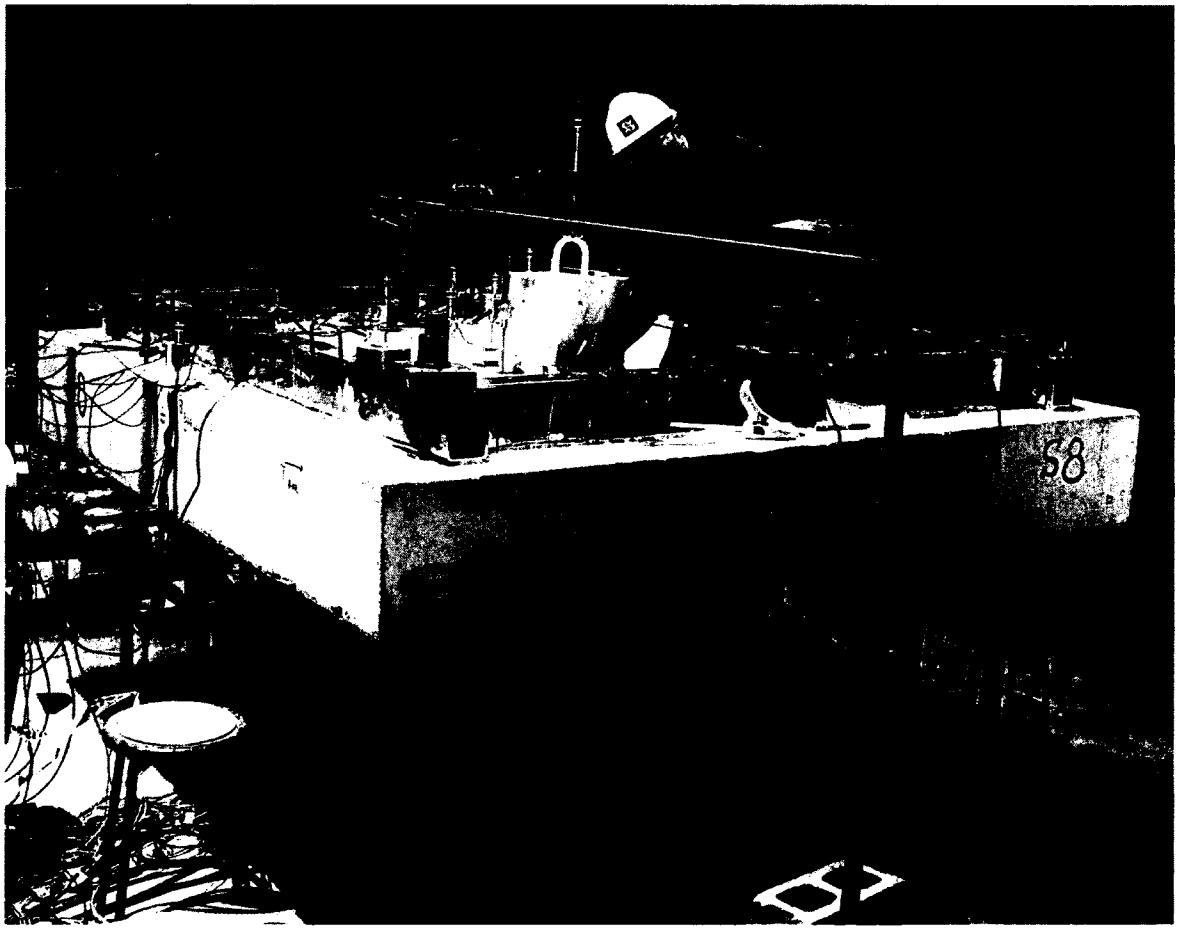

Figure 3.43: A photograph of the test setup of the tested specimens

CHAPTER 4
PUNCHING-SHEAR BEHAVIOUR OF FLAT SLABS REINFORCED WITH GFRP BARS

Foreword

Authors Biographies

Christian Dulude is a master's degree student in the Department of Civil Engineering at the University of Sherbrooke, Sherbrooke, QC, Canada, where he also received his BSc. His research interests include the structural behavior of concrete members reinforced with FRP bars.

Mohamed Hassan is a PhD candidate in the Department of Civil Engineering at the University of Sherbrooke, Sherbrooke, Quebec, Canada. He received his BSc and MSc in civil engineering from Helwan University, Cairo, Egypt. His research interests include the punching shear of flat slabs reinforced with FRP bars.

ACI member **Ehab A. Ahmed** is a postdoctoral fellow in the Department of Civil Engineering at the University of Sherbrooke, Sherbrooke, Quebec, Canada, where he also received his PhD. He received his BSc and MSc from Minoufiya University, Shebin El-Kom, Minoufiya, Egypt. His research interests include structural analysis, design and testing, and structural health monitoring of FRP-reinforced concrete structures.

Brahim Benmokrane, FACI, is an NSERC Research Chair Professor in FRP Reinforcement for Concrete Infrastructures and Tier-1 Canada Research Chair in Advanced Composite Materials for Civil Structures in the Department of Civil Engineering at the University of Sherbrooke, Sherbrooke, QC, Canada. He is a member of ACI Committee 440 FRP Reinforcement and the Canadian Standard Association (CSA) committees on FRP structural

reinforcing materials for buildings (CSA S806), bridges (CSA S6), and specification (CSA S807).

Acceptation date: 14 December 2012

Acceptation state: final version published

Journal: American Concrete Institute (ACI) – *ACI Structural Journal*

Reference: Duldue, C., **Hassan, M.**, Ahmed, E., and Benmokrane, B., 2013, "Punching-Shear Behavior of Flat Slabs Reinforced with Glass Fiber-Reinforced Polymer Bars", American Concrete Institute (ACI) –*ACI Structural Journal*, 110(5): 723-734.

Titre en français: "Comportement au poinçonnement de dalles renforcées de barres d'armature en polymère renforcé de fibres de verre (PRFV)".

Paper's contribution to the project: This paper presents the test results of an experimental investigation on the punching-shear behaviour of 10 interior slab-column connections without shear reinforcement. Factors influencing the strength and deformation capacity such as the effect of reinforcement type (GFRP and steel) and ratio, slab thickness and column dimensions are addressed. Additionally, the test results are employed to evaluate the accuracy of current equations predicting the punching-shear strength of FRP-RC flat slabs provided by codes, design guidelines, and others models from the literature are presented.

Abstract: Results from an experimental study aimed at investigating the behavior of full-scale two-way flat slabs reinforced with glass fiber-reinforced polymer (GFRP) bars and subjected to monotonically-increased concentrated load are presented. A total of 10 interior slab–column prototypes measuring 2.5 m × 2.5 m [98 in. × 98 in.] were constructed and tested up to failure. The test parameters were: (i) reinforcement type (GFRP and steel) and ratio (0.34 to 1.66%); (ii) slab thickness (200 mm and 350 mm [7.9 in. and 13.8 in.]); and (iii) column dimensions (300 mm × 300 mm [11.8 in. × 11.8 in.] and 450 mm × 450 mm [17.7 in. × 17.7 in.]). All test prototypes showed punching-shear failure and the crack patterns at failure were almost the same regardless of reinforcement type or ratio. Besides, the GFRP-reinforced prototypes showed lower punching capacity compared to that of the steel-reinforced ones when the same

reinforcement ratio was employed due to the lower modulus of GFRP bars compared to steel. Predictions using different design guidelines were compared to the experimental results obtained herein. The comparisons showed that the ACI 440.1R equation yielded very conservative predictions with an average V_{test}/V_{pred} equal to 2.10±0.30.

Keywords: punching shear; two-way; flat slab; slab–column; slab; fiber-reinforced polymer; thickness.

4.1 Introduction

The corrosion of steel bars used in reinforced concrete (RC) structures is a major concern in many countries around the world. The extensive use of deicing salt during the winter has created a harsh environment accelerating the corrosion of the steel reinforcement in structures like bridges and parking garages. The corrosion and related deterioration necessitate costly repairs, reduce the service life of concrete structures, and may lead to catastrophic failures. On the one hand, solutions have been proposed to reduce the potential of corrosion and related degradation of parking structures, such as using galvanized steel bars and epoxy-coated steel bars. The former faces some use restrictions in certain countries and the latter is no longer allowed for parking structures under CSA S413-07 (2007) due to the debate on the material's durability. On the other hand, replacing corrodible steel reinforcement with noncorroding FRP bars provides a suitable solution for eliminating the potential of corrosion and its related deteriorations. Recent advances in polymer technology have led to the development of new generations FRP reinforcing bars (in particular, glass FRP (GFRP) bars) such as GFRP bars designated with high modulus of elasticity. These corrosion-resistant bars have shown promise in further protecting bridges and public infrastructure from corrosion-related deteriorations. With the new CSA certification standard (CAN/CSA S807-10) and bars of the highest quality being produced, FRP bars are emerging as a realistic and cost-effective alternative to traditional steel reinforcement for concrete structures under severe environmental conditions.

Flat slabs are commonly used as structural systems because of their construction and architectural advantages. Having the slab supported directly by columns, however, makes the connections susceptible to punching-shear failure which could lead to substantial floor damage or even structural collapse (Cheng and Parra-Montesinos 2010). Thus, a lot of research work

has been conducted to evaluate and increase the punching-shear capacity of steel-reinforced two-way flat slabs. In contrast, few studies (El-Ghandour et al. 1999; Matthys and Taerwe (2000 b); Ospina et al. 2003; Hussein et al. 2004; Zhang et al. 2008; Lee et al. 2009) have been conducted to evaluate the performance and punching capacity of two-way flat slabs reinforced with FRP bars. These studies have demonstrated that the difference in mechanical properties between FRP and steel reinforcement—especially the relatively high tensile strength and the relatively low modulus of elasticity—affect punching-shear behavior and strength. Besides, given the difference in mechanical properties, the punching-shear equations for steel-reinforced concrete flat slabs cannot be directly employed for FRP-reinforced concrete ones. Furthermore, some design equations, which modify the steel-reinforced slab equations to account for the use of FRP have been proposed. Be that as it may, the behavior of FRP-reinforced concrete two-way flat slabs has yet to be investigated and clearly understood.

The main objective of this study was to investigate the behavior of full-scale two-way flat slabs reinforced with GFRP bars subjected to monotonically increased concentrated load and to compare their behavior to that of steel reinforced ones. In addition, the test results were employed to evaluate the accuracy of current equations predicting the punching-shear strength of FRP RC flat slabs provided by (JSCE 1997), El-Ghandour et al. (1999; 2000), Matthys and Taerwe (2000 b), Ospina et al. (2003), El-Gamal et al. (2005), the ACI 440 committee (2006), and the proposed equation for the CSA S806-12 (2012) code for the design and construction of building structures with fiber-reinforced polymers.

4.2 Research Significance

The punching-shear strength of two-way flat slabs reinforced with glass fiber-reinforced polymer (GFRP) bars has yet to be fully investigated. This is due to the limited research work on the subject and to the numerous parameters affecting punching-shear behavior. This study, which presents experimental results of GFRP RC full-scale two-way flat slabs, contributes to understanding the general behavior of such reinforced concrete elements and enriches the state-of-art. Besides, it assesses the accuracy of current equations predicting the punching-shear capacity of FRP RC members.

4.3 Experimental Program

4.3.1 Details of test prototypes

A total of 10 flat-slab prototypes were constructed and tested to investigate the following parameters: (i) reinforcement type (GFRP and steel) and ratio (0.34% to 1.66%); (ii) slab thickness (200 mm and 350 mm [7.9 in. and 13.8 in.]); and (iii) column dimensions (300 mm × 300 mm [11.8 in. × 11.8 in.]; 450 mm × 450 mm [17.7 in. × 17.7 in.]). The test prototypes were designed to represent isolated interior slab–column connections. The geometry of the specimens tested herein was fixed considering the findings of Hallgren et al. (1999). In their study, square- and circular-shaped flat plates were tested to investigate the difference in the punching-shear strengths between the two shapes. They reported that the differences were small and fall within the scatter of the measured punching-shear strengths and geometric properties. Thus, the square geometry was selected as it is not expected to yield significantly different results compared to the circular-shaped one.

The prototypes measured 2500 mm × 2500 mm [98.4 in. × 98.4 in.] with thicknesses of either 200 mm or 350 mm [7.9 in. or 13.8 in.] and 300 mm [11.8 in.] or 450 mm [17.7 in] square column stubs. The column stub extended 300 mm [11.8 in.] beyond the top and bottom surfaces of the slabs. Figure 4.1 shows the geometry and typical reinforcement configuration of the test prototypes. For the entire test prototypes, the clear concrete cover was kept constant at 50 mm [2.0 in.]. This concrete cover was to provide the proper fire-resistance endurance for parking structures because the concrete cover of FRP-reinforced slabs is usually governed by fire-resistance criteria. The prototypes were divided into two series according to thickness: Series I with a thickness of 200 mm [7.9 in.] and Series II with a thickness of 350 mm [13.8 in.]. The 200 mm [7.9 in.] thickness for the first series is common in flat slabs, while the thickness of 350 mm [13.8 in.] represents a 200 mm [7.9 in.] slab with a drop panel of 150 mm [5.9 in.]. Table 4.1 presents the test matrix and characteristics of each test prototype.

As shown in Table 4.1, each of the two series comprised five slab prototypes: four reinforced with GFRP bars and one reinforced with steel for comparison. The four GFRP-reinforced prototypes in each series comprised two pairs of identical prototypes with different column dimensions (300 mm or 450 mm [11.8 in. or 17.7 in.]). On the other hand, the reinforcement amounts of the Series II prototypes (350 mm [13.8 in.] in thickness) were the

same as for the Series I prototypes (200 mm [7.9 in.] in thickness). Thus, the reinforcement ratios of Series I prototypes were 0.71% and 1.56%, while that of Series II prototypes were 0.34% and 0.73%. The reinforcement ratio was selected to cover a wide range of ρ/ρ_b which ranged from 0.6 to 3.32.

The slab prototypes were labeled with a letter denoting the reinforcement type (G for GFRP and S for steel bars) with a subscript indicating the reinforcement ratio, followed by the column dimension in centimeters (30 cm or 45 cm [11.8 in. or 17.7 in.]) and ending with the slab thickness in centimeters (20 cm or 35 cm [7.9 in. or 13.8 in.]). For example, the prototype $G_{(0.7)}30/20$ was reinforced with GFRP bars with a reinforcement ratio of 0.7% in each orthogonal direction, a 30 cm [11.8 in.] square column, and a slab thickness of 20 cm [7.9 in.].

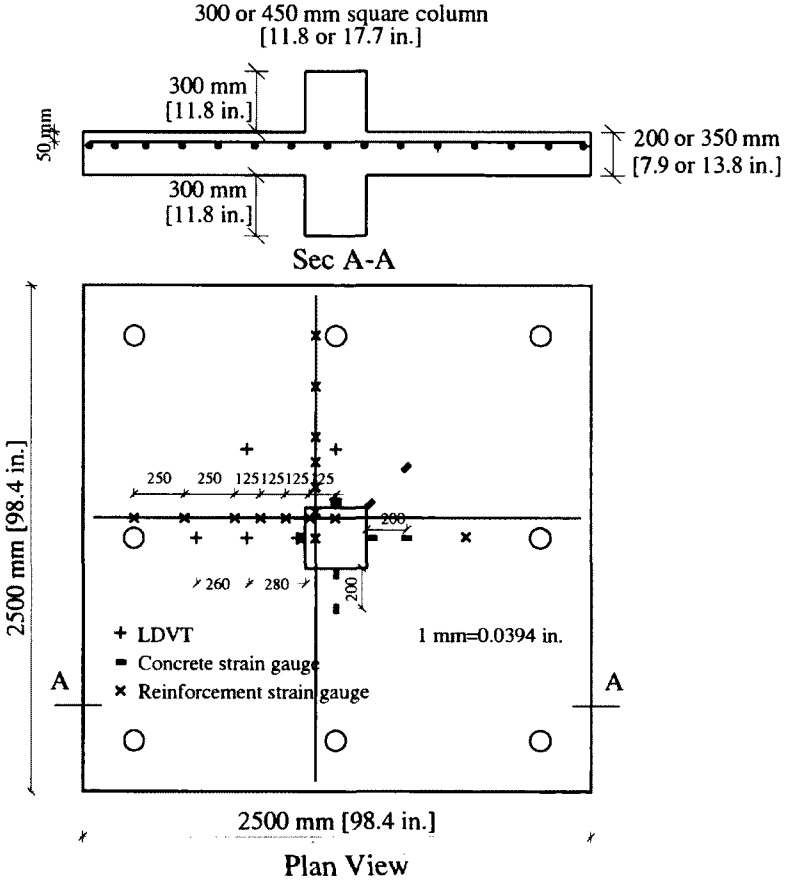

Figure 4.1: Geometry, reinforcement configuration, and instrumentation

Table 4.1: Details of test prototypes

Series	Prototype	Slab thick. mm (in.)	Reinf. type	Reinf.	ρ, %	ρ_b,* %	Column dim., mm (in.)	f'_c,† MPa (ksi)	f_t,† MPa (ksi)
I	$G_{(0.7)}30/20$	200 (7.9)	GFRP	12 No. 15	0.71	0.49	300 (11.8)	34.3 (4.97)	2.5 (0.36)
	$G_{(1.6)}30/20$			18 No. 20	1.56	0.52	300 (11.8)	38.6 (5.60)	2.8 (0.41)
	$G_{(0.7)}45/20$			12 No. 15	0.71	0.57	450 (11.8)	44.9 (6.51)	2.9 (0.42)
	$G_{(1.6)}45/20$			18 No. 20	1.56	0.47	450 (17.7)	32.4 (4.70)	2.3 (0.33)
	$S_{(1.7)}30/20$		Steel	18-20M	1.66	4.56	300 (11.8)	45.4 (6.58)	2.8 (0.41)
II	$G_{(0.3)}30/35$	350 (13.8)	GFRP	12 No. 15	0.34	0.49	300 (11.8)	34.3 (4.97)	2.5 (0.36)
	$G_{(0.7)}30/35$			18 No. 20	0.73	0.53	300 (11.8)	39.4 (5.71)	2.3 (0.33)
	$G_{(0.3)}45/35$			12 No. 15	0.34	0.59	450 (17.7)	48.6 (7.05)	2.6 (0.38)
	$G_{(0.7)}45/35$			18 No. 20	0.73	0.44	450 (17.7)	29.6 (4.29)	2.7 (0.39)
	$S_{(0.8)}30/35$		Steel	18-20M	0.77	3.88	300 (11.8)	38.6 (5.60)	2.8 (0.41)

* Calculated according to ACI 440.1R (2006) for GFRP-RC slabs and ACI 318 (2008) for steel-RC slabs.

† Based on 150×300 mm cylinder testing.

Note: 1 mm = 0.0394 in.

4.3.2 Material Properties

No. 15 and No. 20 sand-coated GFRP reinforcing bars, designated according to the CAN/CSA S807-10 (2010), were used in the GFRP-reinforced prototype. The GFRP bars used herein were manufactured by combining the pultrusion process with an in-line sand-coating process for the bar surface. This sand coating was designed to improve bonding between the GFRP bars and surrounding concrete. The tensile properties of the GFRP bars were determined by testing of five representative bars for each diameter in accordance with the B.2 Test Method of the ACI 440.3R (2004). The ultimate tensile strength and the modulus of elasticity were 769 MPa and 765 MPa [112 ksi and 111 ksi] and 48.2 GPa to 48.1 GPa [6990 ksi and 6976 ksi] for the No. 15 and No. 20 GFRP bars, respectively. Table 4.2 gives the GFRP bar properties, as determined from testing. The reference slab prototypes, however, were reinforced with 20M steel bars (Type 44W) with a yield stress of 470 MPa and modulus of elasticity 200 GPa.

The slab prototypes were cast using a ready-mixed, normal-weight concrete with 5% to 8% of entrained air. The concrete compressive and tensile strengths for each prototype were determined on the day of testing using three concrete cylinders measuring 150 mm × 300 mm [5.9 in. × 11.8 in.] for each test. The concrete compressive strength ranged from 29.6 MPa to 48.6 MPa [4.29 ksi to 7.05 ksi], while the tensile strength determined from split-cylinder

testing ranged from 2.3 MPa to 2.9 MPa [0.33 ksi to 0.42 ksi]. Table 4.1 provides the concrete properties.

Table 4.2: Properties of the GFRP reinforcing bars

Bar size	Area, mm^2 ($in.^2$)	Elastic tensile modulus, E_f, GPa (ksi)	Ultimate tensile strength, MPa (ksi)	Guaranteed tensile strength, MPa (ksi)[1]	Ultimate tensile elongation, %
No. 15	199 (0.31)	48.2±0.4 (6990±58)	769±23 (112±3)	699 (103.4)	1.60±0.05
No. 20	284 (0.44)	48.1±0.7 (6976±102)	765±32 (111±4)	673 (97.6)	1.59±0.08

[1] Guaranteed tensile strength=Average value – 3× standard deviation.

4.3.3 Instrumentation and test setup

Each slab prototype was equipped with 2 instrumented bars in the orthogonal directions in the top reinforcing mat (tension side) with 6 electrical strain gauges attached to each bar. In addition, 8 electrical strain gauges for concrete were glued to the bottom surface of the specimen (compression side) before testing. Moreover, the 8 steel anchors supporting the test prototype were instrumented with electrical strain gauges to verify loading symmetry during the tests. The deflection of the test prototypes at the desired locations was captured using 6 linear voltage differential transformers (LVDTs) whereas the crack width was measured using two LVDTs. The crack appearance was monitored during the test by visual inspection until the first two cracks appeared. Thereafter, their initial widths were measured using a hand-held microscope with a magnifying power of 50X. Then, the two LVDTs were installed at the locations of the first two cracks. The strain gauges and LVDTs were connected to a data-acquisition system to record the readings during the test. Figure 4.1 shows the locations of strain gauges and LVDTs. During the test, the propagation of cracks was marked and the corresponding load recorded.

The prototypes were tested in the structural laboratory at the University of Sherbrooke under monotonic loading till failure. The load was applied at a load-controlled rate of 5 kN/min [1.1 kips/min]. The load was applied using one or two 1500 kN [337.2 kips] hydraulic jacks, according to the expected capacity of each specimen, until slab punching failure. When two hydraulic jacks were used, they were connected to the same pump and were calibrated to work simultaneously. The slab specimens were held against the rigid floor of the laboratory using a rigid steel frame 100 mm [3.9 in.] in width supported by 8 steel anchors, each measuring 38 mm [1.5 in.] in diameter. The tested slabs had clear spans of 1900 mm

[74.8 in.]. Before fixing the steel frame, a 15-mm [0.6 in.] thick cement mortar was placed on the concrete surface at the location of the steel frame. Thereafter, to prevent local failure and to distribute the load uniformly, neoprene sheets 10 mm [0.4 in.] in thickness were used over the loading plate and between the supporting frame and the slab, respectively. Figure 4.2 shows the test setup.

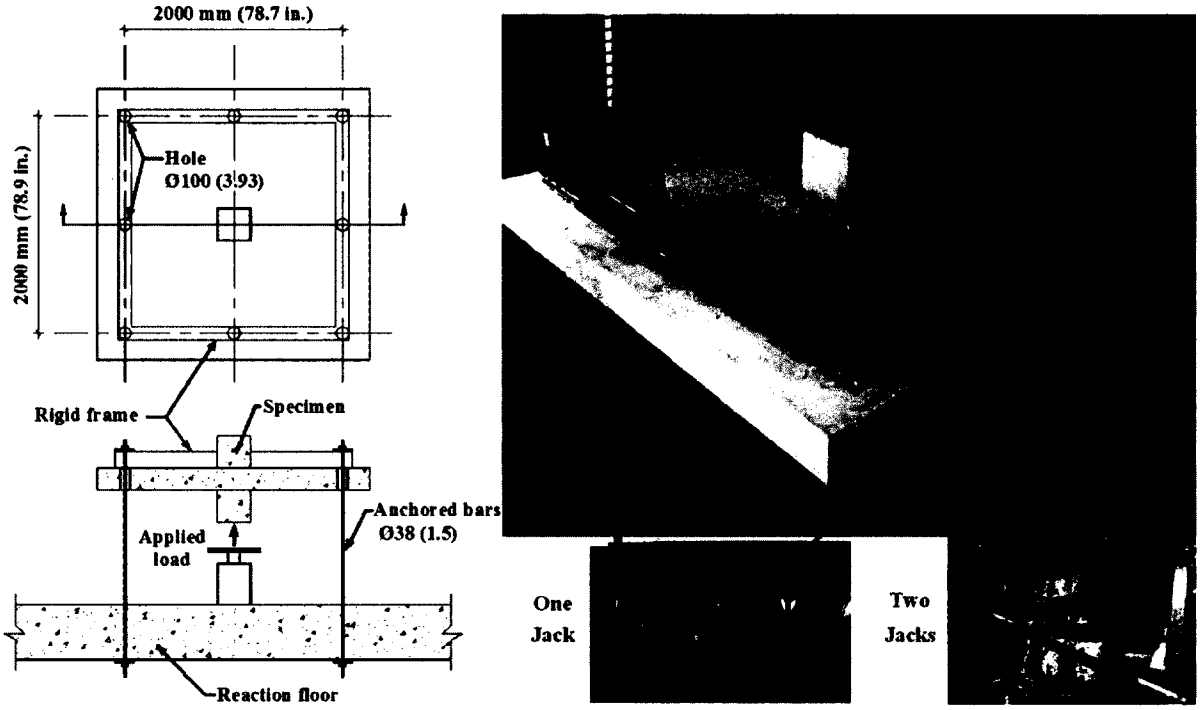

Figure 4.2: Test setup: (a) Schematic and dimensions; (b) Testing of a slab prototype.
(Note: Dimensions in mm [in.]; 1 mm = 0.0394)

4.4 Test Results and Discussion

4.4.1 Cracking and failure mode

The first cracks to appear in the tension side of the slabs (top surfaces) were flexural cracks in the region of the maximum bending moment, which was around the column stub. The cracks started at the corner of the column and extended to the edge of the slab parallel to the orthogonal axes when the load increased. The second type of cracks to appear was

diagonal radial cracks, which formed with deviation angles with respect to the orthogonal axes. At higher loads, small cracks appeared at the column interface along the perimeter. Besides, circumferential cracks were observed near the column connecting the radial cracks together.

Regardless of the reinforcement type and ratio, all the test prototypes showed punching-shear failure. The slab prototypes with low reinforcement ratios showed more flexural cracks surrounding the column and some ductile behavior before the punching-shear failure. The punching-shear failure was evidenced by a sudden drop in the applied load, accompanied by the appearance of a wide, clear crack defining the failure surface of the prototypes around the columns. Figure 4.3 shows the final crack pattern at failure of the 10 prototypes tested. This figure shows that GFRP prototypes $G_{(1.6)}30/20$ and $G_{(0.7)}30/35$ and their steel-reinforced counterparts, $S_{(1.7)}30/20$ and $S_{(0.8)}30/35$, respectively, had similar crack patterns and punching-shear failure surface. This indicates that the crack pattern and failure mode were not affected by the reinforcement type. The failure surface is marked on the slabs as shown in Figure 4.3. The distance from the column face of each prototype until the location of the failure envelope (X_{cone}) was used as to define failure surface. This distance (X_{cone}) was measured at different locations and the average values were calculated and reported in Table 4.3 (multiplications of d). Figure 4.3 shows that the Series I prototypes (200 mm [7.9 in.]) had a smaller failure surface than those in Series II (350 mm [13.8 in.]) due to the slabs' smaller effective depth.

Figure 4.4 shows that increasing the effective reinforcement ratio ($\rho E_r/E_s$, where E_r is the modulus of elasticity of the reinforcing bars) in Series I and II slab prototypes resulted in increased failure surfaces, indicating much flatter inclination of the critical shear crack. This confirms the previous findings of Guandalini et al. (2009) in their investigation, which reported that increasing the steel reinforcement ratio increased the failure surface. This could be explained according to Regan (1981) where it was reported that, in the failure mechanism involving vertical displacement at an inclined fracture surface (shear failure surface), an increase of reinforcement should enhance the restraint available in the plan of the slab. Consequently, with significant increase in the reinforcement amount, flatter inclination angle for the critical shear crack is expected. In addition, there was an upper limit for the X_{cone} distance of about $2.8d$ (where d is the average slab depth), which was observed in the $G_{(1.6)}30/20$ and $S_{(1.7)}30/20$ with effective reinforcement ratios of 0.38% and 1.66%,

respectively. Furthermore, the failure surfaces of the Series I and II tested prototypes exceeded the 0.5*d* or 1.5*d* specified by the available design equations predicting the punching shear capacity of FRP-reinforced concrete slabs, except $G_{(0.3)}30/35$ and $G_{(0.3)}45/35$. The very low effective reinforcement ratio (0.08) of $G_{(0.3)}30/35$ and $G_{(0.3)}45/35$ led to a failure surface located at 1.3*d* and 1.4*d* from the column face, respectively.

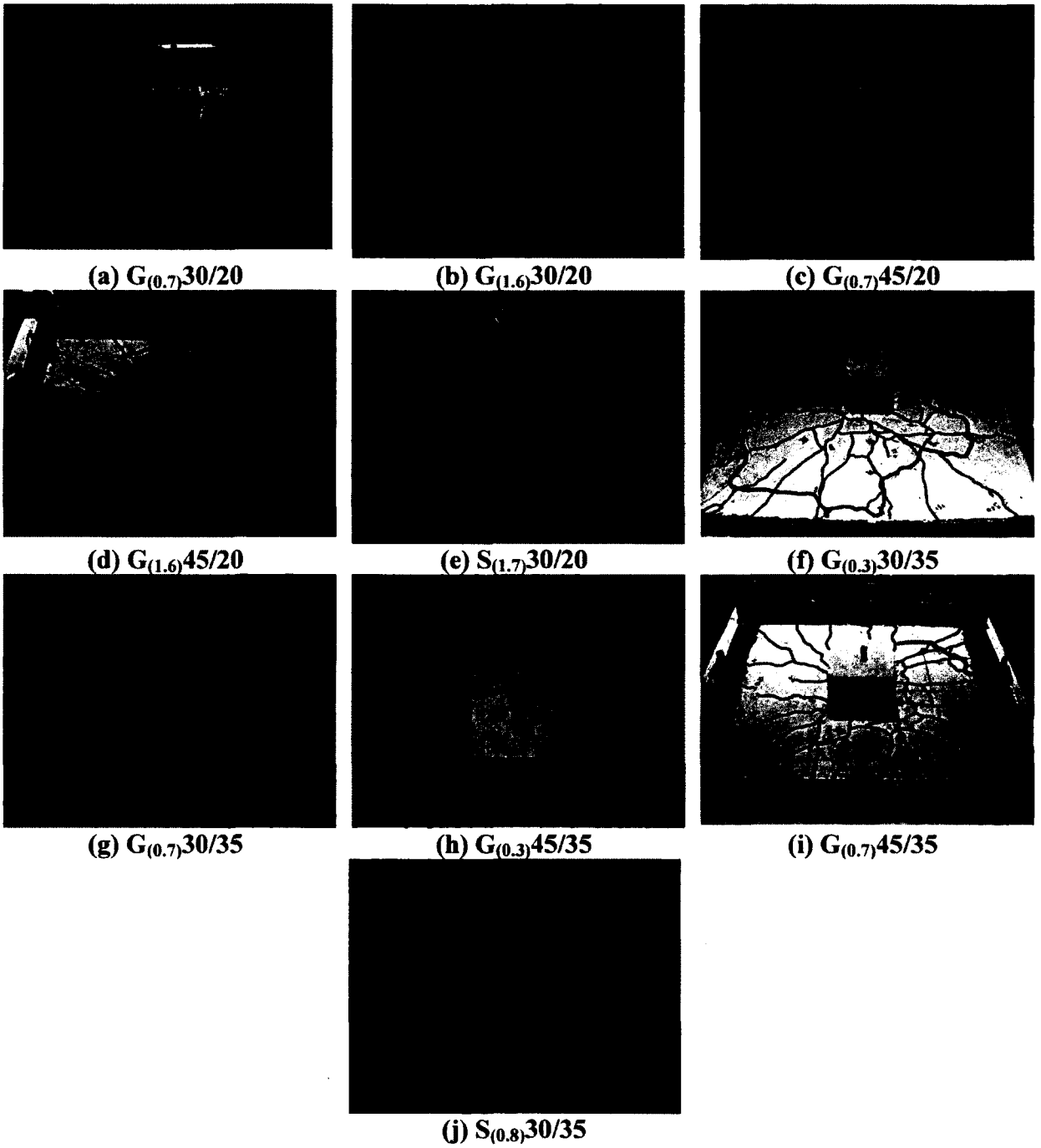

Figure 4.3: Crack pattern and punching-shear failure surface (bold lines).

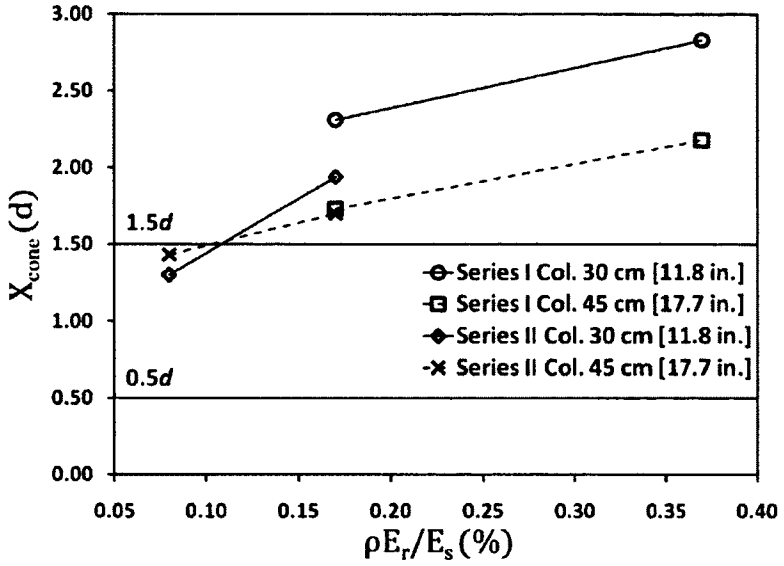

Figure 4.4: Failure surface distance of the GFRP-reinforced prototypes.

As the development of the inner critical shear crack was not visible, four of the tested slab prototypes were sawed allowing the observation of the final crack pattern. Figure 4.5 shows the cross-sections with the critical shear crack emphasized. From this figure, it can be noticed that the prototypes exhibited a main diagonal shear crack starting from the column face with different inclination angles. It should be mentioned that, for $G_{(1.6)}45/20$ prototype where the maximum measured concrete strain was 4195 microstrains, there was no concrete crushing. Moreover, the critical diagonal crack confirms the punching failure of this prototype, as shown in Figure 4.5.

4.4.2 Punching-shear capacity

Table 4.3 presents the normalized ultimate punching-shear capacities and the corresponding normalized punching-shear stresses calculated at the column face of the tested prototypes. It should be noted that the reported load values include prototype dead load. The punching-shear stresses at failure were normalized to the square root of the concrete strength to account for the variation in the concrete strengths. Besides, the effective reinforcement ratios ($\rho E_r/E_s$) of the prototypes were presented to account for the difference between the moduli of elasticity of the GFRP and steel bars. The test results revealed that, with the same reinforcement type, the punching-shear capacity increased as did the reinforcement ratio. Increasing the reinforcement ratio of the GFRP-reinforced prototypes from 0.71% to 1.56% and from 0.34% to 0.73%

increased the normalized punching-shear stress by 39% and 49% on average for Series I and II, respectively. Increasing the reinforcement ratio increased the depth of the uncracked concrete (compression zone) which significantly enhanced the concrete contribution. It also led to smaller strains and consequently smaller crack widths at the same load level which enhanced the aggregate interlock and dowel contributions. Consequently, the punching-shear capacity was enhanced with the increase of the reinforcement ratio.

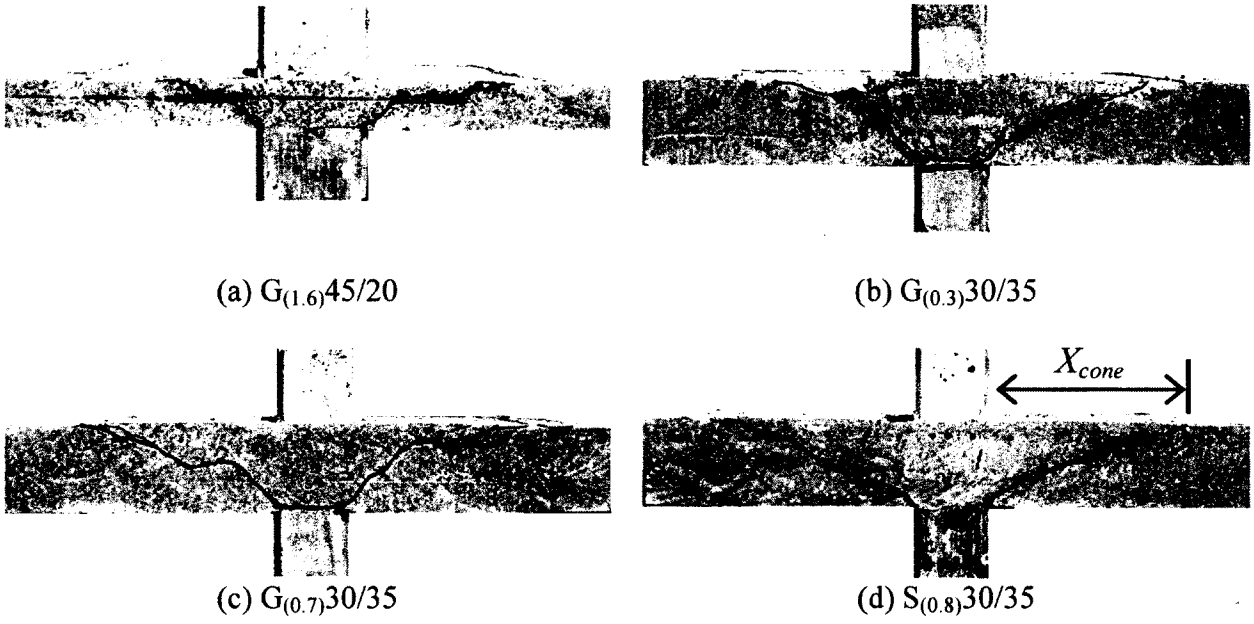

(a) $G_{(1.6)}45/20$ (b) $G_{(0.3)}30/35$

(c) $G_{(0.7)}30/35$ (d) $S_{(0.8)}30/35$

Figure 4.5: Cross-section of slab prototypes after failure showing the critical shear crack.

Slab thickness was one of the parameters that most affected punching-shear capacity, with punching-shear capacity increasing as did slab thickness. For the $G_{(0.7)}30/20$; $G_{(0.7)}30/35$ and $G_{(0.7)}45/20$; $G_{(0.7)}45/35$ prototypes, increasing the slab thickness from 200 mm to 350 mm [7.9 in. to 13.8 in.] increased the normalized punching-shear stress at failure by an average of 63% when the reinforcement ratio remained unchanged (approximately = 0.7%). Increasing slab thickness directly impacts the punching capacity because it significantly increases the surface area that resists the punching-shear stress, which, in turn, increases the punching-shear capacity.

The results in Table 4.3 show that the GFRP-reinforced prototype with the same reinforcement ratio as its steel-reinforced counterpart evidenced lower punching-shear stress at failure (32% lower in Series I and 37% lower in Series II). This was referred to the lower

modulus of elasticity of GFRP reinforcing bars compared to that of steel (≈0.25). Utilizing GFRP reinforcement ratio equal to the steel reinforcement ratio yielded smaller neutral axis depth as well as higher strains and wider cracks at the same load level. Thus, the contributions of the un-cracked concrete zone below the neutral axis (compression side) and the aggregate interlock decreased which, in turn, yielded lower punching-shear capacity.

The effective reinforcement ratio (indicating the axial stiffness of the reinforcing bars) was used to account for the differences in the properties of steel and GFRP bars. The normalized punching-shear stress at failure was plotted against the effective reinforcement ratio, as shown in Figure 4.6. In the Series I and II prototypes, the punching shear capacity increased as did the effective reinforcement ratio. When the effective reinforcement ratio increased from 0.17% to 1.66% (Series I) and from 0.08% to 0.77% (Series II), the normalized punching-shear stress at failure increased by 86% and 98%, respectively. Besides, Figure 4.6 shows that the normalized punching-shear stress at failure was directly proportional to the axial stiffness of the reinforcement. Thus, regardless of the reinforcement type, the two-way flat slabs with bars having the same axial stiffness may yield the same punching-shear stress at failure (and consequently punching-shear capacity). Nonetheless, the FRP grids may not provide the same punching capacity due to the difference in bond behavior between FRP grids and bars, and due to the concentration of stresses in the grids at the intersection of the two forms of orthogonal reinforcement (Ospina et al. 2003).

Increasing the column dimensions also increased failure surfaces and, consequently, reduced the punching-shear stress at failure. Increasing the square column dimensions from 300 mm [11.8 in.] to 450 mm [17.7 in.] decreased the normalized punching-shear stress at failure of the $G_{(0.7)}45/20$, $G_{(1.6)}45/20$, $G_{(0.3)}45/35$, and $G_{(0.7)}45/35$ prototypes by 29%, 14%, 37%, and 12% compared to their counterparts ($G_{(0.7)}30/20$, $G_{(1.6)}30/20$, $G_{(0.3)}30/35$, and $G_{(0.7)}30/35$, respectively). For small values of the ratio of the perimeter of the slab critical section to slab effective depth (b_o/d), shear failure involves a complex three-dimensional failure surface that is well confined by in-plane stresses within the slab. As the ratio b_o/d increases, the confinement is reduced, resulting in a decrease in shear strength (Sherif and Dilger 1996). While the highest decrease in the normalized punching-shear stress at failure observed in prototype $G_{(0.3)}45/35$ which had low reinforcement ratio and associated with more flexural cracks in the tension side. Increasing the column size relative to the slab depth

increases the stress concentration toward to the corners of the column relative to its middle, which in turn, to decreases the punching shear stress.

Table 4.3: Summary of the test results

Prototype	$\rho(E_r/E_s)$, %	V_{cr}, kN (kip)	V_u, kN (kip)	$V_u/\sqrt{f_c'}$,	$v_u/\sqrt{f_c'}$,	Post-cracking stiffness, kN/mm (kip/in.)	X_{cone}	Max. reinf. strain, (με)	Max. conc. strain, (με)
$G_{(0.7)}30/20$	0.17	125 (28.1)	329 (74.0)	56.2 (33.2)	0.35 (0.13)	9.2 (52.5)	2.3*d*	8975	-1280
$G_{(1.6)}30/20$	0.38	211 (47.4)	431 (96.9)	69.4 (40.9)	0.44 (0.17)	15.1 (86.2)	2.8*d*	5010	-340
$G_{(0.7)}45/20$	0.17	216 (48.6)	400 (89.9)	59.7 (35.2)	0.25 (0.09)	10.6 (60.5)	1.7*d*	9250	-1530
$G_{(1.6)}45/20$	0.38	142 (31.9)	504 (113.3)	88.5 (52.3)	0.38 (0.14)	19.1 (109.1)	2.2*d*	4795	-4195
$S_{(1.7)}30/20$	1.66	163 (36.6)	688 (154.7)	102.1(60.3)	0.65 (0.25)	37.9 (216.4)	2.8*d*	2030	-2670
$G_{(0.3)}30/35$	0.08	292 (65.6)	825 (185.5)	140.9 (83.2)	0.41 (0.16)	27.0 (154.2)	1.3*d*	8190	-2300
$G_{(0.7)}30/35$	0.18	415 (93.3)	1071 (240.8)	170.6 (100.8)	0.51 (0.19)	53.6 (306.1)	1.9*d*	4625	-215
$G_{(0.3)}45/35$	0.08	460 (103.4)	911 (204.8)	130.7 (77.1)	0.26 (0.10)	33.1 (189.0)	1.4*d*	8510	-670
$G_{(0.7)}45/35$	0.18	447 (100.5)	1248 (280.6)	229.4 (135.5)	0.45 (0.17)	59.6 (340.3)	1.7*d*	6185	-1270
$S_{(0.8)}30/35$	0.77	444 (99.8)	1692 (380.4)	272.3 (160.7)	0.81 (0.31)	125.7 (717.8)	1.8*d*	6955	-1190

Notes – d is (Slab thickness-50mm- d_b; where d_b is the bar diameter); v_u is ultimate shear stress at the column face; X_{cone} is distance from the column face to the observed failure surface; 1 mm = 0.0394 in.

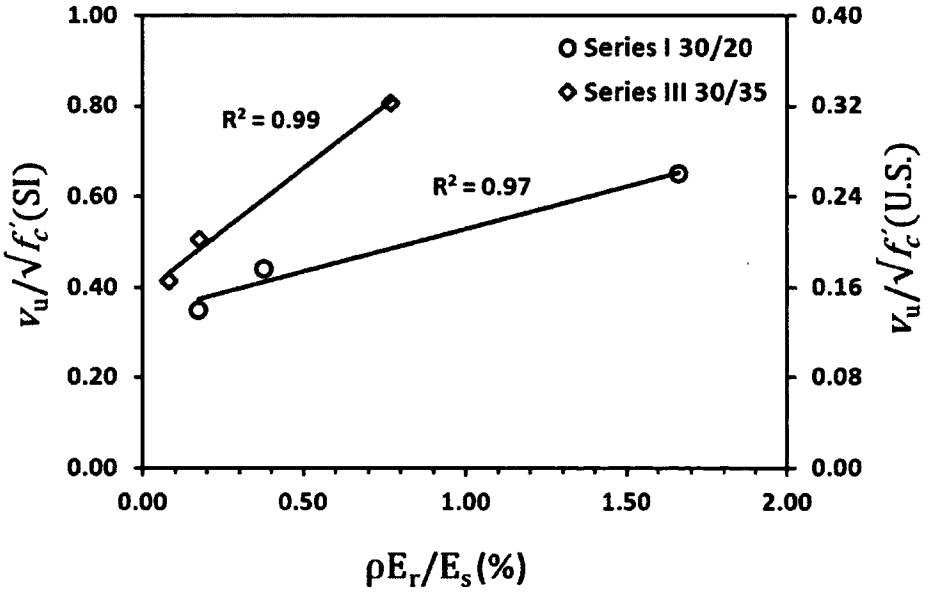

Figure 4.6: Normalized punching-shear stress at failure versus the axial stiffness of the reinforcement of the test prototype with a column dimension of 300 mm [11.8 in.].

4.4.3 Load-deflection responses

Figure 4.7 shows the load-deflection relationships using the LVDTs placed 40 mm [1.6 in.] from the column face. The test prototypes as a whole showed bilinear response till sudden failure due to punching. The first portion is up to the appearance of the first crack. The second portion represents the post-cracking deflection until failure. Series I and II test prototypes evidenced no significant differences in the load-deflection relationships. The post-cracking response, however, was dependent on the reinforcement type and ratio (axial stiffness of the reinforcement). When the same reinforcing-bar material was used and the load level was the same, higher reinforcement ratios resulted in lower deflection values. Moreover, employing the same amounts of GFRP and steel reinforcement in test prototypes yielded higher deflection values at the same load level, because GFRP bars had lower moduli of elasticity values than the steel bars (≈0.25). This, in turn, resulted in reduced effective moment of inertia in the slabs. Furthermore, the deflection of the tested prototypes was also affected by the column dimensions, especially the prototypes with low reinforcement ratios (0.7% in Series I and 0.3% in Series II) as evidenced in Figure 4.7. In case of low reinforcement ratio, the test prototypes exhibited significant flexural cracks with wide widths before punching-shear failure. These cracks impacted the effective moment of inertia which, in turn, yielded larger deflection. Increasing the column dimension directly reduces the shear-span-to-depth ratio and consequently, reduces the deflection of the prototypes. On the other hand, the prototypes with high reinforcement ratio exhibited better flexural performance before the punching-shear failure. The higher reinforcement ratios yielded fewer cracks with smaller widths which minimizes the effect of slight changes in the shear-span-to-depth ratio because the prototypes maintained higher effective moment of inertia. Thus, the effect of the column dimensions in this case was not significant.

The post-cracking stiffness (calculated from the load-deflection relationships in Figure 4.7) was plotted against the axial stiffness of the reinforcing bars, as shown in Figure 4.8 (see the values in Table 4.3). As shown in Figure 4.8 and Table 4.3, higher axial reinforcement stiffness was accompanied by higher post-cracking stiffness. Besides, the post-cracking stiffness was directly proportional to the axial reinforcement stiffness with linear fitting relationships with a corresponding coefficient of correlation of 0.96. In addition, increasing the

column dimensions from 300 mm to 450 mm [11.8 in. to 17.7 in.] increased the post-cracking stiffness due to the smaller clear span-to-depth ratio (a/d).

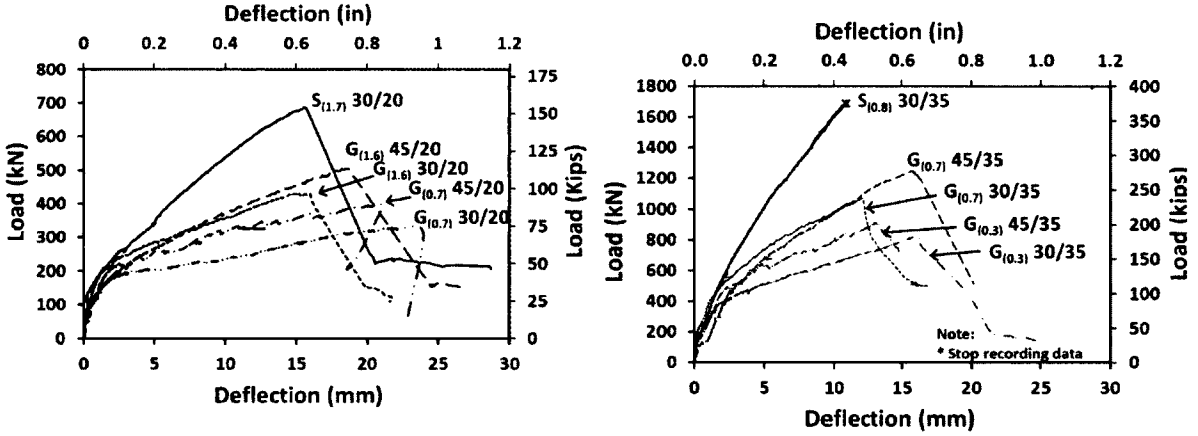

(a) Series I (200 mm [7.9 in.]) (b) Series II (350 mm [13.8 in.])

Figure 4.7: Load-deflection response: (a) Series I (200 mm [7.9 in.]); (b) Series II (350 mm [13.8 in.]).

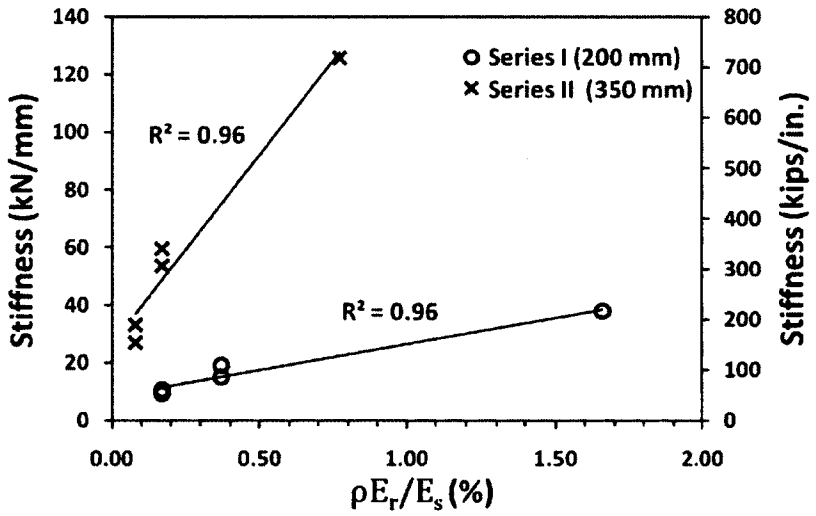

Figure 4.8: Relationships between the post-cracked stiffness and the axial stiffness of the reinforcement. (Note: 1 mm = 0.0394 in).

4.4.4 Strains

Figure 4.9 plots the load versus the reinforcement strain relationships. In this figure, the strain values recorded from the electrical resistance strain gauges located at 125 mm and 250 mm [4.92 in. and 9.84 in.], respectively, from the center of the 300 mm and 450 mm [11.8 in. and 17.7 in.] square columns were used. The prototypes with lower axial reinforcement stiffness showed greater strain at the same load level in Series I and II. The steel-reinforced prototype $S_{(0.8)}30/35$ showed a clear yielding of the steel bars at a corresponding applied load of 1600 kN [360 kips]. In contrast, steel-reinforced prototype $S_{(1.7)}30/20$ showed no signs of yielding as the maximum recorded strain in the steel bars (2030 microstrains) was less than the yield stress of the steel bars (470 MPa/200 GPa=2350 microstrains).

In the case of the GFRP-reinforced prototypes, the maximum measured reinforcement strain was 9250 microstrains, which represented 57% of guaranteed tensile strength. This relatively low strain at ultimate in the slabs reinforced with GFRP bars shows that punching of the slabs was not triggered by rupture of the GFRP bars. The concrete strains of all prototypes (Table 4.3) near the column region were low and below the theoretical crushing failure of 3500 microstrains (CSA S806 2012) except the $G_{(1.6)}45/20$ prototype (4195 microstrains). Moreover, concrete crushing was not observed in any of the tested prototypes. This confirmed that the final mode of failure was punching rather than flexure.

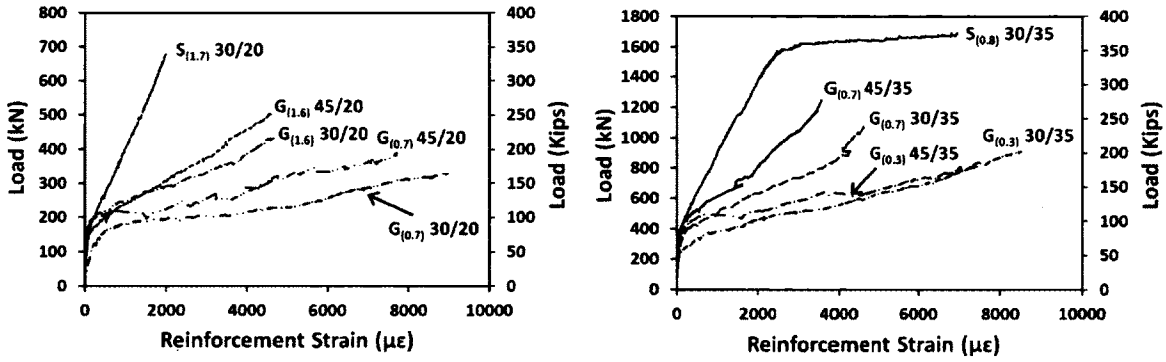

(a) Series I (200 mm [7.9 in.]) (b) Series II (350 mm [13.8 in.])

Figure 4.9: Load-reinforcement strain relationships.

The strain distribution along the span of $S_{(0.8)}30/35$ and $G_{(0.7)}30/35$ is shown in Figure 4.10. Despite the higher strains in the GFRP-reinforced prototype, the two prototypes showed similar profiles until a load below the yielding of the steel-reinforced one. The strain profiles

of the prototypes are similar to that reported by Hussein et al. (2004). In addition, the strain values decreased as the distance from the column face increased until it reached zero at about 1000 mm [39.8 in.] from the column face. This implies that no bond failure or slip occurred during the tests.

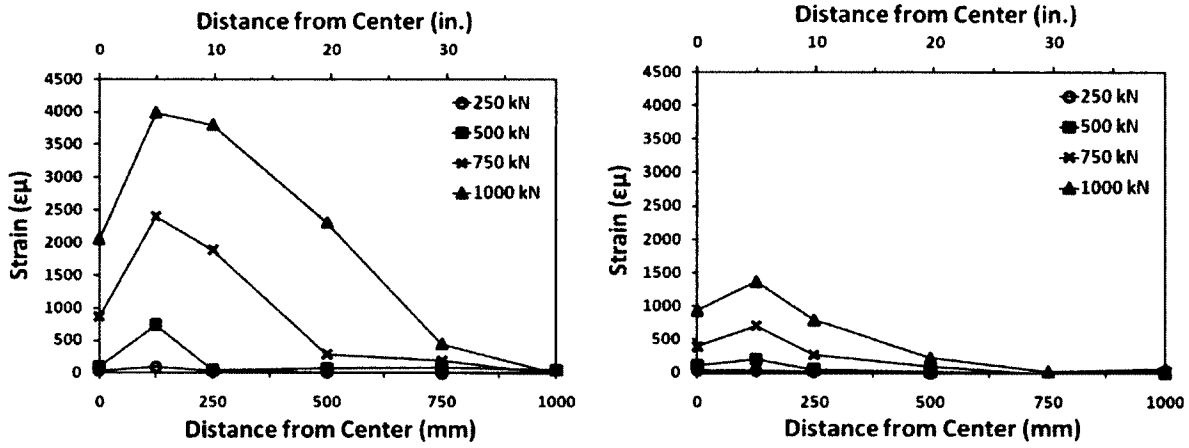

(a) Prototype $G_{(0.7)}30/35$ (b) Prototype $S_{(0.8)}30/35$

Figure 4.10: Reinforcement strain profile. (Note: 1 kN = 0.225 kip.)

4.4.5 Crack width

Figure 4.11 shows the maximum measured crack width versus the applied load and the measured strains for Series I and II. For the GFRP-reinforced prototypes in Series I, the $G_{(0.7)}30/20$ with the lowest effective reinforcement ratio (0.17%) showed the highest crack width relationship. Increasing the effective reinforcement ratio or the column dimensions or both reduced the crack width of the $G_{(0.7)}45/20$, $G_{(1.6)}30/20$, and $G_{(1.6)}45/20$ prototypes at the same load level as shown in Figure 4.11 (a). Similar behavior was observed for the prototypes for the GFRP-reinforced prototypes in Series II, as shown in the same figure. Increasing the effective reinforcement ratio resulted in smaller reinforcement strains at the same load level and consequently, smaller crack widths. While increasing the column dimensions resulted in smaller clear span-to-depth ratio (a/d) which yields smaller flexural moment at the same load level and consequently smaller crack widths.

For both Series, the steel-reinforced prototype showed the smallest crack width. This is due to the high effective reinforcement ratio which ranged from 4.5 to 9.8 times that of GFRP-

reinforced ones in Series I and from 4.5 to 9.6 times that of GFRP-reinforced ones in Series II. To compare the crack width of the different GFRP-reinforced prototypes with that reinforced with steel, reference load values were selected which were 329 kN and 825 kN for Series I and II, respectively. These values represent lowest punching shear capacity in each series (for $G_{(0.7)}30/20$ in Series I and for $G_{(0.3)}30/35$ in Series II). At 329 kN applied load, the crack width of $G_{(1.6)}30/20$ and $G_{(1.6)}45/20$ which had an effective reinforcement ratio equal to 0.22 that of $S_{(1.7)}30/20$ was 1.01 mm and 0.98 mm, respectively. This represents 4.2 times that of $S_{(1.7)}30/20$ (0.24 mm). At 825 kN applied load, the crack width of $G_{(0.7)}30/35$ and $G_{(0.7)}45/35$ which had an effective reinforcement ratio equal to 0.22 that of $S_{(0.8)}30/35$ was 0.70 mm and 0.50 mm, respectively. The pervious represents 2.8 times that of $S_{(0.8)}30/35$ (0.25 mm). This implies that the crack width is strongly related to the axial stiffness of the reinforcement.

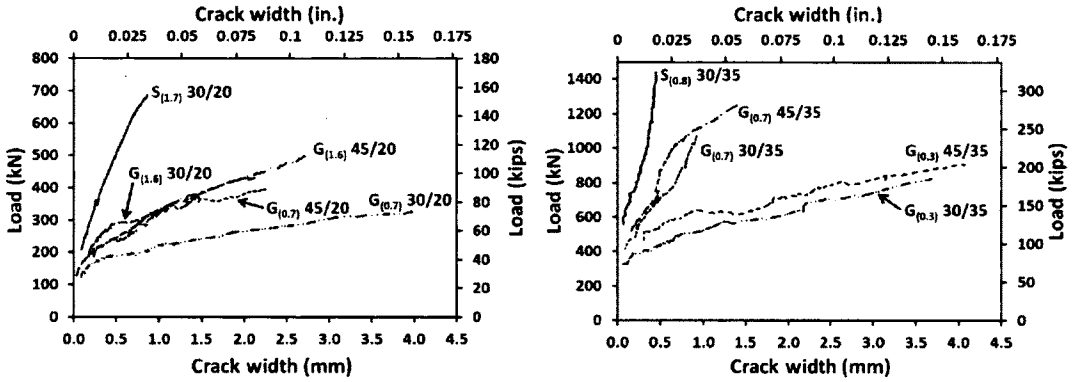

(a) Crack width versus load: Series I and Series II

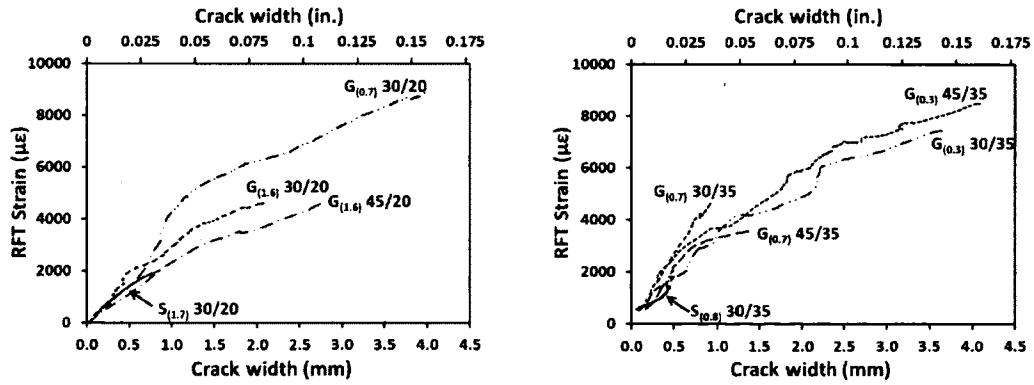

(b) Crack width versus reinforcement strains: Series I and Series II

Figure 4.11: Crack width relationships.

As the crack width is normally related to the strains in the reinforcing bars, the relationships between the measured strains in the reinforcing bars and the measured crack widths were presented in Figure 4.11 (b). This figure confirms the direct relationship between the strains and the crack widths. At early loading stages, only a few cracks appear and their widths are often small. Consequently, the relationships are normally close at early loading stages. The figure also indicates that up to 2,000 microstrains (strain limit provided by ISIS 2007 to keep the crack width less than 0.5 mm), the crack-width strain relationships for each series were close. In addition, at 2,000 the corresponding crack widths were less than 0.5 mm for the two series.

4.5 Comparison of Predictions and Experimental Results

Although there is a multitude of punching-shear provisions in the design codes for steel-reinforced concrete members worldwide, the design codes for FRP-reinforced concrete members do not provide any equations that can be employed to evaluate the punching shear capacity of FRP RC members. On the other hand, there are only two equations provided by Japan Design Recommendations (JCEC 1997) and the ACI 440 committee (2006). Furthermore, El-Ghandour et al. (1999; 2000), Matthys and Taerwe (2000 b), Ospina et al. (2003), and El-Gamal et al. (2005) proposed other equations based on their experimental and analytical investigations to predict the punching capacity of FRP RC members. Current equations were derived by modifying the original steel-reinforced section equations to account for the differences in the mechanical properties of FRP and steel bars. The available equations account for FRP reinforcement instead of steel by introducing the ratio of the modulus of elasticity of the FRP and steel raised to a power of 1/2 or 1/3. Some of the equations—such as JSCE (1997) and Matthys and Taerwe (2000)—introduced other parameters to account for size effect.

Recently, the Canadian Standard Association introduced a new punching-shear strength equation incorporated in the 2012 edition of CSA S806. This section assesses the accuracy of the available equations as well as that of CSA S806-12 by comparing their predictions against the experimental test results from the slabs tested in our investigation. Table 4.4 summarizes the punching-shear capacity equations used for FRP-reinforced concrete slabs.

Table 4.4: Punching strength capacity equations of FRP RC members

Reference	Equation	
JSCE (1997)	$V_c = \beta_d \beta_p \beta_r f_{pcd} b_{o;0.5d} d / \gamma_b f_c$	(4.1 a)
	$\beta_d = (1000/d)^{1/4} \leq 1.5$,	(4.1 b)
	$\beta_p = (100\rho_f E_f/E_s)^{1/3} \leq 1.5$,	(4.1 c)
	$\beta_r = 1 + 1/(1+0.25u/d)$,	(4.1 d)
	$f_{pcd} = 0.2\sqrt{f_c} \leq 1.2$ MPa	(4.1 e)
El-Ghandour et al. (1999)	$V_c = 0.33\sqrt{f_c}\left(\frac{E_f}{E_s}\right)^{1/3} b_{o;0.5d}\, d$	(4.2)
El-Ghandour et al. (2000)	$V_c = 0.79\left[100\rho_f \left(E_f/E_s\right)\cdot\left(0.0045/\varepsilon_y\right)\right]^{1/3} \left(f_{cu}/25\right)^{1/3} \left(400/d\right)^{1/4} b_{o;1.5d}\, d$	(4.3)
Matthys and Taerwe (2000 b)	$V_c = 1.36\frac{\left(100\rho_f E_f/E_s f_c\right)^{1/3}}{d^{1/4}} b_{o;1.5d}\, d$	(4.4)
Ospina et al. (2003)	$V_c = 2.77\left(\rho_f f_c\right)^{1/3}\sqrt{\frac{E_f}{E_s}}\, b_{o;1.5d}\, d$	(4.5)
El-Gamal et al. (2005b)	$V_c = 0.33\sqrt{f_c} b_{o;0.5d}\, d\, \alpha$	(4.6 a)
	$\alpha = 0.5\left(\rho_f E_f\right)^{1/3}\left(1+8d/b_{o;0.5d}\right)$, E_f in GPa	(4.6 b)
ACI 440.1R-06 (2006)	$V_c = \frac{4}{5}\sqrt{f_c} b_{o;0.5d}\, k\, d$	(4.7 a)
	$k = \sqrt{2\rho_f n_f + \left(\rho_f n_f\right)^2} - \rho_f n_f$	(4.7 b)
	where: $n_f = E_f/E_c$; $E_c = 4750\sqrt{f_c}$	
CAN/CSA S806-12 (2012)	The least of the following equations:	
	$V_c = 0.028\lambda\phi_c\left(1+\frac{2}{\beta_c}\right)\left(E_f \rho_f f_c\right)^{1/3} b_{o;0.5d}\, d$	(4.8)
	$V_c = 0.147\lambda\phi_c\left(\frac{\alpha_s d}{b_{o;0.5d}}+0.19\right)\left(E_f \rho_f f_c\right)^{1/3} b_{o;0.5d}\, d$	(4.9)
	$V_c = 0.056\lambda\phi_c\left(E_f \rho_f f_c\right)^{1/3} b_{o;0.5d}\, d$	(4.10)

Notes – SI units; 1 mm=0.0394 in., 1 kN=0.225 kips, 1 MPa=0.145 ksi

Table 4.5 provides the ratios between the experimentally measured and predicted punching capacities (V_{test}/V_{pred}) using the equations in JCEC (1997), El-Ghandour et al. (1999; 2000), Matthys and Taerwe (2000 b), Ospina et al. (2003), El-Gamal et al. (2005), ACI 440.1R-06 (2006), and CSA S806-12 (2012) (see Table 4.4). The safety factors included in all the punching-shear equations were set to 1.0. From the predictions reported in Table 4.5, all

the equations yielded good yet conservative predictions, except for the ACI 440.1R-06 equation (Eq. 4.7). ACI 440.1R-06 yielded very conservative predictions with an average V_{test}/V_{pred} of 2.09±0.30 with a corresponding COV of 14%. The very conservative predictions of the ACI 440.1R-06 equation is referred to that it employs the reinforcement material and ratio only in predicting the depth of the neutral axis. On the other hand, all the other equations include the effect of axial stiffness, such as $(E_f/E_s)^x$, where x = 1/2 or 1/3. Moreover, El-Ghandour et al. (1999) yielded a V_{test}/V_{pred} of 1.18±0.26 with a COV of 22%. This is due to the reinforcement ratio being omitted from this equation (Eq. 4.2). On the other hand, El-Ghandour et al. (2000) which is based on modifying the equation of the BS standard and limiting the strain in the FRP bars to 4,500 microstrains yielded an average V_{test}/V_{pred} of 1.01±0.10 with a COV of 10%.

Table 4.5: Experimental-to-predicted punching capacity (V_{test}/V_{pred})

	Experimental-to-predicted punching capacity V_{test} / V_{pred}							
Prototype	JSCE (1997)	El-Ghandour et al. (1999)	El-Ghandour et al. (2000)	Matthys and Taerwe (2000)	Ospina et al. (2003)	El-Gamal et al. (2005b)	ACI 440.1R (2006)	CAN/CSA S806-12 (2012)[1]
$G_{(0.7)}$30/20	1.11	1.17	0.96	1.21	1.03	1.29	2.08	1.11
$G_{(1.6)}$30/20	1.13	1.50	0.97	1.21	1.04	1.27	1.90	1.11
$G_{(0.7)}$45/20	1.04	0.93	0.88	1.11	0.94	1.13	1.74	0.92
$G_{(1.6)}$45/20	1.10	1.42	0.98	1.23	1.05	1.34	1.74	1.02
$G_{(0.3)}$30/35	1.20	1.03	1.08	1.35	0.95	1.20	2.59	1.25
$G_{(0.7)}$30/35	1.20	1.27	1.05	1.32	0.93	1.14	2.30	1.22
$G_{(0.3)}$45/35	1.11	0.76	0.94	1.18	0.83	0.98	2.08	0.98
$G_{(0.7)}$45/35	1.31	1.36	1.19	1.49	1.05	1.36	2.31	1.24
Mean	**1.15**	**1.18**	**1.01**	**1.26**	**0.98**	**1.21**	**2.09**	**1.11**
S.D.	0.09	0.26	0.10	0.12	0.08	0.13	0.30	0.13
COV (%)	8	22	10	10	8	10	14	11

[1] From equation (4.10).

Furthermore, the JSCE (1997) and Matthys and Taerwe (2000) showed consistently conservative predictions for all test prototypes, because they account for the reinforcement ratio and the size effect. El-Ghandour et al. (1999; 2000), Ospina et al. (2003), El-Gamal et al. (2005), and the CSA S806-12 (2012), however, showed at least one non-conservative prediction. The proposed equation for CSA S806-12 (2012) also showed good, conservative predictions, on average, with an average V_{test}/V_{pred} of 1.11±0.13 and a COV of 11%. The equations proposed by Matthys and Taerwe (2000) and El-Gamal et al. (2005) showed

acceptable agreement with the experimental results with an average V_{test}/V_{pred} of 1.26±0.12 and 1.21±0.13 with corresponding COVs of 10% and 10%, respectively.

4.6 Conclusions

This paper investigated the punching-shear behavior of full-scale, interior slab–column prototypes reinforced with GFRP bars. The following conclusions have been drawn based on the experimental results and discussions presented herein:

- All the tested slab prototypes showed punching-shear failure as well as similar crack patterns, regardless the reinforcement type and ratio. The slab prototypes with low reinforcement ratios showed large plastic deformations prior the punching-shear failure.

- Slab thickness significantly affected punching-shear capacity. Maintaining the same reinforcement ratio and increasing the effective depth by about 115% yielded an average increase of the normalized punching-shear stress at failure by 63%.

- The axial stiffness of the reinforcement significantly affected the punching-shear behavior. Increasing the axial stiffness of the reinforcement increased the punching-shear capacity, decreased reinforcement strains, decreased deflections, and decreased the crack widths.

- The deflection of the tested prototypes was affected by the column dimensions, especially the prototypes with low reinforcement ratios. Due to more and wider cracks in case of low reinforcement ratios, the reduction in the shear-span-to-depth ratio contributes to reducing the deflection as it reduces the moment at the same applied load.

- El-Ghandour et al. (1999; 2000), Ospina et al. (2003), El-Gamal et al. (2005), and the CSA-S806 (2012) equations returned at least one non-conservative prediction for punching-shear capacity. Furthermore, the high standard deviation and coefficient of variation of the El-Ghandour et al. (1999) equation are related to the reinforcement ratio being omitted.

- ACI 440.1R-06 (2006) yielded a very conservative prediction with an average V_{test}/V_{pred} of 2.09±0.30 with a corresponding COV of 14%. JSCE (1997) and Matthys and Taerwe (2000 b) showed consistently reasonable and conservative predictions with

average V_{test}/V_{pred} of 1.15±0.09 and 1.26±0.12, respectively. The equation proposed for CSA S806 (2012) showed accurate yet conservative (on average) predictions with an average V_{test}/V_{pred} of 1.11±0.13.

- Increasing the column dimensions also increased failure surfaces and, consequently, reduced the punching-shear stress at failure. Increasing the square column dimensions from 300 mm [11.8 in.] to 450 mm [17.7 in.] decreased the normalized punching-shear stress at failure of the $G_{(0.7)}45/20$, $G_{(1.6)}45/20$, $G_{(0.3)}45/35$, and $G_{(0.7)}45/35$ prototypes by 29%, 14%, 37%, and 12% compared to their counterparts ($G_{(0.7)}30/20$, $G_{(1.6)}30/20$, $G_{(0.3)}30/35$, and $G_{(0.7)}30/35$, respectively).

CHAPTER 5
PUNCHING SHEAR STRENGTH OF GFRP-REINFORCED SLABS WITHOUT SHEAR REINFORCEMENT

Foreword

Authors Biographies

Mohamed Hassan is a PhD candidate in the Department of Civil Engineering at the University of Sherbrooke, Sherbrooke, Quebec, Canada, J1K 2R1, Phone: 819-821-8000, ext. 63181, Fax: 819-821-7974, E-mail: Mohamed.Hassan@USherbrooke.ca

Ehab A. Ahmed is a Postdoctoral fellow in the Department of Civil Engineering at the University of Sherbrooke, Sherbrooke, Quebec, Canada, J1K 2R1, Phone: 819-821-8000, ext. 62135, Fax: 819-821-7974, E-mail: Ehab.Ahmed@USherbrooke.ca

Brahim Benmokrane, FACI, is a Canada and NSERC Chair Professor in Innovative FRP Materials for Concrete and Civil Structures, Department of Civil Engineering, University of Sherbrooke, Quebec, Canada, J1K 2R1, Phone: 819-821-7758, Fax: 819-821-7974, E-mail: Brahim.Benmokrane@USherbrooke.ca

Acceptation date: 17 April 2013

Acceptation state: published on the web 23 April 2013, 10.1139/cjce-2012-0177

Journal: *Canadian Journal for Civil Engineering (CJCE).*

Reference: Hassan, M., Ahmed, E., and Benmokrane, B., 2012, "Punching-Shear Behavior of Flat Slabs Reinforced with Glass Fiber-Reinforced Polymer Bars", *Canadian Journal for Civil Engineering (CJCE)*, in press.

Titre en français: "Résistance au poinçonnement de dalles en béton renforcé de PRFV".

Paper's contribution to the project: The experimental study was extended in this paper to complete the test matrix presented in the first paper (pervious chapter 2). The punching-shear behaviour of 17 test specimens without shear reinforcement divided into 4 Series was discussed and analysed. Extended parameters such as concrete strength (ranged between 30 MPa to 47 MPa) and GFRP compression reinforcement crossing the column cross section were highlighted. Comparisons between the experimental test results and the theoretical predictions values by the Canadian Standards code CSA S806-12 (2012), design guidelines and different approaches from the literatures are performed.

Abstract: This paper investigates the punching-shear behavior of two-way flat slabs reinforced with glass fiber-reinforced polymer (GFRP) bars. A total of 17 full-scale interior slab-column specimens measuring 2500 mm × 2500 mm reinforced with GFRP and steel bars were constructed and tested under concentric loads till failure. The test parameters were: (i) reinforcement type (GFRP and steel) and ratio (0.34% to 1.66%); (ii) slab thickness (200 mm and 350 mm); (iii) column dimensions (300 mm × 300 mm; 450 mm × 450 mm); (iv) concrete strength (30 to 47 MPa); and (v) GFRP compression reinforcement crossing the column cross section. The test results were reported in terms of cracking behavior, deflection, strains in concrete and reinforcement, punching-shear capacity, and mode of failure. The test results were also employed to assess the accuracy of the available punching-shear capacity equations, including the new punching equation in Canadian Standards CAN/CSA S806-12 (2012).

Keywords: Punching shear; Two-way; Flat slab; Slab–column; Slab; Fiber-reinforced polymer; Thickness; Design.

5.1 Introduction

Steel-reinforced two-way flat slabs are popular as a construction system that simplifies and speeds up site operations, allows easy and flexible partitioning of space, and reduces overall building height. This construction system is often used for parking structures. The optimum design of reinforced-concrete (RC) flat slabs is often compromised by their ability to resist shear stresses at supporting columns. The connections between slabs and supporting columns could be susceptible to high shear stresses and might cause brittle and sudden punching-shear failure. These connections may become the starting points leading to catastrophic punching-shear failure of a flat slab system when the steel reinforcement corrodes due to harsh environmental and exposure conditions (deicing salts, moisture, freeze-thaw cycles, and chlorides).

The use of fiber-reinforced polymer (FRP) bars instead of steel bars, especially where steel corrosion is a major concern, has emerged as an effective solution to reduce structure maintenance costs and extend structure service life. The punching-shear strength of steel-reinforced two-way flat slabs has received a great attention for decades. Few studies, however, have investigated the punching-shear behavior of two-way flat slabs reinforced with FRP bars and grids (El-Ghandour et al. 1999 & 2003; Matthys and Taerwe 2000 b; Ospina et al. 2003; Hussein et al. 2004; Zhang et al. 2005, Lee et al. 2009). This research indicated that GFRP-reinforced two-way flat slabs showed lower punching-shear capacities, lower post-cracking stiffness, and greater crack widths than their counterparts reinforced with steel bars when the same reinforcement amount was used. This is due to the lower axial stiffness of the GFRP bars in comparison to steel bars (E_f/E_s=0.25 approximately). Matthys and Taerwe (2000 b) reported that FRP-reinforced two-way flat slabs and steel-reinforced slabs designed with similar levels of flexural stiffness had similar punching-shear capacities. Ospina et al. (2003) concluded that FRP grids in two-way flat slabs might not provide the same punching-shear capacity as FRP bars due to the difference in bond behavior and concentration of stresses in the grids where the orthogonal reinforcement intersected. Moreover, Lee et al. (2009) showed that concentrating the GFRP top flexural-reinforcement mat within a distance 1.5 times the slab thickness from the column faces resulted in a slightly higher punching-shear capacity. Excessive

concentrations of slab reinforcement (ρ = 3%), however, seemed to be ineffective in increasing the punching-shear capacity of GFRP RC slabs.

The previous research work on FRP-reinforced concrete flat slabs employed slab thicknesses of 75 mm (Banthia et al. 1995), 100 mm (Zaghloul and Razaqpur 2004), 120 and 150 mm (Matthys and Taerwe 2000 b; Hussein et al. 2004; Lee et al. 2009), 155 mm (Ospina et al. 2003) and 175 mm (El-Ghandour et al. 2003). The advancement in FRP manufacturing industry accompanied with the new punching-shear equation of CSA S806-12 (2012) Canadian Standard contributed to the first world-wide parking garages reinforced with GFRP bars in Quebec City, Canada (Benmokrane et al. 2012). In these applications, the thickness of the flat slabs was 250 mm in the flexural areas and 355 mm in the punching areas. Thus, there was a need to investigate the punching-shear performance of full-scale slab-column connections and evaluate the accuracy of the current available punching-shear equations.

This paper presents the results of an extensive research project conducted at the University of Sherbrooke to investigate the behavior of full-scale interior two-way flat slab-column connections reinforced with GFRP bars under concentric loading. It also compares their behavior with that of counterparts reinforced with steel bars. Moreover, the experimental results of this investigation were employed in assessing the accuracy of the new CSA S806-12 (2012) punching-shear equation as well as other equations from codes, guidelines, and the literature.

5.2 Experimental Program

5.2.1 Test Specimen Details

A total of 17 flat slab specimens were constructed and tested to investigate the following parameters: (i) reinforcement type (GFRP and steel) and ratio (0.34% to 1.66%); (ii) slab thickness (200 mm and 350 mm); (iii) column dimensions (300 mm × 300 mm; 450 mm × 450 mm); (iv) concrete strength (30 to 47 MPa); and (v) GFRP compression reinforcement crossing the column cross section. The test specimens were designed to represent isolated interior slab–column connections. The specimens measured 2500 mm × 2500 mm, either 200 mm or 350 mm in thickness, while the square column stub measured 300 mm × 300 mm or 450 mm × 450 mm. The column stub extended 300 mm

beyond the top and bottom surfaces of the slabs. Figure 5.1 shows the geometry and typical reinforcement configuration of the test specimens.

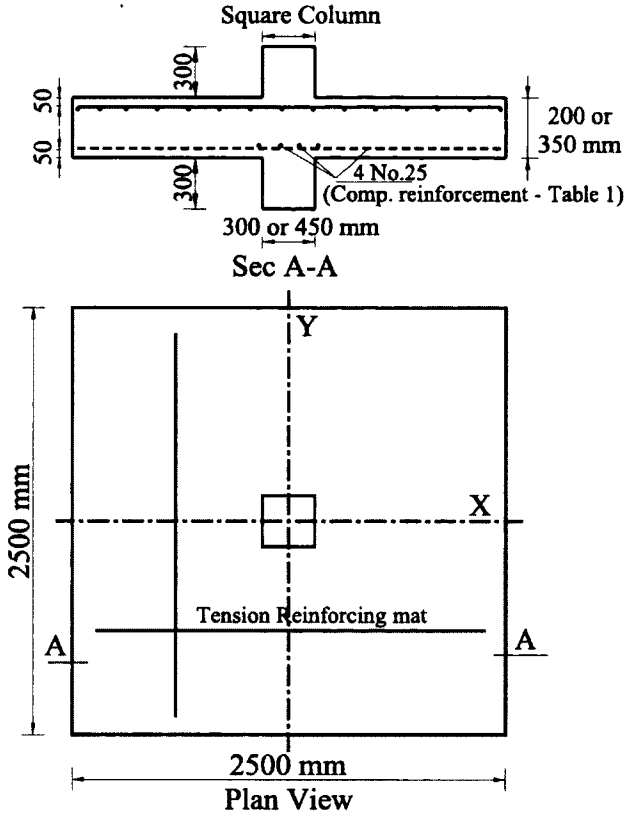

Figure 5.1: Geometry and reinforcement configuration

For the FRP-reinforced specimens, the clear concrete cover was kept constant at 50 mm to satisfy the fire endurance design criteria. The 50 mm clear cover, however, was maintained for the steel-reinforced specimens for comparisons. Two different slab thicknesses were used: the 200 mm thickness represents a common slab thickness in flat slabs; the 350 mm thickness represents a 200 mm slab with a drop panel of 150 mm. The test specimens were designed to simulate real thicknesses flat slabs being used in the field applications (Benmokrane et al. 2012). The specimens were divided into four series (I to IV) according to column dimensions and slab thickness. Series I and II specimens were 200 mm thick and had square sections of 300 mm or 450 mm, respectively. There were 8 specimens in these two series: 7 reinforced with GFRP bars with a reinforcement ratio ranging from 0.71% to 1.56%, and 1 reinforced with steel bars with a reinforcement ratio of 1.66%. Series III and IV specimens were 350 mm thick and had square sections of 300 mm or 450 mm, respectively.

These two series had 9 specimens: 8 reinforced with GFRP bars with a reinforcement ratio ranging from 0.34% to 0.73%, and 1 reinforced with steel bars with a reinforcement ratio of 0.77%. The reinforcement ratio was selected to cover a wide range of ρ/ρ_b from 0.58 to 3.32. Table 5.1 presents the test matrix and characteristics of each test specimen.

Table 5.1: Details of test specimens

Series	Specimen [a]	Slab thick., mm	Reinf. type	Tens reinf.	ρ, %	ρ/ρ_b [c]	Comp. reinf.	Column dim., mm	f'_c [d], MPa	f_t [d], MPa
I	$G_{(0.7)}30/20$	200	GFRP	12 No. 15	0.71	1.45	-	300	34	2.5
	$G_{(0.7)}30/20$-B			12 No. 15	0.71	1.37	4 No. 25	300	39	2.8
	$G_{(1.6)}30/20$			18 No. 20	1.56	3.00	-	300	39	2.8
	$G_{(1.6)}30/20$-B			18 No. 20	1.56	3.32	4 No. 25	300	32	2.3
	$S_{(1.7)}30/20$		Steel	18-20M	1.66	0.36	-	300	45	2.8
II	$G_{(0.7)}45/20$		GFRP	12 No. 15	0.71	1.25	-	450	45	2.9
	$G_{(1.6)}45/20$			18 No. 20	1.56	3.32	-	450	32	2.3
	$G_{(1.6)}45/20$-B			18 No. 20	1.56	2.94	4 No. 25	450	39	2.3
III	$G_{(0.3)}30/35$	350	GFRP	12 No. 15	0.34	0.69	-	300	34	2.5
	$G_{(0.3)}30/35$-B			12 No. 15	0.34	0.64	4 No. 25	300	39	2.3
	$G_{(0.7)}30/35$			18 No. 20	0.73	1.38	-	300	39	2.3
	$G_{(0.7)}30/35$-B-1 [b]			18 No. 20	0.73	1.24	4 No. 25	300	30	2.7
	$G_{(0.7)}30/35$-B-2 [b]			18 No. 20	0.73	1.66	4 No. 25	300	47	2.7
	$S_{(0.8)}30/35$		Steel	18-20M	0.77	0.20	-	300	39	2.8
IV	$G_{(0.3)}45/35$		GFRP	12 No. 15	0.34	0.58	-	450	49	2.6
	$G_{(0.3)}45/35$-B			12 No. 15	0.34	0.74	4 No. 25	450	32	2.3
	$G_{(0.7)}45/35$			18 No. 20	0.73	1.66	-	450	30	2.7

[a] G or $S_{(x.x)}$yy/zz-B: G denotes GFRP, S denotes steel, (x.x) denotes the reinforcement ratio, yy/zz denotes column dimension (yy) and slab thickness (zz), and B refers to the presence of bottom reinforcement in the compression side, if any.

[b] $G_{(0.7)}30/35$-B-1and $G_{(0.7)}30/35$-B-2 differ in concrete strength (30 and 47 MPa, respectively).

[c] ρ_b was calculated according to ACI 440.1R (2006) for GFRP-RC slabs and ACI 318 (2008) for steel-RC slabs.

[d] Based on 150×300 mm cylinder testing.

5.2.2 Material Properties

No. 15, No. 20, and No. 25 sand-coated GFRP reinforcing bars, designated according to CAN/CSA S807-10 (2010), were used in the GFRP-reinforced specimens. The GFRP bars used herein were manufactured by combining the pultrusion process with an in-line process for coating the bar surface with sand. This sand coating was designed to improve bonding between the GFRP bars and surrounding concrete. The tensile properties of the GFRP bars were determined by testing five representative bars for each diameter in accordance with B.2

Test Method of the ACI 440.3R (2004). Table 5.2 gives the mechanical properties of the GFRP bars, as determined from testing. The reference-slab specimens, however, were reinforced with 20M steel bars.

Table 5.2: Properties of the GFRP reinforcing bars

Bar size	Area, mm^2	Elastic tensile modulus, E_f, GPa	Ultimate tensile strength, MPa	Guaranteed tensile strength, MPa[a]	Ultimate tensile elongation, %
No. 15	199	48.2±0.4	769±23	700	1.60±0.05
No. 20	284	48.1±0.7	765±31	672	1.59±0.08
No. 25	510	46.1±0.7	660±11	626	1.43±0.02

[a] Guaranteed tensile strength = Average value – 3 × standard deviation.

The slab specimens were cast using a ready-mixed, normal-weight concrete with 5% to 8% of entrained air. The concrete compressive (f_c') and tensile strength (f_t') for each specimen were determined on the day of testing from three concrete cylinders measuring 150 mm × 300 mm for each test (compression and splitting test cylinders). The concrete compressive strength ranged from 30 MPa to 49 MPa, while the tensile strength ranged from 2.3 MPa to 2.9 MPa. Figure 5.2 shows the fabrication of test specimens while Table 5.1 provides the concrete properties.

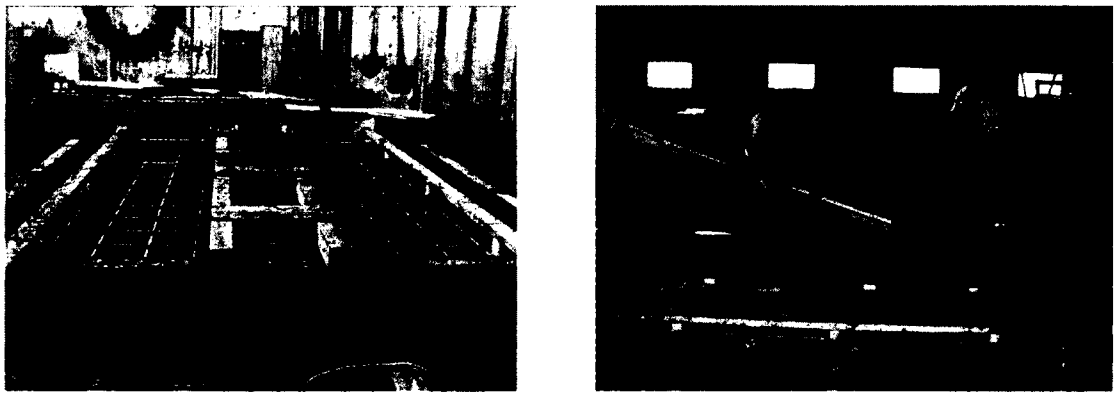

(a) (b)

Figure 5.2: Fabrication of the test specimens: a) Reinforcing cages; b) Concrete casting

5.2.3 Instrumentation and test setup

Each slab specimen was equipped with 2 instrumented bars in the orthogonal directions in the top reinforcing mat (tension side) with 6 electrical strain gauges attached to each bar. In addition, 8 electrical strain concrete gauges were glued to the bottom surface of the slab (compression side) before testing. Moreover, the 8 steel anchors supporting the test specimen were instrumented with electrical strain gauges to verify loading symmetry during the tests. The deflection of the test specimens at the desired locations was captured using 6 linear-voltage differential transformers (LVDTs), whereas the crack width was measured with two LVDTs. Crack appearance was monitored during the test by visual inspection until the first two cracks appeared. Thereafter, their initial widths were measured with a handheld microscope with a magnifying power of 50X. Then, the two LVDTs were installed at the locations of the first two cracks. The strain gauges and LVDTs were connected to a data-acquisition system to record the readings during the test. Figure 5.3 shows the locations of the strain gauges and LVDTs. During the test, crack propagation was marked and the corresponding load recorded.

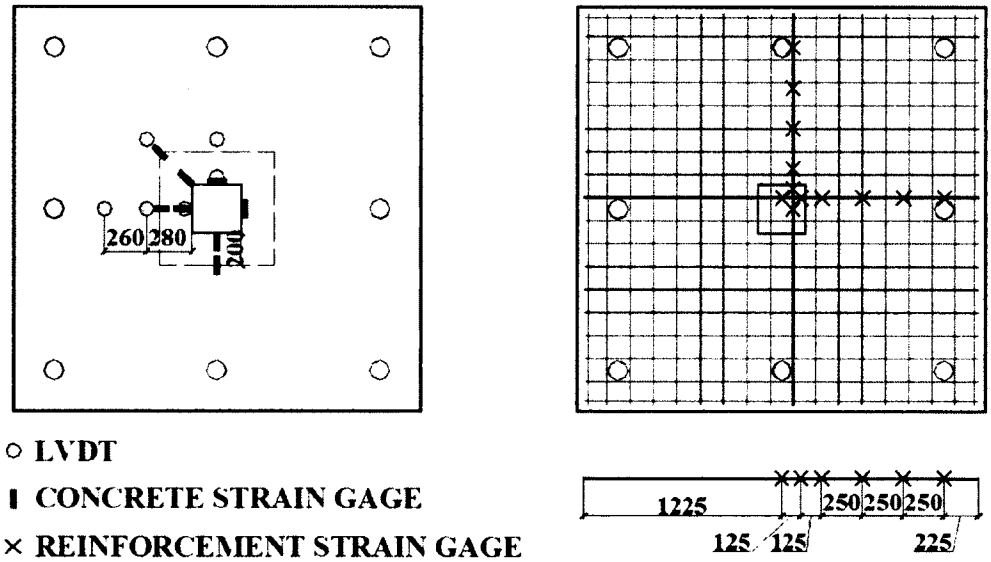

Dimensions in mm

Figure 5.3: Instrumentation plan

The specimens were tested in the structural laboratory at the University of Sherbrooke under monotonic loading till failure. The load was applied at a load-controlled rate of 5 kN/min. The load was applied using one or two 1500 kN hydraulic jacks until slab failure. The slab specimens were held against the rigid floor of the laboratory using a rigid steel frame 100 mm in width supported by 8 steel anchors, each measuring 38 mm in diameter. The slabs tested had clear spans of 1900 mm. Before fixing the steel frame, a 15 mm thick cement mortar was placed on the concrete surface at the location of the steel frame. Thereafter, to prevent local failure and to distribute the load uniformly, 10 mm-thick neoprene sheets were used over the loading plate and between the supporting frame and the slab, respectively. Figure 5.4 provides the details of the test setup.

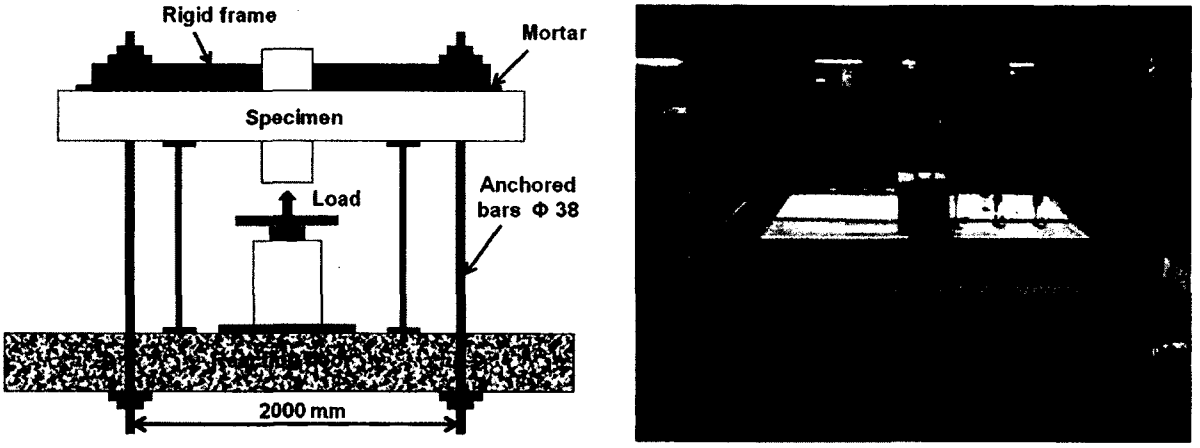

a) b)

Figure 5.4: Test setup: (a) Schematic and dimensions; (b) Specimen testing

5.3 Test Results and Discussion

5.3.1 Cracking and failure characteristics

The first cracks to appear in all the tested specimens were flexural radial cracks in the region of the maximum moment in the tension (top) side of the slab. The cracks started at the column corners parallel to X and Y axes thereafter propagated radially towards the slab edges. At higher loads, small cracks appeared at the column interface along the perimeter. Moreover, circumferential cracks were observed near the column connecting the radial cracks together.

Finally, the circumferential cracks were dominated by a punching-shear crack forming the punching cone.

Regardless of the reinforcement type and ratio, the final failure mode for all test specimens was punching-shear. The punching-shear failure was confirmed by a sudden drop in the applied load, accompanied by the appearance of a wide, clear crack defining the failure surface of the specimens around the columns. The slab specimens with low reinforcement ratios, however, showed more flexural cracks around the column and some ductile behavior before the punching-shear failure. Furthermore, the GFRP specimens with compression reinforcement showed some gradual softening at the peak zone. Figure 5.5 shows a typical crack pattern at failure for some of the tested specimens. As the development of the inner critical shear crack is not visible, some of the tested slab specimens were sawn, allowing observation of the final crack pattern. Figure 5.5 also shows the cross section of some of the test specimens with the critical shear crack emphasized. This figure shows that the specimens exhibited a main diagonal shear crack starting at the column face with variable inclination angles. It should be mentioned that specimen $G_{(1.6)}45/20$, which had a maximum measured concrete strain of 4195 microstrains, exhibited no concrete crushing and, as shown in Figure 5.5, the critical diagonal crack confirms that this specimen failed as a result of punching.

Similar crack patterns and punching-shear surface failure were observed when the same reinforcement ratios of GFRP and steel were used as in specimens $G_{(1.6)}30/20$ and $G_{(0.7)}30/35$ and their steel-reinforced counterparts, $S_{(1.7)}30/20$ and $S_{(0.8)}30/35$, respectively. This indicates that the crack pattern and failure mode were not dependent on reinforcement type. The failure surface was marked on the slabs as shown in Figure 5.5. The distance from the column face of each specimen to the location of the failure surface (X_{cone}) was used to define the observed failure surface. This distance (X_{cone}) was measured at different locations; the average values were calculated and reported in Table 3 (multiples of d). Figure 5.5 and Table 5.3 demonstrated that the 200 mm thick specimens had a smaller failure surface than the 350 mm thick specimens due to the slabs' smaller effective depth. In addition, increasing the effective reinforcement ratio ($\rho E_r/E_s$, where E_r is the modulus of elasticity of the reinforcing bars) increased the observed failure surface (represented by X_{cone}). Furthermore, the observed failure surfaces (X_{cone}) of the test specimens with compression reinforcement were larger than their counterparts without compression reinforcement.

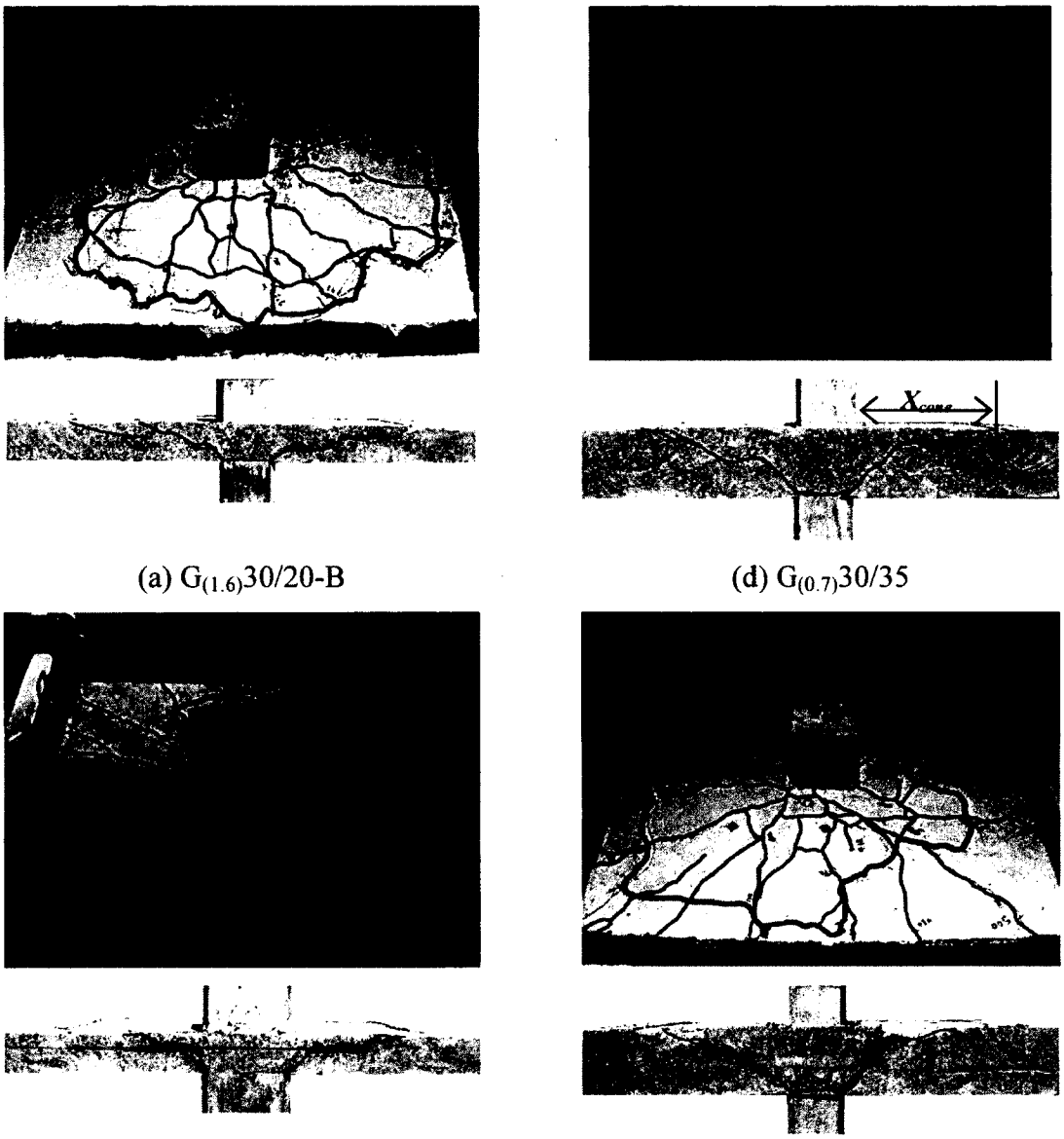

(a) $G_{(1.6)}30/20$-B (d) $G_{(0.7)}30/35$

(b) $G_{(1.6)}45/20$ (c) $G_{(0.3)}30/35$

Figure 5.5: Typical punching-shear failure for the tested specimens

The average X_{cone} distance was $2.5d$ and $1.7d$ for specimens of 200 mm and 350 mm thickness, which corresponds to average angles equal 22° and 30° degree, respectively. Assuming that the critical section for design intersects with the main diagonal shear crack at the middle depth of the slab, the results imply that the critical section is located at $1.25d$ and $0.85d$ from the column face for 200 mm and 350 mm thick specimens, respectively.

Table 5.3: Summary of the test results

Series	Specimen	ρ (E_f/E_s), %	V_{cr}, kN	Δ_{cr}, mm	V_u, kN	ΔV_u, mm	Δ_u, mm	$v_{u,0.5d}/\sqrt{f_c'}$, $\sqrt{\text{MPa}}$	Post-cracking stiffness, kN/mm	X_{cone}	Max. reinf. strain, (με)	Max. conc. strain, (με)
I	$G_{(0.7)}30/20$	0.17	125	0.67	329	21.8	24.0	0.24	7.9	2.3d	8975	-1280
	$G_{(0.7)}30/20$-B	0.17	120	1.52	386	17.0	25.6	0.27	12.2	2.5d	5174	-1384
	$G_{(1.6)}30/20$	0.38	211	1.70	431	15.9	21.7	0.31	15.1	2.8d	5010	-340
	$G_{(1.6)}30/20$-B	0.38	142	1.36	451	15.5	20.7	0.35	19.1	3.3d	4685	-2213
	$S_{(1.7)}30/20$	1.66	163	0.10	688	15.7	28.8	0.45	34.3	2.8d	2030	-2670
II	$G_{(0.7)}45/20$	0.17	216	2.34	400	20.9	21.0	0.19	11.5	1.7d	9250	-1530
	$G_{(1.6)}45/20$	0.38	142	0.94	504	18.7	26.8	0.29	19.5	2.2d	4795	-4195
	$G_{(1.6)}45/20$-B	0.38	173	1.31	511	17.9	22.8	0.27	20.6	2.8d	4814	-2362
III	$G_{(0.3)}30/35$	0.08	338	1.37	825	16.2	24.6	0.21	29.3	1.3d	8190	-2300
	$G_{(0.3)}30/35$-B	0.08	367	1.61	782	12.3	13.9	0.19	31.0	1.7d	5538	-1269
	$G_{(0.7)}30/35$	0.18	415	1.22	1071	12.0	16.8	0.26	53.3	1.9d	4625	-215
	$G_{(0.7)}30/35$-B-1	0.18	401	2.09	1027	12.1	17.3	0.27	56.4	2.1d	5540	-1272
	$G_{(0.7)}30/35$-B-2	0.18	440	1.18	1195	12.6	15.4	0.29	53.5	1.9d	5259	-310
	$S_{(0.8)}30/35$	0.77	444	1.47	1692	10.8	17.4	0.42	123.6	1.8d	6955	-1190
IV	$G_{(0.3)}45/35$	0.08	460	2.01	911	13.3	15.0	0.16	39.0	1.4d	8512	-670
	$G_{(0.3)}45/35$-B	0.08	449	1.90	1020	18.4	23.0	0.21	37.8	1.9d	8326	-1644
	$G_{(0.7)}45/35$	0.18	447	2.41	1248	15.8	20.2	0.28	66.9	1.7d	6185	-1270

Note: $v_{u,0.5d}$ = ultimate shear stress at $d/2$ from the column face; X_{cone}= distance from the column face to the failure surface.

5.3.2 Load-deflection responses

Figure 5.6 shows the load–deflection relationships for the tested specimens. The LVDTs were placed 40 mm from the column face. The test specimens as a whole showed bilinear load-deflection response till sudden failure due to punching, which becomes evident with the immediate, significant drop in applied load. The first portion is up to the appearance of the first crack and reflects the stiffness of the uncracked section. The second portion reflects the decrease in the post-cracking stiffness until failure. The post-cracking stiffness was calculated from the slope of the second portion of load–deflection response and reported in Table 5.3. The GFRP specimens reinforced with bottom GFRP in the compression side of the slab showed some gradual softening response in the peak zone. The post-cracking response, however, was dependent on the reinforcement type and ratio (reinforcement axial stiffness). Higher axial reinforcement stiffness results in higher post-cracking stiffness and lower deflection values (see Figure 5.6). Moreover, employing the same reinforcement ratio of GFRP and steel reinforcement in the test specimens yielded higher deflection values in the

GFRP-reinforced specimens than that of steel-reinforced one at the same load level, because the GFRP bars had lower moduli of elasticity values than steel bars (E_f/E_s=0.25 approximately). This, in turn, resulted in reduced effective moments of inertia in the slabs. Moreover, it should be mentioned that the GFRP-reinforced slab specimens with lower reinforcement ratios exhibited more flexural cracks surrounding the column and larger deformation (Figure 5.6) before punching-shear failure. In addition, the GFRP specimens reinforced with bottom GFRP bars in the compression side showed higher post-cracking stiffness compared to their counterparts.

On the other hand, increasing the column dimensions from 300 mm to 450 mm increased the post-cracking stiffness of the test specimens due to a smaller shear-span-to-depth ratio. Moreover, increasing the concrete compressive strength (f_c') from 30 MPa to 47 MPa increased the cracking load by 10%.

5.3.3 Punching-shear strength

Table 5.3 presents the ultimate punching-shear capacities and the corresponding normalized punching-shear stresses calculated at $d/2$ from the column face of the specimens. It should be noted that the reported load values include specimen dead load. The punching-shear stresses at failure were normalized to the square root of the concrete strength to account for the variation in concrete strengths. Moreover, the effective reinforcement ratios ($\rho E_f/E_s$) of the specimens were presented to account for the difference between the moduli of elasticity of the GFRP and steel bars. The test results revealed that, with the same reinforcement type, the punching-shear capacity increased as did the reinforcement ratio. Increasing the reinforcement ratio of the GFRP-reinforced specimens from 0.71% to 1.56% in series I ($G_{(0.7)}$30/20 & $G_{(1.6)}$30/20) and II ($G_{(0.7)}$45/20 & $G_{(1.6)}$45/20) slabs increased the normalized punching-shear stress at $d/2$ from the column face by 29% and 53%, respectively. Similarly, increasing the GFRP reinforcement ratio from 0.34% to 0.73% in series III ($G_{(0.3)}$30/35 & $G_{(0.7)}$30/35) and IV ($G_{(0.3)}$45/35 & $G_{(0.7)}$45/35) increased the normalized punching-shear stresses at $d/2$ from the column face by 24% and 75%, respectively.

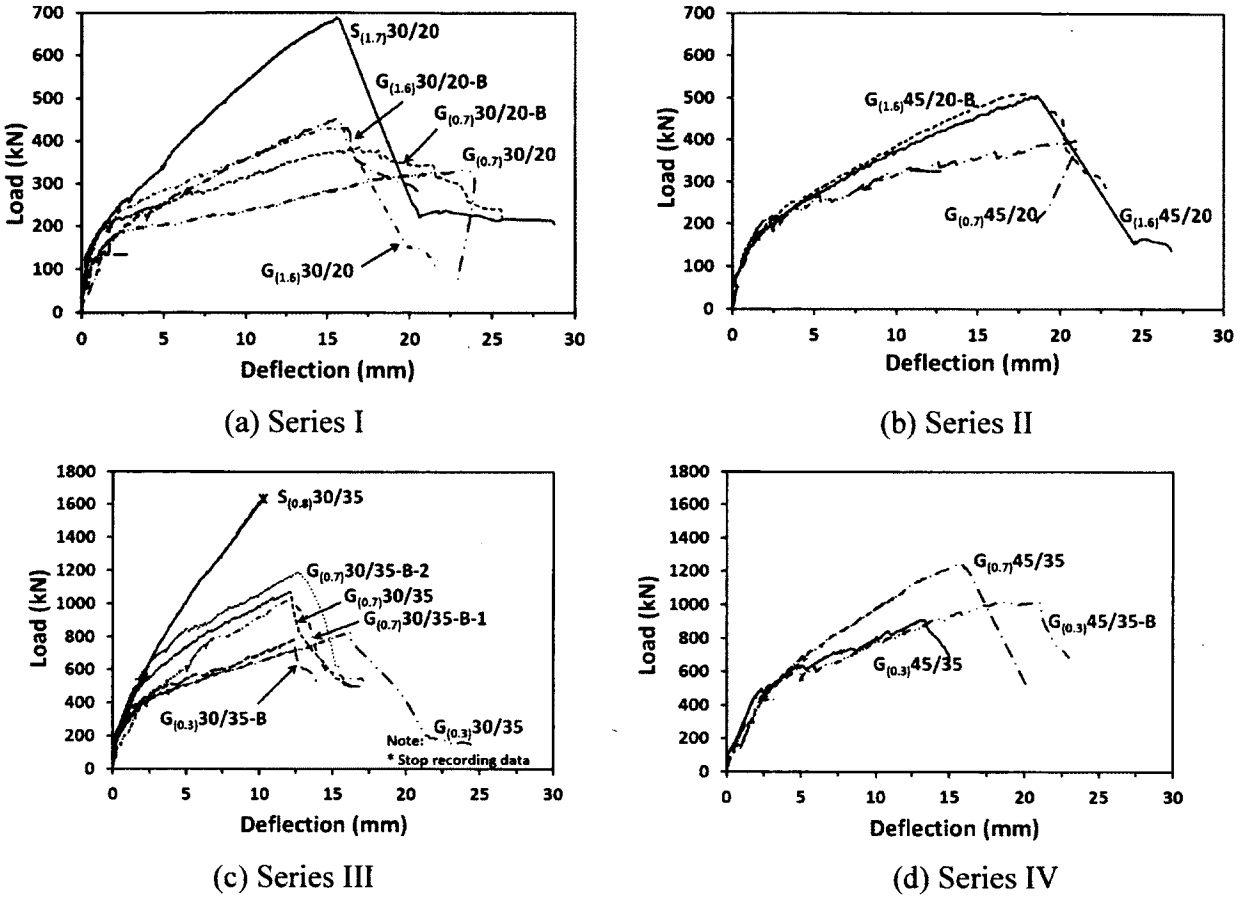

Figure 5.6: Load–deflection responses: (a) Series I; (b) Series II; (c) Series III; (d) Series IV

Slab thickness was one of the parameters most affected the punching-shear capacity, with punching-shear capacity increasing with slab thickness. Increasing the slab thickness from 200 mm to 350 mm in specimens $G_{(0.7)}30/20$ & $G_{(0.7)}30/35$; $G_{(0.7)}30/20$-B & $G_{(0.7)}30/35$-B-2; and $G_{(0.7)}45/20$ & $G_{(0.7)}45/35$, increased the normalized punching-shear stress at failure by 8%, 7% and 47%, respectively. Thus, increasing slab thickness directly impacts on punching capacity because it increases the surface area that resists the punching-shear stress, which, in turn, increases punching-shear capacity. Figure 5.7 shows the variation of the normalized shear stress versus the average effective depth of test specimens. It can be observed from this figure that the trend of the data did not show clearly a size effect with the normalized punching shear stress by increasing slab effective depth from 131 mm to 280 mm. This is in contrast with the steel-reinforced two-way slabs (Mitchell et al, 2005), which the normalized punching-shear stress decreasing with increased values of d. This may due percentage of the (a/d) was varied for the specimens which had an effect on the punching

shear stress. More investigation, however, are needed size effect of the GFRP-reinforced two-way slab.

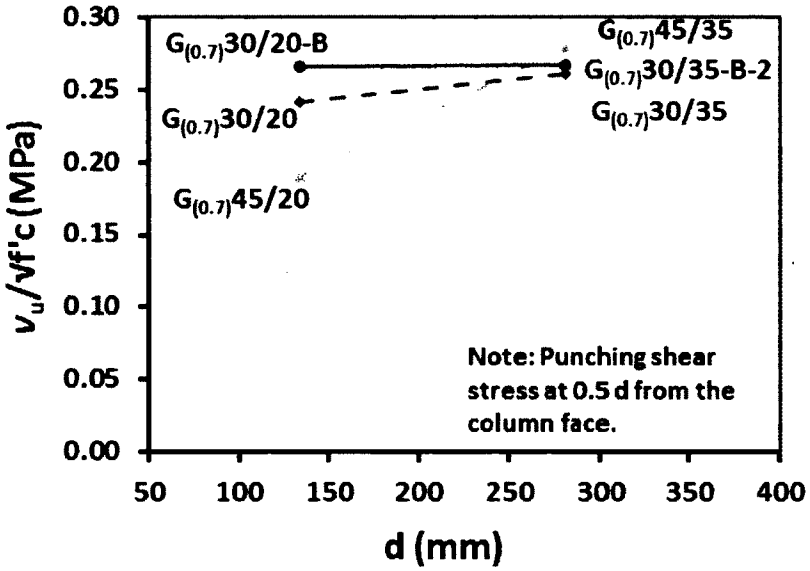

Figure 5.7: Normalized punching shear stress versus average effective depth

The results in Table 5.3 show that the GFRP-reinforced specimen with the same reinforcement ratio as its steel-reinforced counterpart yielded lower normalized punching-shear stress at failure (31% lower in series I and 38% lower in series III). This was attributed to the low modulus of elasticity of GFRP reinforcing bars which equals about 25% that of steel (E_f/E_s=0.25 approximately). In addition, the neutral-axis depth in the cracked sections before failure, calculated from the strain measurements, was very small. The GFRP bars placed in the compression side (in some specimens) contributed to the tension-side reinforcement, which slightly enhanced the punching-shear capacity for some specimens compared to their counterparts without compression reinforcement.

The effective reinforcement ratio, $\rho\ E_f/E_s$, (indicating the axial stiffness of the reinforcing bars) was used to account for the differences in the properties of steel and GFRP bars. The normalized punching-shear stress was plotted against the effective reinforcement ratio, as shown in Figure 5.8. In the series I and III specimens, the normalized punching-shear stress increased as did the effective reinforcement ratio. When the effective reinforcement ratio, $\rho\ E_f/E_s$, increased from 0.17% to 1.66% (series I) and from 0.08% to 0.77% (series III), the normalized punching-shear stress at failure increased by 88% and 100%, respectively. Moreover, Figure 5.8 shows that the normalized punching-shear stress was proportional to the

reinforcement axial stiffness. Thus, regardless of the reinforcement type, the two-way flat slabs with reinforcing bars having the same axial stiffness may fail at the same punching-shear capacity.

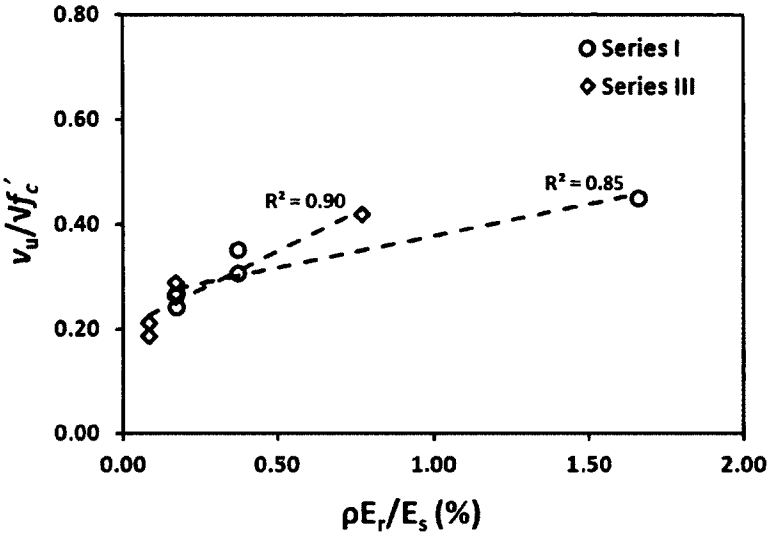

Figure 5.8: Normalized punching-shear stress at $d/2$ from column face versus the reinforcement axial stiffness.

Increasing the column dimensions also increased failure surfaces and, consequently, reduced the punching-shear stress at failure. Increasing the square column dimensions from 300 mm to 450 mm decreased the normalized punching-shear stress at failure of all specimens except specimens $G_{(0.3)}45/35$-B and $G_{(0.7)}45/35$, compared to their counterparts. The decrease ratio in the punching-shear stress at failure ranged from 7% to 24%. Figure 5.9 shows the normalized punching shear stress against the ratio b_o/d. As stated by (Sherif and Dilger 1996) that for small values of the ratio of the perimeter of the slab critical section to slab effective depth (b_o/d), the shear failure involves a complex three-dimensional failure surface that is well confined by the in-plane stresses within the slab. As the ratio (b_o/d) is increased, the confinement is reduced, resulting in a decrease in shear strength. This could explain the decreasing of the normalized punching stress. On the other hand, increasing the column size make a high concentration of the stresses at the corners of the column higher than the stress in the middle, which may have a significant difference led to decreases the punching-shear stress. Figure 5.9 shows effect of b_o/d on the shear strength of the test specimens.

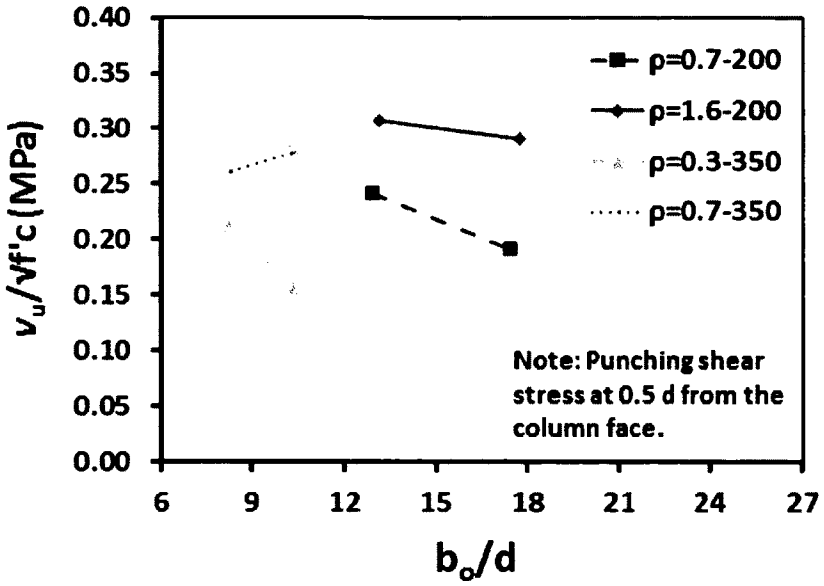

Figure 5.9: Effect of b_o/d on the shear strength of the test specimens

Increasing the concrete compressive strength (f_c') from 30 MPa to 47 MPa increased the normalized punching-shear stress by 17%. Figure 5.10 shows the relationships between the concrete strength and the punching-shear stress at $d/2$ from the column face at failure of similar specimens with different concrete strengths. Neglecting the effect of the reinforcement placed in the compression sides, it could be concluded that increasing the concrete strength increases the punching-shear stress at failure. More investigations, however, are needed.

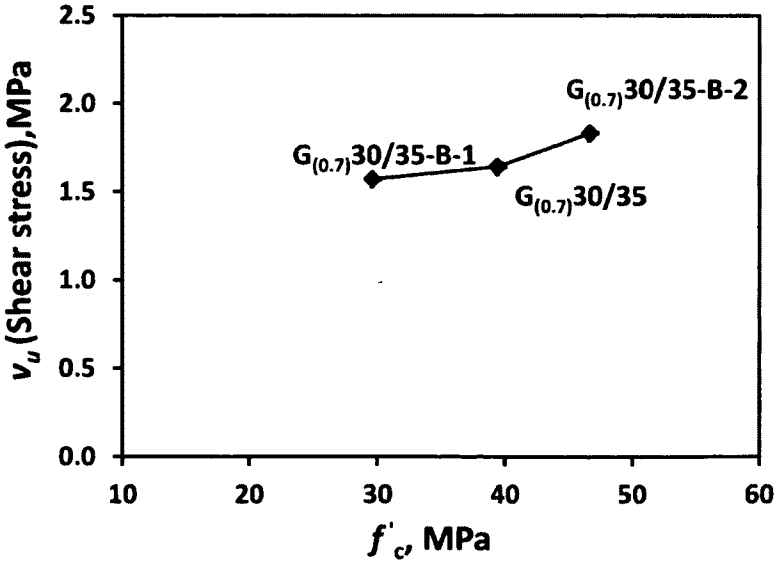

Figure 5.10: Punching-shear stress at $d/2$ from column face versus f'_c.

5.3.4 Reinforcement strains

Figure 5.11 plots the load versus the reinforcement strain relationships. This figure uses the strain values recorded from the electrical resistance strain gauges located at 125 mm and 250 mm from the center of the 300 mm and 450 mm square columns, respectively. The specimens with lower axial reinforcement stiffness showed greater strain at the same load level in series I to IV. The steel-reinforced specimen $S_{(0.8)}30/35$ showed a clear yielding of the steel bars at a corresponding applied load of 1600 kN. In contrast, steel-reinforced specimen $S_{(1.7)}30/20$ showed no signs of yielding.

In the case of the GFRP-reinforced specimens, the maximum measured reinforcement strain was 9250 microstrains, which represents 57% of guaranteed tensile strength. This relatively low strain at ultimate in the slabs reinforced with GFRP bars shows that punching in the slabs was not triggered by GFRP-bar rupture. The concrete strains near the column region in all the specimens (Table 5.3) were low and below the theoretical crushing failure of 3500 microstrains (CSA S806-12 2012) except for specimen $G_{(1.6)}45/20$ (4195 microstrains). At punching failure, however, neither concrete crushing in the compression zone nor rupture of the GFRP reinforcement was observed. Thus, the punching-shear capacity of the compression zone was controlled by concrete splitting tension rather than concrete crushing. Furthermore, Figure 5.11 also confirms that the specimens with GFRP reinforcement in the compression side exhibited lower strains compared to their counterparts without compression reinforcement.

The reinforcement strain distribution along the span of specimens $S_{(0.8)}30/35$ and $G_{(0.7)}30/35$ is shown in Figure 5.12. Despite the higher strains in the GFRP-reinforced specimen, the two specimens showed similar profiles until a load below the yielding of the steel-reinforced one. The strain profiles of the specimens are similar to that reported by Hussein et al. (2004). In addition, the strain values decreased as the distance from the column face increased, until it reached zero at about 1000 mm from the column face. This implies that no bond failure or slip occurred during the tests.

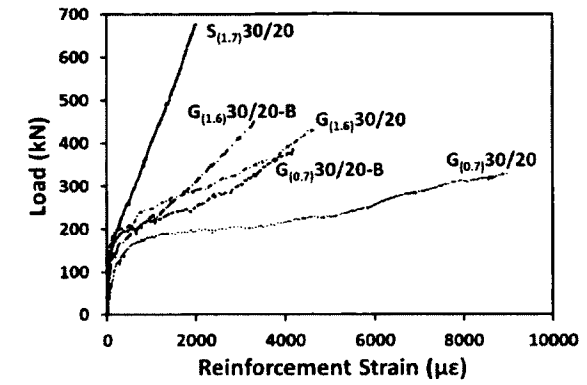

(a) Series I

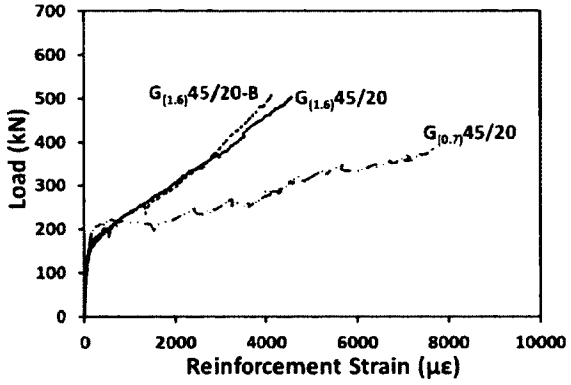

(b) Series II

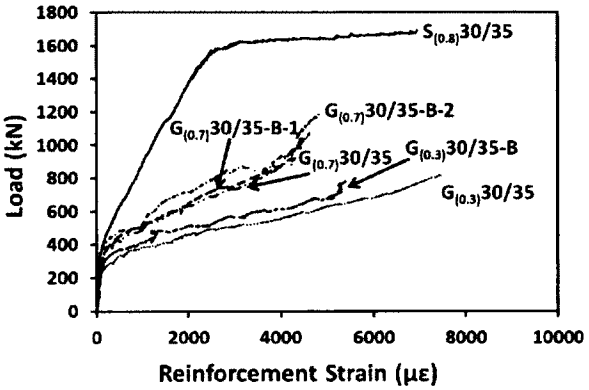

(c) Series III

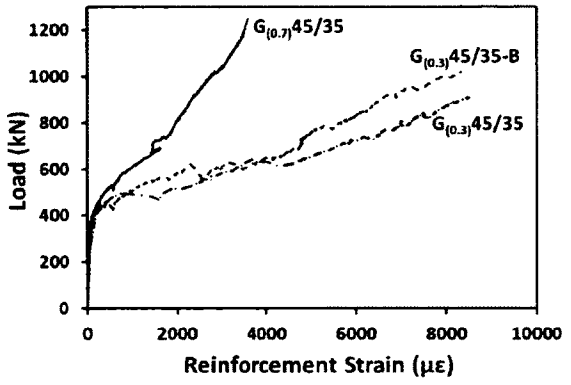

(d) Series IV

Figure 5.11: Load–reinforcement strain relationships.

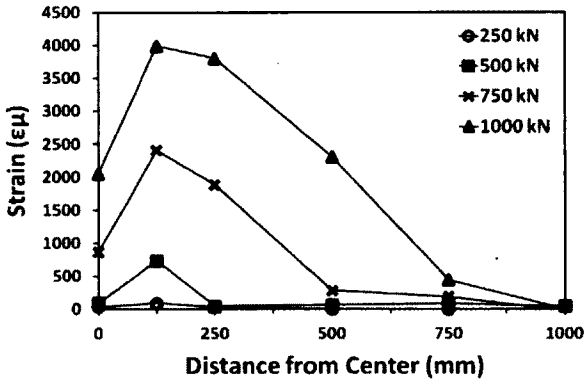

(a) Specimen $G_{(0.7)}30/35$

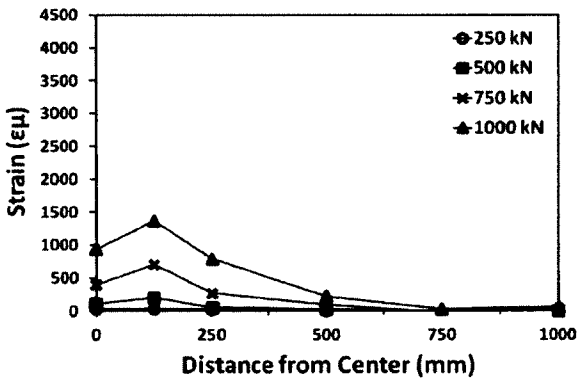

(b) Specimen $S_{(0.8)}30/35$

Figure 5.12: Reinforcement strain profile: (a) Specimen $G_{(0.7)}30/35$; (b) Specimen $S_{(0.8)}30/35$

5.4 Punching-Shear Capacity Equations

The punching-shear strength equations of the FRP-reinforced concrete slabs are forms of the original equations for steel that have been modified to account for the difference in mechanical properties between FRP and steel reinforcement, especially the lower modulus of elasticity. The available punching-shear equations provided by codes and guides (the new equation in CAN/CSA S806-12 2012, ACI 440.1R-06 2006, and JSCE 1997) and those provided by researchers based on their experimental or theoretical investigations (El-Gamal et al. 2005, Ospina et al. 2003, Mattys and Taerwe 2000 b, El-Ghandour et al. 1999 & 2000) are summarized as follows:

5.4.1 CAN/CSA S806-12 (2012)

The punching-shear strength provided by CSA S806-12 (2012) is the smallest of Eqns. (5.1) to (5.3). Clearly, they are the CSA A23.3-04 (2004) equations with modifications to account for FRP instead of steel bars.

The least of the following equations:

$$V_c = 0.028\lambda\phi_c\left(1+\frac{2}{\beta_c}\right)\left(E_f\,\rho_f\,f_c'\right)^{1/3} b_{o;0.5d}\,d \qquad (5.1)$$

$$V_c = 0.147\lambda\phi_c\left(\frac{\alpha_s d}{b_{o;0.5d}}+0.19\right)\left(E_f\,\rho_f\,f_c'\right)^{1/3} b_{o;0.5d}\,d \qquad (5.2)$$

$$V_c = 0.056\lambda\phi_c\left(E_f\,\rho_f\,f_c'\right)^{1/3} b_{o;0.5d}\,d \qquad (5.3)$$

5.4.2 ACI-440.1R-06 (2006)

The ACI 440 equation considers the effect of reinforcement stiffness (FRP bars or grids) to account for the shear transfer in FRP RC flat slabs; as shown in Eq. (5.4):

$$V_c = \frac{4}{5}\sqrt{f_c'}\,b_{o;0.5d}\,k\,d \qquad (5.4\text{ a})$$

$$k = \sqrt{2\rho_f n_f + \left(\rho_f n_f\right)^2} - \rho_f n_f \qquad (5.4\text{ b})$$

where $n_f = E_f / E_c$; $E_c = 4750\sqrt{f_c'}$

5.4.3 Japanese Design Recommendations (JSCE 1997)

The punching-shear strength according to the JSCE (1997) is calculated as given in Eq. (5.5).

$$V_c = \beta_d \beta_p \beta_r f_{pcd} b_{o;0.5d} d / \gamma_b \quad (5.5\text{ a})$$

$$\beta_d = (1000/d)^{1/4} \leq 1.5 \quad (5.5\text{ b})$$

$$\beta_p = (100\rho_f E_f/E_s)^{1/3} \leq 1.5 \quad (5.5\text{ c})$$

$$\beta_r = 1 + 1/(1+0.25u/d) \quad (5.5\text{ d})$$

$$f_{pcd} = 0.2 \leq 1.2 \text{ MPa} \quad (5.5\text{ e})$$

5.4.4 Other Punching-Shear Equations

Based on experimental testing, El-Ghandour et al. (1999) suggested modifying the ACI 318-95 (1995) equation by multiplying it by $(E_f/E_s)^{1/3}$, as shown in Eq. (5.6).

$$V_c = 0.33\sqrt{f_c'}\left(E_f/E_s\right)^{1/3} b_{o;0.5d}\, d \quad (5.6)$$

Later, El-Ghandour et al. (2000) modified the strain correction factor and the equivalent reinforcement ratio in the BS 8110 (1997) design equation. The proposed modification has a strain limit of 0.0045 for FRP reinforcement, yielding this equation for FRP slabs:

$$V_c = 0.79\left[100\rho_f\left(E_f/E_s\right)\cdot\left(0.0045/\varepsilon_y\right)\right]^{1/3}\left(f_{cu}/25\right)^{1/3}\left(400/d\right)^{1/4} b_{o;1.5d}\, d \quad (5.7)$$

Mattys and Taerwe (2000 b) proposed the following equation for the punching-shear strength of flat slabs reinforced with FRP bars or grids, as a modification of the BS 8110 (1997) equation:

$$V_c = 1.36\frac{\left(100\rho E_f/E_s f_c'\right)^{1/3}}{d^{1/4}} b_{o;1.5d}\, d \quad (5.8)$$

Ospina et al. (2003) refined the equation proposed by Matthys and Taerwe (2000 b) by using the square root of the modular ratio instead of the cube root in order to yield better results:

$$V_c = 2.77\left(\rho_f f_c'\right)^{1/3}\sqrt{\frac{E_f}{E_s}}\, b_{o;1.5d}\, d \qquad (5.9)$$

El-Gamal et al. (2005 b) proposed a new parameter (α), which is a function of the axial stiffness of the tensile reinforcement ($\rho_f E_f$), the perimeter of the applied load, and the effective depth of the slab for the ACI 318-05 (2005) design code equation, yielding:

$$V_c = 0.33\sqrt{f_c'}\, b_{o;0.5d}\, d\, \alpha \qquad (5.10\text{ a})$$

$$\alpha = 0.5\left(\rho_f E_f\right)^{1/3}\left(1+8d/b_{o;0.5d}\right), E_f \text{ in GPa} \qquad (5.10\text{ b})$$

5.4.5 Comparison between Experimental and Predicted Results

The accuracy of the available punching-shear equations are assessed herein by comparing their predictions with the experimentally determined punching-shear capacity. Table 5.4 provides the ratio between the experimentally measured and predicted punching capacities (V_{test}/V_{pred}) using the equations in JCEC (1997), El-Ghandour et al. (1999), Matthys and Taerwe (2000 b), Ospina et al. (2003), El-Gamal et al. (2005b), ACI 440.1R-06 (2006), and CAN/CSA S806 (2012). The safety factors included in all the punching-shear equations were set to 1.0. From the predictions reported in Table 5.4, all the equations yielded good yet conservative predictions, except for the ACI 440.1R-06 equation (Eq. 5.4). ACI 440.1R-06 yielded very conservative predictions with an average V_{test}/V_{pred} of 2.18±0.31 with a corresponding COV of 14%. The ACI 440.1R-06 equation is referred to as yielding very conservative predictions because it employs the reinforcement material and ratio only in predicting the depth of the neutral axis. On the other hand, all the other equations include the effect of axial stiffness, such as $(E_f/E_s)^x$, where x = 1/2 or 1/3. Moreover, El-Ghandour et al. (1999) yielded a V_{test}/V_{pred} of 1.23±0.25 with a COV of 20%. This is due to the reinforcement ratio being omitted from this equation (Eq. 5.6). On the other hand, El-Ghandour et al. (2000) equation (Eq. 5.7), based on modifying the BS standard (1997) equation and limiting the strain in the FRP bars to 4500 microstrains, yielded an average V_{test}/V_{pred} of 1.04±0.10 with a COV of 9%.

Furthermore, the JSCE (1997), and Matthys and Taerwe (2000) equations yielded consistently conservative predictions for all test specimens with an average V_{test}/V_{pred} of 1.19±0.10 and 1.30±0.12 with corresponding COVs of 8% and 9%, respectively. These equations seem to be more accurate because of they account for the reinforcement axial stiffness and the size effect. El-Ghandour et al. (1999; 2000), Ospina et al. (2003), El-Gamal et al. (2005b), and the S806-12, however, showed at least one nonconservative prediction. The CSA-S806 (2012) equation also showed good and conservative predictions, on average, with an average V_{test}/V_{pred} of 1.15±0.13 and a COV of 11%.

Table 5.4: Experimental-to-predicted punching-shear capacity (V_{test}/V_{pred})

Series	Specimen	Experimental-to-predicted punching-shear capacity, V_{test} / V_{pred}							
		JSCE (1997)	El-Ghandour et al. (1999)	El-Ghandour et al. (2000)	Matthys and Taerwe (2000 b)	Ospina et al. (2003)	El-Gamal et al. (2005 b)	ACI 440.1R (2006)	CAN/CSA S806-12 (2012)[a]
I	$G_{(0.7)}30/20$	1.11	1.17	0.96	1.21	1.03	1.29	2.08	1.11
	$G_{(0.7)}30/20$-B	1.27	1.30	1.09	1.36	1.16	1.43	2.36	1.25
	$G_{(1.6)}30/20$	1.13	1.50	0.97	1.21	1.03	1.27	1.90	1.11
	$G_{(1.6)}30/20$-B	1.24	1.71	1.07	1.34	1.15	1.45	2.09	1.23
II	$G_{(0.7)}45/20$	1.04	0.93	0.88	1.11	0.94	1.13	1.74	0.92
	$G_{(1.6)}45/20$	1.10	1.42	0.98	1.23	1.05	1.34	1.74	1.02
	$G_{(1.6)}45/20$-B	1.05	1.30	0.94	1.17	1.00	1.23	1.67	0.97
III	$G_{(0.3)}30/35$	1.20	1.03	1.08	1.35	0.95	1.20	2.59	1.25
	$G_{(0.3)}30/35$-B	1.11	0.91	0.98	1.22	0.86	1.06	2.37	1.13
	$G_{(0.7)}30/35$	1.20	1.27	1.05	1.32	0.93	1.14	2.30	1.22
	$G_{(0.7)}30/35$-B-1	1.27	1.41	1.11	1.39	0.98	1.26	2.38	1.29
	$G_{(0.7)}30/35$-B-2	1.34	1.30	1.11	1.39	0.98	1.17	2.45	1.29
IV	$G_{(0.3)}45/35$	1.11	0.76	0.94	1.18	0.83	0.98	2.08	0.98
	$G_{(0.3)}45/35$-B	1.31	1.05	1.20	1.51	1.06	1.35	2.59	1.26
	$G_{(0.7)}45/35$	1.31	1.36	1.19	1.49	1.05	1.36	2.30	1.25
	Mean	**1.19**	**1.23**	**1.04**	**1.30**	**1.00**	**1.24**	**2.18**	**1.15**
	S.D.	0.10	0.25	0.10	0.12	0.09	0.13	0.31	0.13
	COV (%)	8	20	9	9	9	11	14	11

[a] From equation (5.3).

5.5 Conclusions

This paper investigated the punching-shear behavior of full-scale, interior slab-column specimens reinforced with GFRP bars under concentric loads. The following conclusions have been drawn based on the experimental results and discussions presented herein:

- Regardless of the reinforcement type and ratio, the final mode of failure in all the tested specimens was punching-shear failure. The slab specimens with low reinforcement ratios, however, showed large plastic deformations before the punching-shear failure.

- At punching failure, neither concrete crushing in the compression zone nor rupture of GFRP reinforcement was observed. The punching-shear capacity of the compression zone was controlled by concrete splitting tension rather than concrete crushing.

- Punching-shear capacity was proportional to the amount of flexural reinforcement. Increasing the GFRP reinforcement ratio from 0.71% to 1.56% (series I; II) and from 0.34% to 0.73% (series III; IV) increased the normalized punching-shear stress at $d/2$ from column face by 29%, 53%, 24%, and 75% for series I ($G_{(0.7)}30/20$ & $G_{(1.6)}30/20$), II ($G_{(0.7)}45/20$ & $G_{(1.6)}45/20$), III ($G_{(0.3)}30/35$ & $G_{(0.7)}30/35$) and IV ($G_{(0.3)}45/35$ & $G_{(0.7)}45/35$), respectively.

- Concentrating the GFRP reinforcement in the compression side through the column cross section contributed to enhancing the overall slab behavior with a slight increase in the post-cracking stiffness and the ultimate punching-shear capacity.

- The ACI 440.1R-06 (2006) equation overestimates predictions with an average V_{test}/V_{pred} of 2.18±0.31 and a corresponding COV of 14%. JSCE (1997), and Matthys and Taerwe (2000 b) showed consistently reasonable and underestimated predictions with an average V_{test}/V_{pred} of 1.19±0.10 and 1.30±0.12 and corresponding COV of 8% and 9%, respectively.

- The CAN/CSA S806-12 (2012) equation showed accurate yet conservative (on average) predictions with an average V_{test}/V_{pred} of 1.15±0.13 and COV of 11%. It gives rather unsafe predictions for the GFRP-reinforced slabs with large column dimensions.

CHAPTER 6
PUNCHING-SHEAR RESISTANCE OF NORMAL AND HIGH-STRENGTH CONCRETE TWO-WAY SLABS

Foreword

Authors Biographies

Mohamed Hassan is a PhD candidate, Dept. of Civil Eng., University of Sherbrooke, Sherbrooke, Quebec, Canada, J1K 2R1, Phone: 1-819-821-8000, ext. 63181, Fax: 1-819-821-7974, E-mail: Mohamed.Hassan@USherbrooke.ca

Ehab A. Ahmed is a M.ASCE, Postdoctoral fellow, Dept. of Civil Eng., University of Sherbrooke, Sherbrooke, Quebec, Canada, J1K 2R1. Tel. 1-819-821-8000, ext. 62135, Fax 1-819-821-7974, E-mail: Ehab.Ahmed@USherbrooke.ca

Brahim Benmokrane, FACI, is an NSERC & Tier-1 Canada Research Chair Professor, Dept. of Civil Eng., University of Sherbrooke, Sherbrooke, Quebec, Canada, J1K 2R1. Tel. 1-819-821-7758, Fax 1-819-821-7974, E-mail: Brahim.Benmokrane@USherbrooke.ca

Acceptation date: 24 July 2013.

Acceptation state: in press.

Journal: *ASCE Journal of Composite for Construction.*

Title: "Punching-Shear Strength of Normal- and High-Strength Two-Way Concrete Slabs Reinforced with GFRP Bars."

Titre en français: "Résistance au poinçonnement de dalles en béton normal et à haute résistance renforcées de barres en PRFV".

Paper's contribution to the project: In this study, a total of 10 full-scale interior slab-column connections without shear reinforcement were fabricated with normal- and high-strength concretes. The main objective of this paper is to investigate the punching-shear behaviour of two-way flat slabs reinforced with different grades of GFRP bars and constructed with different concrete grades (NSC and HSC). Comparisons between 54 specimens without shear reinforcement tested to date including the specimens in this investigation, using punching-shear design models presented in CSA S806 (2012), ACI 440 (2006), BS 8110 (1997), and JSCE (1997) were assessed.

Abstract: This paper investigated the punching-shear behavior of two-way concrete slabs reinforced with glass fiber-reinforced polymer (GFRP) bars of different grades. A total of 10 full-scale interior slab-column specimens measuring 2500 × 2500 mm with thicknesses 8 of either 200 or 350 mm and 300 × 300 mm square column stubs were fabricated with normal- and high-strength concretes. The specimens were tested under monotonic concentric loading till failure. The effects of concrete strength as well as reinforcement type and ratio were evaluated. The test results revealed that increasing the reinforcement ratio resulted in higher punching-shear capacity, lower reinforcement and concrete strains, and lower deflections. In addition, the high-strength concrete increased the punching-shear capacity, significantly reduced concrete strains, increased strains in the GFRP reinforcing bars, and reduced deflection due to the high tensile strength and modulus of elasticity. The test results and results from literature were used to assess the accuracy of the punching-shear provisions of FRP design codes and guides. Despite the 60 MPa limit of the CSA-S806-12 punching-shear equation, it yielded good predictions for specimens with concrete strengths of 71 to 75.8 MPa.

CE Database Subject Headings: Punching, shear; slab; flat slab; fiber-reinforced polymer; FRP; strain; deflection; prediction; strength; design; concrete.

6.1 Introduction

The reinforced concrete (RC) flat plate/slab is a favorite construction system as it simplifies and speeds up site operations, allows for easy and flexible division of space, and reduces overall building height due to the absence of dropped beams. This construction system is often used for parking structures. The design of flat plates/slabs is often compromised by their ability to resist shear stresses at slab-column connections and to overcome punching-shear failure, which is catastrophic in nature. Corrosion of steel reinforcement due to harsh environmental and exposure conditions (de-icing salts, moisture, freeze-thaw cycles, and chlorides) and the related deterioration may accelerate such failure or reduce the expected service life (Broomfield, 2007). Over the last two decades, the use of fiber-reinforced polymer (FRP) bars instead of steel bars, especially where steel corrosion is a major concern, has been effective in reducing maintenance costs and extending the service life of structures. Recent advances in polymer technology have led to the development of new generations of FRP reinforcing bars such as GFRP bars designated with high modulus of elasticity. The new CSA S807 (2010) "*Specification for Fibre-Reinforced Polymers*" provides a means for standardizing FRP reinforcing bars, which is expected to advance the use of GFRP reinforcing bars in many applications.

The punching-shear design of RC flat plates/slabs has received a great attention for decades. Limited studies, however, have been conducted on the punching-shear behavior of flat plates/slabs reinforced with the FRP bars/grids (El-Ghandour et al., 2003; Matthys and Taerwe, 2000 b; Ospina et al., 2003; Lee et al., 2009, Nguyen-Minh and Rovnak, 2013). The FRP-reinforced flat slabs in these studies evidenced lower punching-shear capacities, lower post-cracking stiffness, and greater crack widths than those of their counterparts reinforced with steel bars when the same reinforcement amount was used. This resulted from smaller dowel action and smaller uncracked compression zone as a result of a lower modulus of elasticity of FRP bars in comparison with that of steel bars (Theodorakopoulos and Swamy, 2007). Matthys and Taerwe (2000 b) reported that the FRP-RC slabs designed with similar flexural stiffness as the steel-RC slabs showed punching-shear capacities close to that of the steel-RC slabs. Moreover, they reported also that there is a strong interaction between flexural and shear effects for all tested FRP-RC slabs. Ospina et al. (2003) concluded that the behavior

of an FRP-RC slab-column connection is affected by the elastic stiffness of the reinforcing mat and the quality of its bond with the concrete. However, the FRP grids may not provide the same punching-shear capacity as the FRP bars. The difference in bond behavior and the concentration of stresses in the grids at the intersections of the orthogonal reinforcement led to more slip in the elastic-cracked stage and more gradual load drop at ultimate. Furthermore, Nguyen-Minh and Rovnak (2013) concluded that both the size factor and the effect of the span-to-effective-depth ratio (L/d) should be taken into account in calculating the punching-shear resistance of the FRP-RC slab-column connections. Recently, the new CSA S806 (2012) standard provided its first punching-shear design equation, which represented a step forward in designing FRP-RC flat slabs and parking structures. Nevertheless, more research is needed to investigate the performance of FRP-RC flat plates/slabs.

High-strength concrete (HSC) is characterized by higher compressive and tensile strengths, and higher modulus of elasticity than normal-strength concrete (NSC). Consequently, the use of HSC can improve the punching-shear capacity, allowing higher forces to be transferred through the slab-column connection. This is due to the increase in tensile strength of HSC (Mendis 2003). The limited research work in this area included only a few specimens reinforced with FRP bars/grids fabricated using HSC. Matthys and Taerwe (2000 b) tested a specimen with a concrete strength of 118 MPa, while Zhang et al. (2005) tested a specimen with a concrete strength of 71 MPa. In addition, FRP design codes and guides normally limit the applicability of the punching-shear equations to a certain range of concrete strengths. One example is CSA S806 (2012), which states that 60 MPa is the maximum concrete strength that should be used in predicting punching-shear capacity. Thus, further investigation is needed to understand the general behavior of RC slabs fabricated with HSC and to verify the possibility of predicting the punching-shear strength accurately with the current punching-shear provisions.

With the main objective of using GFRP bars in RC flat slab parking structures, an extensive research project is being conducted at the University of Sherbrooke to investigate the behavior of GFRP-RC flat plates/slabs. The preliminary tests of this project (Dulude et al., 2010) evaluated the effects of columns' dimensions and reinforcement ratio on the punching-shear capacity of the slab-column connections. It also contributed to field implementation of GFRP bars in flat slab parking structure in a demonstration area (350 m^2) at the Hôtel de Ville

parking garage (Quebec, Canada, 2010). The successful implementation in Hôtel de Ville parking along with the new CSA S806 (2012) punching-shear design equation, helped in designing the world's first flat slab parking garage totally reinforced with GFRP bars: La Chancelière parking garage (Québec, Quebec, Canada, 2011) (Benmokrane et al., 2012).

This paper investigated the punching-shear behavior of interior slab-column connections reinforced with different grades of GFRP bars (Grades I, II, and III according to CSA S807, 2012) and constructed with different concrete types (NSC and HSC). The effects of the concrete strength as well as the reinforcement type and ratio on the punching shear were assessed. In addition, the test results from this investigation and from literature were used in assessing the accuracy of the FRP punching-shear strength design equations in CSA S806 (2012), ACI 440 (2006), BS 8110 (1997), and JSCE (1997).

6.2 Experimental Program

6.2.1 Materiel properties

CSA S807 (2010) classifies glass FRP (GFRP) bars into three grades according to their modulus of elasticity (E_f): Grade I (E_f <50 GPa), Grade II (50 GPa $\leq E_f <$ 60 GPa), and Grade III ($E_f \geq$ 60 GPa). In this investigation, No. 15, No. 20, and No. 25 sand-coated GFRP bars were used and labeled, according their modulus of elasticity, as GFRP-1, GFRP-2, and GFRP-3 (referring to Grades I II, and III, respectively). The GFRP bars were manufactured by combining the pultrusion process with an in-line sand coating to improve the bond between the bars and the surrounding concrete. The tensile properties of the GFRP bars were determined by testing five representative bars for each diameter in accordance with ASTM D7205M (2011). Table 6.1 gives the tensile properties of the GFRP bars, as determined from testing. The reference specimens, however, were reinforced with 20M steel bars (Type 44W) with a yield stress of 470 MPa and a modulus of elasticity of 200 GPa.

The slab-column connections were cast using a ready-mixed, normal-strength concrete (NSC) and high-strength concrete (HSC) with an entrained-air ratio of 5% to 8%. The target compressive strengths of NSC and HSC were 35 and 65 MPa, respectively. The concrete compressive (f_c') and tensile strengths (f_t') for each specimen were determined on the same day of testing from three 150 × 300 mm concrete cylinders for each test (compression and

splitting). The actual concrete compressive strength for the NSC ranged from 34.3 to 45.4 MPa, while that of the HSC was 75.8 MPa. Table 6.2 provides the concrete properties of the tested specimens.

Table 6.1: Properties of the GFRP reinforcing bars

GFRP product	Grade[a]	Bar size [a]	Area[a], mm^2	Elastic tensile modulus, E_f, GPa	Ultimate tensile strength, MPa	Characteristic tensile strength[b], MPa	Ultimate tensile elongation, %
GFRP-1	I	No. 15	199	48.2±0.4	769±23	700	1.60±0.05
		No. 20	284	48.1±0.7	765±31	672	1.59±0.08
GFRP-2	II	No. 20	284	57.4±0.3	1109±21	1046	1.93±0.04
		No. 25	510	56.7±0.3	1065±22	999	1.88±0.04
GFRP-3	III	No. 20	284	64.9±0.6	1334±85	1079	2.07±0.13

[a] According to CSA S807 (2010).

[b] Characteristic tensile strength = Average value – 3× standard deviation (CSA S806, 2012).

6.2.2 Test specimens

A total of 10 full-scale slab-column connections reinforced with different grades of GFRP bars (Grades I, II, and III – CSA S807, 2010) and steel bars were constructed and tested to failure under monotonic concentric loading. The test specimens were designed to represent isolated interior slab-column connections and the slab thicknesses were chosen to simulate the flat slabs used in some parking garage applications (Benmokrane et al., 2012). The slab measured 2500 × 2500 mm with thicknesses of either 200 mm or 350 mm, and a square column stub measured 300 × 300 mm. The column stub extended 300 mm beyond the top and bottom surfaces of the slabs. Figure 6.1 shows the geometry and typical reinforcement configuration of the test specimens.

The specimens were categorized into two series. Series I (200 mm thick) comprised 4 GFRP-RC specimens with a reinforcement ratio ranging from 0.71% to 1.56% and a reference steel-reinforced one. Series II (350 mm thick) comprised 4 GFRP-RC specimens with a reinforcement ratio (ρ) ranging from 0.34% to 1.61% and a reference steel-RC slab. Four slabs in each series were fabricated using a concrete strength of 35 MPa (NSC), while the fifth one was fabricated with a concrete strength of 65 MPa (HSC) to investigate the effects of concrete type and strength. The actual concrete compressive strengths for the NSC ranged from 34.3 to 45.4 MPa, while that of the HSC was 75.8 MPa. In addition, one slab in Series I was reinforced with Grade-III GFRP bars ($G_{(1.2)}30/20$); this slab had the same axial reinforcement

stiffness ($E_f A_f$) as $G_{(1.6)}30/20$ (Grade II). Table 6.2 presents the test matrix and characteristics for each specimen.

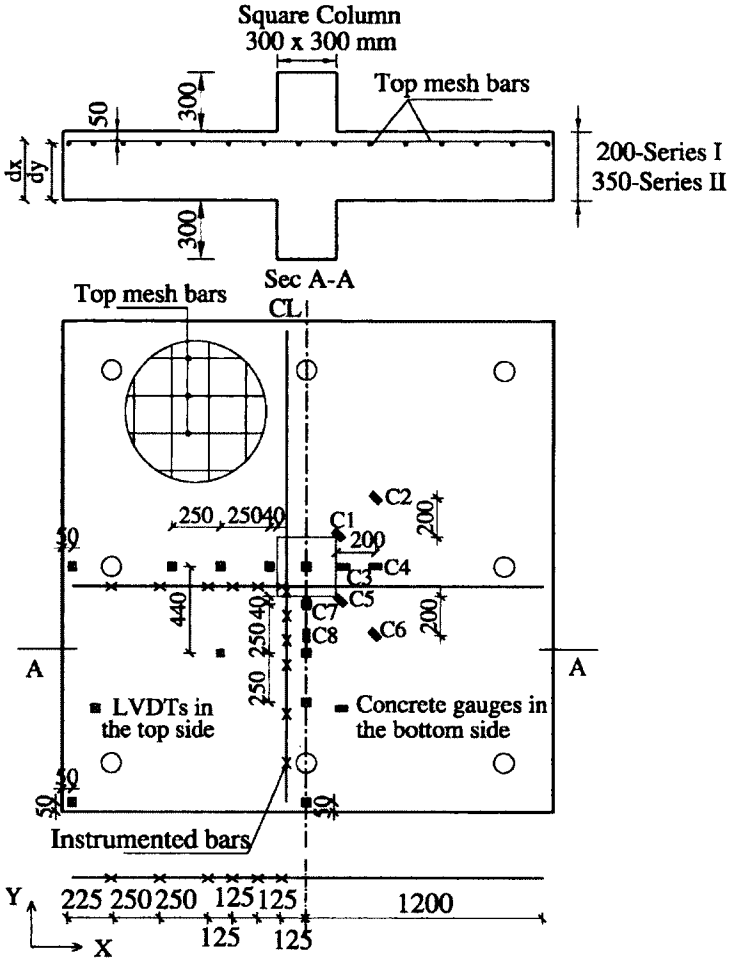

Figure 6.1: Test specimens' geometry, reinforcement configuration, and instrumentations

6.2.3 Instrumentations and test setup

All specimens were tested under monotonic concentrated load, acting on the column stub from the bottom side of the slabs until failure. The specimens were simply supported on all four sides and were held against the laboratory's rigid floor using a rigid steel frame 100 mm in width supported by 8 steel tie rods, each measuring 38 mm in diameter. The specimens were placed supported on temporary frame (Figure 6.2) and its leveling was adjusted. A 15 mm-thick layer of cement mortar was placed on the concrete surface at the location of the rigid steel frame. In addition, 10 mm-thick neoprene sheets were used over the loading plate and between the supporting frame and the slab. Thereafter, the load was applied

using one or two 1500 kN hydraulic jacks according to the expected capacity of each specimen, at a loading rate of 5 kN/min. When two hydraulic jacks were used, they were connected to the same pump and calibrated to work simultaneously. Figure 6.2 provides the details of the test setup.

Table 6.2: Details of test specimens

Series	Specimen [a]	Slab thick. mm	d_x, mm	d_y, mm	S, mm	Reinf. type	Tension reinf.	A_{rx}, mm^2	ρ[b], %	ρ_b[c] %	ρ/ρ_b	$\rho(E_r/E_s)$, %	f'_c[d] MPa	f_t[d] MPa
I	$G_{(0.7)}30/20$	200	142	126	220	GFRP-1	12 No. 15	2388	0.71	0.49	1.45	0.17	34.3	2.5
	$G_{(1.6)}30/20$		141	122	125		18 No. 20	5112	1.56	0.52	3.00	0.38	38.6	2.8
	$G_{(1.6)}30/20$-H		141	122	125	GFRP-2	18 No. 20	5400	1.56	0.51	3.06	0.45	75.8	4.4
	$G_{(1.2)}30/20$		141	122	175	GFRP-3	14 No. 20	3976	1.21	0.24	5.04	0.39	37.5	3.5
	$S_{(1.7)}30/20$		141	122	125	Steel	18-20M	5112	1.66	4.92	0.34	1.66	45.4	2.8
II	$G_{(0.3)}30/35$	350	292	276	220	GFRP-1	12 No. 15	2388	0.34	0.49	0.69	0.08	34.3	2.5
	$G_{(0.7)}30/35$		291	272	125		18 No. 20	5112	0.73	0.53	1.38	0.18	39.4	2.3
	$G_{(1.6)}30/35$		287	262	110	GFRP-2	22 No. 25	11220	1.61	0.33	4.88	0.46	38.2	3.3
	$G_{(1.6)}30/35$-H		287	262	110		22 No. 25	11220	1.61	0.54	2.98	0.46	75.8	4.4
	$S_{(0.8)}30/35$		291	272	125	Steel	18-20M	5400	0.77	4.18	0.18	0.77	38.6	2.8

* Note: the clear concrete cover for all specimens is 50 mm.

[a] G or S $_{(x.x)}$yy/zz: G denotes GFRP; S denotes steel; (x.x) denotes the reinforcement ratio; yy/zz denotes the column dimension (yy); slab thickness (zz); high-strength concrete (H).

[b] $\rho=(\rho_x \cdot \rho_y)/2$

[c] ρ_b calculated according to ACI 440 (2006) and ACI 318 (2008) for GFRP- and steel-RC slabs, respectively.

[d] Compression and splitting testing on 150 × 300 mm concrete cylinders.

Each specimen was provided with 2-instrumented bars in the orthogonal directions in the top reinforcing mat (tension side) with 6 electrical-resistance strain gauges attached to each bar as shown in Figure 6.1. In addition, 8 concrete electrical-resistance strain gauges (C1 to C8) were glued to the slab's bottom surface (compression side) before testing. Moreover, the 8 steel tie rods supporting the test specimen were instrumented with electrical strain gauges to verify loading symmetry during the test. The deflection of the test specimens at the different locations was captured with 11 linear voltage differential transformers (LVDTs) as shown in Figure 6.1. The strain gauges and LVDTs were connected to a data-acquisition system to record the readings during the test. Figure 6.1 also shows the locations of strain gauges (concrete and reinforcement) and LVDTs. During the test, crack propagation was marked and the corresponding loads were recorded.

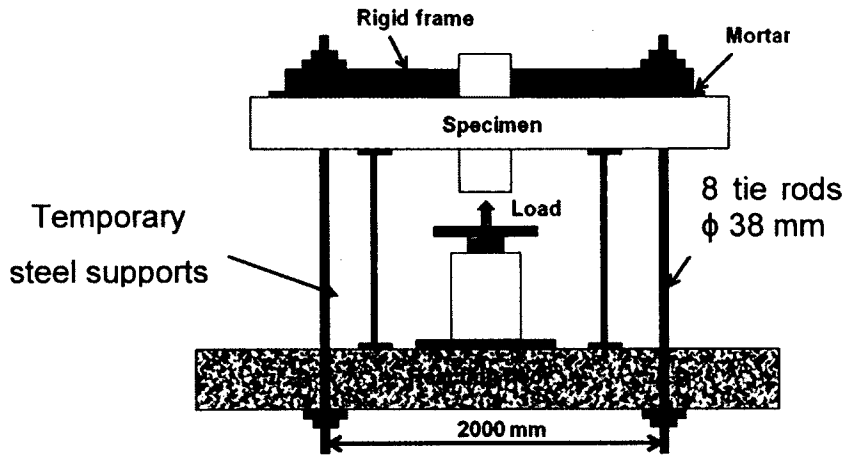

a)

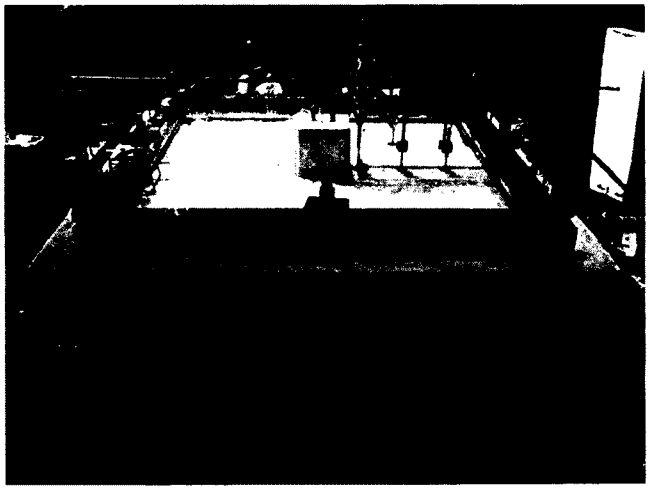

b)

Figure 6.2: Test setup: (a) Schematic and dimensions; (b) Testing of a specimen

6.3 Test Results and Discussion

6.3.1 Cracking and failure

All the test specimens were initially uncracked, except the $G_{(1.2)}30/20$ specimen, which showed hair cracking before testing. During the test, flexural cracks appeared first and propagated radially from the column face toward to the slab edge. The loads corresponding to the appearance of the first crack (cracking load, V_{cr}) as well as the corresponding deflections (Δ_{cr}) were recorded from the maximum deflection LVDTs placed 40 mm from the column face

(See Table 6.3). As the load was increased, these flexural cracks increased and extended beyond the slab supports. Thereafter, a fine circumferential crack appeared at the column interface along the perimeter. At higher loadings (about 50% of the ultimate load), circumferential cracks were observed outside the column location, connecting the flexural cracks together. The slab failed with the final shear crack coinciding with, or located outside, this crack. The final failure developed by the column punching through the slab. Figure 6.3 shows the typical crack pattern at failure for some GFRP reinforced specimens.

Regardless reinforcement type and ratio, the final failure mode for all the specimens was punching-shear. This failure was evidenced by a sudden drop in the applied load, accompanied by the appearance of a wide, clear crack defining the failure surface of the specimens around the columns. The specimens with low reinforcement ratios such as $G_{(0.7)}30/20$ and $G_{(0.3)}30/35$, however, exhibited large deflections prior to failure and more flexural cracks around the column as well as showed more plastic deformations before the punching-shear failure. Furthermore, the GFRP-RC specimens with the same axial reinforcement stiffness (E_fA_f) (as in case of $G_{(1.2)}30/20$ and $G_{(1.6)}30/20$) displayed a similar crack pattern.

Since the development of the inner diagonal shear cracks were not visible, some specimens were sawed to allow observing the inner diagonal shear cracks. Table 6.3 and Figure 6.3 show the angle of the punching-shear cone of some of the tested specimens. From Figure 6.3, it can be noticed that the sawed specimens exhibited a main diagonal shear crack starting at the column face with different inclination angles, α_{cone}, (where α_{cone} is the average angle for punching-shear cone with the horizontal direction) as shown in Figure 6.3. The inclination angle of the diagonal punching-shear crack (α_{cone}) was significantly affected by the flexural reinforcement ratio rather than the concrete compressive strength. The distance defining the failure surface (X_{cone}) (the observed distance from column face to the location of the failure surface) was measured at different locations and the average values were calculated and reported in Table 6.3 (multiplications of d). The X_{cone} distance for the GFRP-RC specimens in Series I and II varied approximately from $2.3d$ to $2.8d$ and $1.3d$ to $2.0d$, respectively. The corresponding failure surface angels (α_{Xcone}) varied from 28.6° to 33.0° and from 32.0° to 43.5°, respectively. In general, at the same flexural reinforcement ratio, the observed angels of the shear crack of Series II (350 mm thick) were steeper than those

observed in Series I (200 mm thick). Increasing the flexural reinforcement ratio enhanced the slab's in-plane restraint and led to a much flatter inclination of the critical shear crack which, in turn, decreased the angle of the punching-shear cone. On the other hand, increasing the concrete strength from 38.2 MPa to 75.8 MPa in the GFRP-RC specimens showed a slight effect on the angle of the punching-shear cone; however, more investigation is needed to cover a wide range of concrete strengths.

The two specimens fabricated with the HSC ($G_{(1.6)}30/20$-H and $G_{(1.6)}30/35$-H) showed the highest cracking loads in both groups due to the concrete's higher tensile strength. The concrete strength significantly affected the first cracking load because the higher the concrete strength, the higher the concrete tensile strength. In addition, the HSC specimens evidenced fewer and narrower cracks. Considerable splitting of the concrete cover was observed, however, once punching failure occurred. This behavior is similar to that observed in steel-RC slabs by Marzouk et al. (1996).

6.3.2 Punching-shear capacity

Table 6.3 presents the ultimate punching-shear capacities and the corresponding normalized punching-shear stresses calculated at $0.5d$ from the column face of the tested specimens. It should be noted that the reported load values include specimen dead load (39 kN and 67 kN for Series I and II, respectively). The punching-shear stresses at failure were normalized to the cubic root of the concrete strength to account for the variation in the concrete strengths. Besides, the effective reinforcement ratios ($\rho E_f/E_s$) of the specimens were used to account for the difference between the moduli of elasticity of the GFRP and steel bars.

The results in Table 6.3 show that the GFRP-RC specimen with the same reinforcement ratio as its steel-RC counterpart evidenced lower punching-shear stress at failure (33% lower in Series I and 38% lower in Series II). This was related to the smaller dowel action and the lower modulus of elasticity of GFRP reinforcing bars compared to that of steel (E_f / E_s = 0.25 approximately). Using a GFRP reinforcement ratio equal to the steel reinforcement ratio yielded smaller neutral-axis depth as well as higher strains and deeper and wider cracks at the same load level. Thus, both the contributions of the uncracked concrete zone (compression side), and the aggregate interlock decreased, which, in turn, yielded lower punching-shear capacity.

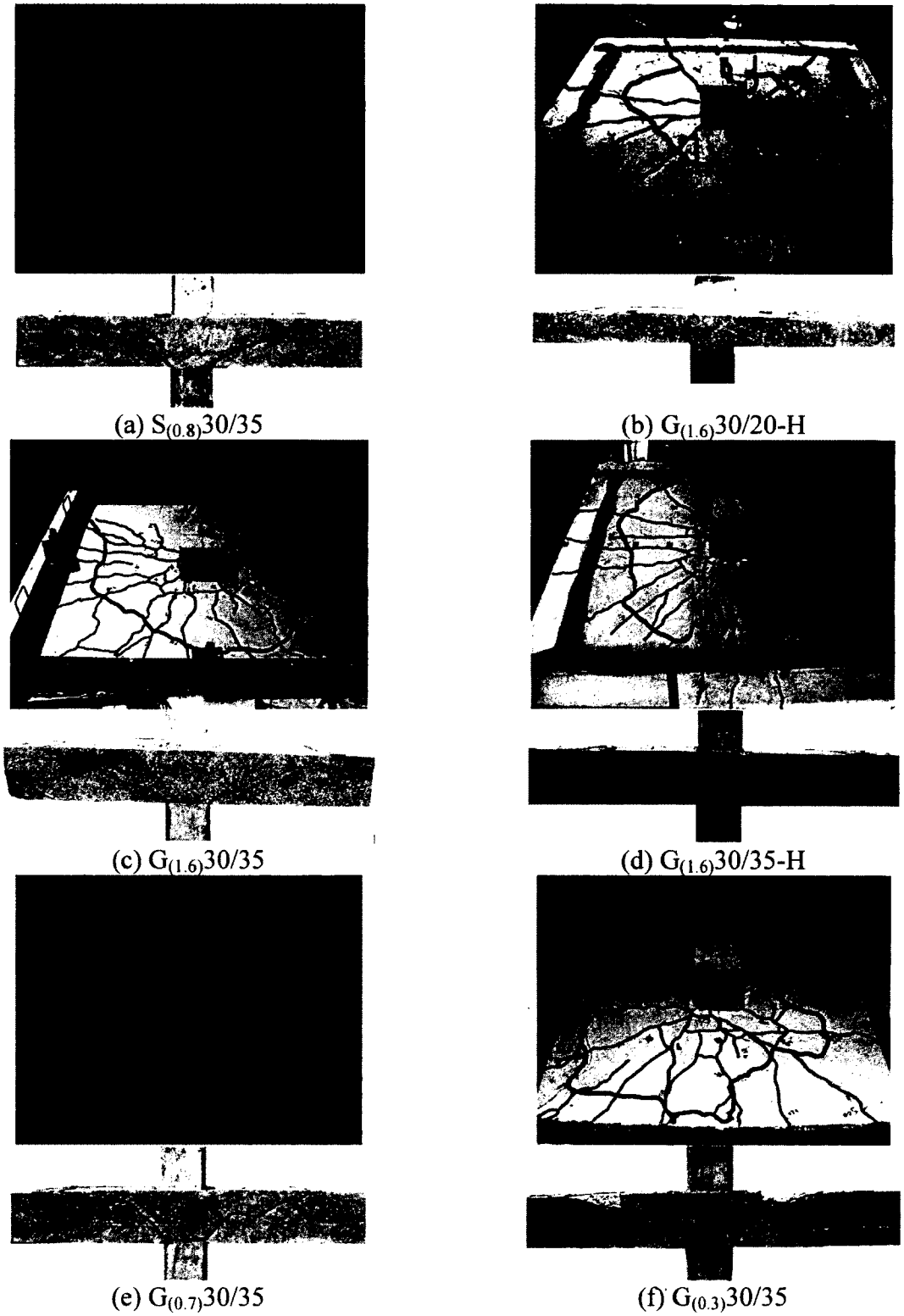

(a) $S_{(0.8)}30/35$ (b) $G_{(1.6)}30/20$-H

(c) $G_{(1.6)}30/35$ (d) $G_{(1.6)}30/35$-H

(e) $G_{(0.7)}30/35$ (f) $G_{(0.3)}30/35$

Figure 6.3: Typical punching-shear failure and main shear crack for some specimens

Table 6.3: Summary of test results

Prototype	ρ (E_r/E_s), %	k_i, kN/mm	k_p, kN/mm	k_p/k_i	V_{cr}, kN	v_{cr}, MPa	Δ_{cr}, mm	V_u, kN	Δ_u, mm	$v_{u,0.5d}$, MPa	$v_n = v_{u,0.5d}/\sqrt[3]{f_c'}$, MPa$^{(2/3)}$	X_{cone}	α_{Xcone} (degrees)	α_{cone} (degrees)	ε_{rmax}, (με)	ε_{cmax}, (με)
$G_{(0.7)}30/20$	0.17	80.3	8.0	0.10	125	0.54	0.67	329	21.8	1.41	0.43	2.3d	33.0	—	8975	-1280
$G_{(1.6)}30/20$	0.38	124.8	14.8	0.12	211	0.93	1.70	431	15.9	1.91	0.56	2.8d	28.6	—	5010	—
$G_{(1.6)}30/20$-H	0.45	152.4	14.2	0.10	237	1.05	1.50	547	20.4	2.42	0.57	2.5d	31.4	34.0	5830	-1870
$G_{(1.2)}30/20$	0.39	84.8	14.6	0.17	160	0.71	1.35	438	17.9	1.94	0.58	2.5d	31.4	34.7	4471	-3713
$S_{(1.7)}30/20$	1.66	163.7	36.3	0.22	163	0.72	0.10	688	15.7	3.05	0.85	2.8d	28.6	—	2630	-2670
$G_{(0.3)}30/35$	0.08	144.0	27.3	0.19	338	0.51	1.37	825	16.2	1.24	0.38	1.3d	43.5	42.0	8190	-2300
$G_{(0.7)}30/35$	0.18	233.4	48.4	0.21	415	0.64	1.22	1071	12.0	1.64	0.48	1.9d	33.2	36.4	4625	—
$G_{(1.6)}30/35$	0.46	187.8	84.4	0.45	384	0.59	1.77	1492	—	2.30	0.68	1.7d	36.4	26.1	3200	-2385
$G_{(1.6)}30/35$-H	0.46	282.8	83.0	0.29	611	0.94	2.05	1600	12.7	2.47	0.58	2.0d	32.0	28.4	3881	-1446
$S_{(0.8)}30/35$	0.77	245.8	115.8	0.47	444	0.68	1.47	1692	10.8	2.05	0.77	1.8d	34.7	27.9	6955	-1190

Notes: d = slab thickness; — 50 mm — d_b; where d_b is the bar diameter; V_u= ultimate failure load; $v_{u,0.5d}$ = ultimate shear stress at 0.5d from the column face; Δ_u; ultimate deflection at failure load; X_{cone}= average distance from the column face to the observed surface failure;

The results also indicated that increasing the reinforcement ratio of the GFRP-RC specimens from 0.71% to 1.56% and from 0.34% to 1.62% in Series I and Series II, respectively, increased the punching-shear stress by 35 and 81%, respectively. Furthermore, the $G_{(1.2)}30/20$ designed with similar axial reinforcement stiffness ($E_f A_f$) as $G_{(1.6)}30/20$ and fabricated with the same concrete strength exhibited similar punching-shear capacity (438 and 431 kN, respectively). The normalized punching-shear stress was plotted against the effective reinforcement ratio ($\rho_f E_f/E_s$), as shown in Figure 6.4. This figure illustrates that the normalized punching-shear stress is not linearly proportional to the effective reinforcement ratio. The normalized punching-shear stress to the cubic root of the concrete compressive strength is proportional to the effective reinforcement ratio to the power of 0.34. This is close to the punching-shear design equation in CSA S806 (2012), BS 8110 (1997), and JSCE (1997), which account for FRP axial stiffness to the power of 1/3.

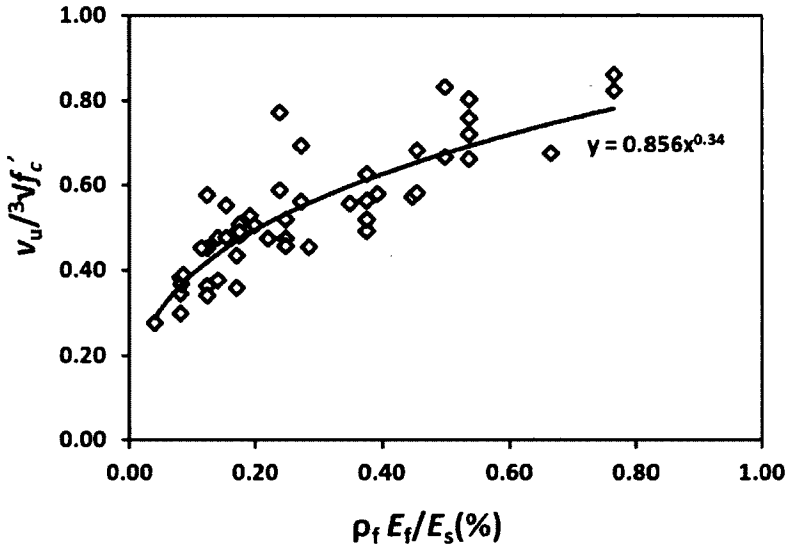

Figure 6.4: Normalized punching-shear stress at 0.5*d* from the column face versus the effective reinforcement ratio.

The slab thickness was one of the parameters that most affected the punching-shear capacity. Increasing the slab thickness of GFRP-RC specimens $G_{(0.7)}30/35$, $G_{(1.6)}30/35$, and $G_{(1.6)}30/35$–H from 200 mm to 350 mm (effective depth from 134 mm to 280 mm), while maintaining the same reinforcement ratio, the normalized punching-shear stresses increased by 12%, 21%, and 1%, respectively, compared to their counterparts $G_{(0.7)}30/20$, $G_{(1.6)}30/20$, and $G_{(1.6)}30/20$-H. The lowest increase ratio may give an indication for the size effect in punching-

shear strength. However, it was not possible to quantify this effect because the shear-span-to-depth ratio (a/d) was not constant for all specimens. CSA S806 (2012) states that, when the effective depth of structural slabs exceeds 300 mm, a sized effect of $(300/d)^{0.25}$ should be applied in punching-shear prediction equations. In Series II specimens, however, the effective depth ranged from 275 to 285 mm (average of 280 mm).

The use of HSC increased the punching-shear capacity of the specimens. The higher concrete strength contributes to the punching-shear strength in two different ways: (1) it enhances slab cracking load and (2) it enhances the contribution of the compressive block below the neutral axis after cracking, which yields higher punching-shear strength. The ultimate punching-shear stresses of $G_{(1.6)}30/20$-H and $G_{(1.6)}30/35$-H increased by 27% and 7% compared to their counterparts $G_{(1.6)}30/20$ and $G_{(1.6)}30/35$, respectively.

6.3.3 Load–deflection response

Figure 6.5 shows the load-deflection relationships for the tested specimens measured from the LVDTs placed 40 mm from the column face. All slabs showed typical bilinear load-deflection behavior. The first line of the load-deflection curve illustrates the initial stiffness (k_i) of the uncracked specimen, while the second line shows the postcracking stiffness (k_p). Using HSC directly enhanced the uncracked stiffness of the test specimens, as evidenced by Figure 6.5. Table 6.3 shows that $G_{(1.6)}30/20$-H in Series I displayed an uncracked stiffness of 152.4 kN/mm, which was higher than those of the other GFRP-RC specimens in the same series. Specimen $G_{(1.6)}30/35$-H in Series II had an uncracked stiffness of 282.8 kN/mm, which was higher than all the specimens in this series, including the steel-RC one. On the other hand, $G_{(1.2)}30/20$ seems to be affected by pre-existing cracks. It had an uncracked stiffness of 84.8 kN/mm, compared to 124.8 kN/mm for $G_{(1.6)}30/20$, which had the same axial reinforcement stiffness and very close concrete strength.

GFRP-RC specimens $G_{(1.6)}30/20$ and $G_{(0.7)}30/35$ showed higher deflection values at the same load level than of their steel-RC counterparts ($S_{(1.7)}30/20$ and $S_{(0.8)}30/20$). The ultimate deflections of specimens $G_{(1.6)}30/20$ and $G_{(0.7)}30/35$ increased by 1.3% and 11% compared to $S_{(1.7)}30/20$ and $S_{(0.8)}30/20$, respectively. This is due to the GRFP bars having lower moduli of elasticity than the steel bars ($E_f / E_s = 0.25$ approximately). This, in turn, reduced the effective moment of inertia in the slabs. It should be noted the LVDTs for specimens $S_{(0.8)}30/20$ were

released at about 1600 kN because of a problem with the acquisition system. Increasing the reinforcement ratio in the GFRP specimens in Series I and II from 0.71% to 1.56% ($G_{(0.7)}30/20$ and $G_{(1.6)}30/20$) and from 0.34% to 0.73% ($G_{(0.3)}30/35$ and $G_{(0.7)}30/35$) decreased the ultimate deflections by 27% and 26%, respectively. This illustrates the effectiveness of increasing the reinforcement ratio in reducing deflection. Moreover, $G_{(1.2)}30/20$ showed a 13% increase in ultimate deflection compared to $G_{(1.6)}30/20$, which had the same axial reinforcement stiffness, due to the pre-existing cracks observed before testing. These cracks affected the initial and postcracking stiffness, which is reflected in the effective inertia and, consequently, the deflection.

Furthermore, the ultimate deflection of specimen $G_{(1.6)}30/20$-H (Series I) was 30% higher than that of $G_{(1.6)}30/20$. This indicates that using the HSC in the GFRP-RC slabs increased the punching-shear capacity and the deformability of the test specimen and made it possible to achieve significantly higher deflections at failure. A similar trend was observed in $G_{(1.6)}30/35$-H (Series II), but comparison with $G_{(1.6)}30/35$ was not possible because its LVDT stopped recording before the failure.

It is worth mentioning that, increasing the slab thickness from 200 mm in Series I to 350 mm in Series II while maintaining a constant reinforcement ratio decreased the ultimate deflection by 42% (on average). This is expected due to the very high increase in slab moment of inertia, which significantly reduced the deflection.

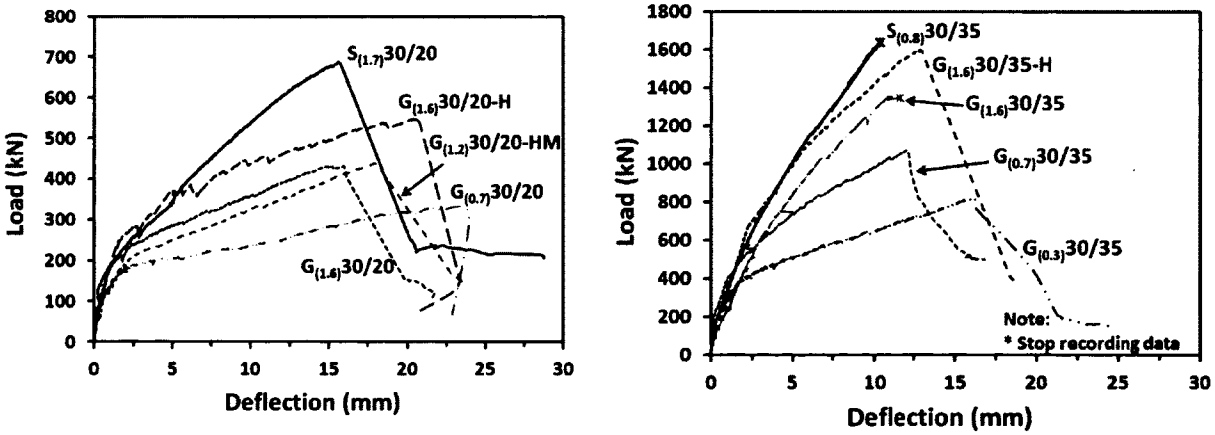

(a) Series I (b) Series II

Figure 6.5: Load–deflection relationships: (a) Series I; (b) Series II

6.3.4 Reinforcement and concrete strains

Figure 6.6 plots the load versus reinforcement and concrete strains relationships. It presents the reinforcement strain values recorded from the strain gauges located at 125 mm from the column centerline and the concrete strain figured at the column face (gauge C3). Generally, the specimens with higher axial reinforcement stiffness (E_fA_f) showed smaller concrete and reinforcement strains at the same load level when the concrete strength did not vary significantly.

In the GFRP-RC specimens, the maximum measured reinforcement strain was 8975 microstrains, representing 56% of the characteristic tensile strength and indicating that the punching of the slabs was not triggered by GFRP-bar rupture. The concrete strains in all the specimens (Table 6.3) near the column region were less than the theoretical crushing failure of 3500 microstrains (CSA S806, 2012), except in the $G_{(1.2)}30/20$ specimen (3713 microstrains). At failure, however, neither concrete flexural crushing on the compression zone nor GFRP reinforcement rupture was observed. On the other hand, steel-RC specimen $S_{(0.8)}30/35$ showed a clear yielding of the steel bars in both gauges of 125 mm and 250 mm from the column center line at a corresponding applied load of 1600 kN. In contrast, steel-RC specimen $S_{(1.7)}30/20$ showed no signs of yielding.

Figure 6.6 clearly depicts the effect of using HSC on the concrete and reinforcement strains in both series (I and II). Regardless of the reinforcement type and ratio, the concrete strains of the HSC specimen were lower than those of the NSC specimens. This relates to the high tensile strength, which delays slab cracking, and the higher modulus of elasticity, which contributes to reducing induced strains. On the other hand, using HSC yielded lower strains in GFRP bars at early loading stages than in their NSC counterparts reinforced with the same type and ratio of GFRP bars. At higher loading stages, the induced strains were slightly higher than that of their NSC counterparts.

Figure 6.7 provides the strain distribution for outer (tension face) reinforcement layer along the span of the test specimens. The strain values decreased with distance from the column face until reaching zero at about 1000 mm from the column center. This implies that no bond failure or slip occurred during the tests. Furthermore, it can be noticed that the strains in the GFRP-RC specimen $G_{(1.6)}30/20$ were higher than that of steel-RC $S_{(1.7)}30/20$ specimen due to the lower axial stiffness. The steel- and GFRP-RC specimens showed similar profile

regardless the strain values which are similar to that reported by (Hussein et al. 2004). On the other hand, the specimen $G_{(1.2)}30/20$ which, was designed with the same axial stiffness as the specimen $G_{(1.6)}30/20$, evidenced similar ultimate strain values at failure. However, the strain profile of specimen $G_{(1.2)}30/20$ showed high strains at 750 mm from the column center line compared with $G_{(1.6)}30/20$ which may imply effect of gauge location with respect to the crack location.

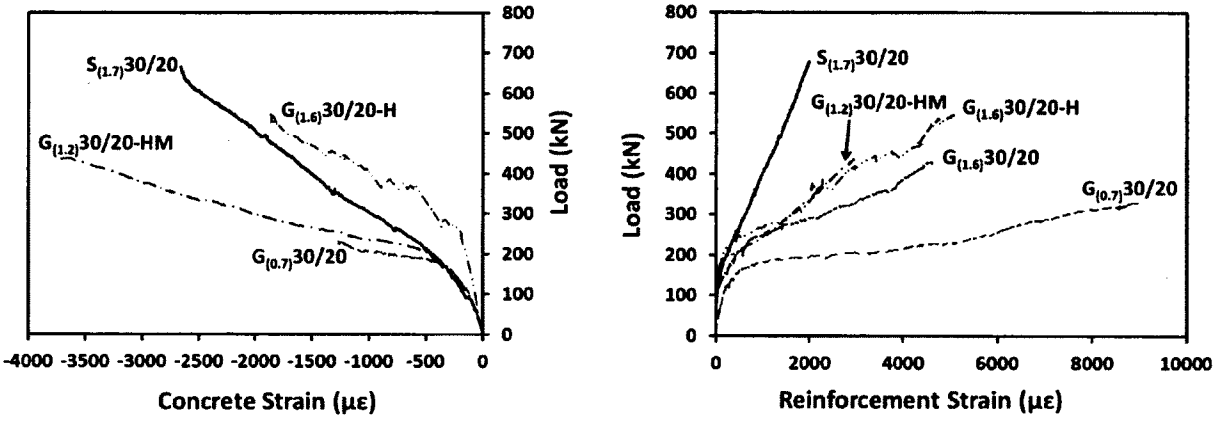

(a) Series I

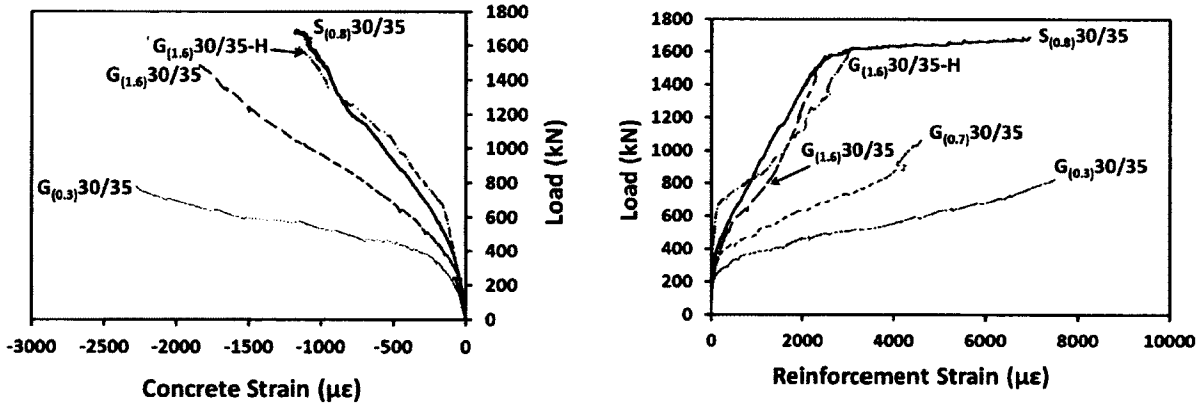

(b) Series II

Figure 6.6: Load-strain reinforcement and concrete relationships: (a) Series I; (b) Series II

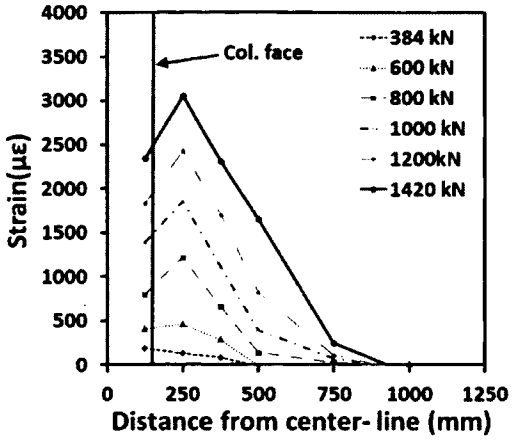

(a) Specimen $G_{(1.6)}30/35$

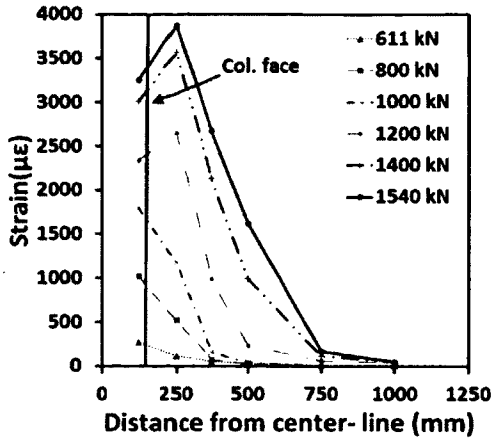

(b) Specimen $G_{(1.6)}30/35$-H

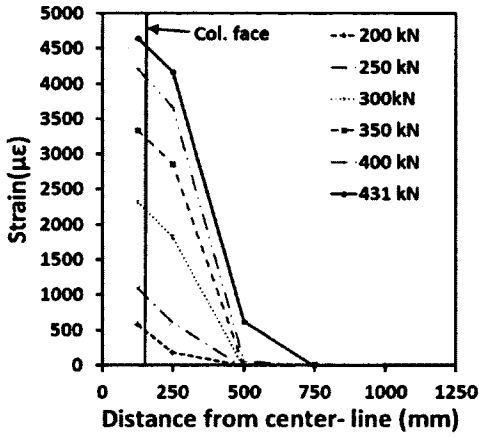

(c) Specimen $G_{(1.6)}30/20$

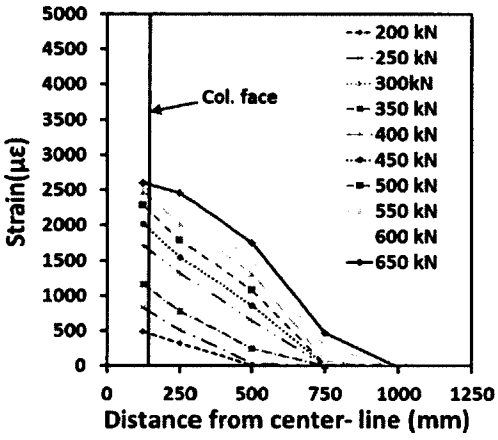

(d) Specimen $S_{(1.7)}30/20$

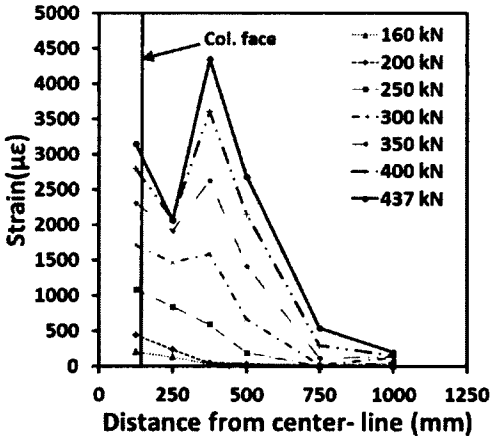

(e) Specimen $G_{(1.2)}30/20$

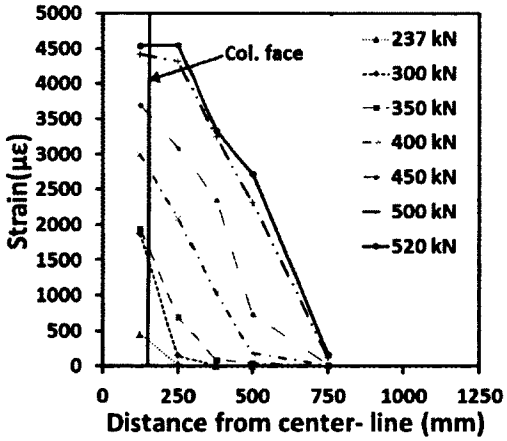

(f) Specimen $G_{(1.6)}30/20$-H

Figure 6.7: Reinforcement strain profiles for some tested specimens

6.3.5 Initial and Post-cracking Stiffness

Table 6.3 gives the calculated values of the initial stiffness (k_i), postcracking stiffness (k_p), and stiffness degradation (k_p/ k_i) for the test specimens. The k_i and k_p were calculated from the slopes of the first and second lines of the load-deflection relationships presented in Figure 6.5. From Table 6.3 and Figure 6.5, it can be noted that the concrete compressive strength and the slab thickness had direct effect on the initial slopes of the load–deflection curves of the GFRP specimens. In both series (I and II), the initial stiffness of the HSC was higher than that of the NSC. The initial stiffness of specimens $G_{(1.6)}30/20$-H and $G_{(1.6)}30/35$-H increased by 22% and 51% compared to their counterparts $G_{(1.6)}30/20$ and $G_{(1.6)}30/35$, respectively, because of the HSC's higher compressive strength and modulus of elasticity in comparison to the NSC. In addition, increasing the slab thickness from 200 to 350 mm increased the initial stiffness by 51% and 86% in specimens $G_{(1.6)}30/20$ and $G_{(1.6)}30/20$-H, respectively, compared to their counterparts $G_{(1.6)}30/35$ and $G_{(1.6)}30/35$-H. This reflects the direct effect of the slab thickness on the slab stiffness.

The postcracking stiffness, however, was dependent on the reinforcement type and ratio (axial reinforcement stiffness) rather than the concrete strength. There were no differences between the postcracking stiffness of the HSC specimens ($G_{(1.6)}30/20$-H and $G_{(1.6)}30/35$-H) and that of the NSC specimens ($G_{(1.6)}30/20$ and $G_{(1.6)}30/35$). On the other hand, increasing the axial reinforcement stiffness yielded higher postcracking stiffness. Besides, specimens $G_{(1.6)}30/20$ and $G_{(1.2)}30/20$ (with the same axial-reinforcement stiffness) had the same postcracking stiffness. In addition, the slab thickness has a direct impact on the postcracking stiffness. Increasing the slab thickness results an increase in the slab moment of inertia which, in turn, increases the postcracking stiffness significantly.

The ratio between the postcracking and initial stiffness (k_p/ k_i) was also evaluated for the tested specimens. For GFRP reinforced specimens in Series I, the k_p/ k_i ratio ranged from 0.10 to 0.17, whereas, for those in Series II, it ranged from 0.19 to 0.45. The degradation in the case of HSC was higher than that for the NSC specimens as given in Table 6.3.

6.4 Predications of Punching-Shear Capacity

Most of the empirical punching-shear strength equations for FRP-RC slabs are modified forms of the original ones for steel with some modifications to account for the difference in mechanical properties between the two materials, especially the lower modulus of elasticity.

This section assesses the accuracy of the available punching-shear equations for FRP-RC flat slabs in codes and design guidelines in CSA S806 (2012), ACI 440 (2006), BS 8110 (1997), and JSCE (1997). The accuracy of the design equations was assessed by comparing their predictions against the experimental results. The available punching-shear equations provided by FRP design codes and guides are summarized below.

6.4.1 CSA S806-12 (CSA S806, 2012)

The punching-shear strength provided by CSA S806 (2012) is the smallest of Eqs. (6.1) to (6.3). When calculating V_c using Eqns. (6.1) to (6.3), the concrete strength f'_c should not exceed 60 MPa.

$$V_c = 0.028\lambda\phi_c\left(1+\frac{2}{\beta_c}\right)\left(E_f\,\rho_f\,f'_c\right)^{1/3} b_{o;0.5d}\,d \tag{6.1}$$

$$V_c = 0.147\lambda\phi_c\left(\frac{\alpha_s d}{b_{o;0.5d}}+0.19\right)\left(E_f\,\rho_f\,f'_c\right)^{1/3} b_{o;0.5d}\,d \tag{6.2}$$

$$V_c = 0.056\lambda\phi_c\left(E_f\,\rho_f\,f'_c\right)^{1/3} b_{o;0.5d}\,d \tag{6.3}$$

6.4.2 ACI-440.1R-06 (ACI 440, 2006)

The ACI 440 equation considers the effect of reinforcement stiffness (FRP bars or grids) to account for the shear transfer in FRP-RC flat slabs, as shown in Eq. (6.4):

$$V_c = \frac{4}{5}\sqrt{f'_c}\,b_{o;0.5d}\,k\,d \tag{6.4 a}$$

$$k = \sqrt{2\rho_f n_f + \left(\rho_f n_f\right)^2} - \rho_f n_f \tag{6.4 b}$$

where $n_f = E_f / E_c$; $E_c = 4750\sqrt{f_c'}$

6.4.3 British Standards (BS 8110, 1997)

The BS 8110 (1997) modifies Eq. (6.5) for punching-shear capacity of steel-RC to Eq. (6.6) FRP-RC by replacing ρ_s by $\rho_f (E_f/E_s)$.

$$V_c = 0.79[100\rho_s]^{1/3}(f_{cu}/25)^{1/3}(400/d)^{1/4} b_{o;1.5d}\, d \text{ (Steel-RC)} \quad (6.5)$$

$$V_c = 0.79\left[100\rho_f (E_f/E_s)\right]^{1/3}(f_{cu}/25)^{1/3}(400/d)^{1/4} b_{o;1.5d}\, d \text{ (FRP-RC)} \quad (6.6)$$

6.4.4 Japanese Design Recommendations (JSCE, 1997)

The punching-shear strength according to JSCE (1997) is calculated as given in Eq. (6.7).

$$V_c = \beta_d \beta_p \beta_r f_{pcd} b_{o;0.5d} d/\gamma_b \quad (6.7\text{ a})$$

$$\beta_d = (1000/d)^{1/4} \leq 1.5 \quad (6.7\text{ b})$$

$$\beta_p = (100\rho_f E_f/E_s)^{1/3} \leq 1.5 \quad (6.7\text{ c})$$

$$\beta_r = 1 + 1/(1+0.25u/d) \quad (6.7\text{ d})$$

$$f_{pcd} = 0.2\sqrt{f_c'} \leq 1.2 \text{ Mpa} \quad (6.7\text{ e})$$

6.4.5 Comparison between experimental and predicted results

The accuracy of the available punching-shear equations in CSA S806 (2012), ACI 440 (2006), BS 8110 (1997), and JSEC (1997) are assessed herein by comparing their predictions with the experimentally determined punching-shear capacity of the 8 GFRP reinforced specimens and 46 other specimens from the literature. The safety factors included in all the punching-shear equations were set to 1.0. The tested-to-predicted punching shear ratios (V_{test}/V_{pred}) are presented in Table 6.4, while Figure 6.8 shows the V_{test}/V_{pred} ratio against the effective reinforcement ratio.

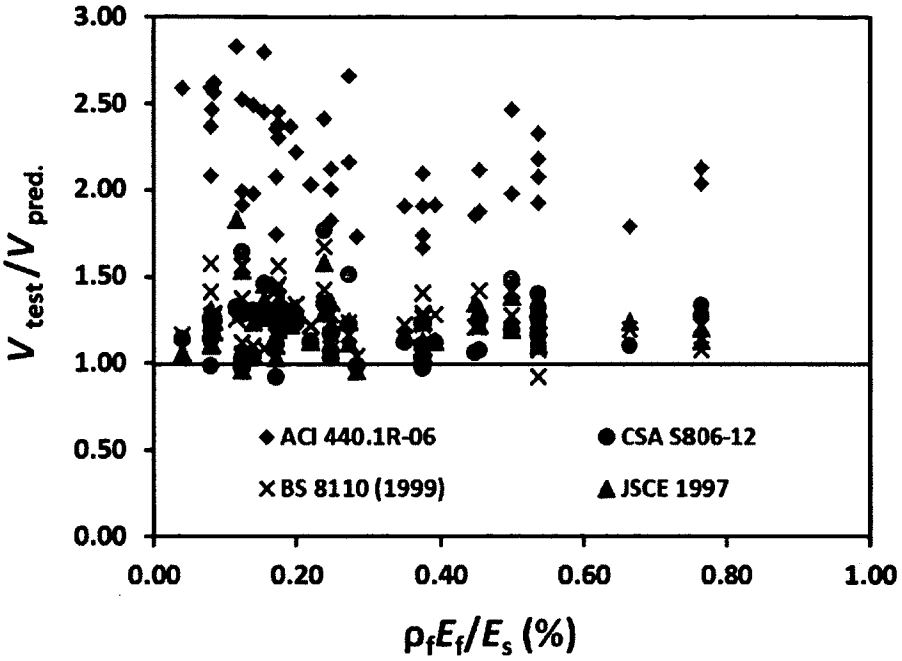

Figure 6.8: Tested-to-predicted capacity versus effective reinforcement ratio.

From the predictions reported in Table 6.4, it can be concluded that CSA S806 (2012), BS 8110 (1997), and JSCE (1997) equations yielded good yet conservative predictions with average V_{test}/V_{pred} of 1.21±0.17, 1.22±0.15, and 1.27±0.15 and a COV of 14%, 13%, and 12%, respectively, while ACI 440 (2006) showed very conservative predictions with average V_{test}/V_{pred} of 2.23±0.35. The direct implementation of the FRP axial stiffness into the punching-shear equations of CSA S806 (2012), BS 8110 (1997) through replacing ρ_s by $\rho_f E_f/E_s$ in the punching-shear equations gives good predications such as in case of CSA S806 (2012), BS 8110 (1997), and JSCE (1997). On the other hand, Eq. (6.4) of ACI 440 (2006) employs the FRP reinforcement ratio to calculate the depth of the neutral axis and consequently, the punching-shear strength is calculated from compression area of the cross-section. The contribution of the compression area itself; however, is dependent on the axial stiffness of the reinforcement. Thus, the absence of the axial stiffness of the reinforcement from the punching shear equation itself may be the reason for the high conservativeness level of this equation. In addition, the results showed that using the cubic root of the concrete strength in predicting the punching-shear capacity of the HSC GFRP prototypes yielded better predictions than using the square root of the concrete strength.

It should be mentioned that CSA S806 (2012) limits the applicability of its equation to a maximum concrete strength of 60 MPa. Using the CSA S806 (2012) equations for the high-strength concrete, specimens $G_{(1.6)}30/20$-H and $G_{(1.6)}30/35$-H with a compressive concrete strength of 75.8 MPa, yielded V_{test}/V_{pred} of 1.06 and 1.07, respectively. In addition the predictions for specimen H1 with a concrete strength of 118 MPa (Matthys & Taerwe, 2000 b) and specimen GSHS with a concrete strength of 71 MPa (Zhang et al., 2005) yielded V_{test}/V_{pred} of 1.32 and 1.07, respectively. Employing the 60 MPa in the punching-shear equation of CSA S806 (2012) for $G_{(1.6)}30/20$-H, $G_{(1.6)}30/35$-H, GSHS, and H1 yielded V_{test}/V_{pred} of 1.15 and 1.16, 1.13, and 1.65, respectively. Thus, the CSA S806 (2012) punching-shear equation may be applicable for a wider range of concrete strengths. That notwithstanding, further investigation is warranted.

Table 6.4: Tested-to-predicted punching-shear capacity (V_{test}/V_{pred})

Reference	Specimen	L (mm)	C (mm)	d (mm)	f'_c (MPa)	ρ_f (%)	E_f (GPa)	V_{test} kN	V_{test}/V_{pred} CSA S806 (2012)[a]	ACI 440 (2006)	BS 8110 (1997)	JSCE (1997)
This study	$G_{(0.7)}30/20$	2000	S300	134	34.3	0.71	48.2	329	1.11	2.08	1.26	1.11
	$G_{(1.6)}30/20$	2000	S300	131	38.6	1.56	48.1	431	1.11	1.90	1.26	1.13
	$G_{(1.6)}30/20$-H	2000	S300	131	75.8	1.56	57.4	547	1.15[b]	1.85	1.21	1.35
	$G_{(1.2)}30/20$	2000	S300	131	37.5	1.21	64.9	438	1.12	1.91	1.28	1.13
	$G_{(0.3)}30/35$	2000	S300	284	34.3	0.34	48.2	825	1.25	2.59	1.41	1.20
	$G_{(0.7)}30/35$	2000	S300	281	39.4	0.73	48.1	1071	1.22	2.30	1.38	1.20
	$G_{(1.6)}30/35$	2000	S300	275	38.2	1.61	56.7	1492	1.26	2.12	1.42	1.22
	$G_{(1.6)}30/35$-H	2000	S300	275	75.8	1.61	56.7	1600	1.16[b]	1.88	1.21	1.31
Dulude et al. (2010)	$G_{(0.7)}30/20$-B	2000	S300	134	38.6	0.71	48.2	386	1.25	2.36	1.43	1.27
	$G_{(0.7)}45/20$	2000	S450	134	44.9	0.71	48.2	400	0.92	1.74	1.16	1.04
	$G_{(1.6)}45/20$-B	2000	S450	131	39.4	1.56	48.1	511	0.97	1.67	1.23	1.05
	$G_{(0.3)}30/35$-B	2000	S300	284	39.4	0.34	48.2	781	1.13	2.37	1.28	1.11
	$G_{(0.7)}30/35$-B-2	2000	S300	281	46.7	0.73	48.1	1195	1.29	2.45	1.45	1.34
	$G_{(0.3)}45/35$	2000	S450	284	48.6	0.34	48.2	911	0.98	2.08	1.23	1.11
	$G_{(1.6)}30/20$-B	2000	S300	131	32.4	1.56	48.1	451	1.23	2.09	1.40	1.24
	$G_{(1.6)}45/20$	2000	S450	131	32.4	1.56	48.1	504	1.02	1.74	1.29	1.10
	$G_{(0.7)}30/35$-B-1	2000	S300	281	29.6	0.73	48.1	1027	1.29	2.38	1.45	1.27
	$G_{(0.3)}45/35$-B	2000	S450	284	32.4	0.34	48.2	1020	1.26	2.59	1.58	1.31
	$G_{(0.7)}45/35$	2000	S450	281	29.6	0.73	48.1	1248	1.24	2.30	1.56	1.31
Lee et al.(2009)	GFU1	2000	S225	110	36.3	1.18	48.2	222	0.98	1.73	1.04	0.96
Zhang et al.(2005)	GS2	1830	S250	100	35	1.05	42.0	218	1.12	2.03	1.22	1.13
	GSHS	1830	S250	100	71	1.18	42.0	275	1.13[b]	2.00	1.17	1.35
Zaghloul & Razaqpur (2004)	ZJF5	1500	S 250	75	44.8	1.33	100.0	234	1.10	1.79	1.20	1.24
Hussien & Rashid (2004)	GS1	1830	S 250	100	40.0	1.18	42.0	249	1.17	2.12	1.28	1.22
	GS2	1830	S 250	100	35.0	1.05	42.0	218	1.12	2.03	1.22	1.13
	GS3	1830	S 250	100	29.0	1.67	42.0	240	1.12	1.91	1.22	1.17
	GS4	1830	S 250	100	26.0	0.95	42.0	210	1.23	2.22	1.34	1.31
Ospina et al. (2003)	GFR-1	1670	S 250	120	29.5	0.73	34.0	199	1.03	1.99	1.12	1.04
	GFR-2	1670	S 250	120	28.9	1.46	34.0	249	1.03	1.82	1.12	1.04
	NEF-1	1670	S 250	120	37.5	0.87	28.4	203	0.97	1.91	1.06	0.96
El-Ghandour et al. (2003)	SG1	1700	S 200	142	32.0	0.18	45.0	170	1.14	2.59	1.16	1.06
	SC1	1700	S 200	142	32.8	0.15	110.0	229	1.20	2.47	1.23	1.11
	SG2	1700	S 200	142	46.4	0.38	45.0	271	1.25	2.62	1.28	1.24
	SG3	1700	S 200	142	30.4	0.38	45.0	237	1.26	2.56	1.29	1.18
	SC2	1700	S 200	142	29.6	0.35	110.0	317	1.29	2.37	1.32	1.22

Table 6.4 (cont.): Tested-to-predicted punching-shear capacity (V_{test}/V_{pred})

Reference	Specimen	L (mm)	C (mm)	d (mm)	f'_c (MPa)	ρ_f (%)	E_f (GPa)	V_{test} kN	V_{test}/V_{pred} CSA S806 (2012)[a]	ACI 440 (2006)	BS 8110 (1997)	JSCE (1997)
Matthys&Taerwe (2000 b)	C1	900	C 150	96	36.7	0.27	91.8	181	1.64	3.22	1.56	1.54
	C1'	900	C 230	96	37.3	0.27	91.8	189	1.28	2.52	1.37	1.30
	C2	900	C 150	95	35.7	1.05	95.0	255	1.49	2.47	1.42	1.39
	C2'	900	C 230	95	36.3	1.05	95.0	273	1.19	1.98	1.27	1.20
	C3	900	C 150	126	33.8	0.52	92.0	347	1.76	3.16	1.67	1.58
	C3'	900	C 230	126	34.3	0.52	92.0	343	1.34	2.41	1.43	1.29
	CS	900	C 150	95	32.6	0.19	147.6	142	1.30	2.49	1.24	1.24
	CS'	900	C 230	95	33.2	0.19	147.6	150	1.03	1.98	1.10	1.05
	H2	900	C 150	89	35.8	3.76	40.7	231	1.28	2.04	1.22	1.20
	H2'	900	C 80	89	35.9	3.76	40.7	171	1.34	2.13	1.08	1.13
	H3	900	C 150	122	32.1	1.22	44.8	237	1.23	2.16	1.17	1.12
	H3'	900	C 80	122	32.1	1.22	44.8	217	1.51	2.66	1.23	1.24
	H1	900	C 150	95	118.0	0.62	37.3	207	1.65[b]	2.83	1.26	1.83
Banthia et al. (1995)	I	500	C 100	55	41.0	0.31	100.0	65	1.46	2.80	1.26	1.46
	II	500	C 100	55	52.9	0.31	100.0	61	1.26	2.45	1.09	1.37
Ahmad et al. (1993)	CFRC-SN1	590	S 75	61	42.4	0.95	113.0	93	1.40	2.33	1.12	1.32
	CFRC-SN2	590	S 75	61	44.6	0.95	113.0	78	1.16	1.93	0.92	1.11
	CFRC-SN3	590	S 100	61	39.0	0.95	113.0	96	1.26	2.08	1.08	1.21
	CFRC-SN4	590	S 100	61	36.6	0.95	113.0	99	1.32	2.18	1.14	1.25
								Mean	**1.21**	**2.23**	**1.22**	**1.27**
								S.D.	0.17	0.35	0.15	0.15
								COV (%)	14	16	13	12

Note: L; Loaded span (mm); C circular and S square column
[a] From equation (6.3).
[b] Using concrete strength of 60 MPa (CSA S806, 2012)

6.5 Conclusions

This paper assessed the performance and punching-shear strength of two-way flat plates/slabs reinforced with glass fiber-reinforced polymer (GFRP) bars of different grades using normal- and high-strength concretes (NSC & HSC). Based on the experimental results and discussions presented herein, the following conclusions can be drawn:

- The tested specimens showed punching-shear failure as the final mode with no signs of concrete flexural crushing, and with no rupture or slippage failure of the reinforcing bars.
- Increasing the GFRP reinforcement ratio yielded higher punching-shear capacities, lower strains in the reinforcement, and smaller slab deflections. Increasing the reinforcement ratio from 0.71% to 1.56% in Series I and from 0.34% to 1.62% in Series II increased the punching-shear stresses at failure by 35% and 81%, respectively. The specimen $G_{(1.2)}30/20$

designed with the axial reinforcement stiffness (E_fA_f) as $G_{(1.6)}30/20$ yielded the same punching-shear capacity.

- Using HSC for the GFRP-RC specimens improved the punching-shear capacity. The ultimate punching-shear capacity of $G_{(1.6)}30/20$-H and $G_{(1.6)}30/35$-H increased by 27% and 7% over their counterparts, respectively ($G_{(1.6)}30/20$ and $G_{(1.6)}30/35$). The smaller increase (7%) in case of the thick slabs (350 mm) might imply a size-effect contribution.

- The HSC directly enhanced the load-deflection relationships in specimens $G_{(1.6)}30/20$-H and $G_{(1.6)}30/35$-H. The two specimens evidenced lower deflections at the same load level than the other GFRP-RC with NSC ones. In addition, they showed the same load-deflection relationships as their steel-RC counterparts until about 60% of the ultimate capacity.

- Concrete compressive strength had a significant effect on the initial stiffness (uncracked stiffness) of the GFRP-RC specimens. The initial stiffness increased by 22% and 51% in test specimens $G_{(1.6)}30/20$-H and $G_{(1.6)}30/35$-H compared to their counterparts $G_{(1.6)}30/20$ and $G_{(1.6)}30/35$, respectively. The post-cracking stiffness, however, was similar to the GFRP reinforced specimens made with NSC.

- The punching-shear stress at failure was proportional to the effective reinforcement ratio ($\rho_f E_f/E_s$) to the power of 0.34. Thus, CSA S806 (2012) and BS 8110 (1997) yielded good yet conservative predictions as they incorporate $(\rho_f E_f/E_s)^{1/3}$ along with the cubic root of the concrete compressive strength, which agrees with the experimental findings. CSA S806 (2012) and BS 8110 (1997) showed an average V_{test}/V_{pred} of 1.21±0.17 and 1.22±0.15, respectively. On the other hand, ACI 440 (2006) yielded very conservative predictions with an average V_{test}/V_{pred} of 2.23±0.35.

- Despite the 60 Mpa concrete strength limit in the CSA S806 (2012) punching-shear provision, it yielded good predictions for two specimens with a concrete strength of 75.8 MPa. The V_{test}/V_{pred} ratios for those two prototypes were 1.06 and 1.07, respectively. Further investigation, however, is needed.

CHAPTER 7
PUNCHING-SHEAR BEHAVIOUR OF GFRP TWO-WAY SLABS USING FRP SHEAR REINFORCEMENT

Foreword

Authors Biographies

Mohamed Hassan is a PhD candidate, Dept. of Civil Eng., University of Sherbrooke, Sherbrooke, Quebec, Canada, J1K 2R1, Phone: 1-819-821-8000, ext. 63181, Fax: 1-819-821-7974, E-mail: Mohamed.Hassan@USherbrooke.ca

Ehab A. Ahmed is a M.ASCE, Postdoctoral fellow, Dept. of Civil Eng., University of Sherbrooke, Sherbrooke, Quebec, Canada, J1K 2R1. Tel. 1-819-821-8000, ext. 62135, Fax 1-819-821-7974, E-mail: Ehab.Ahmed@USherbrooke.ca

Brahim Benmokrane , FACI, is an NSERC & Tier-1 Canada Research Chair Professor, Dept. of Civil Eng., University of Sherbrooke, Sherbrooke, Quebec, Canada, J1K 2R1. Tel. 1-819-821-7758, Fax 1-819-821-7974, Corresponding author, E-mail: Brahim.Benmokrane@USherbrooke.ca

Submitted date: 17 August 2013

Journal: Journal of Composite for Construction–*American Society of Civil Engineers (ASCE)*

Title: "Punching-Shear Behavior of Two-Way Slabs Reinforced with FRP Shear Reinforcement".

Titre en français: "Comportement au poinçonnement de dalles bidirectionnelles renforcé par des barres de cisaillement en PRF".

Paper's contribution to the project: This paper presents the results of an experimental investigation on the behaviour of behavior of GFRP-RC two-way flat slabs reinforced with and without FRP shear reinforcement. A total of 10 full-scale interior slab- column connections were tested under concentrated load up to failure. The tests were performed to evaluate the effectiveness and contribution of using the FRP as shear reinforcement in the GFRP-RC slabs. Research findings indicated that using FRP stirrups as shear reinforcement in the test specimens was an effective way in increasing the punching-shear and deformation capacity, in particularly when the flexural reinforcement is high.

Abstract: This study investigated the punching-shear behavior of two-way concrete slabs with glass-fiber-reinforced polymer (GFRP) bars as flexural reinforcement and FRP stirrups (Glass or Carbon) as shear reinforcement. Ten full-scale interior slab–column specimens measuring 2500 × 2500 mm with thicknesses of either 200 or 350 mm, and 300 × 300 mm square column stubs were fabricated and tested under monotonic concentric loading until failure. These tests aimed at assessing the effectiveness and contribution of FRP stirrups as shear reinforcement in two-way concrete slabs. The investigated parameters were the flexural reinforcement ratio and the shear reinforcement type (Glass FRP and Carbon FRP stirrups) and ratio. The test results revealed that using FRP stirrups as shear reinforcement increased the punching-shear strength and the deformation capacity of the test specimens. The increased punching-shear strength and deformation capacity were proportional to the flexural- and shear-reinforcement ratios. In addition, the brittle punching-shear failure mode may be prevented and transformed into ductile mode when FRP stirrups are used as shear reinforcement assuming that no rupture of stirrups occurs.

Keywords: Punching-shear; Two-way; Slab-column; Slab; Fiber-reinforced polymer; GFRP; Thickness; Design; Shear reinforcement.

7.1 Introduction

The deterioration of reinforced-concrete (RC) structures due to corrosion of steel bars limits their service life and increases their maintenance costs. RC slabs are the component most vulnerable to corrosion-related deterioration because they are directly exposed to high concentrations of chlorides used for snow and ice removal. To overcome the corrosion-related problems, steel bars should be protected against corrosion or replaced with noncorrodible materials, such as fiber-reinforced polymer (FRP) bars. Using FRP bars in RC slabs, such as in parking garages, can extend the service life, reduce maintenance costs, and improve life-cycle cost efficiency.

The punching-shear failure of the slab–column connection can lead to catastrophic collapse of the entire floor system. The punching-shear failure of RC slabs without shear reinforcement is brittle in nature with limited deflections and accompanied by a sudden loss of the load-carrying capacity. Well-designed punching-shear reinforcement significantly improves slab behavior, as it not only increases slab punching-shear strength but also the structure's deformation capacity (Lips et al. 2012). A few studies have been conducted to investigate the punching-shear behavior of two-way FRP-RC slabs without shear reinforcement (Matthys and Taerwe 2000 b; El-Ghandour et al. 2003; Ospina et al. 2003; Zaghloul 2007; Lee et al. 2009; Nguyen-Minh and Rovank 2013). Very limited research work, however, has been done on two-way FRP-RC slabs with shear reinforcement (El-Ghandour et al. 2003; Li et al. 2006; Zaghloul 2007).

El-Ghandour et al. (2003) tested three specimens with FRP bars for flexural reinforcement and carbon-FRP (CFRP) shear bands for shear reinforcement. The test results indicated that the shear bands increased the punching-shear capacity by an average ratio of 15.9%. They also played a role in delaying bond slip and preventing punching-shear failure at lower load levels. In addition, the slabs with shear bands evidenced larger deformability than the slabs without shear reinforcement. Li et al., (2006) conducted an experimental study to investigate the behavior of two-way steel-RC flat slabs with CFRP rods as shear reinforcement under constant gravity loading and lateral displacements in a reversed-cyclic manner. The results indicated that the specimen with CFRP rods as shear reinforcement exhibited significant flexural yielding and sustained deformations up to a drift ratio of 9% without

significant loss of strength. Furthermore, punching-shear failure was not observed in this specimen. Zaghloul (2002 & 2007) tested two interior slab–column specimens with CFRP grids as flexural reinforcement and specially-manufactured CFRP shear rails as shear reinforcement under shear and unbalanced moments. The results revealed that the CFRP shear rails increased the punching-shear capacity of the interior slab–column connection by 24.6% and 30.4%, when the first leg of the shear reinforcement was located $0.5d$ and $0.85d$, respectively. This increase in punching-shear capacity is comparable to the increase that can be achieved with steel-headed studs. Moreover, despite CFRP's lack of ductility, the CFRP-RC connections exhibited essentially the same amount of ductility as steel-RC connections. More investigation, however, is needed to understand the structural behavior of FRP-RC flat slabs with FRP shear reinforcement in different configurations, such as FRP stirrups.

An extensive two-phase research project was carried out at the University of Sherbrooke to investigate the behavior of two-way GFRP-RC slabs. Phase I focused on two-way GFRP-RC slabs without shear reinforcement, considering the reinforcement ratio, slab thickness, column dimensions, and concrete strength as testing parameters. The phase was completed (Dulude et al. 2013) and its findings contributed to the field implementation of GFRP bars in two parking garages in Québec (Quebec, Canada): Hotel de Ville in 2010 and La Chancelière in 2011 (Benmokrane et al. 2012). Phase II, which is presented herein, aimed at investigating the punching-shear behavior of two-way GFRP-RC slabs reinforced with carbon and glass (CFRP and GFRP) stirrups as shear reinforcement.

7.2 Experimental Program

7.2.1 Test specimens

A total of 10 full-scale two-way specimens were constructed and tested up to failure under monotonic concentrated loading. The test specimens were designed to simulate the real thicknesses of slabs used in field applications (Benmokrane et al. 2012). The specimens measured 2500 × 2500 mm with thicknesses of either 200 mm (Series I) or 350 mm (Series II), and a square column stub measuring 300 × 300 mm. The column stub extended 300 mm beyond the top and bottom surfaces of the slabs. Table 7.1 presents the test matrix and characteristics for each specimen. All the specimens had GFRP bars as flexural reinforcement,

but seven specimens had CFRP and GFRP stirrups as shear reinforcement and the remaining three served as reference specimens to assess stirrup contribution to punching-shear capacity and deformation capacity. The GFRP flexural reinforcement ratios (ρ_f) ranged from 0.34% to 1.61% to assess the efficiency of the FRP stirrups in relatively low and high flexural-reinforcement ratios. The clear concrete cover was between 45 to 50 mm. Figure 7.1 shows the geometry and typical reinforcement configuration of the test specimens. The test specimens were provided with GFRP flexural reinforcement ratios (ρ_f) ranged from 0.34% to 1.61%. This range was chosen to evaluate the efficiency of the FRP stirrups in relatively low and high flexural reinforcement ratios.

The test matrix was divided into two series according to slab thickness. Series I (200 mm thick) comprised three specimens with GFRP bars as flexural reinforcement at a ratio (ρ_f) of 1.21%. Two specimens were reinforced with discrete GFRP and CFRP closed stirrups, while the third one served as the reference slab without shear reinforcement. The GFRP and CFRP stirrups were #10 and distributed along the orthogonal directions with a spacing of $d/2 = 70$ mm. Figure 7.1 and Figure 7.2 show the test specimen geometry and the investigated shear reinforcement configurations, respectively.

Series II (350 mm thick) comprised seven specimens with GFRP bars as flexural reinforcement at a ratio of 0.34% or 1.61%. Five specimens were fabricated with GFRP and CFRP spiral stirrups, including one specimen ($G_{(1.6)}$350-GBSS(d/4) with GFRP spiral stirrups in a bundled configuration (see Figure 7.2). In this test series, spiral stirrups were used because of their fast and easy installation during construction in comparison to discrete closed ones. Both of the GRRP and CFRP spirals used were #13 and distributed along the orthogonal directions of the slabs with spacing ranging from $d/3$ to $d/4$ (100 mm to 70 mm). The shear reinforcement ratio (ρ_{fv}) was calculated with the cross-sectional area of the FRP stirrups on a concentric line parallel to the perimeter of the column at $0.5d$ from the column face as specified by ACI 318 (2008) and CSA 23.4 (2004).

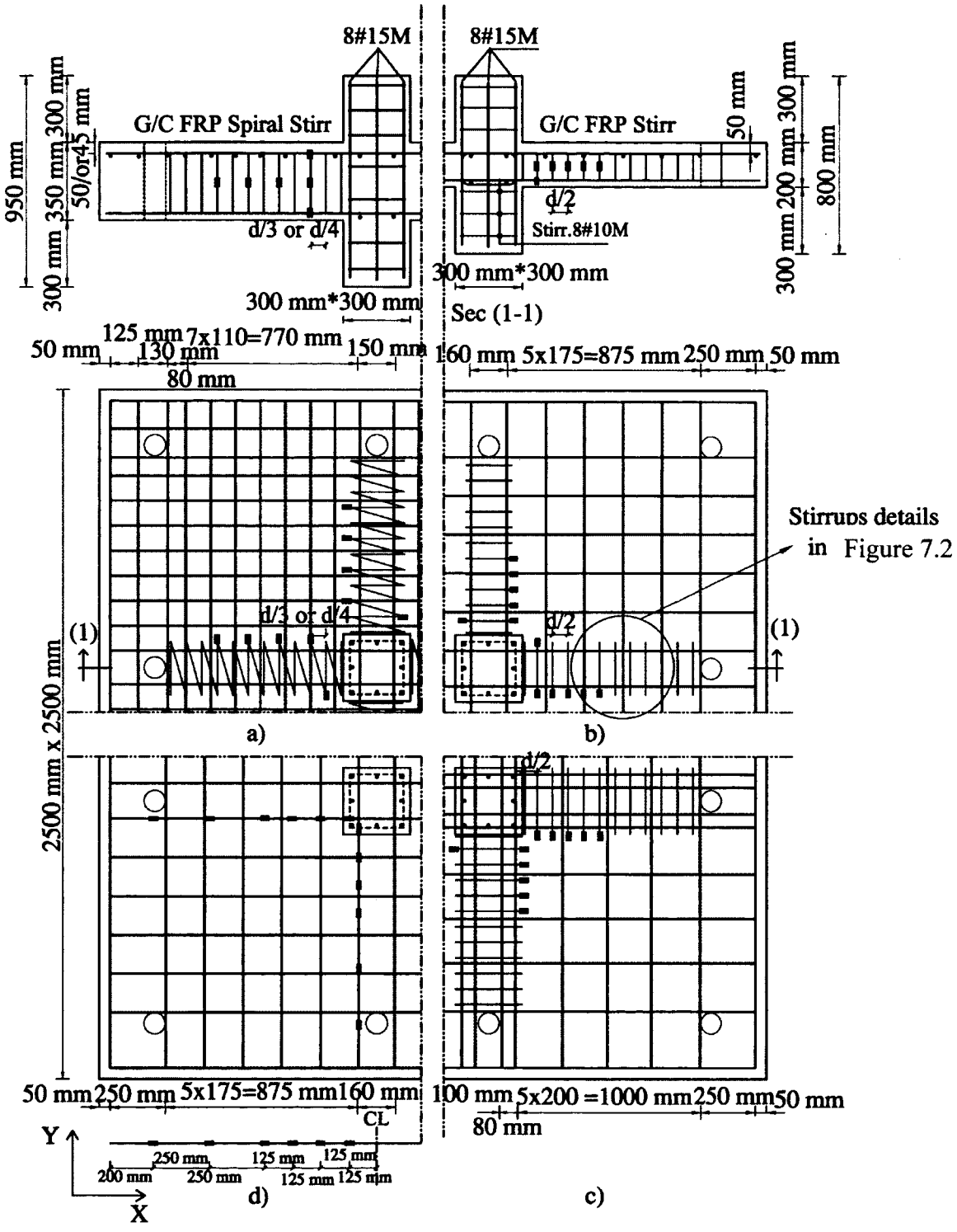

Dimensions in mm; Stirrups details are shown in Fig. 7.2

Figure 7.1: Test specimens' geometry, reinforcement configuration and instrumentations: a) G/CSS and GBSS; b) CCS; c) GCS; d) slabs without shear reinforcement

Table 7.1: Details of test specimens

Series	Specimen [a]	Slab thick. mm	d, effective depth. mm	Tens Reinf.	ρ_f, %	ρ_{fb} %	ρ_{fv}, %	$\rho_{fv}E_{fv}$, GPa%	f'_c [b], MPa	f_t [b], MPa	Shear Reinforcement			
											RFT type	Diam.	Spacing mm	Shape (Width x height)[c], mm
I	$G_{(1.2)}200$	200	131	14 No. 20	1.21	0.24	-	-	37.5	3.5	-	-	-	-
	$G_{(1.2)}$ 200-GCS(d/2)		131	14 No. 20	1.21	0.24	0.94	42	37.5	3.5	GFRP	No.10	70	C240×140
	$G_{(1.2)}$ 200-CCS(d/2)		131	14 No. 20	1.21	0.24	0.47	61	37.5	3.5	CFRP	No.10	70	C240×140
II	$G_{(0.3)}350$	350	284	12 No. 15	0.34	0.49	-	-	34.3	2.5	-	-	-	-
	$G_{(0.3)}350$-GSS(d/4)		284	12 No. 15	0.34	0.43	0.63	28	29.5	2.3	GFRP	No.13	70	S300×290
	$G_{(1.6)}350$		280	22 No. 25	1.61	0.33	-	-	38.2	3.3	-	-	-	-
	$G_{(1.6)}$ 350-GSS(d/4)		280	22 No. 25	1.61	0.34	0.64	28	40.2	3.3	GFRP	No.13	70	S300×290
	$G_{(1.6)}$ 350-GBSS(d/4)		280	22 No. 25	1.61	0.32	1.27	57	37.5	3.5	GFRP	No.13	70	S300×290
	$G_{(1.6)}$ 350-CSS(d/4)		280	22 No. 25	1.61	0.33	0.64	79	38.2	3.3	CFRP	No.13	70	S300×290
	$G_{(1.6)}$ 350-CSS(d/3)		280	22 No. 25	1.61	0.34	0.45	55	40.2	3.3	CFRP	No.13	100	S300×290

[a] $G_{(aa)}$bb-cdd(S_{fv}): G denotes GFRP tension reinforcement, (aa) denotes the reinforcement ratio, bb denotes the slab thickness in mm; c denotes the FRP punching shear reinforcement material (GFRP and/or CFRP); dd denotes stirrups configuration (SS single spiral stirrups and BSS denotes bundle spiral stirrups; CS denotes closed stirrups; and S_{fv} denotes stirrups spacing relative to the effective depth; if any.

[b] Based on 150×300 mm cylinder testing.

[c] S spiral and C closed stirrups cross section dimensions (width × height).

7.2.2 Materiel properties

Sand-coated GFRP bars of sizes No. 15, No. 20, and No. 25, designated according to the CSA S807 (2010), were used as flexural reinforcement of the test specimens. The GFRP bars were manufactured by combining the pultrusion process with an in-line sand coating to enhance the bond between the bars and the surrounding concrete. The tensile properties of the GFRP bars were determined by testing five representative bars for each diameter in accordance with ASTM D7205M (2011). Table 7.2 summaries the mechanical properties of the GFRP bars as determined from testing.

For the shear reinforcement (stirrups), two types of sand-coated FRP stirrups were used namely CFRP and GFRP. Closed discreet and spiral continuous stirrups diameters No. 10 and No. 13 were used in Series I and II, respectively. Figure 7.2 shows the configurations of the investigated stirrups. The mechanical properties of the straight and bend portions of the stirrups were determined by testing five representative sample of each FRP type and diameter according to ASTM D7205M (2011) and B.5 test method of ACI 440 (2004), respectively. The mechanical properties of the GFRP and CFRP stirrups are reported in Table 7.3.

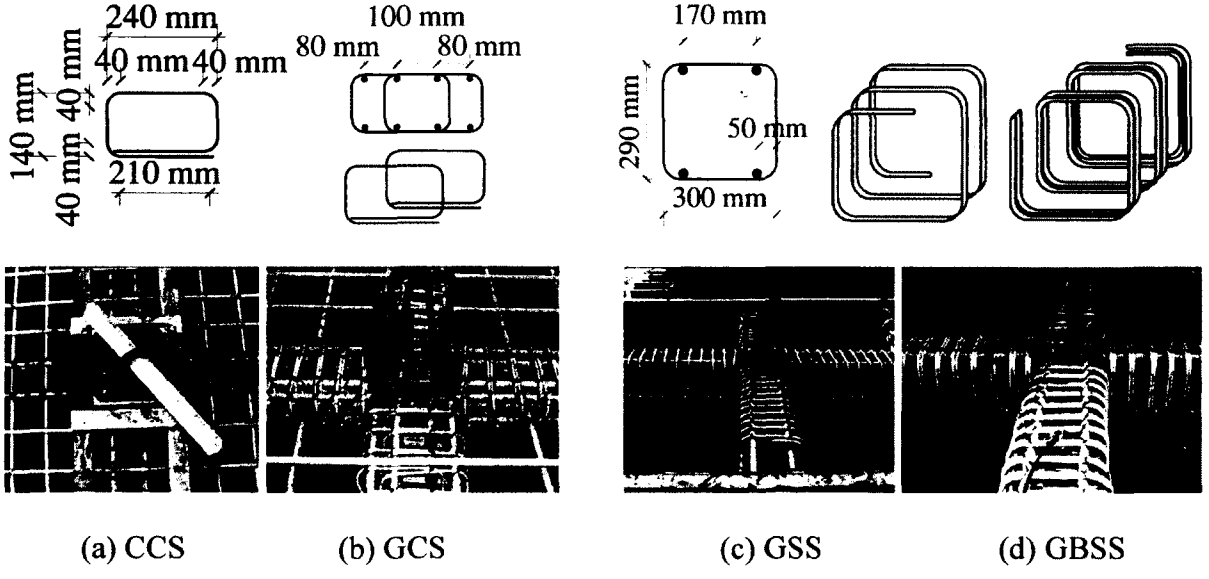

(a) CCS (b) GCS (c) GSS (d) GBSS

Figure 7.2: Details and configurations of investigated stirrups

The test specimens were cast using a ready-mixed, normal-weight concrete with a 28-day target concrete compressive strength of 35 MPa and 5% to 8% of entrained air. The concrete compressive (f_c') and tensile strength (f_t') were determined, on the day of testing, using three 150 × 300 mm concrete cylinders for each of the compression and splitting tests. The compressive strength ranged from 29.5 to 40.2 MPa, while the tensile strength ranged from 2.3 to 3.5 MPa. Table 7.1 also provides the concrete strengths.

Table 7.2: Mechanical properties of GFRP flexural reinforcement

Bar Size	Area (mm^2)	Elastic tensile modulus, E_f (GPa)	Ultimate Tensile Strength, f_{fu} (MPa)	Characteristic Tensile Strength[a], f_{fu} (MPa)	Ultimate Tensile Elongation (%)
No. 15	199	48.2±0.4	769±23	700	1.60±0.05
No. 25	510	56.7±0.3	1065±22	999	1.88±0.04
No. 20	284	64.9±0.6	1334±85	1079	2.07±0.13

[a] Characteristic tensile strength=Average value – 3× standard deviation.

Table 7.3: Mechanical properties of FRP stirrups

FRP Product	Bar Size	r_b (mm)	d_b (mm)	Area (mm^2)	Elastic Tensile Modulus (straight), E_{fv} (GPa)	Ultimate Tensile Strength (straight), f_{fv} (MPa)	Ultimate Tensile Strength, (bent)[a] f_{fvb} (MPa)	f_{fvb}/f_{fuv}	Ultimate Tensile Elongation, (straight) (%)
GFRP	No. 10	40	9.53	71	44.8±0.5	948±39	485±42	0.48	2.11±0.08
	No. 13	50	12.7	129	44.6±0.4	1004±19	551±46	0.53	2.25±0.06
CFRP	No. 10	40	9.53	71	130.0±0.6	1562±24	780±75	0.49	1.20±0.04
	No. 13	50	12.7	129	124.4±0.7	1562±30	774±80	0.50	1.26±0.03

[a] f_{fvb} is the ultimate tensile bend strength obtained from B.5 test method according to ACI 440 (2004).

7.2.3 Test setup and instrumentation

The specimens were tested under monotonic concentrated loading, acting on the column stub from the bottom side of the slabs until failure. The specimens were simply supported on all four sides and were held against the laboratory's rigid floor by a rigid steel frame 100 mm in width supported by eight steel tie rods 38 mm in diameter. The specimens were supported on a temporary frame (Figure 7.3) which leveled. A 15 mm thick layer of cement mortar was placed on the concrete surface at the location of the rigid steel frame. In addition, 10 mm thick neoprene sheets were used over the loading plate and between the supporting frame and the slab. Thereafter, the load was applied with one or two 1500 kN

hydraulic jacks according to the expected capacity of each specimen at a loading rate of 5 kN/min. When two hydraulic jacks were used, they were connected to the same pump and calibrated to work simultaneously. Figure 7.3 provides the details of the test setup.

Each specimen was equipped with two instrumented bars in the orthogonal directions in the top reinforcing mat (tension side) with six electrical strain gauges attached to each bar. Six electrical strain gauges in each orthogonal direction were glued to the straight, bend locations top and bottom of the stirrups, as shown in Figure 7.1. In addition, eight concrete electrical strain gauges—labeled C1 to C8—were glued to the slab's bottom surface (compression side) before testing. Moreover, the eight steel anchors supporting the test specimen were instrumented with electrical strain gauges to verify the loading symmetry during the test. The deflection at the different locations (see Figure 7.3) was captured with eleven linear variable differential transducers (LVDTs). The strain gauges and LVDTs were connected to a data-acquisition system to record the readings. Figure 7.3 shows the locations of strain gauges and LVDTs. During the test, crack propagation was marked and the corresponding loads were recorded.

7.3 Test Results and Discussions

7.3.1 Cracks and failure envelop

The specimens showed similar crack propagation in the top surface (tension side) during testing. At failure, however, the punching-shear cone was considerably large in the specimens with FRP shear reinforcement. Figure 7.4 shows the final punching-shear failure (in bold) of the specimens. The flexural cracks occurred first (radially) and advanced from the column corners along the central four axes of symmetry (X and Y directions and 2 diagonals) towards the slab edges. As the load increased, the radial cracks increased and a tangential crack appeared at the column interface along the perimeter. Thereafter, at higher loading (~51% to 56% of the peak load), tangential cracks developed outside the column, thereby connecting the radial cracks. Table 7.4 provides the loads at the appearance of first radial and tangential cracks (V_{cr} and V_{tang}) as well as the corresponding deflections (Δ_{cr} and Δ_{tang}). Finally, the slabs failed by the column punching through the slab, except in specimens $G_{(1.6)}$350-CSS(d/4) and $G_{(1.6)}$350-GBSS(d/4), which were characterized by high flexural and shear

reinforcement ratios. The high reinforcement ratios in specimens $G_{(1.6)}$350-CSS(d/4) and $G_{(1.6)}$350-GBSS(d/4) increased the their punching-shear strength, which resulted in further shear cracks around the middle points of the supporting steel anchorages. At higher loading, the maximum strain in the middle steel anchorage was approximately 3 times the strain in the corner anchorages. Consequently, the slabs ($G_{(1.6)}$350-CSS(d/4) and $G_{(1.6)}$350-GBSS(d/4)) behaved like a slab supported on four points rather than line support due to the differential deformation of the supporting anchors. This behavior could explain the formation of the diagonal shear cracks that appeared outside the slab (side view), as shown in Figure 7.4 (f) and Figure 7.4 (h).

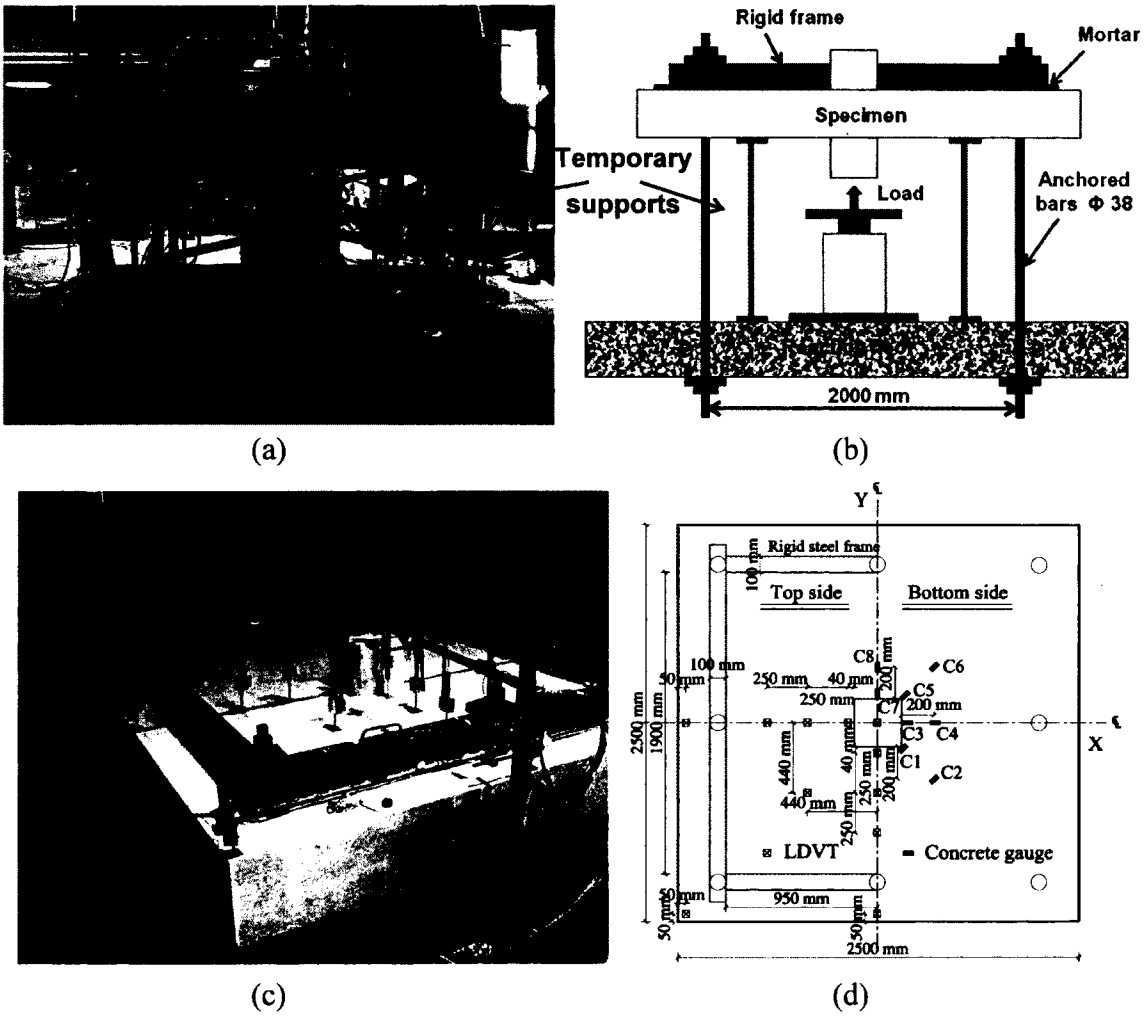

Figure 7.3: Test setup and instrumentation: (a) Supports and loading jacks; (b) Schematic; (c) LVDTs locations; (d) Instrumentation details

The specimens with high flexural reinforcement ratios and without shear reinforcement showed brittle punching-shear failure at corresponding small deflections. At low flexural reinforcement ratios, such as in specimen $G_{(0.3)}350$, large deflections prior to failure, more flexural cracks around the column, and some ductile behavior were observed before punching-shear failure. Figure 7.5 shows the sawn-off sections of the specimens, which clarify that specimens without shear reinforcement exhibited a main critical shear crack starting from the column face to the tension slab side with different inclination angles. The inclination angle of the critical shear crack was affected by the flexural reinforcement ratio: the higher the flexural reinforcement ratio, the flatter the inclination angle of the critical shear crack, as illustrated by specimen $G_{(1.6)}350$. Increasing the flexural reinforcement ratio enhanced the in-plane restraint of the slab and led to a much flatter inclination of the critical shear crack. This observation is in agreement with the findings of Guandalini et al. (2009), in which increasing the steel reinforcement ratio led to a much flatter inclination of the critical shear crack. The distance defining the failure surface (X_{cone}) (the observed distance from column face to the location of the failure envelope) was measured at different locations; the average values were calculated and reported in Table 7.4 (multiplications of d). The reported X_{cone} values confirm the effect of the flexural reinforcement ratio on the angle of the critical shear crack.

7.3.2 Shear reinforcement effects on the failure mode

The FRP shear-reinforcement ratio plays a significant role in failure mode, in particular when the flexural-reinforcement ratio is high enough to ensure punching-shear failure at relatively low strains in the flexural reinforcement. The brittle punching-shear failure in the specimens with FRP shear reinforcement may be eliminated and converted into a ductile failure mode (Marzouk and Jiang 1997), assuming that no rupture occurred in the stirrups. The sawn specimens with FRP stirrups (Figure 7.5) developed two types of cracks. The first type was extensively distributed inclined shear cracks starting from the column face and ending with a horizontal splitting crack at the level of the flexural reinforcement in the slab's tension side. The second type was a horizontal splitting crack in the compression side in the concrete cover. Andersson (1963), through testing of specimens with a large amount of shear reinforcement, reported that the radial compressive force in the concrete near the column acts in a nearly horizontal direction. Therefore, a substantial portion of this force is transmitted into

the region around and under the lower part of the shear reinforcement. Furthermore, in this region, the radial compressive force changes its direction. Consequently, tensile stresses are produced in a horizontal section through the lower part of the shear reinforcement. In addition, the large amount of shear reinforcement caused an increase in the eccentricity of the radial compressive force in the concrete, which increased the radial tensile stresses in the slab's top surface. This could explain the development of the two horizontal splitting cracks in Figure 7.5 in the specimens with shear reinforcement.

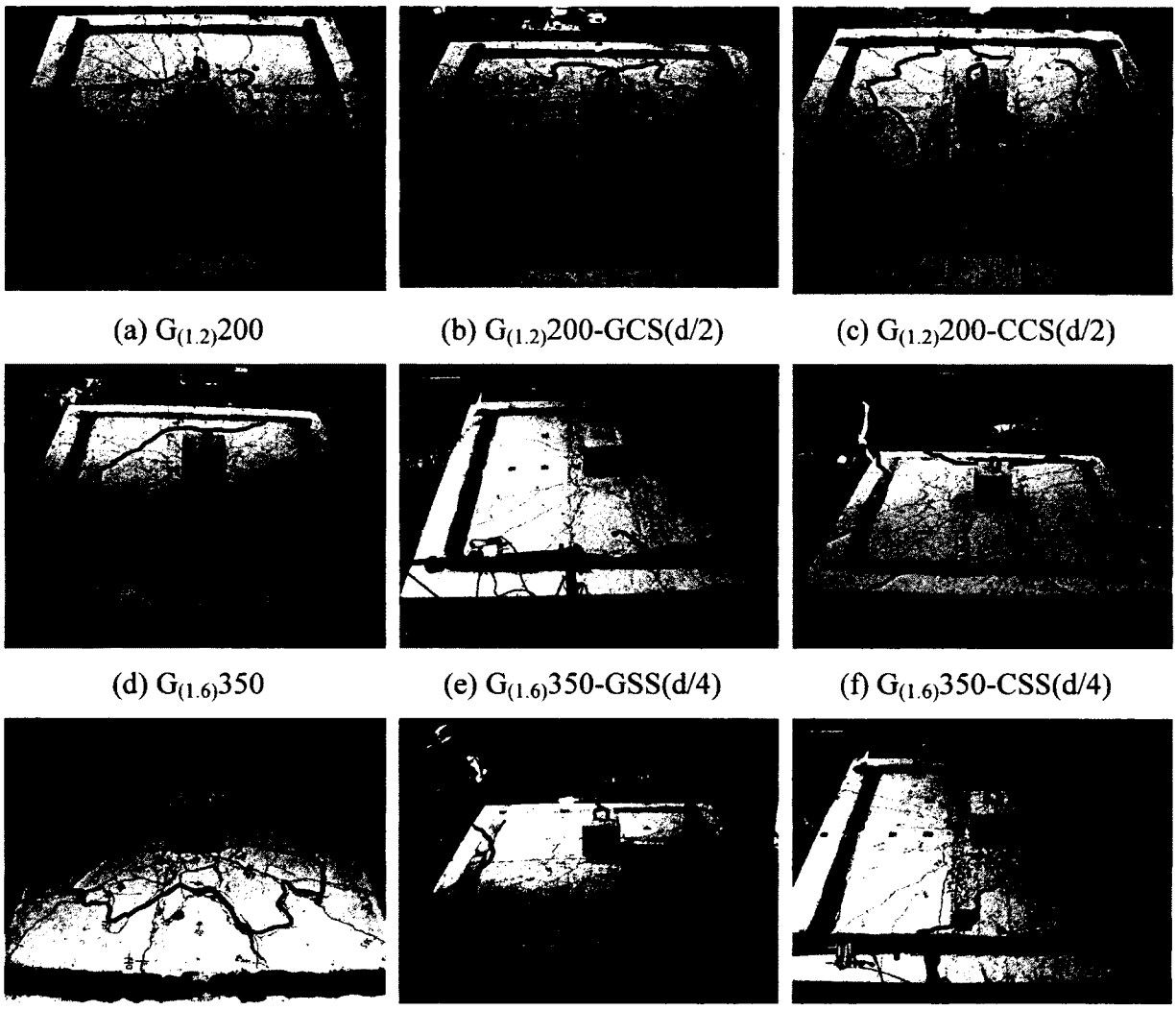

(a) $G_{(1.2)}200$ (b) $G_{(1.2)}200$-GCS(d/2) (c) $G_{(1.2)}200$-CCS(d/2)

(d) $G_{(1.6)}350$ (e) $G_{(1.6)}350$-GSS(d/4) (f) $G_{(1.6)}350$-CSS(d/4)

(g) $G_{(0.3)}350$-GSS(d/4) (h) $G_{(1.6)}350$-GBSS(d/4) (i) $G_{(1.6)}350$-CSS(d/3)

Figure 7.4: Final punching-shear failure surface for the tested specimens (in Bold)

Table 7.4: Test results

Series	Specimen	V_{cr}, kN	Δ_{cr} mm	$V_{tang.}$ kN	$\Delta_{tang.}$ mm	V_u, kN	Δ_{Vu}, mm	Δ_u, mm	$v_u/\sqrt[3]{f_c'}$, MPa	X_{cone}	ε_{fVu}, (με)	ε_{fmax}, (με)	$X\,\varepsilon_{fmax}$	ε_{cmax}, (με)
I	$G_{(1.2)}200$	160	1.35	189	1.92	438	17.9	23.5	0.58	2.5d	4350	4471	2.86d	-3713
	$G_{(1.2)}$ 200 GCS(d/2)	168	1.58	207	3.22	614	35.8	52.8	0.81	3.5d	8786	11058	1.91d	-3437
	$G_{(1.2)}$ 200-CCS(d/2)	165	1.61	247	5.15	514	24.0	44.2	0.68	2.9d	7161	10002	1.91d	-3046
II	$G_{(0.3)}350$	338	1.37	492	4.45	825	16.2	24.6	0.38	1.3d	9039	9039	1.32d	-2298
	$G_{(0.3)}$350-GSS(d/4)	334	2.09	482	5.80	885	30.5	44.0	0.43	1.2d	11299	-	0.88d	-1806
	$G_{(1.6)}350$	583	1.77	645	3.28	1492	-	-	0.68	1.7d	3199	3199	0.89d	-2385
	$G_{(1.6)}$ 350-GSS(d/4)	631	3.23	782	4.32	1761	20.9	45.6	0.79	2.0d	4265	4265	0.45d	-1770
	$G_{(1.6)}$ 350-GBSS(d/4)	646	3.81	808	5.47	1869	28.2	48.9	0.86	2.4d	5231	5774	0.45d	-2860
	$G_{(1.6)}$ 350-CSS(d/4)	619	3.03	881	4.54	2024	-	-	0.93	2.5d	6801	8131	0.45d	-3740
	$G_{(1.6)}$ 350-CSS(d/3)	646	3.13	915	5.29	1886	27.6	44.3	0.85	2.3d	5671	6136	0.89d	-2079

Note -- d= (slab thickness-50 or 45mm- d_b; where d_b is the bar diameter);

Considering the case of low flexural-reinforcement ratio (0.34%), that is, specimen $G_{(0.3)}$350-GSS(d/4), the FRP stirrups did not significantly contribute to the punching-shear strength. The specimens with low flexural-reinforcement ratios exhibited wide and deep cracks, which decreased the contribution of the uncracked concrete zone below the neutral axis (compression side) and the aggregate interlock. In addition, it limited the contribution of the stirrups to the punching-shear capacity. On the other hand, since the GFRP spiral stirrups have good anchorage, they contributed to confining the flexural reinforcement passing through the column cross-section, which forced the flexural reinforcement to achieve higher strains and, in turn, higher deformation capacity. It should be noted that, after the concrete cover on the slab's top surface was removed, some bars around the column face (~1.2*d* from the column face) were ruptured. This issue was not observed in the slabs with high flexural-reinforcement ratios, since increasing the reinforcement ratio reduced the strains at failure.

The specimens with high flexural-reinforcement ratios (1.2 and 1.6%) in Series I (200 mm) and II (350 mm) and reinforced with FRP stirrups, evidenced different failure patterns. In Series I, the GFRP closed stirrups were more efficient in enhancing the slab behavior than the CFRP ones. This is due to (1) stirrup configuration (see Figure 7.2), in which the GFRP stirrups had four legs, which contributed to the shear-resistance mechanism and failure was not governed by stirrup strength, and (2) the number of flexural reinforcement bars enclosed inside the stirrups. Nielsen (1999) and Braestrup et al. (1976) reported that the concrete stresses have to be transferred to the longitudinal bars supported by stirrups and the number of enclosed bars and their distribution along the concrete section may increase the effective concrete strength. Consequently, the stress concentrations around the supported bars led to a highly complicated state of microcracking. This explains the increased number of shear cracks in the specimens. Similar behavior was observed in Series II specimens ($G_{(1.6)}$350-GSS(d/4), $G_{(1.6)}$350-GBSS(d/4), $G_{(1.6)}$350-CSS(d/4), and $G_{(1.6)}$350-CSS(d/3)).

7.3.3 Punching-shear capacity

Table 7.4 summarizes the punching-shear capacities and the corresponding normalized punching-shear stresses calculated at 0.5*d* from the column face. The punching-shear stresses at failure were normalized to the cubic root of the concrete strength to account for the variation

in the concrete strengths. It should be noted that the reported loads include specimen self-weight.

The test results in Table 7.4 show that increasing the GFRP flexural-reinforcement ratio increased the punching-shear capacity of the test specimens. Increasing the flexural reinforcement ratio from 0.34% to 1.61% in Series II specimens increased the normalized punching-shear stress by an average ratio of 82%. More details concerning the effect of FRP flexural-reinforcement ratio on the punching-shear capacity of two-way concrete slabs can be found elsewhere (Dulude et al. 2013).

The FRP stirrups increased the punching-shear capacity of the test specimens compared to their counterparts without shear reinforcement. Lips et al. (2012) reported that, even small amounts of shear reinforcement increase the punching-shear strength and deformation capacity of slabs. The FRP stirrup confines the region adjacent to the column and contributes significantly to the punching-shear resistance mechanism and, consequently, the punching-shear capacity, especially when the flexural reinforcement ratios are high. Specimens $G_{(1.2)}$200-GCS(d/2), $G_{(1.2)}$200-CCS(d/2), $G_{(0.3)}$350-GSS(d/4), $G_{(1.6)}$350-GSS(d/4), $G_{(1.6)}$350-GBSS(d/4), $G_{(1.6)}$350-CSS(d/4), and $G_{(1.6)}$350-CSS(d/3) evidenced increases in punching-shear capacity by 40%, 17%, 7%, 18%, 25%, 36%, and 26%, compared to their counterparts without shear reinforcement, respectively. The lowest punching-shear increase was evidenced in slab $G_{(0.3)}$350-GSS(d/4), which had the lowest flexural-reinforcement ratio and developed higher strains in the flexural reinforcement as well as wide and deep cracks. Thus, the FRP stirrups did not effectively contribute to punching-shear capacity. This confirms the findings of Marzouk and Jiang (1997), in which the punching-shear capacity of the test specimens was ultimately governed by the flexural-reinforcement ratio.

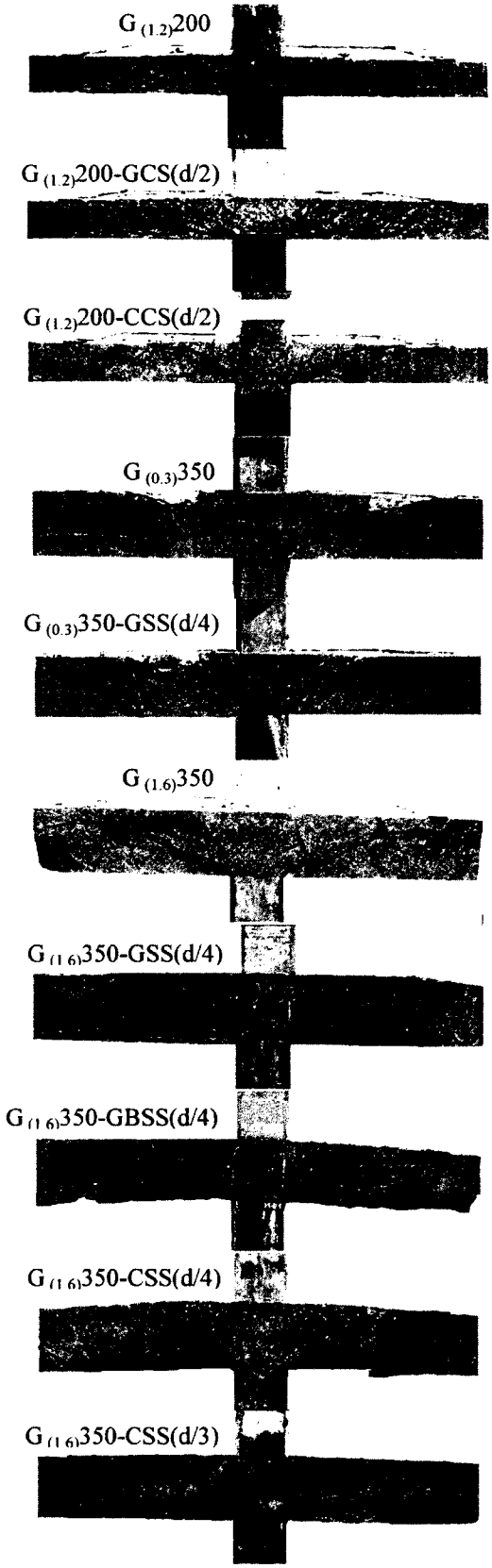

Figure 7.5: Cross-section failure envelop

The punching-shear capacity was related to the shear-reinforcement index (shear-reinforcement ratio × E_f). The shear-reinforcement index of $G_{(1.6)}$350-CSS(d/4) (CFRP stirrups @ d/4) was higher than that of $G_{(1.6)}$350-GBSS(d/4) (bundled GFRP stirrups @ d/4) by about 39%; consequently, the punching-shear capacity was higher by 8%. Furthermore, maintaining the same shear-reinforcement index in specimens $G_{(1.6)}$350-GBSS(d/4) and $G_{(1.6)}$350-CSS(d/3) yielded similar punching-shear capacities (1869 and 1886 kN, respectively).

7.3.4 Load–deflection characteristics

Figure 7.6 shows the load–deflection relationships for the tested specimens plotted from the LVDTs placed 40 mm from the column face on the X axes. Table 7.4 also summarizes the measured deflections at the peak load (ΔV_u), as well as the post-peak deflection at failure (Δ_u). The specimens without FRP stirrups showed typical bilinear load–deflection responses. The first line corresponds to the stiffness of the uncracked section and the second line corresponds to the stiffness of the cracked slab. After the peak load, the failure occurred suddenly in a brittle manner.

The test specimens with FRP stirrups, however, exhibited gradual failure with considerable post-peak deformation. This large post-peak deflection can be attributed to the presence of the FRP stirrups in the punching-shear zone around the column. The FRP stirrups resulted in a flexible punching-shear mechanism due to the mobilization of the shear reinforcement before the punching-shear failure (El-Ghandour et al. 2003). The deflection at peak load (ΔV_u) and the post-peak deflection (Δ_u) of the specimens in Series I ($G_{(1.2)}$200-GCS(d/2), and $G_{(1.2)}$200-CCS(d/2)) increased by 100% and 34% and by 125% and 88%, respectively. A similar trend was observed in the test specimens in Series II, but comparison was not possible because the LVDTs for some specimens stopped recording before specimen failure. In general, the FRP stirrups (spiral and closed stirrups) effectively improved slab behavior and prevented brittle punching-shear failure. The post-peak behavior, however, was significantly enhanced in the test specimen with high ratios of GFRP stirrups ($G_{(1.6)}$350-GBSS(d/4)).

It is worth mentioning that increasing the flexural-reinforcement ratio strongly influenced the post-cracking stiffness, in comparison to increasing the amount of shear reinforcement (see Figure 7.6). Increasing the flexural-reinforcement ratio in the test

specimens increased the post-cracking stiffness and the ultimate punching-shear capacity, decreased specimen deformation capacity, and resulted in more brittle punching-shear failure.

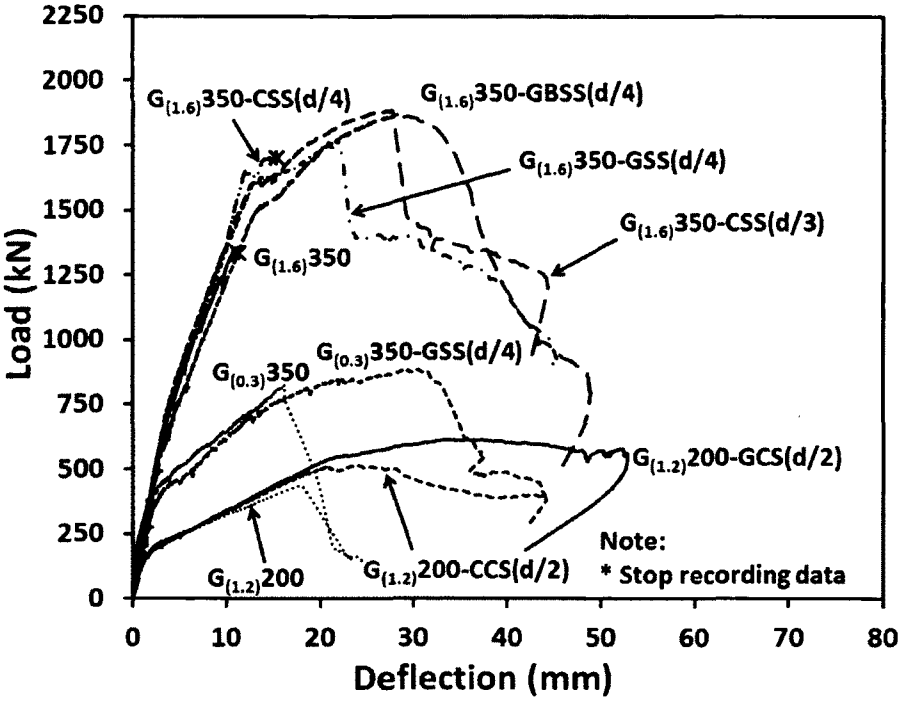

Figure 7.6: Load-deflection relationships of the test specimens (LVDT placed @ 40mm in X direction).

7.3.5 Flexural reinforcement and concrete strains

Figure 7.7 plots the relationships between the load and FRP reinforcement and concrete strains, while Table 7.4 lists the maximum strains for each specimen. In Figure 7.7, the reinforcement strains were recorded from the strain gauges located at 125 mm from the column centerline, while the concrete strains were plotted from concrete gauge C3 (see Figure 7.3). Generally, the specimens with higher flexural-reinforcement ratios showed lower reinforcement and concrete strains at the same load level. In the test specimens without shear reinforcement, the maximum flexural-reinforcement strain was 9039 microstrains, which represents 61% of characteristic tensile strength (referred to as guaranteed tensile strength by ACI 440 2006 = average −3×standard deviation). Besides, the maximum concrete strains near the column region were below the theoretical crushing failure of 3500 microstrains (CSA S806 2012), except specimen $G_{(1.2)}$200 (3713 microstrains). At punching-shear failure, however,

neither concrete crushing on the compression zone nor rupture of the GFRP reinforcement was observed.

Using the FRP stirrups around the column zone area of the test specimens mobilized the flexural reinforcement to achieve higher strains, which may have led to a decrease in the compressive strain in slab soffit. In Series I (200 mm), providing carbon- or glass-FRP stirrups decreased the concrete strain at the same load level compared to the reference specimen $G_{(1.2)}200$. The strains in the GFRP reinforcing bars, however, were higher than in the reference specimen. In addition, the strains in the GFRP reinforcing bars were very close to that in the specimens with carbon- and glass-FRP stirrups with the same stirrup spacing ($G_{(1.2)}200$-CCS(d/2) and $G_{(1.2)}200$-GCS(d/2)). In Series II (350 mm), the FRP stirrups significantly reduced the concrete strain at failure (from 2400 to 1000 microstrains) for the specimen with ρ_f = 0.34%. Specimens with higher reinforcement ratios (ρ_f = 1.61%) also showed some variations with respect to the reference specimen without shear reinforcement, although no specific trend is evident. The highest recorded strain in the GFRP reinforcing bars was 11299 microstrains in the specimen with the lowest flexural reinforcement ratio: $G_{(0.3)}350$-GSS(d/4). It was observed that some of GFRP top bars were ruptured in the column zone area, but no signs of concrete crushing in the compression side of the slab were observed. Therefore, it may be concluded that brittle punching-shear failure may be prevented and transformed into flexural-like failure by using FRP stirrups as shear reinforcement.

Figure 7.8 provides the strain distribution in the flexural reinforcement in the strong and weak directions of all the test specimens. The strain values were inversely proportional to the distance from the column for all slabs. Besides, the strains at 1000 mm from the column center reached approximately zero, implying that no bond failure or slip occurred during the tests. In addition, strains in the strong direction were higher than that in the weak direction of the slabs.

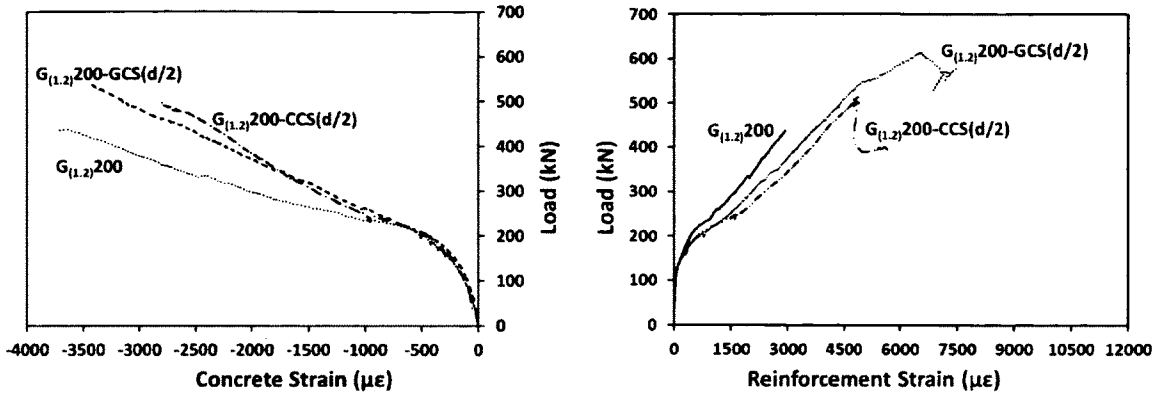

(a) Series I

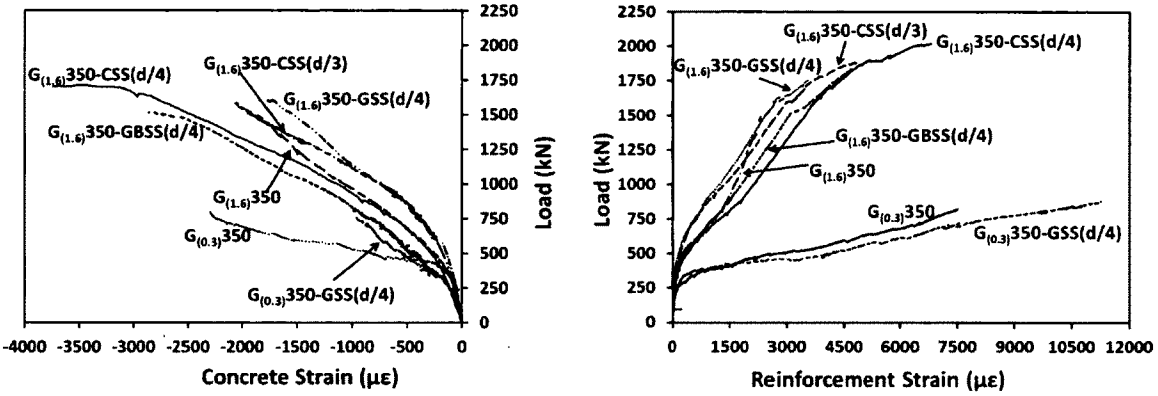

(b) Series II

Figure 7.7: Load-flexural strains relationships: (a) Series I; (b) Series II

Note: Reinforcement strains @ 125 mm from the column face and concrete @ C3

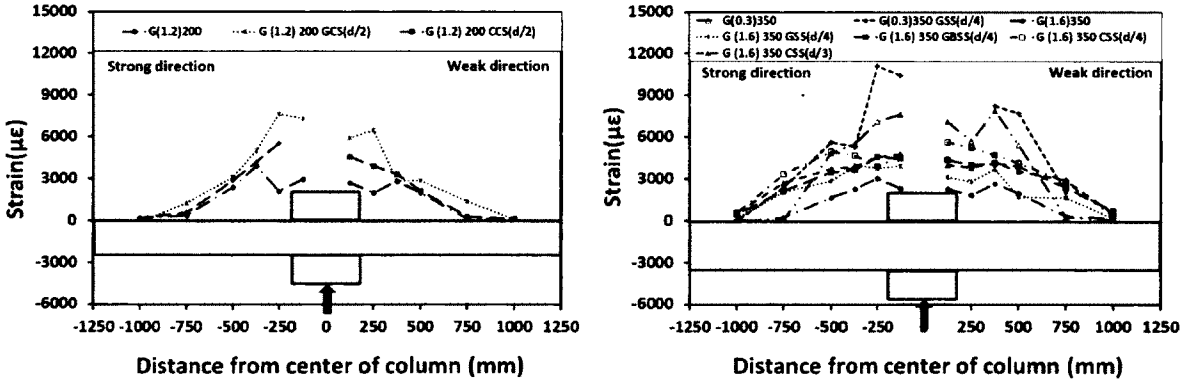

(a) Series I (b) Series II

Figure 7.8: Strain profile in the flexural reinforcement at 0.95 V_u: (a) Series I; (b) Series II

7.3.6 FRP stirrups strains

Figure 7.9 shows the measured strains at mid-height of the straight portions of the FRP stirrups located at *d*/2 and *d*, where *d* is the slab effective depth. The figure confirms that the FRP stirrups at *d*/2 started contributing to the punching-shear resistance before those at *d* because they are closer to the first shear cracks. As evidenced in Figure 7.9, the contribution of the FRP stirrups to the punching-shear resistance before cracking was insignificant. After the development of inclined shear cracks, however, the shear reinforcement (FRP stirrups) transferred most of the forces across the shear cracks and delayed further widening. This, in turn, increased the punching-shear and the deformation capacity of the test specimens (Rizk et al. 2011).

In Series I specimens, (Figure 7.9 (a)), the strains in the GFRP stirrups were less than that of the CFRP at the same load levels because the GFRP stirrups had four legs and enclosed four flexural bars compared to the two-legged CFRP stirrups enclosing only two flexural bars. On the other hand, in the Series II specimens (Figure 7.9 (b)) with a flexural reinforcement ratio of 1.61%, the strains in the FRP stirrups were close to about 80% to 90% of the ultimate capacity regardless of the stirrup material and spacing. The exception was specimen $G_{(1.6)}$350-GBSS(d/4) with bundled GFRP stirrups, which showed the lowest strains until about 1500 kN. In addition, Figure 7.9 (b) indicates that the effectiveness of the FRP stirrups in enhancing the punching-shear capacity increased by increasing the flexural-reinforcement ratios. The flexural reinforcement controlled the flexural cracks and enhanced the concrete's contribution (v_c), and the punching-shear resistance increased as a result of the contribution of the FRP stirrups (v_{fv}).

It should be mentioned that the strains in the FRP stirrups were relatively low compared to their strain capacity, since the punching-shear failure was not controlled by FRP-stirrup rupture. No rupture in the FRP stirrups at bent locations was observed, except in specimen $G_{(1.6)}$350-CSS(d/3). The maximum recorded strain before the rupture of the CFRP stirrups was 6522 microstrains (about 52% of the ultimate strain of the straight portions of the stirrups) at a distance of *d*/3 from the column face. Consequently, the test specimens did not reveal significant differences between the GFRP and CFRP stirrups.

Figure 7.10 shows the strain profile in the straight portions of the FRP stirrups at $0.95V_u$. As shown, the stirrups strain decreased as the distance from the column face increased. In addition, the maximum strains were recorded in the FRP stirrups at a distance of $0.5d$ to

1.0*d* from the column faces. Furthermore, the strains in the FRP stirrups started to decrease at 1.0*d* from the column and completely diminished at 2.5*d* and 2.0*d* from the column face in Series I and II (200 and 350 mm), respectively. Thus, the FRP stirrups may be provided at a distance of 2.5*d* from the column face. It should be mentioned that CSA A23.4 (2004) states that the shear reinforcement shall extend to a distance of at least 2*d* from the column face.

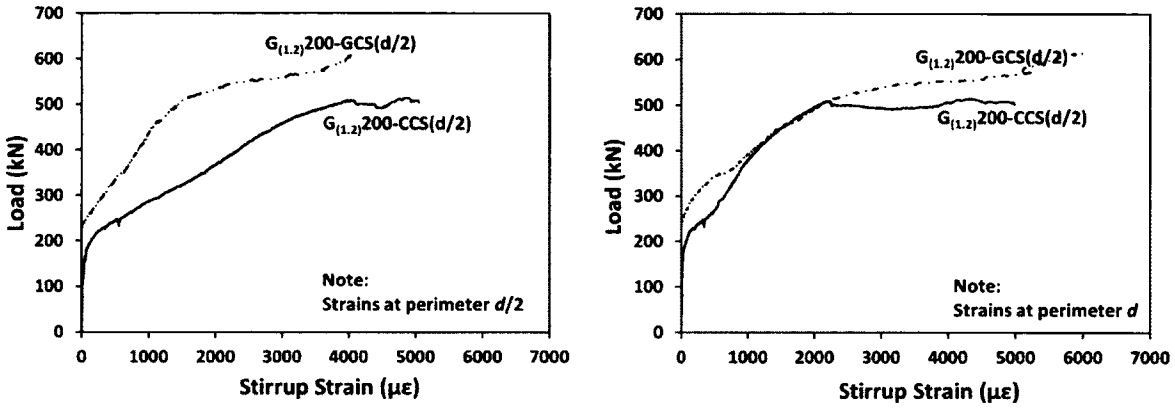

(a) Series I

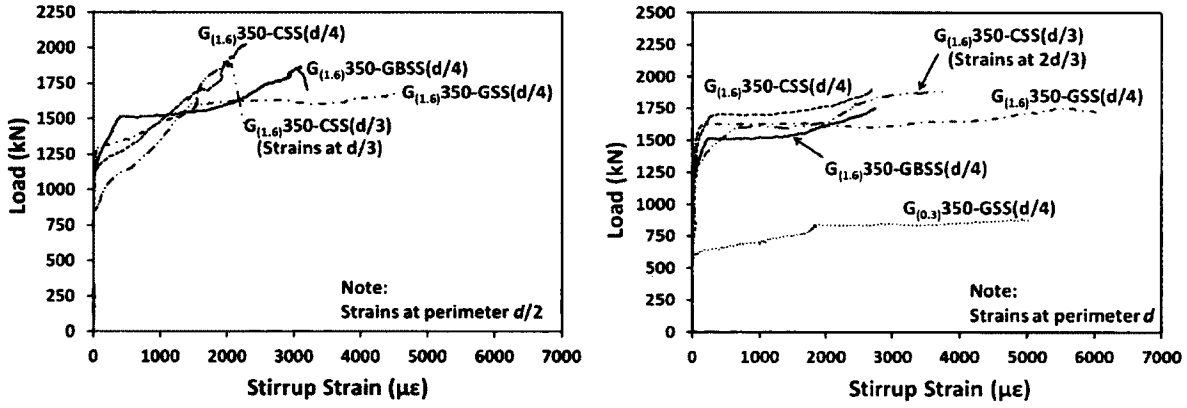

(b) Series II

Figure 7.9: Stirrups strains in the straight portion located at *d*/2 and *d* perimertes: (a) Series I; (b) Series II

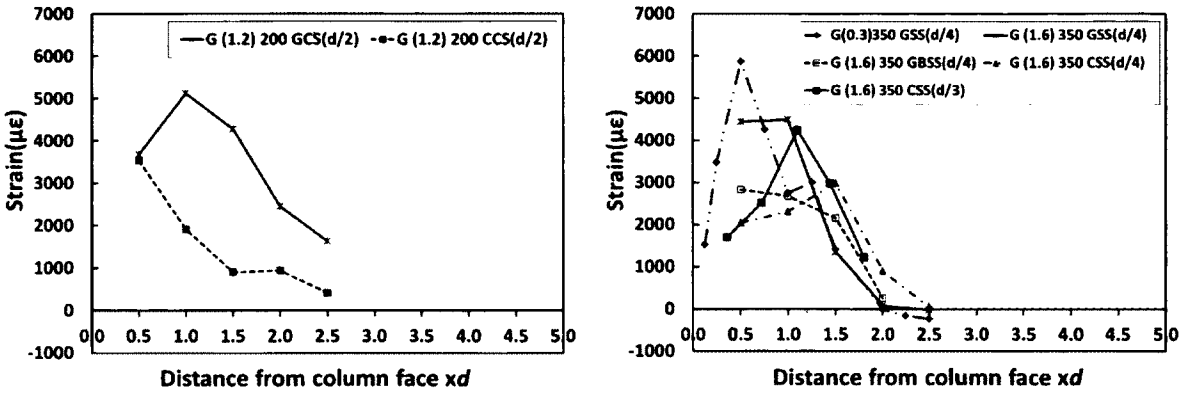

(a) Series I (b) Series II

Figure 7.10: Strain profile in the straight portion of the stirrups at $0.95V_u$: (a) Series I; (b) Series II

7.4 Conclusions

A total of ten full-scale interior slab-column specimens were constructed and tested to investigate the punching-shear behavior of two-way GFRP-RC slabs reinforced with FRP stirrups. The tests were performed to assess the effectiveness and contribution of the FRP stirrups as shear reinforcement in the two-way GFRP-RC slabs. Based on the experimental results and discussions presented herein, the following conclusions can be drawn:

1. The test specimens showed similar crack propagation in the top surface of the slab (tension side). Nevertheless, the single critical shear crack in the specimens without FRP stirrups changed to extensive inclined cracks when FRP stirrups were used as shear reinforcement.

2. The test specimens without shear reinforcement showed a sudden and brittle punching-shear failure, especially when the flexural-reinforcement ratio was high. The use of FRP stirrups in the test specimens, however, yielded to a softer punching-shear failure than the slabs without stirrups.

3. The use of FRP stirrups not only enhanced the punching-shear strength but also the specimen deformation capacity, which was more pronounced in the slabs reinforced with higher flexural reinforcement ratios. The average increase in the punching-shear capacity

was 29% and 23% in Series I and II, respectively. In addition, the average increase in the deflection at failure of Series I specimens was 107%.

4. The strain measurements confirmed that the FRP stirrups contributed to the punching-shear strength were located within a distance of 2.5*d* from the column face, which is in agreement with CSA A23.4 (2004), which states the shear reinforcement should extend to at least 2*d* of the column face.

5. The FRP stirrups with more legs resulted in a better performance than those with less legs (even with higher modulus of elasticity).

6. The test specimens reinforced with the same flexural-reinforcement type and ratio, and reinforced with FRP stirrups with the same shear-reinforcement index (shear rft ratio × E_f) may yield similar behavior and punching-shear capacity, as evidenced by specimens $G_{(1.6)}$350-GBSS(d/4) and $G_{(1.6)}$350-CSS(d/3).

7. Based on the test results, the GFRP and CFRP stirrups can be used in two FRP RC slabs as shear reinforcement. It may be designed using a strain value of 4000 or 5000 micro-strains as recommended by ACI 440 (2006) or CSA S806 (2012), respectively.

CHAPTER 8
SUMMARY AND CONCLUSIONS

8.1 Summary

The research work conducted herein focused on experimental and analytical investigations of the punching-shear behaviour of GFRP-reinforced interior slab-column connections under applied concentric loading. The principle objective is to increase the understanding of the phenomena of punching-shear failure in GFRP-reinforced flat slab provided with and without FRP-shear reinforcement.

The experimental work consists of twenty-six full-scale flat slab reinforced with GFRP bars and two specimens reinforced with steel bars for comparisons, which are divided into two phases. The investigated parameters of the test specimen in the first phase (Phase I) are: (i) flexural reinforcement ratio (ranged from 0.34% to 1.66%) and type (steel and GFRP); (ii) GFRP compression reinforcement; (iii) slab thickness (200 mm and 350 mm); (v) column dimensions (300 x 300 mm and 450 x 450 mm); (iv) concrete strength (normal and high-strength concretes). Whilst, the use of FRP shear reinforcement (stirrups) in the slab as well its effectiveness and contribution to the punching-shear capacity are evaluated the second phase. The test variables considered in the second phase (Phase II) are the material of the stirrups, shear reinforcement ratio, stirrup spacing, and the effect of flexural reinforcement ratio on the effectiveness of the FRP shear reinforcement on punching-shear capacity.

On the other hand, the analytical study included assessing the accuracy of the current punching-shear design provisions through comparing the test results of the specimens tested herein and 35 specimens from literature. The provisions included CSA S806-12 (2012), ACI 440 (2006), BS 8110 (1997), and JSCE (1997).

The results of this research work are presented in four articles. However, the following are the general conclusions of this work:

8.2 Conclusions

The following general conclusions can be drawn based on the experimental and analytical research work presented in this dissertation:

8.2.1 Slabs without shear reinforcement

1. All the tested specimens showed punching-shear failure as the final mode of failure with similar crack patterns, regardless the reinforcement type and ratio.

2. The GFRP test specimens without shear reinforcement depicted a sudden and brittle punching-shear failure in particularly when the flexural reinforcement was high. At low flexural reinforcement ratio, however, exhibited wider, deeper, and larger plastic deformation prior the punching failure.

3. At punching failure, neither rupture nor anchorage slippage of the GFRP bars observed, even in the most lightly GFRP-reinforced test specimens.

4. The punching-shear failure of the compression zone for the tested specimens was triggered by concrete tension splitting rather than concrete crushing.

5. The amount and type of reinforcement had a considerable effect on the slab stiffness and deflection after occurrence of the first crack.

6. Due to the lower modulus of elasticity of the GFRP-reinforced specimens designed with a similar flexural reinforcement ratio as the steel ones, the obtained punching-shear capacity and stiffness were considerable less. The punching-shear capacity of $G_{(1.6)}30/20$ and $G_{(0.7)}30/35$ were 37.4% and 36.7% lower than those of companion slabs $S_{(1.7)}30/30$ and $S_{(0.8)}30/35$, respectively.

7. Increasing the GFRP reinforcement ratio for the tested specimens yielded higher punching-shear capacities, lower stains in the flexural reinforcement, and smaller slab deflections whilst, the test specimens designed with same axial stiffness showed similar slab behaviour and punching-shear capacity.

8. Increasing the column dimensions also increased failure surface and consequently reduced the punching-shear stresses at failure.

9. Concentrating the GFRP reinforcement in the compression side through the column cross-section contributed to enhance the overall slab behaviour with a slight increase in the post-cracking stiffness and ultimate punching-shear capacity.

10. Increasing the slab thickness from 200 mm to 350 mm, increase the punching-shear capacity, initial and post-cracking stiffness, and decreased the slab deformability, significantly.

11. In general, the estimated angle of the punching-shear cone for the GFRP thick slabs were much steeper than the shear crack slopes observed in slender slabs, at the same reinforcement was used.

12. Increasing the flexural reinforcement ratio enhanced the slab's in-plane restraint and led to a much flatter inclination of the critical shear crack which, in turn, decreasing the punching-shear angle cone with the horizontal direction.

13. Increasing the concrete strength in the GFRP specimens from 38 MPa to 76 MPa showed slightly variances between the specimens in the punching-shear angle cone, however, more investigation is needed to exam the former with a wide range of concrete strengths.

14. Using HSC for the GFRP specimens improve the punching-shear capacity, allowing higher forces to be transferred through the slab-column connection.

15. Concrete compressive strength had a significant effect on the initial stiffness (uncracked stiffness) of the GFRP specimens. However, the post-cracking stiffness was similar as the GFRP specimens with NSC.

16. The post-cracking stiffness of the GFRP-reinforced specimens was dependent on the reinforcement type and ratio (axial stiffness) rather than increasing the concrete strength.

17. The CSA S806 (2012), BS 8110 (1997), and JSCE (1997) yielded good yet conservative predictions an average V_{test}/V_{pred} of 1.21±0.17, 1.22±0.15, and 1.27±0.15 and a COV of 14%, 13%, and 12%, respectively. On the other hand;

18. ACI 440 (2006) yielded very conservative predictions with an average V_{test}/V_{pred} of 2.23±0.35 with a higher corresponding COV of 16%.

19. The use of the cubic root of the concrete strength in HSC GFRP specimens yielded better predictions than using the square root of the concrete strength.

20. The CSA S806 (2012) punching-shear equation may be applicable for a wider range of concrete strengths. That notwithstanding, further investigation is warranted.

8.2.2 Slabs with shear reinforcement

21. On the whole specimens with and without shear reinforcement showed similar cracks propagation in the top surface of the slab (tension side). However, the punching shear cone produced at failure was considerably larger in the test specimens with shear reinforcement.

22. Using the FRP shear reinforcement in the test specimens exhibited more flexible punching-shear failure mechanism due to the mobilization of the shear reinforcement before failure.

23. FRP shear reinforcement amount plays a significant role in enhancing the punching-shear strength and the deformation capacity of the test specimens, thus increase their safety, in particularly when the flexural reinforcement ratio is high.

24. The central deflection of the test specimens with FRP shear reinforcement is even more pronounced when post-failure behaviour is examined.

25. The test specimens with FRP shear reinforcement exhibited a significant increase in the number of cracks and showed more complex crack pattern failure.

26. The failure angle of a punching cone of slabs with shear reinforcement cannot be distinguished by one value, since the confided zones have a different angle from the zone between the rows of shear reinforcement.

27. The efficiency of the FRP shear reinforcement systems is strongly influenced by their development conditions (anchorage, modulus of elasticity, bond) and detailing rules.

28. The maximum-recorded strains for test specimens were located at 0.5d and/or d perimeter.

29. The GFRP stirrups showed the highest strain values rather than the CFRP stirrups due to the lower modulus of elasticity of GFRP materials.

30. The FRP stirrups contribution to the punching-shear resistance before cracking is insignificant. After the development of inclined shear cracks, however, the shear reinforcement transfers most of the forces across the shear cracks and delays further widening.

31. This study confirms the efficiency of the FRP stirrups in increasing the punching-shear and deformation capacity of the test specimens. This indicates that using FRP as shear reinforcement in the GFRP-RC two-way slabs has a reasonable potential to research further.

8.3 Conclusions en French

Les conclusions générales suivantes découlent des résultats analytiques et expérimentaux présentés dans la dissertation.

8.3.1 Dalles sans armature de cisaillement

1. Tous les échantillons ont eu comme mode de rupture final le poinçonnement ainsi que des motifs de fissuration semblables, peu importe le type ou le taux d'armature.

2. Les échantillons de PRFV sans armature de cisaillement ont démontré une rupture soudaine et fragile, en particulier lorsque le taux d'armature de flexion était élevé. Pour un taux d'armature faible en flexion, cependant, les spécimens ont subi des déformations plastiques plus importantes avant la rupture en poinçonnement.

3. À la rupture en poinçonnement, aucune rupture ou glissement des barres en PRFV a été observé, même dans les échantillons les plus légèrement renforcés.

4. Pour les échantillons testés, la rupture en poinçonnement de la zone en compression a été déclenchée par la fissuration du béton en traction plutôt que par l'écrasement du béton en compression.

5. La quantité et le type d'armature ont eu un effet considérable sur la rigidité de la dalle et sur la déflection après l'apparition de la première fissure.

6. Les échantillons renforcés de PRFV, conçus avec un taux d'armature en flexion similaire aux échantillons renforcés d'acier, ont démontré une rigidité et une résistance au poinçonnement moindre en raison du plus faible module d'élasticité des armatures en

PRFV. La résistance au poinçonnement des échantillons $G_{(1,6)}$ 30/20 et $G_{(0,7)}$ 30/35 était de 37,4% et 36,7% inférieures à celles des dalles partenaires $S_{(1,7)}$ 30/30 et $S_{(0,8)}$ 30/35.

7. Sur les échantillons testés, augmenter le taux d'armature en PRFV a augmenté la résistance au poinçonnement, réduit les contraintes dans l'armature de flexion et diminué les déflections des dalles tandis que les échantillons conçus avec la même rigidité axiale ont montré un comportement et une résistance au poinçonnement semblable.

8. Augmenter les dimensions de la colonne a également augmenté la surface de rupture et par conséquent réduit les contraintes de poinçonnement à la rupture.

9. La concentration de l'armature en PRFV du côté de la compression à travers la colonne a contribué à améliorer le comportement global de la dalle avec une légère augmentation de la rigidité post-fissuration et de la résistance au poinçonnement.

10. L'augmentation de l'épaisseur de la dalle de 200 mm à 350 mm a augmenté la résistance au poinçonnement, la rigidité initiale, la rigidité post-fissuration et a diminué la déformabilité de la dalle de manière significative.

11. En général, l'angle estimé du cône de poinçonnement pour les dalles épaisses renforcées de PFRV était beaucoup plus abrupte que l'angle des fissures de cisaillement observées sur les dalles minces lorsque la même armature avait été utilisé.

12. L'augmentation du taux d'armature en flexion a augmenté la retenue en plan de la dalle et a conduit à une inclinaison moindre de la fissure de cisaillement critique, ce qui, à son tour, diminue l'angle du cône de poinçonnement avec l'horizontale.

13. L'augmentation de la résistance en compression du béton dans les échantillons de PRFV de 38 MPa à 76 MPa a montré de légers écarts dans l'angle du cône de poinçonnement. Cependant, une enquête plus approfondie avec une plus grande gamme d'échantillons est nécessaire pour obtenir des résultats plus concluants.

14. L'utilisation de béton à haute résistance pour les échantillons renforcés de PRFV a amélioré la résistance au poinçonnement, permettant à des efforts plus élevés d'être transférés via la connexion dalle-colonne.

15. La résistance à la compression du béton a eu un effet significatif sur la rigidité initiale (rigidité non-fissurée) des échantillons renforcés de PFRV. Toutefois, la rigidité post-fissuration était similaire à celle des échantillons renforcés de PRFV avec un béton normal.

16. La raideur post-fissuration des échantillons renforcés de PRFV dépendait du type et du taux d'armature (raideur axiale) plutôt que d'augmenter avec la résistance du béton.

17. Les normes CSA S806 (2012), BS 8110 (1997), et JSCE (1997) ont donné de bonnes prédictions, quoique conservatrices : une moyenne V_{test}/V_{pred} de 1,21 ± 0,17, 1,22 ± 0,15 et 1,27 ± 0,15 et un coefficient de variation de 14%, 13% et 12%, respectivement. Par contre;

18. La norme ACI 440 (2006) a donné des prédictions très conservatrices avec une moyenne V_{test}/V_{pred} de 2,23 ± 0,35 avec un coefficient de variation correspondant plus élevé, soit de 16%.

19. L'utilisation de la racine cubique de la résistance du béton dans des échantillons renforcés de PRFV avec un béton à haute résuistance a donné de meilleures prédictions qu'en utilisant la racine carrée de la résistance du béton.

20. L'équation de poinçonnement de la norme CSA S806 (2012) peut s'appliquer à une large gamme de résistances de béton. Malgré cela, des études plus poussées sont recommandées.

8.3.2 Dalles avec armature de cisaillement

21. Globalement, les échantillons avec ou sans armature de cisaillement montrent une propagation de fissure similaire sur la face supérieure de la dalle (côté en traction). Toutefois, le cône de poinçonnement à la rupture était beaucoup plus grand pour les échantillons avec armature de cisaillement.

22. Utilisation de l'armature de cisaillement en PRFV dans les échantillons provoquait un mécanisme de rupture en poinçonnement plus flexible grâce à la mobilisation de l'armature de cisaillement avant la rupture.

23. La quantité d'armature de cisaillement en PRFV a une grande influence sur la résistance au poinçonnement et sur la capacité de déformation des échantillons. Ceci affecte donc la sécurité, en particulier lorsque le taux d'armature en flexion est élevé.

24. La flèche à mi-portée des échantillons avec armature en cisaillement en PRFV est encore plus importante lorsque le comportement post-rupture est examiné.

25. Les échantillons renforcés de PRFV en cisaillement ont montré une augmentation significative du nombre de fissures et présentaient un motif de fissures plus complexe.

26. L'angle du cône de poinçonnement à la rupture des dalles avec armature de cisaillement ne peut pas être décrit par une seule valeur puisque les zones confinées ont un angle différent de la zone située entre les lignes de l'armature de cisaillement.

27. L'efficacité de l'armature de cisaillement en PRFV est fortement influencée par les conditions de développement (ancrage, module d'élasticité, adhérence) et leurs configurations.

28. Les contraintes maximale enregistrées dans les échantillons sont situés à 0,5 d et /ou d.

29. Les étriers en PRFV ont montré des valeurs de déformation plus élevées que les étriers en PRFC en raison de leur plus faible module d'élasticité.

30. La contribution des armatures en PRFV à la résistance au poinçonnement avant fissuration est négligeable. Après le développement de fissures inclinées de cisaillement, cependant, le renforcement en cisaillement transfère la plupart des forces à travers les fissures de cisaillement et retarde leur élargissement.

31. Cette étude confirme l'efficacité des étriers en PRF en augmentant la résistance au poinçonnement et la capacité de déformation des échantillons. Ceci indique que l'utilisation de PRF comme armature de cisaillement dans les dalles bidirectionnelles en béton armé de PRFV a un potentiel raisonnable pour réaliser des recherches plus poussées.

8.4 Recommendations for Future Work

Through the experience that was gained during this research project, the following recommendations are made for future research work:

1. Investigate the size effect on the punching-shear strength of FRP-reinforced two-way flat slabs.

2. Study the effect of HSC for the FRP two-way flat slabs with and without FRP shear reinforcement.

3. Investigate the effect of the FRP shear reinforcement considering different shapes, arrangement, and layout.

4. Testing of edge and corner slab-column connection reinforced with FRP reinforcement.

5. Testing of FRP reinforcement slab-column connection with different sizes of drop panels.

6. Examine the serviceability requirements in two-way flat slabs reinforced with FRP bars.

REFERENCES

ACI 318-95/ACI 318R-95, (1995), "Building Code Requirements for Reinforced Concrete and Commentary.", *American Concrete Institute*, Detroit, USA.

ACI Committee 440, (2004), "Guide Test Methods for Fiber-Reinforced Polymers (FRPs) for Reinforcing or Strengthening Concrete Structures.", (ACI 440.3R-04), *American Concrete Institute*, Farmington Hills, MI, USA, 40 p.

ACI 318-05/ACI 318R-05, (2005), "Building Code Requirements for Reinforced Concrete and Commentary.", *American Concrete Institute*, Detroit, USA.

ACI Committee 440, (2006), "Guide for the Design and Construction of Concrete Reinforced with FRP Bars.", (ACI 440.1R-06), *American Concrete Institute*, Farmington Hills, MI, USA, 44 p.

ACI 318-05/ACI 318R-08, (2008), "Building Code Requirements for Reinforced Concrete and Commentary.", *American Concrete Institute*, Detroit, USA.

Ahmad, S.H.; Zia, P.; Yu, T.; and Xie, Y., (1993), "Punching Shear Tests of Slabs Reinforced with 3-D Carbon Fiber Fabric.", *ACI Concrete International*, 16 (6): 36-41.

Ahmed, E., (2009), " Shear Behaviour of Concrete Beams Reinforced with Fibre-Reinforced Poylmer (FRP) Stirrups.", *PhD Thesis,* Department of Civil Engineering, University of Sherbrooke, Sherbrooke, Québec, Canada, 291 p.

Andersson, J., (1963), "Punching of Concrete Slabs with Shear Reinforcement.", Transactions 212, *Royal Institute of Technology*, Stockholm, 65 p.

ASTM D7205, (2011), "Tensile Properties of Fiber Reinforced Polymer Matrix Composite Bars.", *American Society for Testing and Materials*, Conshohocken, USA, 12 p.

Banthia, N.; Al-Asaly, M.; and Ma S., (1995), "Behavior of Concrete Slabs Reinforced with Fiber-Reinforced Plastic Grid.", *Journal of Materials in Civil Engineering*, 7 (4): 252-257.

Benmokrane, B.; El-Salakawy, E.; El-Ragaby, A.; and Lackey, T., (2006), "Designing and Testing of Concrete Bridge Decks Reinforced with Glass FRP Bars.", *ASCE Journal of Bridge Engineering*, 11(2): 217-229.

Benmokrane, B.; El-Salakawy, E.; El-Ragaby, A.; and Wisman, A., (2006a), "Rehabilitation of the Structural Slabs of Laurier-Tache Parking Garage (Gatineau, Quebec) Using Glass FRP Bars.", *35th CSCE Annual Conference*, Calgary, AB, Canada, May 23-26, 9 p. (CD-ROM).

Benmokrane, B.; El-Salakawy, E.; El-Gamal, S. E.; and Sylvain, G., (2007), "Construction and Testing of an Innovative Concrete Bridge Deck Totally Reinforced with Glass FRP Bars: Val-Alain Bridge on Highway 20 East.", *ASCE Journal of Bridge Engineering*, 12(5):632-645.

Benmokrane, B.; Ahmed, E.; Dulude, C.; and Boucher, E., (2012), "Design, Construction, and Monitoring of the First Worldwide Two-Way Flat Slab Parking Garage Reinforced with GFRP Bars.", *Proceedings of the 6th International Conference on FRP Composites in Civil Engineering*, Rome, Italy, June 13-15, 8 p.

Braestrup, M.; Nielsen, M.; Bach, F.; and Jensen, B., (1976), "Shear Tests on Reinforced Concrete T-beams: Series T.", Rapport NF.R72, *Structural Research Laboratory, Technical University of Denmark.*

British Standards Institution, (1997), "Structural Use of Concrete, BS8110: Part 1-Code of Practice for Design and Construction.", London, UK, 172 p.

Birkle, G., (2004), "Punching of Flat Slabs: The Influence of Slab Thickness and Stud Layout.", *PhD thesis*, Civil Engineering Department, Calgary University, Canada, 217 p.

Broomfield, P. J., (2007), "Corrosion of Steel in Concrete: Understanding, Investigation and Repair.", *2nd Ed., Taylor & Francis*, London.

Canadian Standards Association (CSA), (2002), "Design and Construction of Building Components with Fibre Reinforced Polymers (*CAN/CSA S806–02*).", Rexdale, ON, Canada.

Canadian Standards Association (*CSA-A23.3 M-04*), (2004), "Design of concrete structures for buildings.", Rexdale, Ontario, Canada, 240 p.

Canadian Standards Association (*CAN/CSA-S6-06*), (2006), "Canadian Highway Bridge Design Code.", Canadian Standards Association, Mississauga, Ontario, Canada.

Canadian Standards Association (CSA), (2007), "Parking structures (CAN/CSA 413-07).", Rexdale, ON, Canada, 107 p.

Canadian Standards Association (CSA), (2010), "Specification for Fibre-Reinforced Polymers.", *(CAN/CSA S807–10)*, Rexdale, Ontario, Canada, 27 p.

Canadian Standards Association (CSA), (2011), "Design and Construction of Building Structures with Fibre Reinforced Polymers.", (*CAN/CSA S806–11*)," Draft, Rexdale, ON, Canada.

Canadian Standards Association (CSA), (2012), "Design and Construction of Building Structures with Fibre Reinforced Polymers.", *(CAN/CSA S806–12)*, Rexdale, Ontario, Canada, 198 p.

Cheng, M.-Y.; and Parra-Montesinos, G.J., (2010), "Evaluation of Steel Fiber Reinforcement for Punching Shear Resistance in Slab-Column Connections-Part I: Monotonically Increased Load.", *ACI Structural Journal*, 107(1): 101-109.

CNR-DT 204/2006, (2006), "Guide for the Design and Construction of Fiber-Reinforced Concrete Structures.", *National Research Council, Advisory Committee on Technical Recommendations for Construction*, Rome.

Dulude, C.; Hassan, M.; Ahmed, E.; Benmokrane, B., (2010), "Conception et essais expérimentaux sur des dalles de stationnements étagés en béton armé d'armature en matériaux composites de PRFV.", (Projet de recherche MDEIE, N/Réf.: 08-09-PSVT2-13462), *Dept. of Civil Engineering, Université de Sherbrooke*, Québec, Canada, 74 p.

Dulude, C., (2011), "Poinçonnement des dalles bidirectionnelles en béton armé d'armature de polymères renforcés de fibres de verre.", *Master Thesis,* Department of Civil Engineering, University of Sherbrooke, Sherbrooke, Quebec, Canada, 142 p.

Dulude, C.; Hassan, M.; Ahmed, E.A.; and Benmokrane, B., (2013), "Punching Shear Behaviour of Two-Way Flat Concrete Slabs Reinforced with GFRP Bars.", *ACI Structural Journal*, 110(5): 723–734.

Dragosavic, M., and Van den Beukel, A., (1974), "Punching Shear.", Heron, Delft, Netherlands, 20 (2), 48 p.

El-Gamal, S.; El-Salakawy, E.; and Benmokrane, B., (2005a), "Behavior of Concrete Bridge Deck Slabs Reinforced with Fiber-Reinforced Polymer Bars under Concentrated Loads.", *ACI Structural Journal,* 102 (5): 727-735.

El-Gamal, S.E.; El-Salakawy, E.F.; and Benmokrane, B., (2005b), "A New Punching Shear Equation for Two-Way Concrete Slabs Reinforced with FRP Bars.", *Fiber-Reinforced*

Polymer Reinforcement for Concrete Structures, American Concrete Institute, Farmington Hills, MI, SP-230-50: 877-894.

El-Ghandour, A.W.; Pilakoutas, K.; and Waldron, P., (1999), "New Approach for Punching Shear Capacity Prediction of Fiber Reinforced Polymer Reinforced Concrete Flat Slabs.", *Fiber Reinforced Polymer Reinforcement for Reinforced Concrete Structures*, American Concrete Institute, Farmington Hills, MI, SP 188-13: 135-144.

El-Ghandour, A.W.; Pilakoutas K.; Waldron P., (2000), "Punching shear behavior and design of FRP RC flat slabs.", *Proceedings of the International Workshop on Punching Shear Capacity of RC Slabs*, Dedicated to Professor Sven Kinnunen. Stockholm: TRITA-BKN Bulletin 57, 359–366 p.

El-Ghandour, A.W.; Pilakoutas, K.; and Waldron P., (2003), "Punching Shear Behavior of Fiber Reinforced Polymers Reinforced Concrete Flat Slabs: Experimental Study.", *ASCE Journal of Composites for Construction*, 7(3): 258–265.

El-Salakawy, E.; Benmokrane, B.; El-Ragaby, A.; and Nadeau, D., (2005), "Field Investigation on the First Bridge Deck Slab Reinforced with Glass FRP Bars Constructed in Canada.", *ASCE Journal of composites for construction*, 9(6): 470-479.

Fédération Internationale du Béton, FIB (2007), "FRP reinforcement in RC structures.", *Task Group 9.3*, Lausanne, Switzerland.

Guandalini, S.; Burdet, O. L.; and Muttoni, A., (2009), "Punching Tests of Slabs with Low Reinforcement Ratios.", *ACI Structural Journal*, 106 (1): 87-95.

Hassan, M., Ahmed, E.A., and Benmokrane, B., (2012), "Punching-Shear Strength of GFRP-Reinforced concrete Flat Slabs.", *Canadian Journal of Civil Engineering*, 36 p. (in press).

Hallgren, M.; Kinnunen, S.; and Nylander, B., (1999), "Punching Shear Tests on Column Footings.", *Royal Institute of Technology*, Department of Structural Engineering, Stockholm, Sweden, 23 p.

Hawkins, N.M.; Criswell, M.E.; and Roll, F. (1974), "Shear Strength of Slabs without Shear Reinforcement.", ACI Publication, Shear in Reinforced Concrete, 42 (30): 677-720.

Hawkins, N.M. (1974), "Shear Strength of Slabs with Shear Reinforcement.", ACI Publication, Shear in Reinforced Concrete, 42 (34): 785-815.

Hussein, A.; Rashid I.; and Benmokrane B., (2004), "Two-Way Concrete Slabs Reinforced with GFRP Bars.", Advanced Composite Materials in Bridges and Structures, *Proceeding*

of the 4th International Conference on Advanced Composite Materials in Bridges and Structures, CSCE, Calgary, AB, Canada, 8 pp.

Institution of Structural Engineers, (1999), "Interim guidance on the design of reinforced concrete structures using fibre composite reinforcement.", *Published by SETO Ltd*, London, 116 p.

ISIS Canada, (2006), "Specifications for product Certification on Fibers Reinforced Polymer (FRPs) as internal Reinforcement in Concrete Structures.", Product Certification of FRP Materials, the Canadian Network of Centers of Excellent on Intelligent Sensing for Innovation Structures, *ISIS Canada*, University of Manitoba, Winnipeg, Manitoba, Canada.

ISIS Design Manual No. 3, (2007), "Reinforcing Concrete Structures with Fiber Reinforced Polymers.", *ISIS Canada,* Intelligent Sensing for Innovative Structures, A Canadian Networks of Centres of Excellence. University of Manitoba, Winnipeg, Manitoba, Canada.

Japan Society of Civil Engineers (JSCE), (1997), "Recommendation for Design and Construction of Concrete Structures Using Continuous Fibre Reinforcing Materials.", *Concrete Engineering Series 23*, A. Machida, Ed., Tokyo, Japan, 325 p.

Kinnunen, S.; and Nylander, H., (1960), "Punching of Concrete Slabs Without Shear Reinforcement.", Transactions No. 158, *Royal Institute of Technology*, Stockholm, 112 pp.

Komová, E.; Varga, M.; Varga, R.; Vojtan, P.; Torrejon, J.; Provencio, M.; and Vazquez, M., (2008). "Stress Dependence of the Switching Field in Glass Coated Microwires.", Acta Phys. Pol. A, 113(1), 135–138.

Lee, J.H.; Yoon, Y.S.; and Mitchell, D, (2009), "Improving Punching Shear Behavior of Glass Fiber-Reinforced Polymer Reinforced Slabs.", *ACI Structural Journal*, 106(4): 427–434.

Li, R.; Cho, Y.S.; and Zhang, S., (2006), "Punching Shear behavior of Concrete Flat plate Slab Reinforced with Carbon Fiber Reinforced Polymer Rods.", *Composites: Part B,* 38(5-6): 712–719.

Lips S.; Ruiz M.F.; and Muttoni A., (2012), "Experimental Investigation on Punching Strength and Deformation Capacity of Shear-Reinforced Slabs.", *ACI Structural Journal*, 109(6): 889–900.

MacGregor, J., (1997), "Reinforced Concrete: Mechanics and Design.", 3rd Edition, Prentice Hall, Englewood Cliffs, N.J., 939 p.

Marzouk, H.; Emam, M.; and Hilal, S., (1996), "Effect of High-Strength Concrete Columns on the Behavior of Slab-Column Connections.", *ACI Structural Journal*, 93(5): 545-555.

Marzouk, H.; Jiang, D., (1997), "Experimental Investigation on Shear Enhancement Types for High-Strength concrete Plates.", *ACI Structural Journal*, 94(1): 49-58.

Matthys, S.; and Taerwe, L., (2000 a), "Concrete Slabs Reinforced with FRP Grids. I: one-way bending.", *ASCE Journal of Composites for Constructions*, 4(3): 145–153.

Matthys, S.; and Taerwe, L., (2000 b), "Concrete Slabs Reinforced with FRP Grids. II: Punching Resistance.", *ASCE Journal of Composites for Constructions*, 4(3): 154–161.

Mitchell, D.; Cook W.D.; and Dilger, W., (2005), "Effects of Size, Geometry, and Material Properties on Punching Shear Resistance.", *ACI Special Publication*, 232(3): 39-56.

Mendis, P., (2003), "Design of High-Strength Concrete Members: State-of-the-Art.", *Progress in Structural Engineering Materials*, 5(1): 1-15.

Muttoni A., (2008), "Punching Shear Strength of Reinforced Concrete Slabs without Transverse Reinforcement.", *ACI Structural Journal*, 105(4): 440-450.

Nguyen-Minh L.; and Rovnak M., 2013, "Punching-Shear Resistance of Interior GFRP Reinforced Slab-Column Connection.", *ASCE Journal of Composites for Constructions*, 17(1): 2–13.

Ospina, C.E.; Alexander, S.D. B.; and Roger Cheng, J.J., (2003), "Punching of Two-Way Concrete Slabs with Fiber-Reinforced Polymer Reinforcing Bars or Grids.", *ACI Structural Journal*, 100(5): 589–598.

Park, R.; and Gamble, W., (2000), "Reinforced Concrete Slabs.", 2nd Edition, *John Wiley & Sons*, Inc. 715p.

Regan, P.E., (1981), "Behaviour of Reinforced Concrete Flat Slabs.", Technical Report 89, *Construction Industry Research and Information Association* (CIRIA), London, UK, 89p.

Regan, P.E., and Bræstrup, M.W., (1985), "Punching Shear in Reinforced Concrete.", Comité Euro-International du Béton, Bulletin d'Information, No. 168, Jan. 1985, 232 p.

Rizk, E.; Marzouk, H.; and Hussein, A., (2011), "Punching Shear of Thick Plates with and without Shear Reinforcement.", *ACI Structural Journal*, 108 (5): 581-591.

Ruiz, M.F.; and Muttoni, A., (2010), "Performance and Design of Punching Shear Reinforcing Systems.", *3rd fib International Congress*, Maryland, 14 p.

Sherif, A., (1996), "Behavior of Reinforced Concrete Flat Slabs.", *PhD Thesis*, Civil Engineering Department, Calgary University, Canada, 395 p.

Serbescu, A., (2009), "Tensile Properties of Basalt FRP Rebars "ROCKBAR.", Test Report Sheffiled of university, Civil Engineering Department, UK. 28 p.

Theodorakopoulos, D.D.; and Swamy, R.N., (2007), "Analytical Model to Predict Punching Shear Strength of FRP-Reinforced Concrete Flat Slabs.", *ACI Structural Journal*, 104(3): 257–266.

Whitney, C.S., (1957), "Ultimate Shear Strength of Reinforced Concrete Flat Slabs, Footings, Beams, and Frame Members without Shear Reinforcement.", *Journal of the American Concrete Institute*, 54 (4): 265-298.

Zaghloul A.; and Razaqpur A., (2004), "Punching Shear Strength of Concrete Flat Plates Reinforced with CFRP Grids.", Advanced Composite Materials in Bridges and Structures, *Proceeding of the 4th International Conference on Advanced Composite Materials in Bridges and Structures*, CSCE, Calgary, AB, Canada, 8 p.

Zaghloul, A., (2002), "Behaviour and Strength of CFRP Reinforced Flat Plate Interior Column Connections Subjected to Shear and Unbalanced Moments.", *Master thesis*, Department of Civil and Environmental Engineering, Carleton University, Ottawa, Ontario.

Zaghloul, A., (2007), "Punching Shear Strength of Interior and Edge Column-Slab Connections in CFRP Reinforced Flat Plate Structures Transferring Shear and Moment.", *PhD thesis*, Department of Civil and Environmental Engineering, Carleton University, Ottawa, Ontario, 372 p.

Zhang, Q.; Marzouk, H.; and Hussein, A., (2005), "A Preliminary Study of High-Strength Concrete Two-Way Slabs Reinforced with GFRP Bars.", *Proceeding of the 33rd CSCE Annual Conference: General Conference and International History Symposium*, CSCE, Toronto, ON, Canada, 10 p.

APPENDIX A: CROSS-SECTION FAILURE ENVELOP

Figure A.1: Cross-section failure envelope of slab $G_{(1.2)}200$

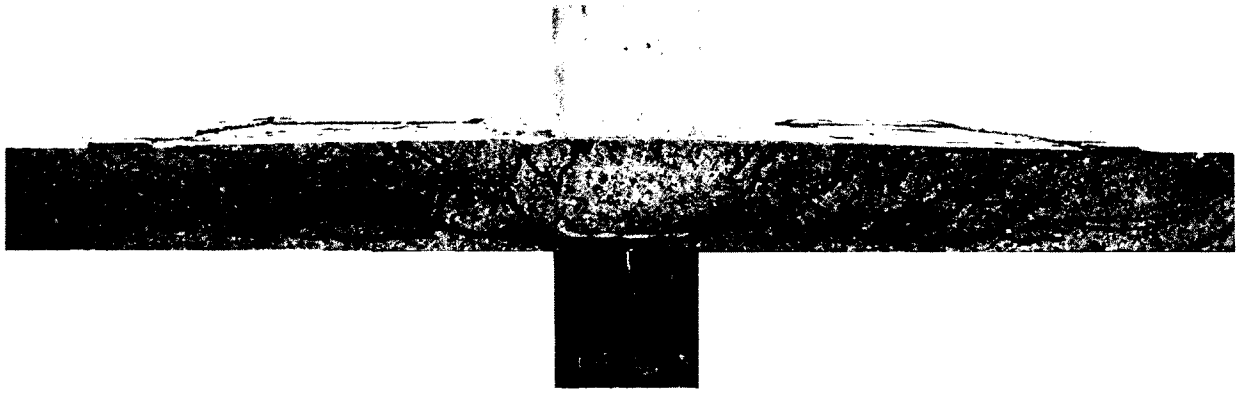

Figure A.2: Cross-section failure envelope of slab $G_{(1.2)}200$-GCS(d/2)

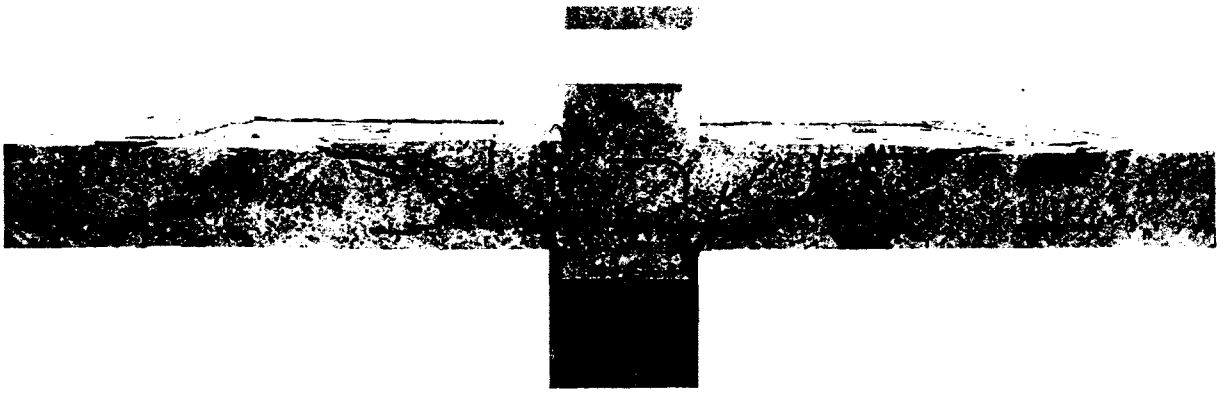

Figure A.3: Cross-section failure envelope of slab $G_{(1.2)}$200-CCS(d/2)

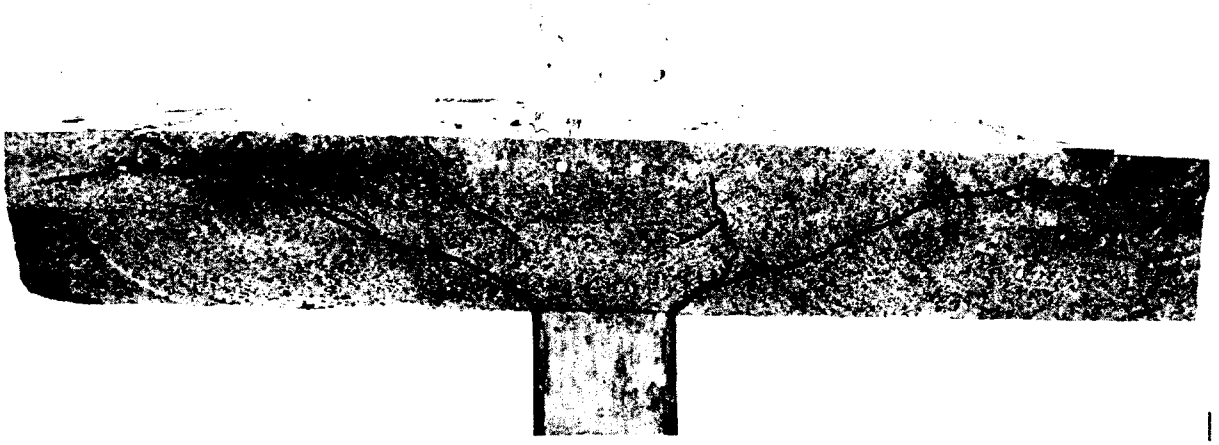

Figure A.4: Cross-section failure envelope of slab $G_{(1.6)}$350

Figure A.5: Cross-section failure envelope of slab $G_{(1.6)}$350-GSS(d/4)

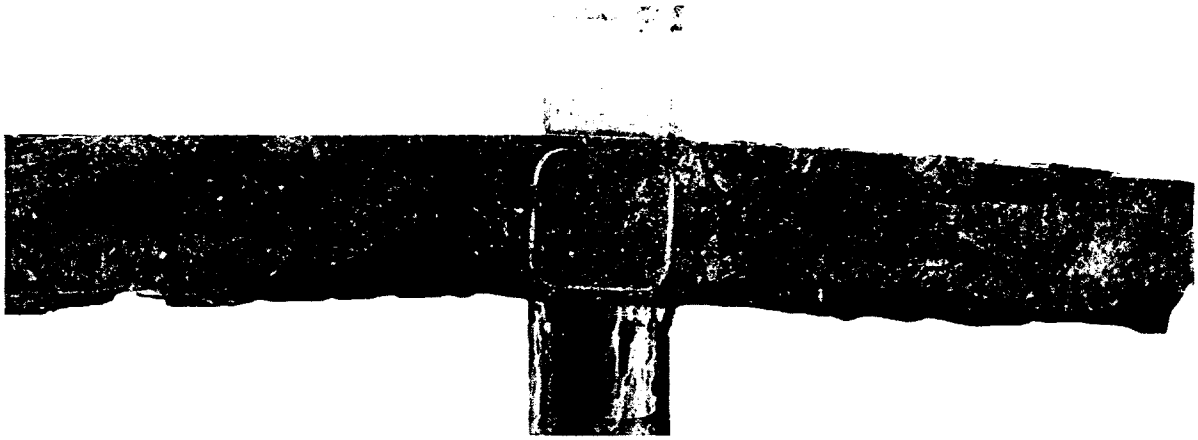

Figure A.6: Cross-section failure envelope of slab $G_{(1.6)}350$-GBSS(d/4)

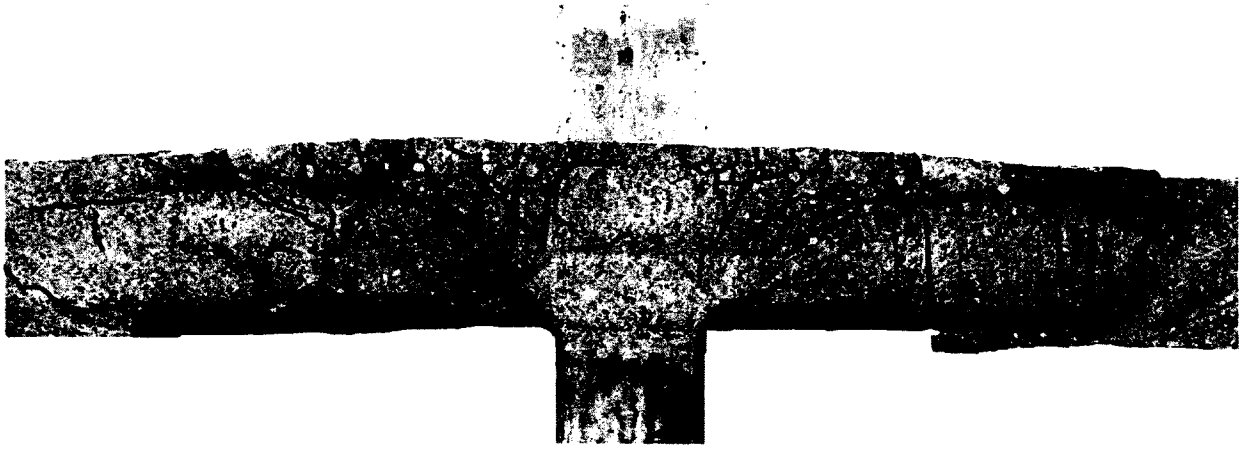

Figure A.7: Cross-section failure envelope of slab $G_{(1.6)}350$-CSS(d/4)

Figure A.8: Cross-section failure envelope of slab $G_{(1.6)}350$-CSS(d/3)

Figure A.9: Cross-section failure envelope of slab $G_{(0.3)}350$

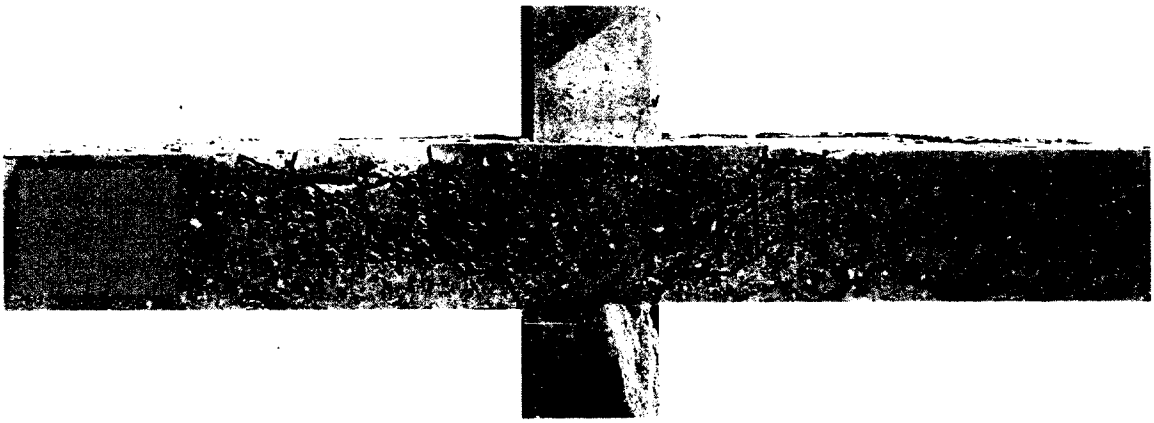

Figure A.10: Cross-section failure envelope of slab $G_{(0.3)}350$-GSS(d/4)

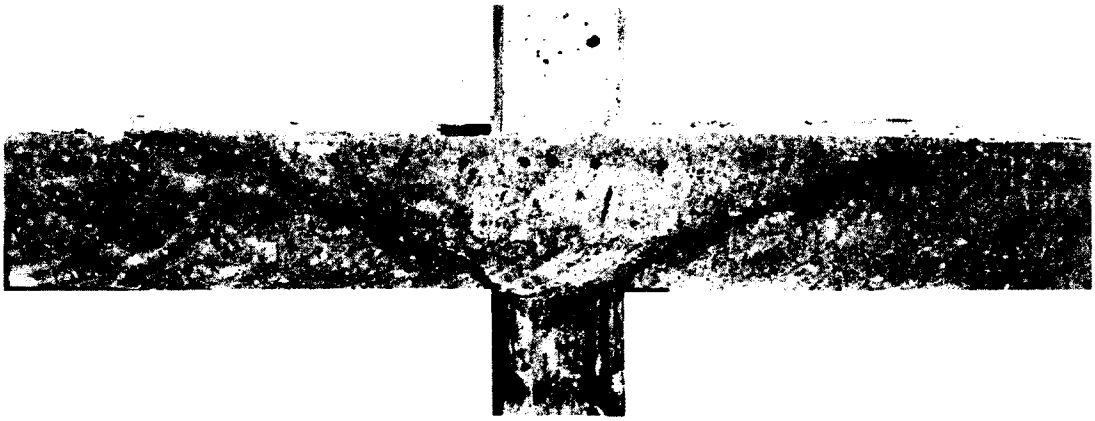

Figure A.11: Cross-section failure envelope of slab $S_{(0.8)}30/35$

Figure A.12: Cross-section failure envelope of slab $G_{(1.6)}30/20$-H

Figure A.13: Cross-section failure envelope of slab $G_{(1.6)}30/35$-H

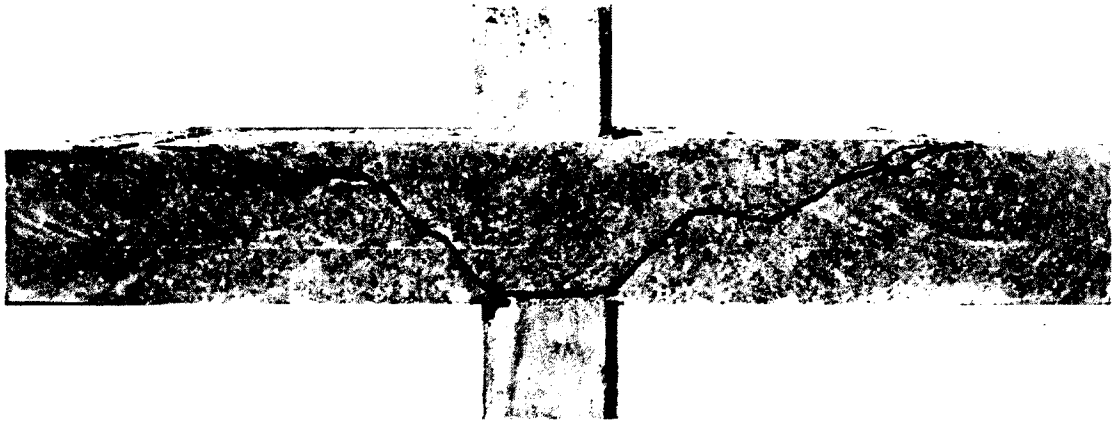

Figure A.14: Cross-section failure envelope of slab $G_{(0.7)}30/35$

Figure A.15: Cross-section failure envelope of slab $G_{(1.6)}30/20$-B

Figure A.16: Cross-section failure envelope of slab $G_{(1.6)}45/20$

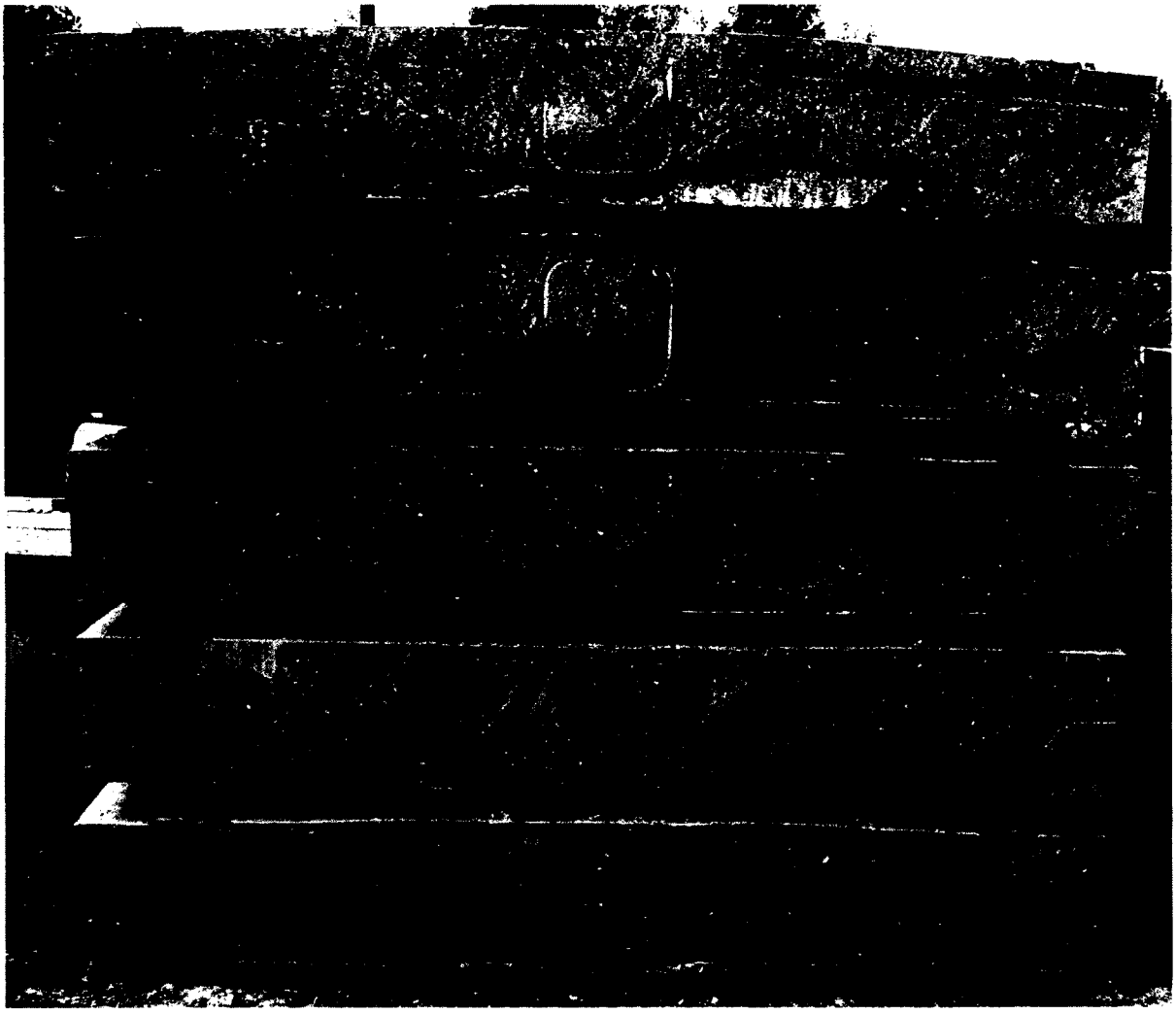

Figure A.17: Cross-section failure envelope of specimens other parts

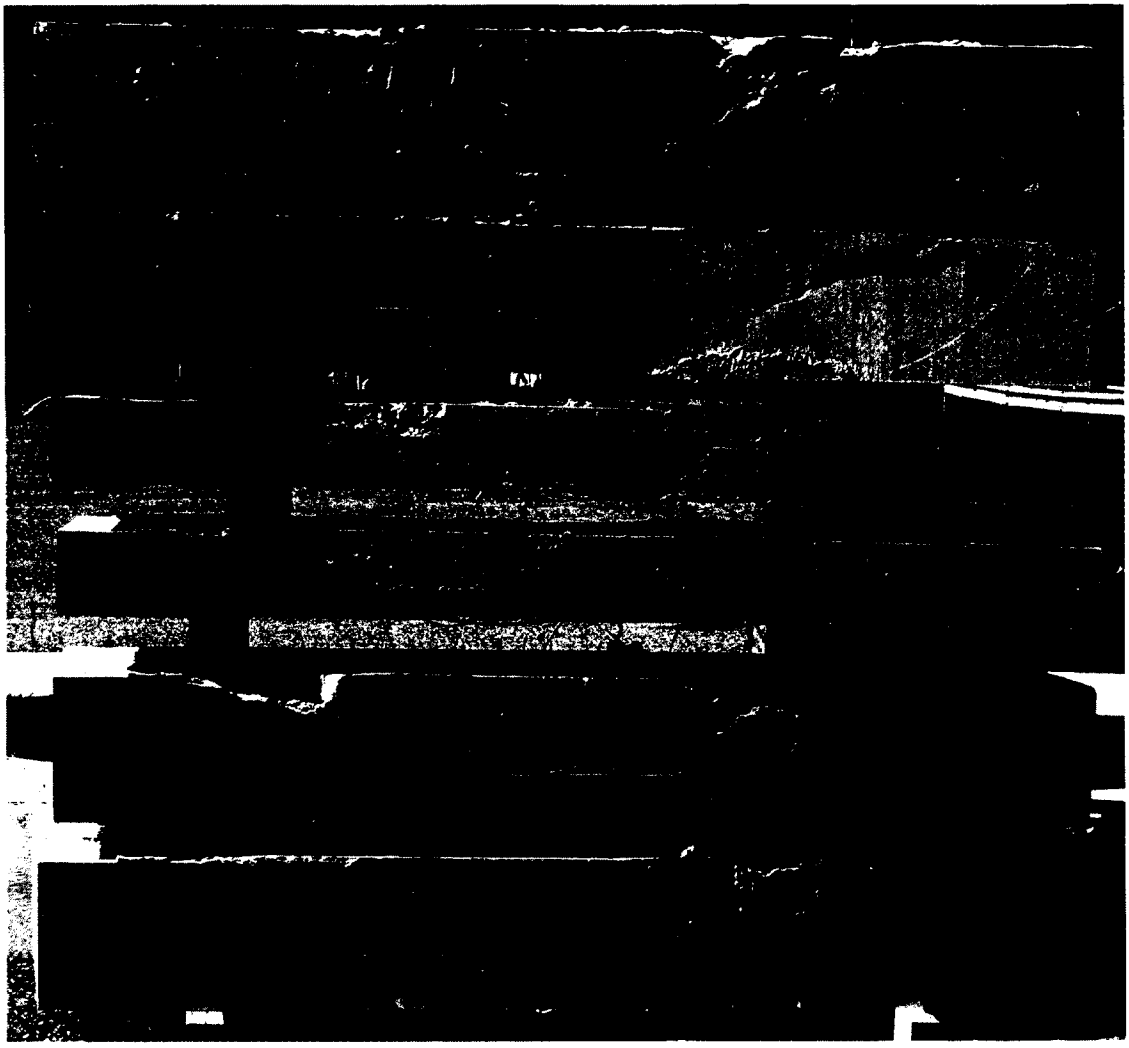

Figure A.18: Cross-section failure envelope of specimens other parts

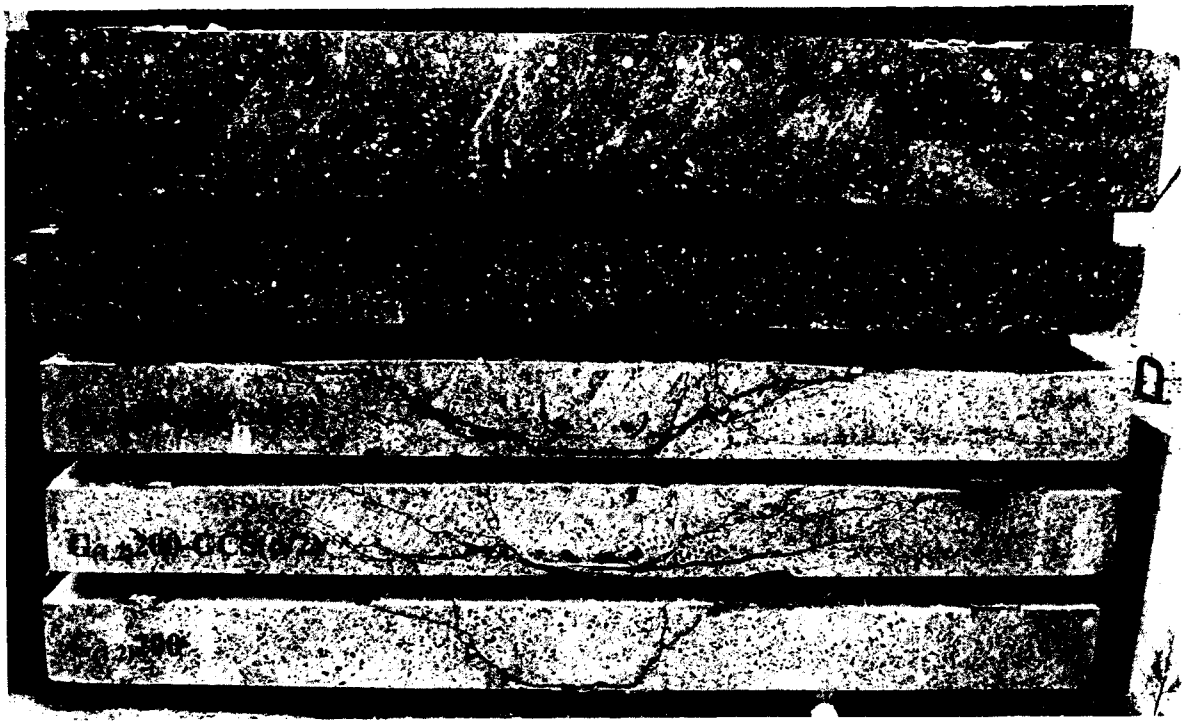

Figure A.19: Cross-section failure envelope of specimens other parts